

MINERAL TRANSFORMATIONS WITHIN AMPHIBOLITES
AT ELDORA, COLORADO

K.E.Prince

A thesis submitted for the degree of Doctor of Philosophy

University of Edinburgh

1992



'Hart (1964) and Steiger and Hart (1967) have convincingly demonstrated that the contact metamorphism around the Eldora Stock occurred by the 'dry' conduction of heat without major mineralogic changes, unlike near other area intrusives where there is associated evidence of hydrothermal alteration. It seems reasonable therefore to describe the loss of argon under the conditions at Eldora as a volume diffusion process.'

Berger (1975)

ABSTRACT

Detailed petrological and geochemical investigations performed upon amphibolites from Eldora, Colorado have clearly demonstrated the heterogeneous nature by which rocks situated within the lower crust adapt to changes in the physico-chemical environments imposed upon them through time.

The Eldora Amphibolites formed and attained both chemical and textural equilibration during the initial PreCambrian metamorphism of the Idaho Springs Formation *c.*1850my ago. Several alteration events have affected the Amphibolites since their formation. Migmatization, with the widespread injection of leucocratic seams, occurred *c.*1750my ago. At least two phases of PreCambrian re-heating, caused by the intrusions of the Silver Plume and Pike's Peak Granites, have also taken place. The re-heating associated with the intrusion of the Silver Plume Granite *c.*1410my ago resulted in the re-setting of the K-Ar ages of the rocks. Both PreCambrian and Laramide (60-100my) mineralisation have been previously documented within other rocks from the Formation. It has been difficult to conclusively distinguish between these different aged mineralising events in many of the rocks at Eldora since both types produced similar textural and chemical changes within the amphibolites. A quartz monzonite stock which also intruded into the Amphibolites during the Laramide orogenic event has been shown to have had little noticeable effect upon the surrounding country-rocks except those within approximately 2m. of the contact. This conflicts with the classic text of Hart (1964), who postulated temperature-related modifications in an approximately 30m. wide aureole surrounding the Stock.

This study has concentrated upon characterising, and establishing the relative timing of the modifications which took place to original ferroan-pargasitic-hornblende crystals within the amphibolites. Four slightly different amphibole alteration types (termed Boundary, Microvein, Extensive single crystal and Extensive multi-crystal alterations) have been recognised and fully characterised using optical, electron microprobe and electron microscope techniques. Extensive single crystal and Extensive multi-crystal alterations are only seen in rocks situated within 2m. of the Stock. All the alteration types, irrespective of their proximity to the Stock contact are only ever present within certain parts of the rock, termed permeation zones and microfracture networks. These zones are believed to represent the routes via which fluids gained access to the rocks. The majority of the mineral alterations identified resulted from crystal-fluid interactions and are not the result of diffusive exchange associated with any re-heating (PreCambrian and/or Laramide) that may have affected

the rocks. The 2m. zone surrounding the Stock is probably the product of alteration caused by the passage of metasomatic fluids emanating from within the Stock.

Coupled thin-section/electron microprobe studies have shown that most secondary hornblendes formed during the PreCambrian migmatisation event, whilst most actinolites formed during either the younger mineralisation events (PreCambrian or Laramide) or from fluids emanating from the Laramide Stock.

Most of the secondary hornblendes and secondary actinolites have sharp gradients against their host hornblendes. However, no grain boundary is visible between the two phases. Evidence is presented which indicates that the secondary amphiboles are not the result of a miscibility gap within the calcic amphibole series and that the alterations probably represent epitaxial replacements and/or overgrowths of the original grains.

Geochronological investigations have been performed which show that the ages of the amphiboles were not re-set by heat dissipated by the Laramide quartz-monzonite stock, as was previously suggested by Hart (1964). Age re-setting has occurred. However, in contrast to the previous isotopic study of Hart (op.cit.), no direct correlation between the bulk age of the rock and its proximity to the Stock was observed. In addition to the examination of the K-Ar ages of amphibole separates, the $^{40}\text{Ar}/^{39}\text{Ar}$ ages of individual amphibole crystals have been determined in-situ using laser spot dating techniques. The age patterns observed are complex. Original hornblendes are zoned in age with cores of approximately 1450my surrounded by ages which gradually decrease to c.900-600my. A periphery of erratic ages at the edges of the crystals are suggested as representing the incorporation of excess argon. Analyses of secondary hornblendes and actinolites generally give ages slightly older, c.500my or less, than was expected. Many of these "ages" are the result of laser volatilisation from areas consisting of both original and secondary amphiboles and thus represent mixed ages. The age variations within the original hornblendes are thought to have formed during one of the PreCambrian re-heating events whilst the ages of the secondary amphiboles represent the times at which the relevant fluids pervaded, and facilitated the formation of secondary phases within, the rocks. The apparent age re-setting of the rocks recorded by Hart (1964) has been shown to reflect the abundance of secondary phases within his separates and does not represent diffusive activity controlled by the rocks position within a thermal aureole.

ACKNOWLEDGMENTS

This thesis is the culmination of three years toil against the "elements"! The studies presented herein are the result of continued encouragement, advice and assistance from the lecturing and technical staff of both Edinburgh and Leeds Universities.

I am most particularly grateful to my supervisor, Ben Harte, who had faith (often in the face of extreme opposition) and persevered until I managed to explain what I'd seen. I have learnt much about scientific practice, thought and presentation from Ben and I hope my thesis justifies all his efforts.

Amongst the staff of Edinburgh University I wish to thank Pete Hill, Stuart Kearns, John Craven and Richard Hinton for their considerable help in enhancing my interest in the analytical sides of geology. With their help and guidance I eventually managed to master the electron microprobe and had several adventures into the realm of ion microprobe analysis. Roy Gill is thanked for his advice on aspects of the ore mineralisation within the amphibolites and for his general interest and optimism. John Finley is thanked for his help on the S.E.M. over at the Botany Department. Ian Parson's is acknowledged for his help in arranging the laser microprobe work and for the use of his microscope and camera from which some of the colour pictures in this thesis were obtained.

At Leeds University I wish to acknowledge Eric Condliffe and Andy Barnicoat for their assistance and training on the S.E.M. The "K-Ar Crew", particularly Dave Rex and Philip Guise, are thanked for fitting me in at short notice, obtaining the K-Ar ages of my separates and for many enjoyable tea-breaks. Martin Dodson is thanked for supplying the initial samples from the contact aureoles which enabled me to begin my studies and culminated in my trip to the U.S.A.

Thanks go to Ray Burgess at S.U.R.R.C., who "zapped" my hornblendes using the laser microprobe (eventually) and supplied all the $^{40}\text{Ar}/^{39}\text{Ar}$ dates. This technique has only really just become available for use and I feel particularly lucky to have been involved at a relatively early stage of it's development. Laser "spot" dating will undoubtedly become one of the more useful techniques available for unravelling the geological histories of rock samples.

Many thanks to Diana Batty and Yvonne Cooper for all their help on the visual aspects of my studies, and to all the other technical staff at Edinburgh for expertise in a variety of different skills.

Julia Cousens is thanked for being a sterling field assistant and good friend throughout the course of my studies. Many thanks for putting me up during my many visits to Leeds and for bravely proof reading some of my chapters.

Finally I wish to thank my close friends and family for their continual interest and support over the past three years. I hope I wasn't too unbearable!

CONTENTS

CHAPTER 1: INTRODUCTION AND FIELD STUDIES

1.1. Introduction.	1
1.2. Geological setting and fieldwork.	5
1.2.1. Snowbank Lake Aureole.	8
1.2.2. Giant's Range Aureole.	14
1.2.3. Christmas Lake Aureole.	20
1.2.4. Eldora Aureole.	24
1.3. Research Appraisal.	45
1.3.1. Giant's Range Aureole.	45
1.3.2. Eldora Aureole.	46
1.4. Resume.	49

CHAPTER 2: THEORETICAL BACKGROUND

2.1. Diffusion.	51
2.1.1. Principles of diffusion.	51
2.1.2. The Closure Temperature concept.	58
2.2. The Amphibole Group.	69
2.2.1.(i) Structure.	70
2.2.1.(ii) Classification and nomenclature.	72
2.2.2. Substitutions and mineral reactions.	77
2.2.3. Amphibole equilibria and phase relations.	79
2.2.4. Deformation and recrystallisation mechanisms.	83

CHAPTER 3: TECHNIQUES

3.1. Transmitted light petrography.	84
3.2. Chemical petrography.	84
3.2.1. Electron microprobe.	84
3.2.2. Back-scattered-electron imagery.	86
3.2.3. Ion microprobe.	90
3.3. Isotopic analysis.	94
3.3.1. K-Ar age determinations from mineral separates.	94
3.3.2. $^{40}\text{Ar}/^{39}\text{Ar}$ laser spot age determinations.	98

CHAPTER 4: PETROGRAPHY AND SPATIAL DISTRIBUTION OF ALTERATIONS WITHIN THE ELDORA AMPHIBOLITES

4.1. Petrography.	104
4.1.1 Terminology.	104
4.1.2. Eldora rock types.	106
4.1.3. Detailed rock descriptions.	107
4.2. Summary of the alteration phenomena observed.	132
4.2.1. Pristine regions of amphibolitic rock.	132
4.2.2. Altered/less pristine regions of amphibolitic rock.	132
4.3. Distributions of alterations within the amphibolites.	150
4.3.1. Distribution within individual thin-sections.	150
4.3.2. Alteration distribution at outcrop scale.	158
4.4. Conclusions/interpretations.	160

CHAPTER 5: MINERAL CHEMISTRY, THERMOBAROMETRY AND DIFFUSION CALCULATIONS

5.1. Amphibole chemistry.	166
5.1.1. Electron probe analysis and B.S.E. images.	166
(i) Pristine amphibole compositions.	166
(ii) Altered amphibole compositions.	169
5.1.2. Summary of the optical and chemical characteristics of the major alteration types.	200
5.1.3. Summary of the chemical profile types.	200
5.1.4. Discussion of B.S.E. images.	202
5.1.5. Relation of secondary amphibole compositions to alteration zones within the amphibolites.	206
5.1.6. Miscibility between original and secondary amphiboles.	206
5.1.7. Ion probe analysis.	213
(i) Mass surveys.	213
(ii) Element profiles of altered grains.	213
(iii) Spot analysis of different amphibole chemistries.	217
(iv) Ion imaging.	218
(v) Summary of ion probe analysis.	219
5.2. Feldspar, pyroxene and biotite chemistry.	221
5.2.1. Feldspar chemistry.	221
5.2.2. Pyroxene chemistry.	227
5.2.3. Biotite chemistry.	227
5.3. Summary of chemical data.	230
5.4. Thermobarometry and diffusion calculations.	232
5.4.1. Thermobarometry.	232
5.4.2. Diffusion calculations and curve fitting.	234

CHAPTER 6: SUMMARY AND DISCUSSION OF THE OPTICAL AND GEOCHEMICAL INFORMATION OBTAINED ON THE ELDORA AMPHIBOLITES

6.1. Summary of optical and B.S.E./microprobe observations.	238
6.2. Conclusions.	241

CHAPTER 7: GEOCHRONOLOGY

7.1. Previous work.	244
7.2. K-Ar age determinations from mineral separates.	256
7.3. $^{40}\text{Ar}/^{39}\text{Ar}$ age determinations using laser spot analysis.	257
7.4. Conclusions of isotopic studies.	277
7.5. Discussion of previous work.	278

CHAPTER 8: CONCLUSIONS

General conclusions and suggestions for future work.	281
--	-----

APPENDIX A

Tables 1- 9: Laser Spot Ages.	283
-------------------------------	-----

BIBLIOGRAPHY

CHAPTER 1. INTRODUCTION AND FIELD STUDIES

1.1. INTRODUCTION

The studies presented in this thesis are aimed at gaining some insight into the kinetic processes by which a given set of mineral grains within solid rocks change chemical composition and move towards equilibrium. It is therefore a study of metamorphism, but differs crucially from normal metamorphic studies which are commonly concerned with changing mineral assemblages and textures. In this instance the objective has been to study situations where full recrystallisation¹ did not occur, and the assemblage of minerals and their textures did not change, but where there were nonetheless changes in mineral composition which could be compared at different temperatures. It was expected that these changes would have been caused by diffusion² and that the studies would provide at least relative empirical data on various element mobilities in ferromagnesian minerals. Given good data on the conditions and timing of metamorphism, it was hoped that the kinetic data might be semi-quantitatively defined. Some progress in these objectives has been made, but the studies most particularly revealed the detailed chemical complexity of natural rocks at the grain scale and the heterogeneous nature of their 'reaction' changes. The research presented clearly demonstrates the depth of detailed information that can be gathered by integrating modern geochemical and classic petrographic techniques. These have provided essential information from which the geological histories of rocks have been determined.

The contact metamorphic environment was considered to be the most suitable setting in which the temperature and time circumstances of metamorphism could be constrained; here modelling of the pressure and temperature of metamorphism can be made from estimates of intrusion composition, size, shape and temperature. Classic contact metamorphic aureoles in which extensive recrystallisation have been documented were inappropriate for these studies, but several aureoles which had been the subject of geochronological studies appeared highly appropriate and much of this first chapter is concerned with examination of these and the choice of Eldora, Colorado, as the focus of much study. Thus this research is a follow-up to an original geochronological study made by Hart (1964) on the Eldora Aureole,

¹ The structural and chemical reconstitution of an existing grain to a mineralogically similar phase.

² Diffusion being a spontaneous process by which atoms, molecules or ions move from one position to another without advection. Further discussion can be found in chapter 2.

Colorado. In this now classic isotopic study Hart outlined how K-Ar, U-Pb and Rb-Sr mineral ages in Pre-Cambrian regional metamorphic rocks could be reset in a contact aureole to the age of the associated Tertiary igneous intrusive; the results of this work are presented in Figure 1.1.

The thermal significance of isotopic dates has been an area of intense research since the early 1960's. The concepts of diffusion kinetics and blocking temperatures³ have been used by geochronologist's and metamorphic petrologist's alike in an attempt to elucidate the thermal histories of metamorphic terrains. Theoretically in a contact metamorphic environment the intrusive body raises the rocks of it's associated aureole above the blocking temperature range of the mineral systems concerned. Diffusion may then occur at a rate depending on the samples temperatures, which depend on the rock's position within the aureole. Ideally samples originating closest to the intrusive, having been subjected to the highest temperatures and thus showing most diffusion, retain the least concentrations of radiogenic nuclides and therefore have the youngest ages. This contrasts with samples furthest from the contact, unaffected by the thermal event, which remain closed systems retaining their age prior to intrusion. An aureole showing minerals with reduced ages is therefore created symmetrically around the intrusion.

The specific aim of this study was to re-examine aureoles in which geochronological studies had shown a re-setting of mineral ages, with a view to gaining knowledge of the major, minor and trace element, as opposed to isotopic mobilities within ferromagnesian minerals. There were initially 5 main objectives:-

- (i) To compare and contrast, both texturally and chemically, samples collected at various distances from the contact establishing the extent of equilibration and degree of recrystallisation of the ferromagnesian phases.
- (ii) To investigate by which processes equilibration has taken place within the contact metamorphic environment.

³ The temperature (or range of temperatures) at which geologically significant diffusion ceases. Further explanations can be found in chapter 3.

- (iii) To document the 'plateau' concentrations and diffusion widths for each mobile element within zoned grains and highlight any variation with distance from the contact. The electron microprobe was to be used to measure any change in concentrations of major and minor elements and the ion microprobe for changes in trace element populations.
- (iv) To pinpoint distances at which individual elements become mobile in specific minerals and examine their diffusion kinetics in a temperature/distance framework, with the aim of establishing the blocking temperatures of particular element/mineral systems.
- (v) To model both the heating-cooling history of an aureole and thus the diffusion/closure behaviour of particular element/mineral systems

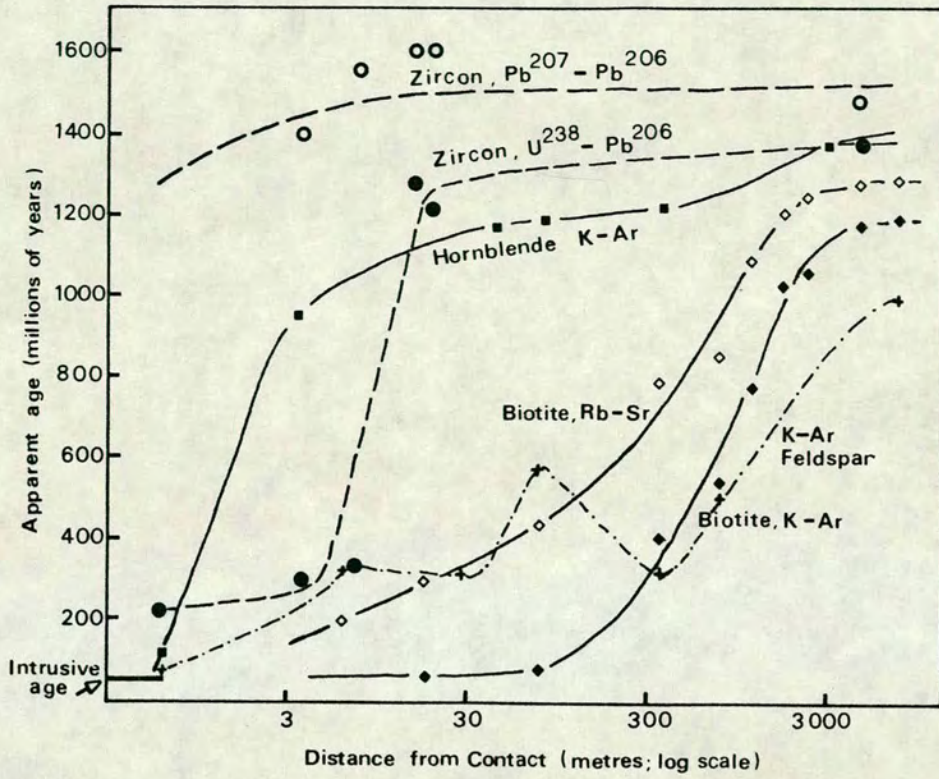


FIG. 1.1. Apparent K-Ar, Rb-Sr, U-Pb and Pb-Pb mineral ages as a function of distance from the Eldora Stock (compiled from Hart, 1964 and Tilton *et al.*, 1964)

1.2. GEOLOGICAL SETTING AND FIELDWORK

Although this study concentrates on the Eldora Aureole, some preliminary studies were also made on other aureoles in an endeavour to establish patterns of mineral behaviour and choose the best possible material for detailed study. This section summarises these general studies and establishes why the Eldora Aureole was considered the best setting in which to perform detailed investigations.

The criteria considered important in the initial selection of a suitable aureole within which to base this research were:-

- (i) An aureole with a relatively uncomplicated metamorphic history ideally comprising either an initial regional metamorphic episode or igneous event followed by contact metamorphism with little or no subsequent late stage processes.
- (ii) Relatively simple mineralogy with a lack of recrystallisation of original grains, uniformity of texture, grain-size and mode throughout the aureole. In addition grain sizes should be sufficient to allow study of zoned chemical composition profiles developed in the minerals as a result of contact metamorphism.

The most desirable country rocks to study are those which reached a state of equilibrium prior to thermal metamorphism. Any mineralogical adjustment within the original grains can therefore be assumed to be a direct consequence of the contact metamorphic event. Uniformity of grain-size, original textures *etc.* are desirable because any effect of contact metamorphism is most noticeable in rocks of an otherwise constant nature. Recrystallisation is undesirable because it eradicates evidence of volume diffusion.

- (iii) Despite the aspects of lack of change during contact metamorphism noted under (ii), there must nonetheless be changes in mineral compositions associated with the contact metamorphism.
- (iv) There is some knowledge of the thermal gradient and cooling history of the aureole.

It will then be possible to make a reasonable attempt at modelling the diffusivities of the elements based on a framework of well constrained external parameters.

Existing geochronological studies of the re-setting of mineral ages in contact aureoles which appeared to fulfill most or all of these criteria include:

- The Snowbank Lake Aureole, Minnesota (Hanson & Gast, 1967)
- The Giant's Range Aureole, Minnesota (Hanson *et al.*, 1971,1975)
- The Christmas Lake Aureole, Wyoming (Hanson & Gast, 1967)
- The Eldora Aureole, Colorado (Hart, 1964)

The results of these studies are presented in Figures 1.1 and 1.2; a decrease in the ages with closeness to the intrusive contacts is apparent in each case.

A set of specimens collected along identical traverses to each of these geochronological studies were available from Dr. Martin Dodson (Leeds University). Preliminary hand-specimen observations of the rock-types within these aureoles indicated that they were suitable for consideration as settings in which to carry out the specified research. The rocks of the Eldora and Giant's Range Aureoles appeared particularly suitable; thin-section and electron-microprobe work was commenced upon the specimens from these two localities in the first year of research.

Fieldwork undertaken 5th-24th July 1989 enabled the four aureoles to be further critically assessed. Limited time available in the field meant it was not possible to undertake detailed mapping of each locality, however, published information provided an adequate base from which to work. Emphasis was predominantly toward sample collection, although some effort was made at establishing the nature of the country-rock/intrusive contact and gaining an overall knowledge of the geological environment within which limited contact metamorphism had operated.

In the following sections the field and petrographic observations of the rock-types within each aureole are summarised. This is followed by a critical appraisal of the localities, providing the basis for the selection of the rocks at Eldora for detailed studies.

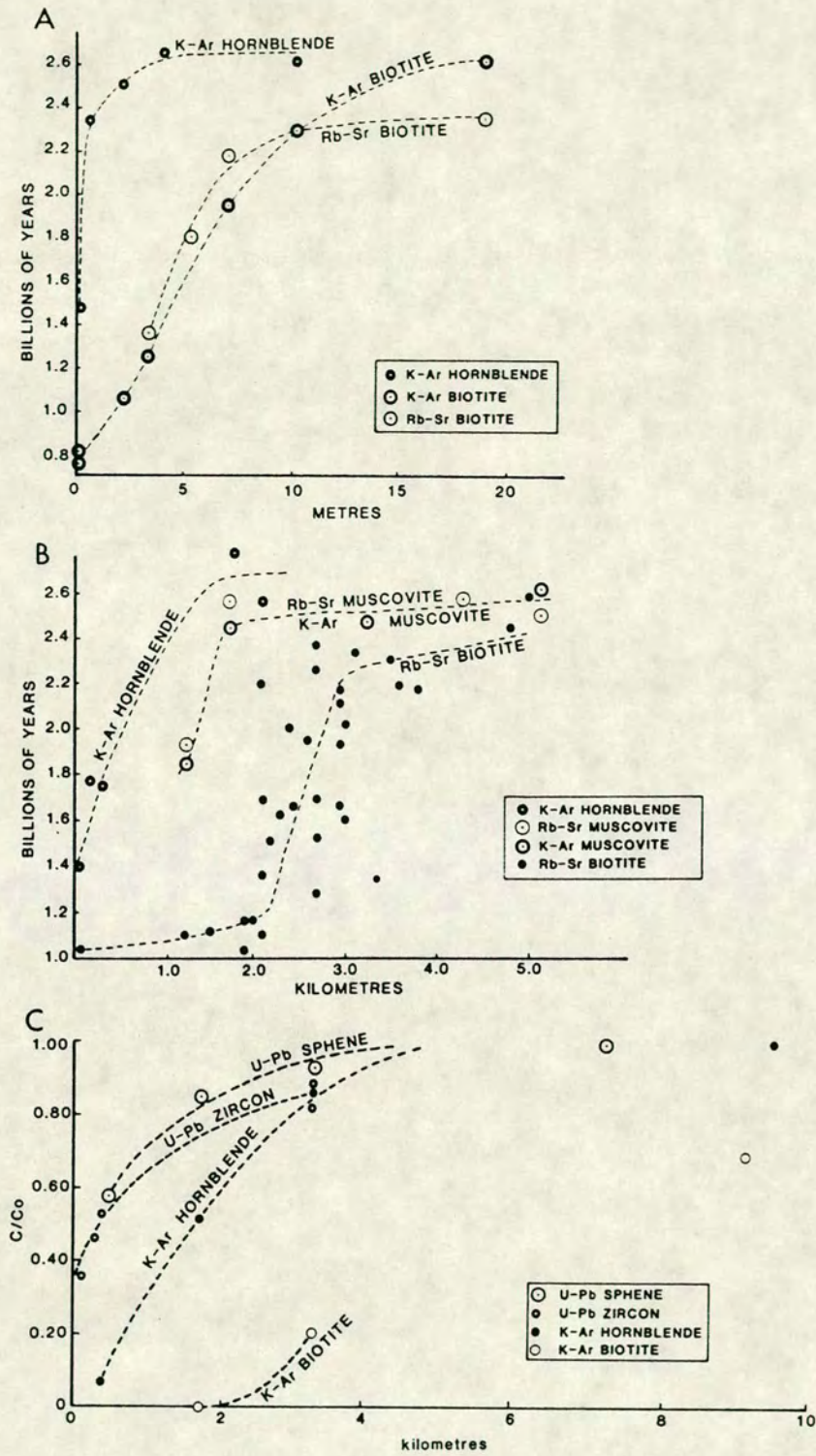


FIG. 1.2. Apparent K-Ar, Rb-Sr, U-Pb mineral ages versus distance from:
 (A) The Christmas Lake Dyke (reproduced from Hanson and Gast, 1967).
 (B) The Duluth Gabbro contact with the Snowbank Lake Granite (compiled from Hanson and Gast, 1967).
 (C) The Duluth Gabbro Contact with the Giants Range Porphyry (reproduced from Hanson *et al.*, 1971).
 Ages in (C) expressed as a fraction of parent to daughter ratio (C/Co).

1.2.1. THE SNOWBANK LAKE STOCK IN THE DULUTH GABBRO AUREOLE

The Snowbank Stock is found within the 'Boundary Water Canoe Wilderness', east of Ely, northern Minnesota (Figure 1.3). The position of the stock is now marked by one of Minnesota's 10,000 lakes, however some exposure remains around the foreshore and on small islands within the lake from which sampling is possible - if unconventional ! (Plate 1a,b).

Numerous studies were made on the stock between 1918 and 1967 (e.g. Grout, 1918; Anderson, 1964; Goldich *et al.*, 1961; Hanson and Gast, 1967). According to the Rb-Sr and K-Ar ages of Hanson and Gast (1967) the Stock was intruded between 2560 and 2610 million years ago. The stock and surrounding rocks of this Archean terrain were subsequently transgressed by the Duluth Gabbro Complex 1100 million years ago (Hanson *et al.* 1971). The geological map of the area is reproduced in Figure 1.4.

Petrographically the stock varies in composition from a quartz-monzonite to a diorite; constituent minerals being plagioclase, alkali-feldspar, augite, hornblende, biotite and quartz (Hanson and Gast, 1967). Sanders (1929) considered the stock to consist of four facies, whilst Hanson and Gast (1967) recognised two facies but did not attempt to delimit definite boundaries. The contact effects of the Duluth Gabbro upon the Snowbank Stock have been petrographically examined by Hanson and Gast (1967). They report that

"as the contact is approached the plagioclase has been unaffected except within 40m. of the contact where twinning and extinction may be wavy and indistinct. Pyroxene becomes more abundant at the expense of hornblende; however even within 2m. of the contact hornblende is present. The augite becomes globular as the rock texture becomes more granoblastic. Biotite does not change color as the contact is approached and within 2km. of the gabbro exsolved rutile is no longer found in biotite. Within 200m. of the contact chlorite, which is commonly interlayered with the biotite, becomes rare, and the biotite is less abundant."

They go on to infer from this that the dominant chemical effect produced by the gabbro is largely a dehydration episode.

FIELD OBSERVATIONS

Due to the rather remote setting, access to the stock/gabbro contact itself was not achieved, none-the-less a complete coverage of rocks between 0.1 and

6.5 kilometres from the contact were examined; the sample localities are displayed in Figure 1.3.

Though retaining a fairly uniform mineralogy the modal percentage and grain size of each phase within the aureole is somewhat variable. These fluctuations in grain size and mode probably reflect facies changes within the stock. The dominant rock-type is a pink-weathering, medium-grained, subhedral, homogeneous monzonite (Plate 1a) comprising approximately 70-80% subhedral feldspar (1.5-2mm size range); 10-15% aggregates and subhedral laths of hornblende (1.5-3mm. size range) which occasionally show alteration to chlorite; \pm biotite (0-10%); \pm quartz (\leq 5%); \pm sphene (\leq 2%). Increases in the modal percentage of mafics of up to 70% were observed in texturally similar lithologies, as well as variations in rock-type to fine grained biotite-aplites and coarse grained plagioclase-phyric granites (Plate 2a,b). Additional complexities noted in the field were the presence of mafic xenoliths with a diverse size and shape (Plate 2c) and a series of cross-cutting basaltic dykes.



FIG. 1.3. Location of samples within the Snowbank Lake Stock, Minnesota.

PLATE 1. SNOWBANK LAKE AUREOLE.

(a) Typical granitic outcrop exposed along the shore of Snowbank Lake.

(b) Essential field equipment!

(c) Monzonite 'facies' of the Snowbank Stock.

Oar for scale



PLATE 1

FIGURE 1.4.

(a) Geological map of the Snowbank Lake Aureole (reproduced from Minnesota Geological Survey Two Harbors Sheet; Green, 1982). Scale 1:250000 (grid square ~8 miles).

gr=Giant's Range Granite/Adamellite (Archean).

dt=Duluth Complex-troctolite (Middle Proterozoic).

kvf,kcg=Ely Greenstone-acid volcanics (Archean).

ksc=Knife Lake Group-metasediments (Archean).

(b) Geological map of the Giant's Range Aureole (reproduced from Minnesota Geological Survey Two Harbors Sheet; Green, 1982). Scale 1:250000 (grid square~8.5 miles).

grd/grp/gru=Giant's Range Batholith (Archean)

da/dt=Duluth Gabbro-anorthosites and troctolites (Middle Proterozoic).

evm=Ely Greenstone-metabasalt (Archean).

eif=Ely Greenstone-banded ironstone formation (Archean).

PLATE 2. SNOWBANK LAKE AUREOLE.

(a) Coarser-grained, plagioclase phyric granite facies of the Snowbank Lake Stock.

Lens cap for scale.

(b) Coarser-grained patch (arrow 1) and small mafic xenoliths (arrowed 2) within a dioritic facies of the Stock.

Lens cap for scale.

(c) Boudinaged xenolith within the Stock.

Lens cap for scale.

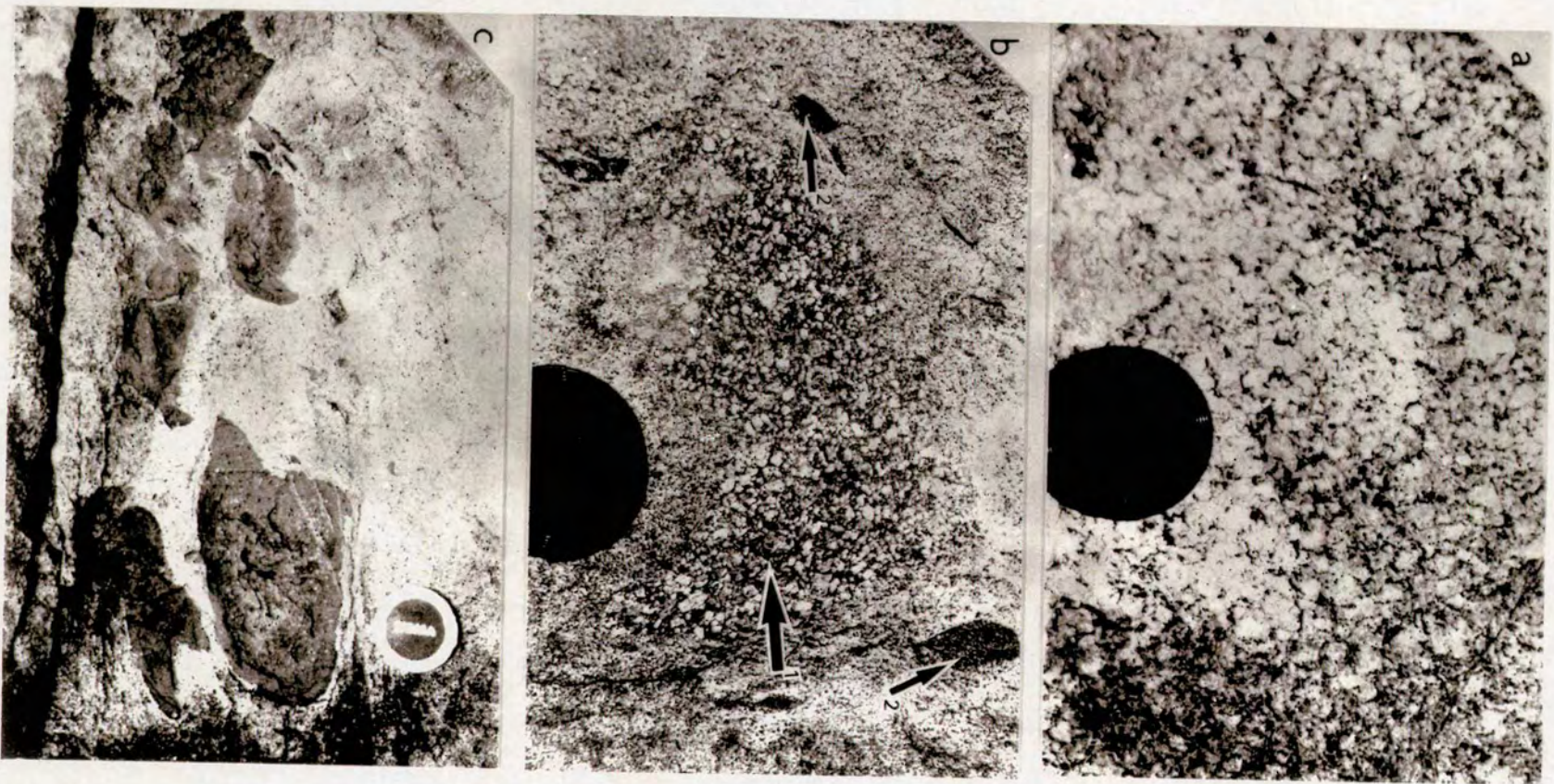


PLATE 2

1.2.2. THE GIANT'S RANGE GRANITE IN THE DULUTH GABBRO AUREOLE

The Giant's Range Granite is found southeast of Ely, northern Minnesota approximately 20 miles west of Snowbank Lake. Easy access to the rocks is available along state Highway 1 (see Figure 1.5 and Plate 3a).

Previous studies performed between the early 1960's and 1980's have largely been of either a regional mapping or geochronological nature (Goldich *et al.*, 1961; Green *et al.*, 1966; Hanson, 1968; Sims and Morey, 1972; Hanson *et al.*, 1971, 1975; Green, 1982).

The Giant's Range Granite intruded the Ely Greenstone 2700-2750 million years ago (Hanson *et al.*, 1971) and was itself intruded by the Duluth Gabbro Complex 1100 million years ago (Hanson *et al.*, 1971). Green's (1982) geological map is reproduced in Figure 1.4. The contact between the Granite and the Duluth Gabbro Complex is marked, within the Gabbro, by the presence of a "contact zone formation", described by Green (*op.cit.*) as:-

"Irregularly coarse-to fine-grained poikilitic augite- and hypersthene-bearing troctolite; contains inclusions of hornfels and sulfide-bearing zones."

The sulphide minerals within this formation are dominantly anhedral grains of pyrite and chalcopyrite.

Hanson *et al.* (1971) note that within the granite

"The hornblende tends to have biotite as inclusions within 2km of the contact."

Hanson *et al.* (1971) also observe:-

"...gridiron twinning in the microcline disappears at about 3km. from the contact. The chlorite in the biotite gradually becomes resorbed, although some chlorite not associated with the biotite is still present at 0.5km. from the contact. Epidote is absent within 2km. suggesting that it is not stable....The sericite in the plagioclase is resorbed and becomes minor within 0.9km. There does not appear to be a change in the appearance of sphene which occurs both as anhedral blebs associated with the hornblende and biotite and as subhedral to euhedral crystals. Sphene becomes rare within 0.5km. along this section..."

Hanson *et al.* (1971) consider some of these features may have a primary igneous origin and may not be the result of thermal metamorphism.

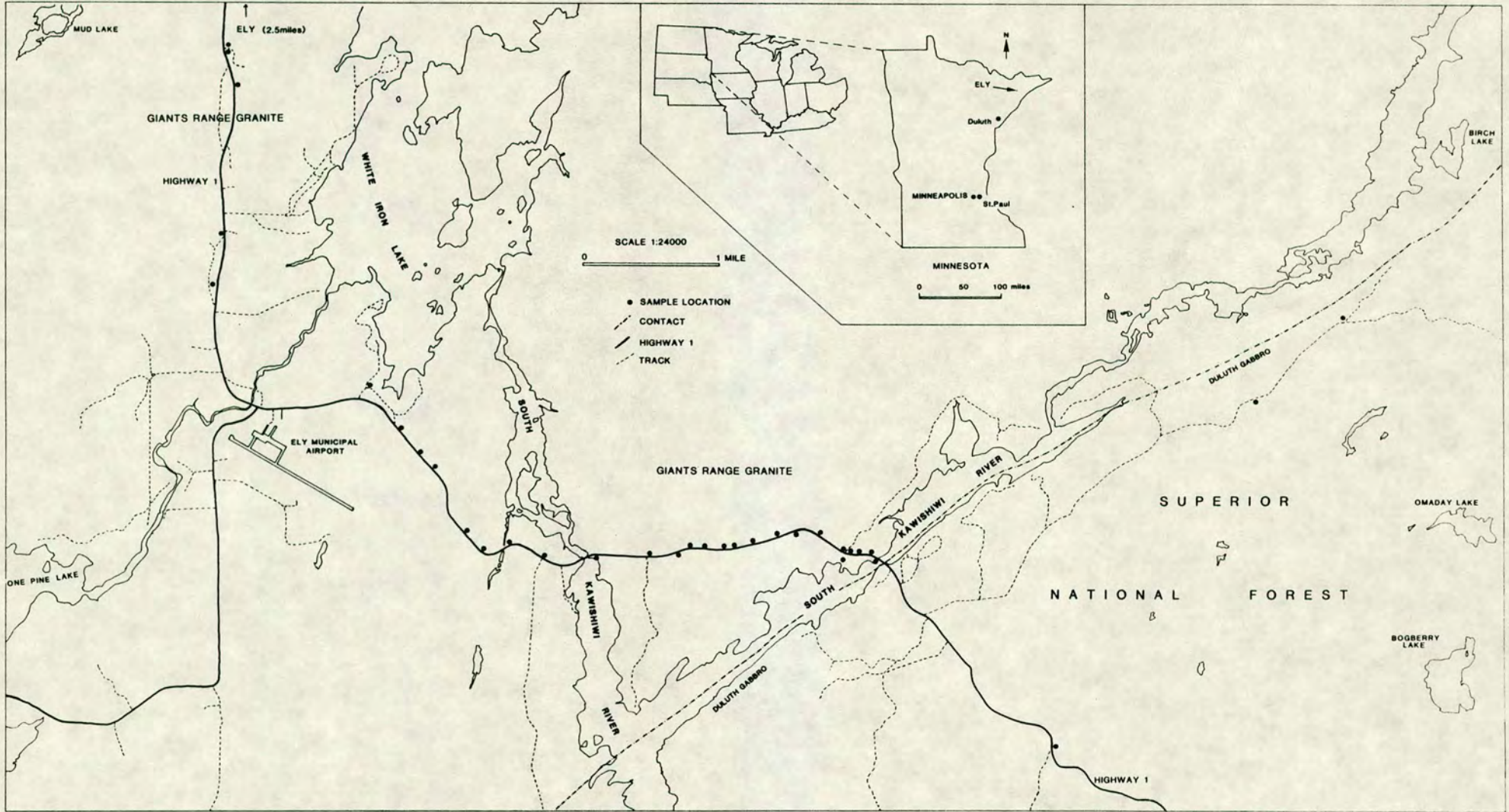


FIG. 1.5. Location of samples within the Giants Range Granite, Minnesota.

PLATE 3. GIANT'S RANGE AUREOLE.

(a) Typical outcrop of Giant's Range Granite exposed adjacent to Minnesota State Highway 1.

(b) Medium to coarse-grained porphyritic quartz-monzonite. Pencil indicates Carlsbad twin plane within an alkali feldspar phenocryst.

Pencil as scale

(c) Subhedral aggregates of hornblende and biotite (arrow 1). Note also euhedral amphiboles within the groundmass (arrow 2).

Pencil for scale.



PLATE 3

FIELD OBSERVATIONS

An extensive investigation of the aureole was made, samples being collected at regular intervals from between 0.1 and 10 kilometres from the contact; sample localities are displayed in Figure 1.5. Two specimens were obtained from alternate outcrops to ensure representative facies were being collected. The rock type remained quite uniform throughout the aureole.

The "Granite" itself is texturally quite similar to Shap Granite, though some slight facies variation was observed; it predominantly comprises a medium-coarse grained, homogeneous, porphyritic quartz-monzonite. Euhedral phenocrysts (20-30% mode) of pink, perthitic, alkali feldspar with distinct Carlsbad twinning (Plate 3b), ranging from 1.5-5cm.ⁱⁿ length, occur within a groundmass of sub-euhedral plagioclase, quartz and mafic minerals (10-15% mode). The majority of the mafics are anhedral to subhedral aggregates of hornblende and biotite, ranging in size from 1mm.-1cm. (Plate 3c). Euhedral amphibole crystals are also present within the groundmass; these show evidence of alteration to epidote/chlorite along grain-boundaries and cleavage planes. Euhedral inclusions of pristine hornblende and biotite (0.5-1mm.) are present within both the phenocrysts and matrix feldspars; these were thought to be potentially of great value to this study. Magnetite, sphene, apatite, zircon and epidote occur as accessories. The larger crystals, including both the phenocrysts and euhedral altered amphiboles, commonly define a flow foliation and lineation within the rock.

The most common departure from the above features is variation in the modal percentage of phases, changes in the mafic population of up to 75% mode have been recorded. In places the rock is better described as a diorite.

Streaked lenses or pods of amphibolitic rock are present within much of the granite (Plate 4a,b). These occur in a great diversity of size (ranging from 0.5-30cm.) and shape, often being elongated in the same direction as the flow foliation. The pods are essentially dominated by subhedral crystals of hornblende and plagioclase, with sizes ranging from 0.1-2mm. No chilling was observed at the contact between amphibolitic lenses and granite host and it is likely that these pods actually represent xenoliths of country-rock incorporated at the time of intrusion (*pers. com.* Bruce Brasaemle, University of Minnesota, 1989). Green (1982) describes these as:-

"amphibolite and augite amphibolite inclusions within the Giant's Range Batholith."

Small 5-10cm. thick, fine-grained, quartz-feldspar rich aplite veins cross-cut the granite in many places. Late stage faulting noted approximately 7km. from the contact is distinguished by either a reddish discolouration (reflecting feldspar alteration) or by a bright green, micaceous epidote/chlorite-rich surface (Plate 4c). Little movement has occurred along these fault horizons and they are believed to be only of local significance.

The boundary between the "contact zone" formation and the Giant's Range Batholith was located to within 3m. At this distance from the contact the granite is largely as seen elsewhere in the aureole, though being of the dioritic rather than monzonitic facies. The euhedral hornblendes are here recrystallised to aggregates of hornblende, biotite and chlorite.

The author observed very little textural or mineralogical change within the granite as the contact was approached. Apart from the slight facies variation the only modification observed was an increase in the abundance of altered euhedral amphiboles; these appear to be relatively fresh beyond approximately 2km. and recrystallising to aggregates of hornblende/biotite/chlorite within 2km. of the contact.

PLATE 4. GIANT'S RANGE AUREOLE.

(a) & (b) Amphibolitic xenoliths incorporated within the Giant's Range porphyry.

Lens cap for scale in (a)

Xenolith approximately 5cm. width in (b).

(c) Epidotised/chloritised fault horizon within the "granite".

Field note-book for scale (c.12cm. width).



PLATE 4

1.2.3. THE CHRISTMAS LAKE DYKE AUREOLE

Christmas Lake is one of many such lakes found approximately 20 miles south-west of Red Lodge, Montana within the 13000ft Beartooth Plateau (Northern Rockies) bordering Montana/Wyoming. Access is available from the Beartooth Highway, Interstate 212, weather and nerve permitting ! A locality map is presented in Figure 1.6.

The dyke, located adjacent to the Lake (Plate 5a), and it's surrounding gneisses have been previously studied by, amongst others, Gast and Long (1957), Pierce (1965), Printz (1964) and Hanson and Gast (1967).

The gneisses and amphibolites of the Beartooth Plateau were subjected to regional metamorphism 2600 million years ago (Gast, Kulp and Long, 1958) and were intruded by the dyke approximately 800 million years ago (Hanson and Gast, 1967). Printz (1964) considered it to be one of the late PreCambrian dolerites.

The quartz-dolerite dyke is 36-50m. thick with a near vertical dip (Hanson & Gast, 1967), well developed chilled borders and a uniform chemical composition (Printz, 1964). The surrounding country rock (Plate 5b) consists of "well foliated para-amphibolites" and "pink leucogranitic gneisses" (Hanson & Gast, 1967). Hanson and Gast (*op.cit.*) note

"there was little if any development of a granoblastic texture as the contact of the dike is approached."

Hanson and Gast (*op.cit.*) also investigated the orthoclase-microcline inversion within the aureole with the objective of "setting limits on the temperature and rate of reaction" for the inversion. They report

"The potassium feldspar is microcline with an obliquity of about 0.90 at and beyond 5m. from the contact. However at and within 4m. of the contact the potassium feldspar has an obliquity of 0.00. If there is a zone of transition, it is only 1m. wide from 4-5m. from the contact."

FIELD OBSERVATIONS

The Dyke has a brownish colour and in-weathering nature in outcrop. It comprises plagioclase, clinopyroxene, hornblende, quartz, orthopyroxene \pm magnetite. For the purpose of this study a single closely spaced traverse was made from the north-east dyke-country rock contact, sampling at intervals of 10-

15m., out to a distance 150m. Samples collected within 74m. of the contact comprise a leucocratic medium-grained quartz-feldspar-biotite gneiss with an average grain-size ranging 0.5-2mm. The quartz and feldspar form well developed alternate bands of 1-2cm. thickness, the biotite occurring in rather discontinuous layers and lenses of variable thickness (average \approx 1cm.). At and beyond 74m. the rock-type consists of a medium-grained, foliated amphibolite comprised predominantly of subhedral hornblende, biotite, feldspar and quartz (0.5-1.5mm). The amphibolites are cut by < 1cm., > 3cm. thick quartz veins which exhibit complex small scale minor folding of a ptygmatic nature (Plate 5c).

The author observed little textural or mineralogical variation, other than the major change in rock-type, as the contact was approached.

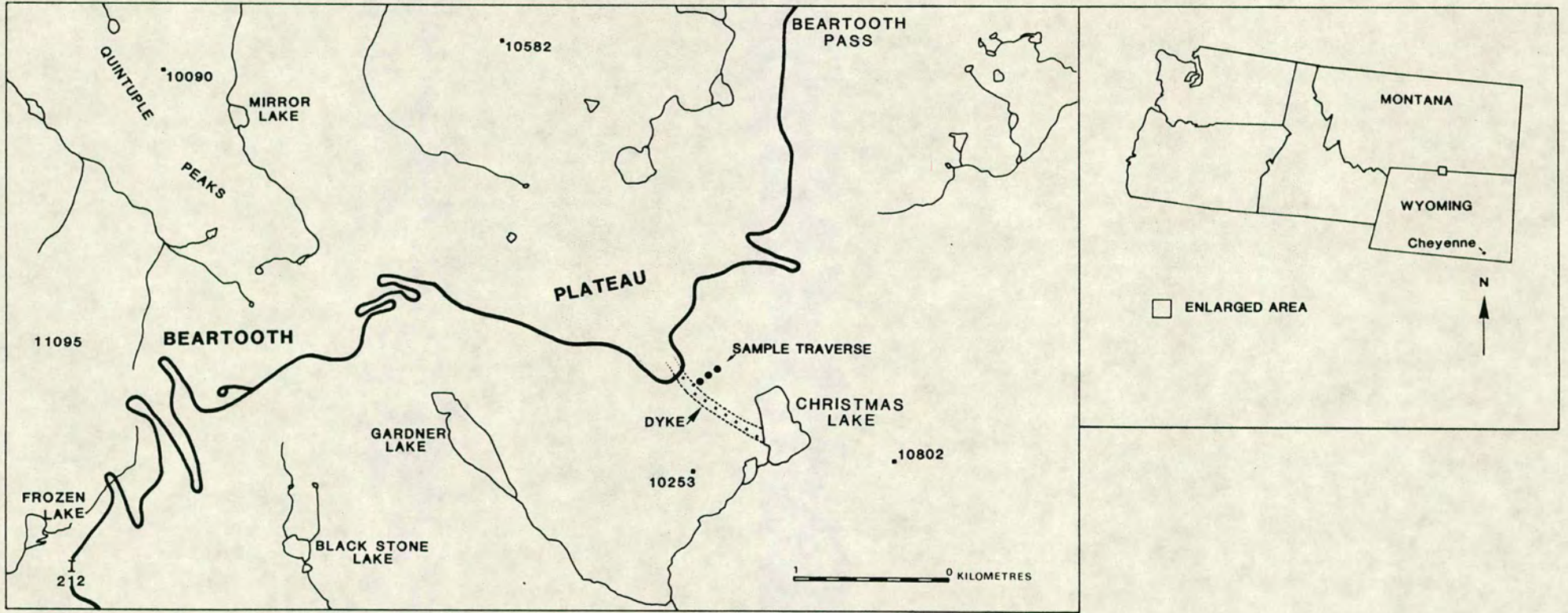


FIG. 1.6. Location of samples within amphibolitic/gneissic rock surrounding the Christmas Lake Dyke, Northern Wyoming.

PLATE 5. CHRISTMAS LAKE AUREOLE.

(a) Christmas Lake; the snow in the foreground (arrow) marks the position of the dolerite dyke (approx. 50m. wide).

(b) A view of the dyke (arrow 1) and it's aureole; gneisses (arrow 2) and amphibolites (arrow 3).

(c) Close-up view of the amphibolitic rock displaying a ptigmatic vein (arrowed).

Hammer head for scale.

1.2.4. THE ELDORA STOCK AUREOLE, COLORADO

Eldora is a small resort (Plate 6a) located in the north-central part of the southern foothills of the Rocky Mountains, known as the Front Range, Colorado. It is situated approximately 20 miles west of Boulder and can be accessed from a country road leading west from state highway 119 at Nederland. The location of Eldora within the Front Range, Colorado is shown in Figure 1.7.

The aureole has been the setting of numerous studies (Cree, 1948; Lovering and Goddard, 1950; Gable, 1969; Steiger and Hart, 1967; Wright, 1967; Berger, 1975) with the geochronological work of Hart (1964) being considered the classic text of it's kind. The geology and ore deposits of the Front Range have been extensively studied as a consequence of their economic value. The majority of early work carried out on the region has been summarised by Lovering and Goddard (1950). Tweto (1966) and Peterman *et al.* (1968) have summarised recent concepts concerning the geological history of the area.

REGIONAL SETTING

The oldest rocks in the Front Range are gneisses and schists referred to as the Idaho Springs Formation (Plate 6b). The rocks represent an approximately 14000 foot thick accumulation of sandstones, shales, minor amounts of quartzites, carbonates and probably some volcanic rocks that have been metamorphosed to almandine-amphibolite facies schists and gneisses over most of the area (Peterman and Hedge, 1967). Cree (1948) suggests the hornblende amphibolites ("Swandyke Hornblende Gneisses") may represent original dioritic intrusive and related extrusive rocks that were in part contemporaneous with but mostly younger than the upper most part of the Idaho Springs Formation. During regional metamorphism the original sediments and volcanics of the Formation were intruded by an extensive series of PreCambrian granitic and pegmatitic rocks (Hart, 1964).

The PreCambrian rocks of the Front Range have undergone a long and complex geological history involving multiple periods of metamorphism, deformation, and intrusive activity (Peterman *et al.*, 1968). A geological map of the Front Range is displayed in Figure 1.8. The original sedimentary-volcanic pile was converted to greenschist facies rocks approximately 1750 to 1850my ago (Olsen, 1982). A second regional orogeny of amphibolite facies *c.*1750my ago resulted in the extensive migmatitisation of the Formation. During the waning

stages of this migmatisation event, *c.*1700my ago (Peterman and Hedge, 1967), the synkinematic Boulder Creek Granodiorite was emplaced. A second period of major plutonic activity *c.*1390-1450my ago (Peterman and Hedge, 1967) resulted in the emplacement of the Silver Plume and Sherman Granites. Regional heating of the surrounding rocks at this time re-set most of the Rb-Sr and K-Ar mineral ages and probably caused the retrogressive metamorphism which locally affected the gneisses and schists (Peterman *et al.*, 1968). The final PreCambrian event was the emplacement of the Pike's Peak batholith approximately 1040my ago (Peterman and Hedge, 1967). This had local thermal effects only. Peterman and Hedge (1967) report no evidence for subsequent PreCambrian metamorphic or plutonic events within the Front Range.

The most recent, Laramide, event to affect the PreCambrian country-rocks resulted in the emplacement of ten major hypabyssal intrusive rocks and their associated ore deposits; see Figure 1.9. The intrusive porphyries of monzonitic-granodioritic rock occupy a narrow belt about 5 miles wide extending southwestwards across the PreCambrian core of the Front Range; known as the "Colorado Mineral Belt" (see Figure 1.7). The mineral belt has been the source of more than \$3 billion in gold, silver, lead, zinc, molybdenum, tungsten and fluorspar. The intrusives occur as stocks, laccoliths, sills and dykes; their associated ore deposits are mesothermal and epithermal veins and replacement bodies which occupy fissures or small faults of Laramide and PreCambrian ages (Tweto and Sims, 1963). Cree (1948) reports hydrothermal minerals, chiefly quartz and pyrite within both the Laramide intrusives and adjacent parts of the country rocks. Mineralised faults and veins trend between north-northeast and east and are clustered in swarms each of which constitutes a mining district (Tweto and Sims, 1963). The intrusive activity and mineralisation took place at different times in different places within the belt; the magmatic activity that characterises the belt was not all synchronous (Tweto and Sims, *op.cit.*). However, the ore deposits are believed in most cases to be younger than the intrusive porphyries.

PLATE 5



PLATE 6. ELDORA AUREOLE.

(a) The town of Eldora within the foot-hills of the Rocky Mountain Range, Colorado.

(b) A road cutting exposure of part of the Idaho Springs Formation.
Field assistant as scale.



9



2

PLATE 6

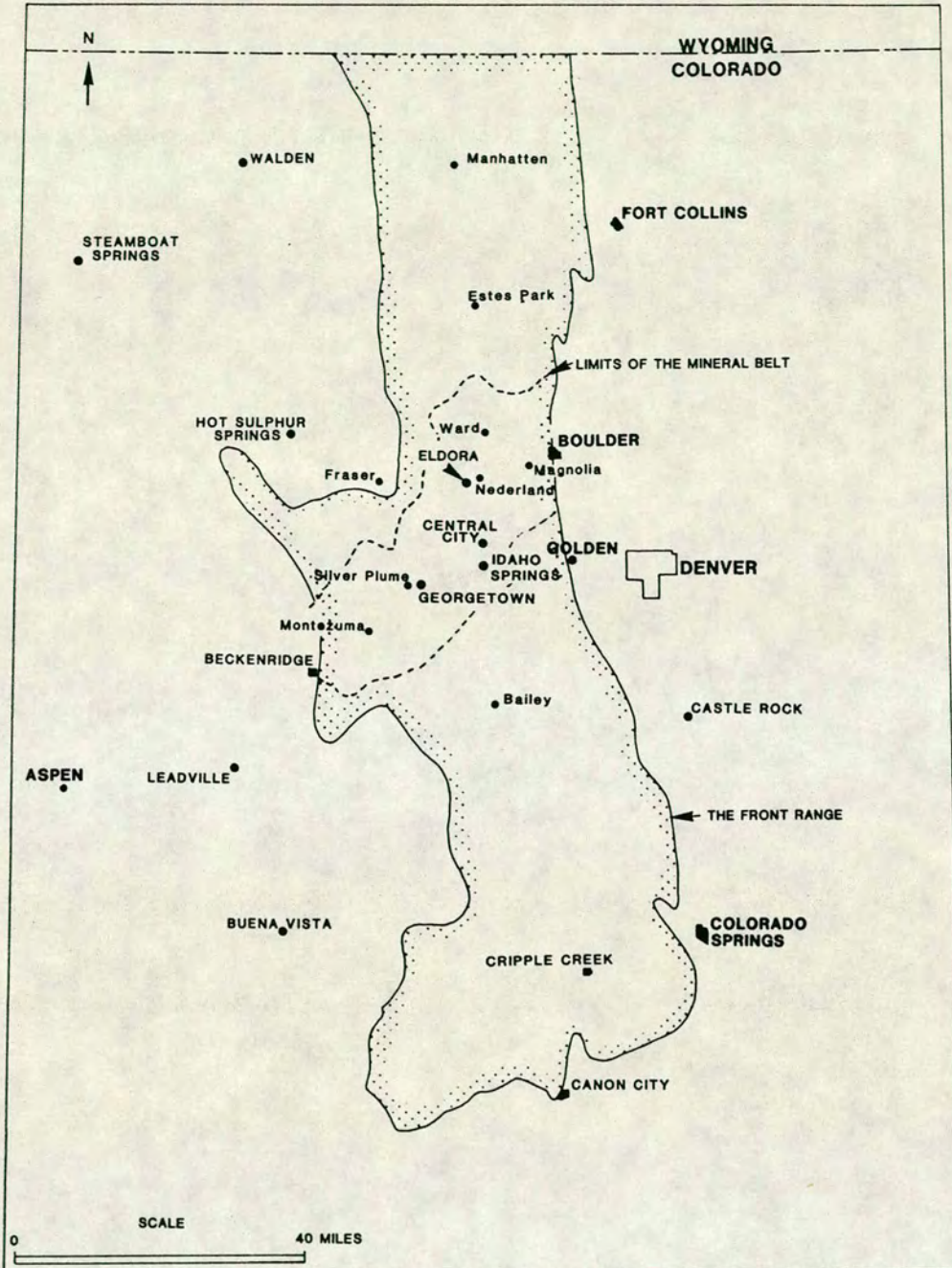


FIG. 1.7. Location of Eldora within the 'Front Range', Colorado. Also depicted is the limit to the Laramide "Mineral Belt" discussed in the text. (reproduced from Lovering and Goddard, 1950).

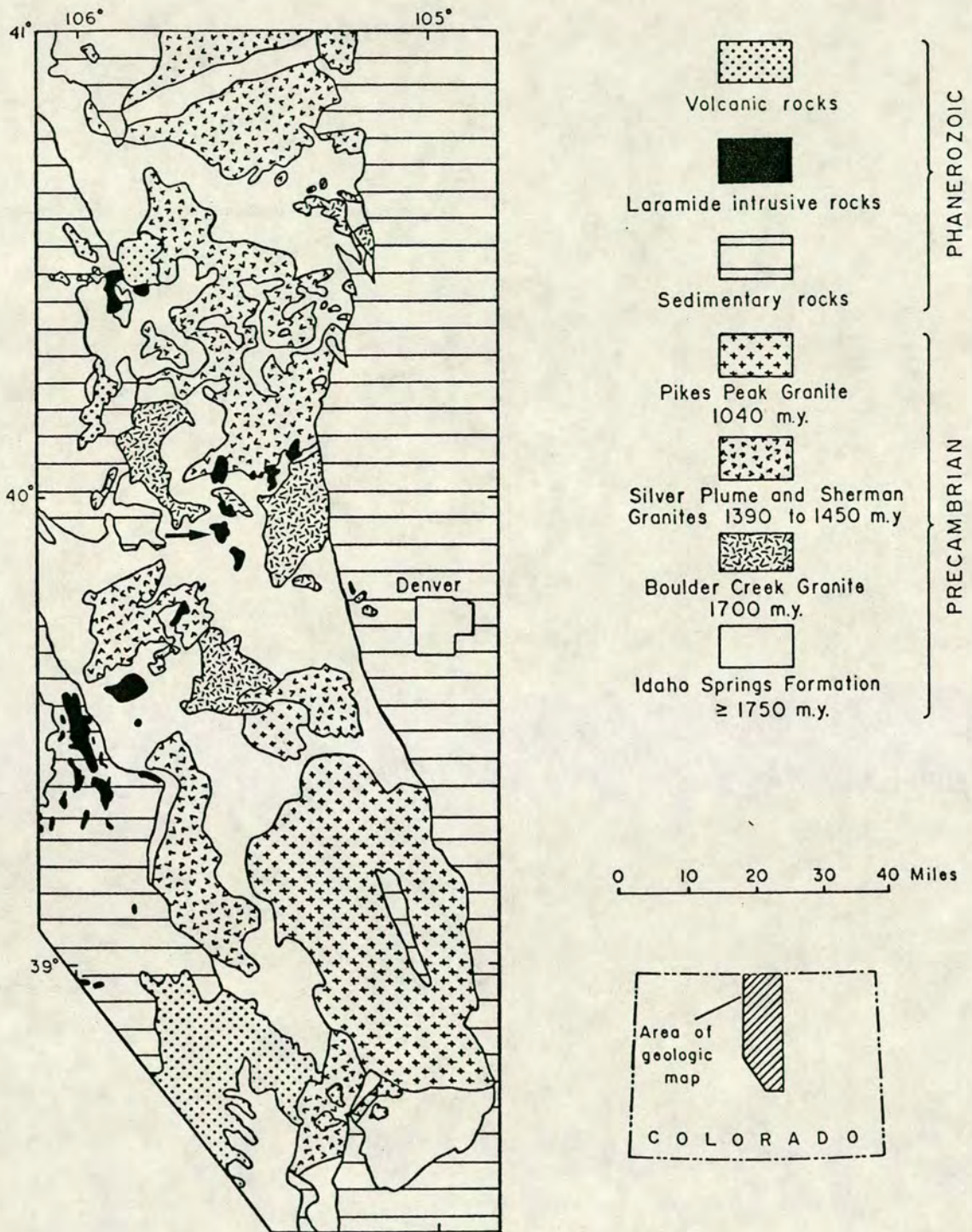


FIG. 1.8. Geological map of the Front Range, Colorado depicting the positions of the major PreCambrian intrusives in relation to the Eldora Aureole (arrowed). Reproduced from Peteman and Hedge, 1967.

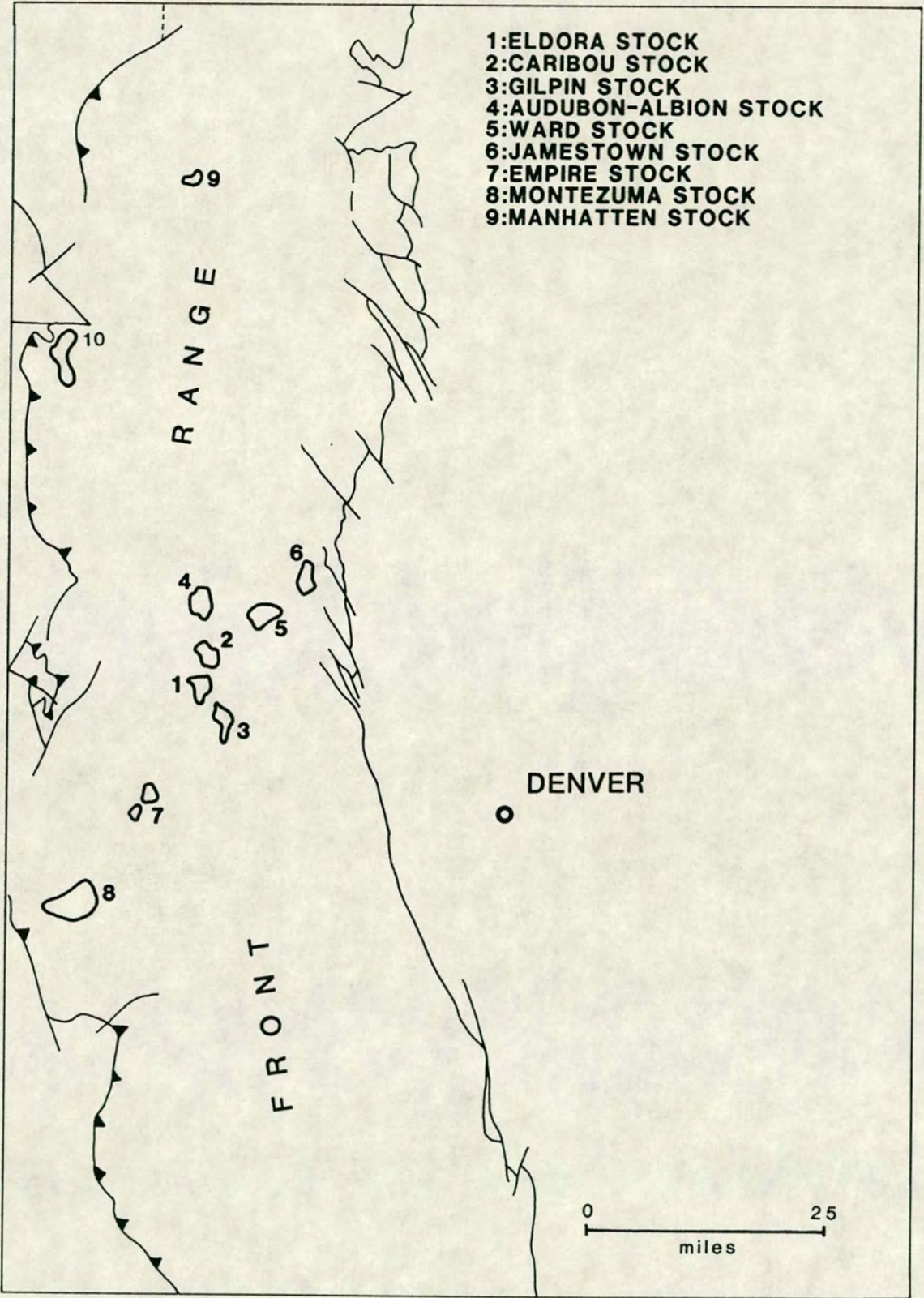


FIG. 1.9. Position of the major Laramide Intrusives within the Front Range, Colorado (reproduced from Lovering and Goddard, 1950).

According to the summary of Lovering and Goddard (1950) the Idaho Springs Formation within the Front Range as a whole have been subjected to three main mineralisation events:-

- (i) A PreCambrian episode of mineralisation associated with hypothermal deposits (including bornite, pyrrhotite, chalcopyrite, gold, pyrite and magnetite) and alteration of the country-rocks to tremolite, garnet and feldspar. These occur chiefly in areas of hornblende gneisses and at the borders of Stocks of PreCambrian granite. They show little relation to the rocks or structure of the Laramide revolution.
- (ii) A Laramide (late Cretaceous-early Tertiary) episode associated with the intrusion of the dominantly quartz-monzonite porphyritic stocks (outlined above). These occur as fissure fillings and replacement deposits which formed at moderate depth and temperature.
- (iii) A geographically restricted Tertiary episode of ore deposition associated with extrusive volcanics. This has not affected the rocks under study.

THE ELDORA STOCK AUREOLE

Eldora lies approximately centrally within the "Mineral Belt" of the Laramide intrusives (Figure 1.7). Here the PreCambrian country-rock consists of hornblende gneisses and biotite-sillimanite gneisses with a common foliation and regular interlayering. These correlate with the 'Hornblende Gneisses (Gnh)' and 'Biotite Gneisses (Gnb & Gnbc)' of Gable (1969), see Figure 1.10, who describes the Hornblende Gneisses as

"Predominantly amphibolite interbedded with biotite-quartz-plagioclase gneiss, microcline gneiss, locally calc-silicate gneiss and cordierite amphibole gneiss. The amphibolite is dark-gray to black fine- to medium-grained well foliated rock consisting dominantly of hornblende and plagioclase and subordinate amounts of pyroxene, biotite and quartz."

and the Biotite Gneisses as

"Gray fine- to medium-grained migmatitic biotite gneiss

gnb: dominantly sillimanitic biotite-quartz gneiss, interlayered with biotite-quartz-plagioclase gneiss, and biotite-quartz gneiss.

gnbc: garnet- and cordierite-bearing facies of sillimanitic biotite-quartz gneiss; grades into sillimanitic biotite-quartz gneiss."

Small bodies of dominantly concordant pegmatitic rock are ubiquitous. These are generally a few feet thick and have a small lateral extent only (Hart

et al., 1969). Hart (1964) suggests they represent "sweat" or "secretion" pegmatites formed during the regional metamorphism of the Idaho Springs Formation.

The Eldora Stock (Plate 7a) is approximately 3km. in diameter comprising predominantly three rock types; quartz-monzonite, granodiorite and syenodiorite (Hart, 1964). These grade into one another (Hart, 1964), and Cree (1948) suggests they do not represent separate intrusions but are formed from a common magma by differentiation and variable assimilation of the country rock. Hart (*op.cit.*) determined the intrusive age to be *c.*54ma., he suggests metasomatism as one method of emplacement, especially along the north-east lobe of the stock where igneous rock grades into metamorphic rock through a zone several feet wide. Cree (1948) describes wide zones of contact breccia, windows of stock within the PreCambrian rocks, and inclusions and roof pendants of schists and gneisses within the intrusive. He believes these represent portions of the roof of the stock which were being actively stopped at the time of final consolidation. Cree (1948) reports vertical fractures developed in a general east-west direction within the PreCambrian metamorphic rocks into which later stage Tertiary hydrothermal solutions deposited pyrite. Mineralised fracture zones are called "mineralised shears" by Cree (1948), and within the portion of the Stock exposed west of Eldora they commonly trend north-east, whilst those in the adjacent country rocks trend north-west.

Amongst his field observations Hart (1964) reports

"The only observable contact effect in the country rock is the weakening of the foliation in the first several feet."

and that within the pegmatitic phases:

"The biotites show a faint color change from brown with an orange tinge far out to brown near the contact....The major mineralogical contact effect is a change in the alkali feldspar from perthitic microcline to non-perthitic orthoclase."

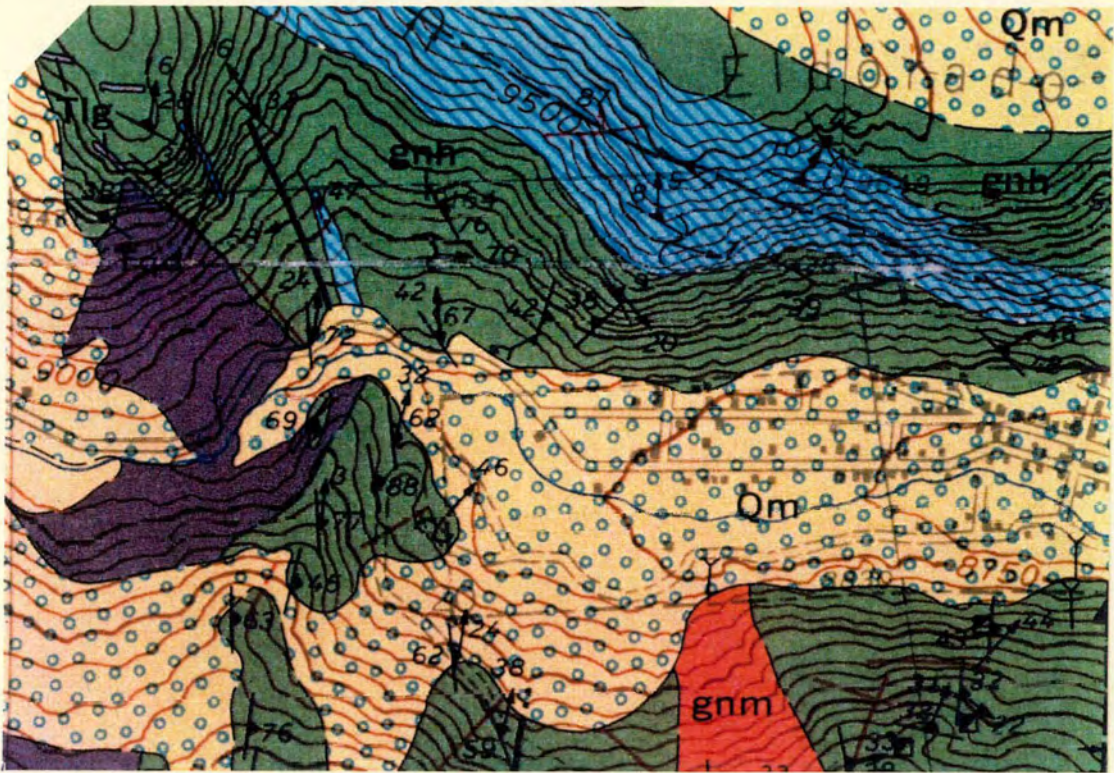


FIG. 1.10. Geological map of the Eldora Aureole. Reproduced from U.S.G.S. Geologic Map of the Nederland Quadrangle (Gable, 1969). Scale 1:24000 (3cm-0.5mile).

Tqd=Quartz Monzonite Group (Tertiary) gnh=Hornblende Gneiss (PreCambrian)
 gnm=Microcline Gneiss (PreCambrian) blue=Biotite Gneiss (PreCambrian)
 Qm=Glacial Material (Quaternary).

PLATE 7. ELDORA AUREOLE.

(a) Typical, blocky Stock outcrop.

Field assistant as scale.

(b) Close-up view of the Stock rock-type; medium-grained monzonite with phenocrysts of K-feldspar.

Lens cap as scale.

(c) Inclusions of amphibolitic (arrow 1) and gneissic (arrow 2) material within the monzonitic stock.

Field note-book as scale (c.12cm. wide).



PLATE 7

FIELD OBSERVATIONS

The intrusive Stock is a fairly homogeneous, leucocratic, medium-grained, granular rock (Plate 7b). Phenocrysts (5% mode) of simply-twinned potassium-feldspar, ranging in size from 0.5-1cm., occur within a groundmass of subhedral feldspar, quartz and mica crystals with an average size of 0.5-1mm. Occasionally the biotites form anhedral to subhedral crystals or aggregates intergrown with the matrix feldspar. Large (c.3mm.) grains of hornblende occur occasionally (c.1% mode). There is no apparent lineation within the rock though the feldspar phenocrysts may possess a slight foliation. Exposures are generally massive, well-jointed, smooth weathering and mottled with black lichen.

The contact between Tertiary Stock and PreCambrian metamorphic rock varies from place to place. The almost vertical contact is sharp in many places but gradational in others. Some interdigitation occurs resulting in a stepped interface, alternately subparallel to and transecting the foliation within the country-rock. Within the stock a transitional boundary of 5-10m. width is observed as the stock-country-rock contact is approached. Within this zone the rock adjacent to the contact (within 2m.) is more medium-grained with a gradual increase in the modal hornblende constituent towards the contact. Beyond 2m. within the transitional region, the 'monzonite' may contain abundant inclusions of the country-rock (Plates 7c & 8a).

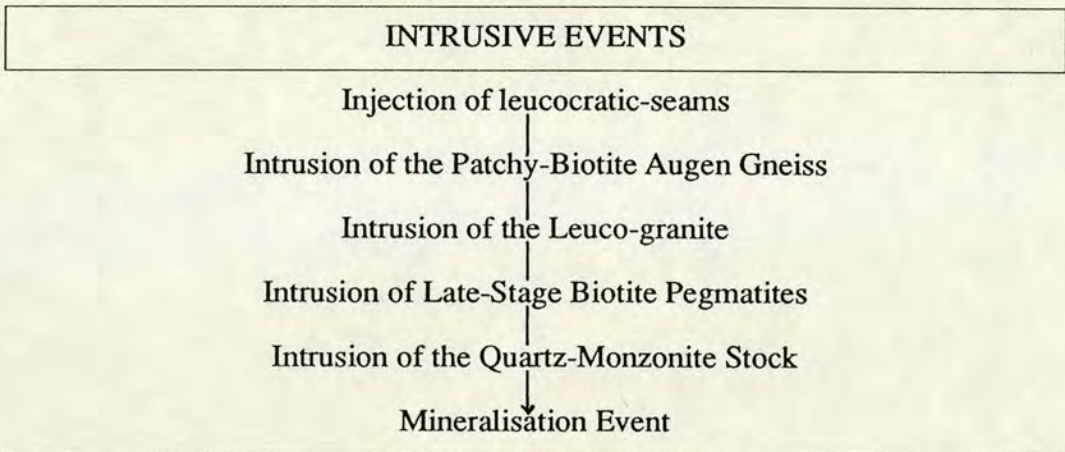
Field investigations of the PreCambrian country-rocks found a greater degree of heterogeneity existed than was suggested in descriptions within the literature. Although the hornblende gneisses and amphibolites were the centre of attention some time was also devoted to establishing their spatial and age relationships to the other rock-types present; the following paragraphs describe these observations and suggest a possible sequence of events.

The oldest rock types present, termed "The Early Gneiss Complex", comprise the hornblende gneisses and biotite-sillimanite gneisses of Gable (1969). The hornblende gneisses essentially consist of melanocratic, medium-grained amphibolites with a fairly homogeneous textured, well-foliated matrix of sub-idioblastic amphibole and feldspar crystals with an average size of 1mm. Variations in mineralogy to more pyroxene and/or biotite rich lithologies are observed, these generally being of a paler-grey, more leucocratic colouration. The amphibolites are characterised by the presence of leucocratic-seams (Plate 8b) composed of quartz-feldspar rich, fine to medium-grained, sharply-bounded

'sheets' which range in thickness from 1mm.-2cm. They are largely orientated parallel or subparallel to the overall foliation but are occasionally also observed in crosscutting or pygmatic relationships (Plate 8c). In places their complexity is such that they may well reflect more than one intrusive set (Plate 9a).

The biotite gneiss (Plate 9c) is a largely meso-leucocratic rock composed of medium-grained, biotite mica, sillimanite, quartz and feldspar. It was far less abundant in the area under study and as such wasn't examined in detail. In those localities where it was encountered, it was found to be intruded by granitic material resulting in classic "lit par lit" textures, widely associated with migmatitic rocks.

Field studies by the author showed that the hornblende- and biotite-sillimanite-gneisses of the Early Gneiss Complex have been subjected to at least 6 intrusive events which are outlined below:-



The 'Patchy-Biotite Augen Gneiss' is a leucocratic, orangy-pink weathering, coarse-grained quartz-feldspar rich rock interspersed with biotite aggregates (Plate 9b). The sub-idioblastic to idioblastic quartz and feldspar crystals vary in grain-size from 2mm.≥5cm. The biotite aggregates are comprised of masses of 1-2mm. sub-idioblastic biotite flakes which define a foliation within the rock. Rafts and blocks of amphibolitic material with a diverse size and shape occur as inclusions within the Augen Gneiss; at one location these have a distinctly boudinaged appearance. The Augen Gneiss predominantly appears to discretely intrude and interdigitate with the Early Gneiss Complex. It may additionally occur in the form of 5-15cm. thick veins subparallel to the foliation within the amphibolites.

PLATE 8. ELDORA AUREOLE.

(a) Amphibolitic 'ghost' within the transitional monzonite region of the contact zone.

Lens cap for scale.

(b) Amphibolitic rock characterised by the presence of quartz-feldspar rich leucocratic seams. Note cross-cutting and ptygmatitic relationships of some of these seams and foliation-concordant nature of others.

Hammer shaft as scale.

(c) Ptygmatitic, leucocratic seam within amphibolitic rock.

Pencil for scale.

PLATE 8

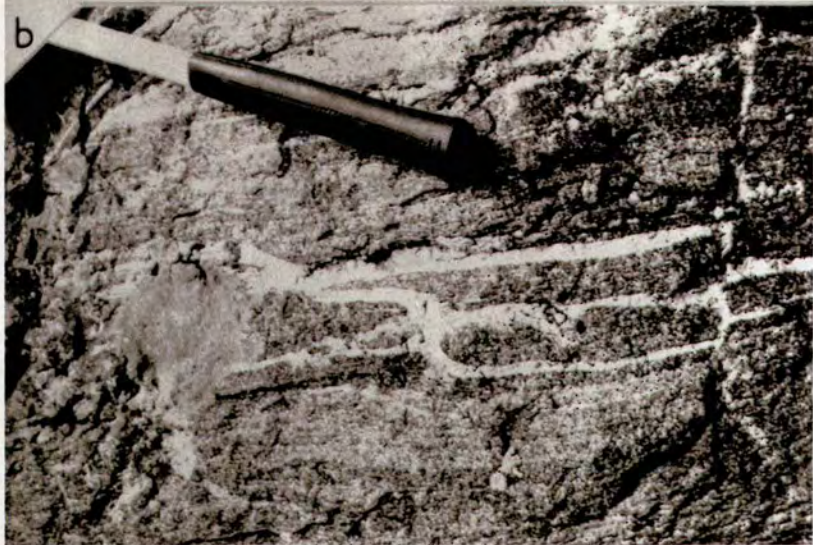


PLATE 9. ELDORA AUREOLE.

(a) Complex, almost 'flow-like', seam relationships within amphibolitic rock.
Hammer-head as scale.

(b) The Patchy-Biotite Augen Gneiss; a coarse-grained quartz-feldspar rich rock interspersed with foliated biotite aggregates.
Chisel for scale (c.10cm. length).

(c) Biotite gneiss displaying classic "lit par lit" textures.
Hammer-head as scale.

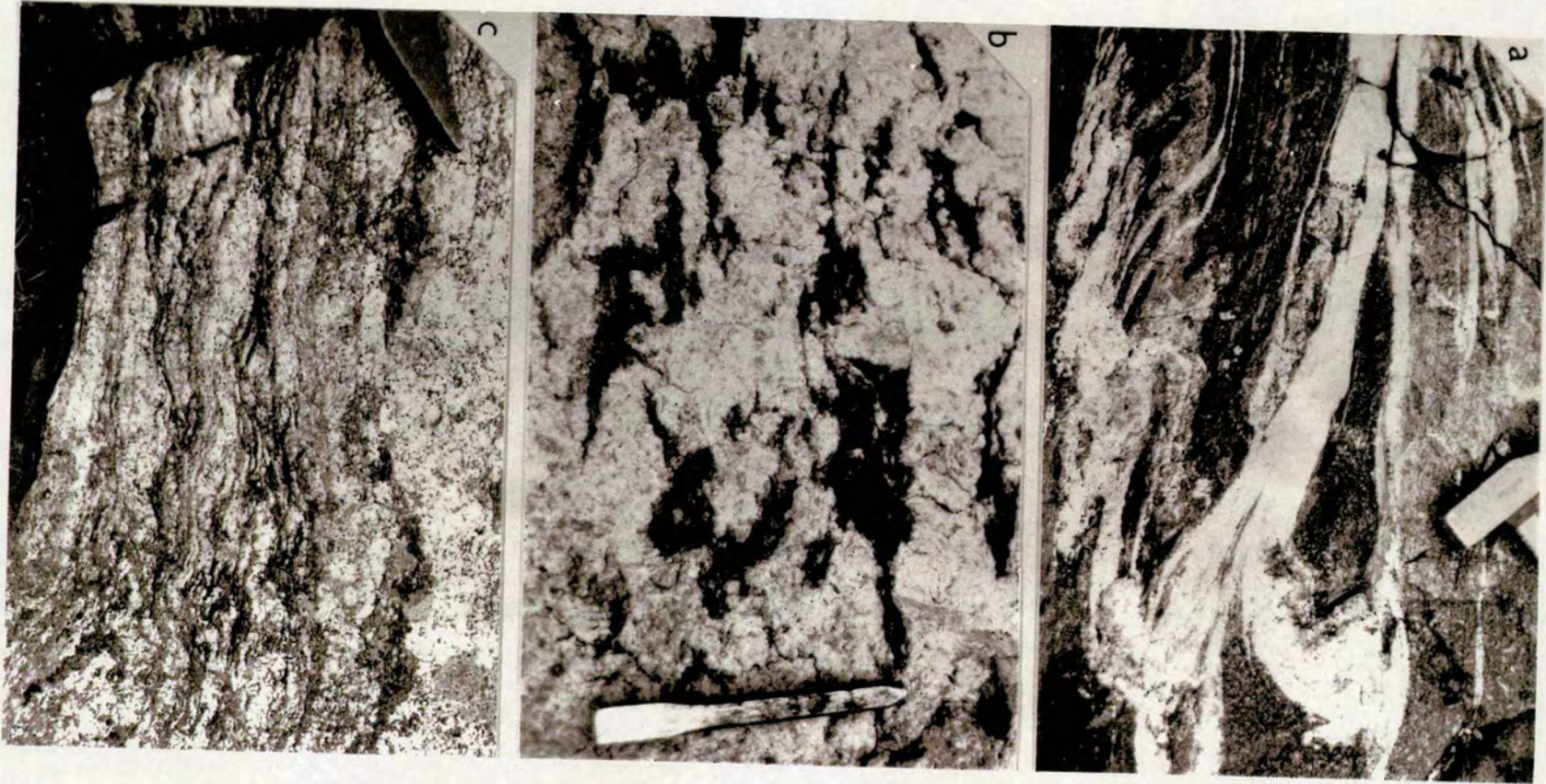


PLATE 9

PLATE 10. ELDORA AUREOLE.

(a) Close-up view of the quartz-feldspar rich, granular textured, Leuco-granite.
Pencil as scale.

(b) Leuco-granite (LG) 'invading' amphibolitic rock.
Hammer as scale.

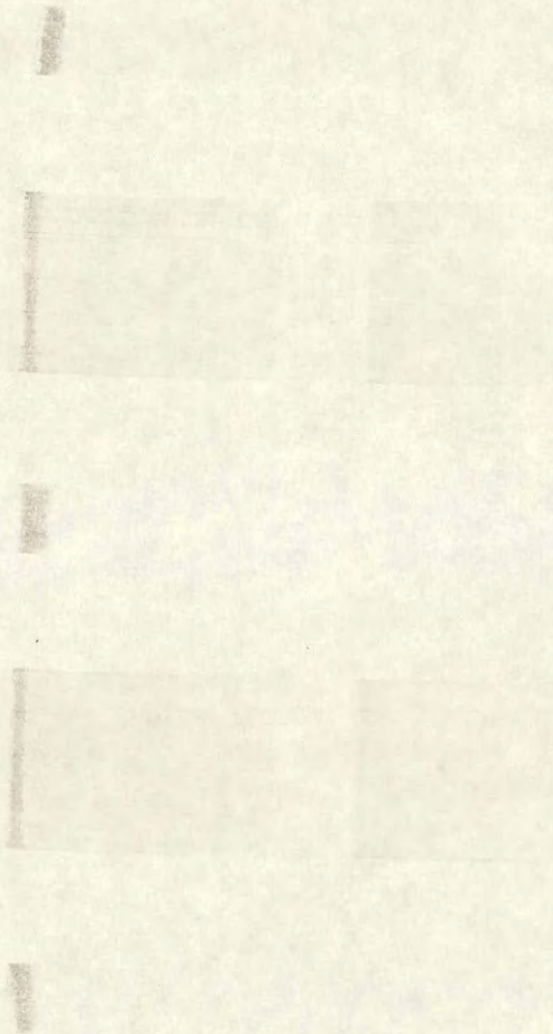




PLATE 10

The 'Leuco-granite' ("Granite Gneiss" of Cree, 1948) is a granular textured rock consisting of ~2mm. sized crystals of subhedral quartz and feldspar, though this tends to vary depending on the proportion of included metasediments; biotite-quartz-feldspar and occasionally hornblende-biotite-quartz-feldspar assemblages have also been observed (Plate 10a). No alignment of the sparse biotite flakes is detected and the proportion of mafic minerals is generally very low. Grain-size varies from medium-grained (1-2mm.) to coarser pegmatites (1-2cm.) within the same intrusive unit; the coarser grain-sizes probably representing the final stages of crystallisation. The Leuco-granite is interpreted as having invaded the Early Gneiss Complex (Plate 10b) causing partial re-melting of the leucocratic-seams and passive disruption of the gneisses - now seen as enveloped rafts (Plate 11a) and inclusions within the Leuco-granite (ranging from fist-sized to 5x5m. blocks). Injection of sheets of the Leuco-granite into the biotite gneisses probably resulted in their migmatisation.

The 'Late-Stage Biotite Pegmatites' ("Aplite Dykes" of Cree, 1948) represent the youngest granitic composition intrusive event of the area (Plate 11b), with distinct cross-cutting relationships with the Leuco-granite (Plate 11c), Early Gneiss Complex (Plate 12a) and Patchy-Biotite Augen Gneiss (Plate 12b). The late-stage pegmatites range in thickness from 0.1-0.5m. with a mineralogy dominated by subhedral-anhedral, medium to coarse-grained quartz and feldspar with a variable biotite concentration. The biotite tends to occur as individual flakes rather than the aggregates and/or patches seen within the patchy biotite augen gneisses; there is no distinguishable foliation.

The final intrusive event, other than emplacement of the stock, is marked by fracture zones (shears in Cree's (1948) terminology) associated with alteration \pm sulphide mineralisation within the country-rocks (Plate 13a). These shears have a variable thickness between 0.5-3m. and a characteristically orangy-brown, in-weathering nature. They are vertical, approximately perpendicularly transecting the foliation of the earlier lithologies and occasionally intruding along prominent joint horizons, having a general orientation approximately parallel/sub-parallel to the stock-country-rock contact to the north-east of the stock.

PLATE 11. ELDORA AUREOLE.

(a) Amphibolitic raft (arrow) within the Leuco-granite (LG). The foliation within the amphibolitic rock preserves an identical orientation to undisturbed amphibolites suggesting passive disruption.

Compass-clinometer as scale.

(b) Close-up view of a Late-Stage Biotite Pegmatite. Note non-alignment of individual biotite flakes (*c.f.* Patch Biotite Augen Gneiss).

Pencil for scale

(c) Late-Stage Biotite Pegmatite (arrow 1) with few visible biotite flakes cutting Leuco-granite (finger) which has invaded amphibolite (arrow 2).

Lens cap and finger for scale.

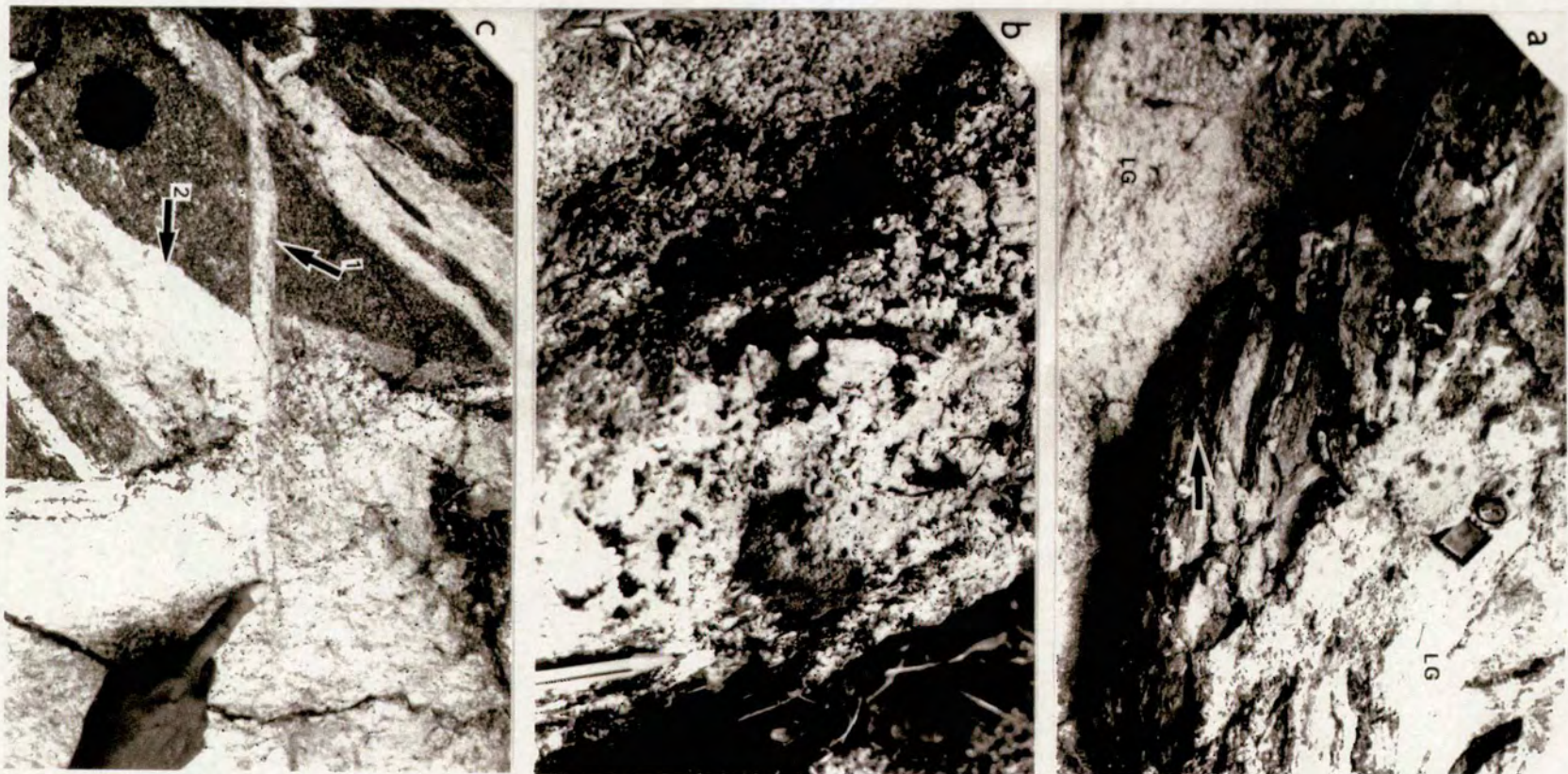


PLATE 11

PLATE 12. ELDORA AUREOLE.

(a) Late-Stage Biotite Pegmatite (arrow) cutting amphibolitic rock and leucocratic-seams. Note leucocratic-seams themselves display off-setting relationships.

Edge of compass-clinometer as scale.

(b) Late-Stage Biotite Pegmatite (arrowed 1) cutting both amphibolitic rock (A) and overlying Patchy-Biotite Augen Gneiss (AG).

Field assistant as scale.



PLATE 13. ELDORA AUREOLE.

(a) Rusty weathering mineralised shear (arrowed) cutting Idaho Springs Formation amphibolites.

Field assistant as scale.

(b) The sharp contact between the Eldora Stock and the amphibolitic country rocks. Note the presence of a rusty-weathering patch (arrow).

Lens cap as scale.

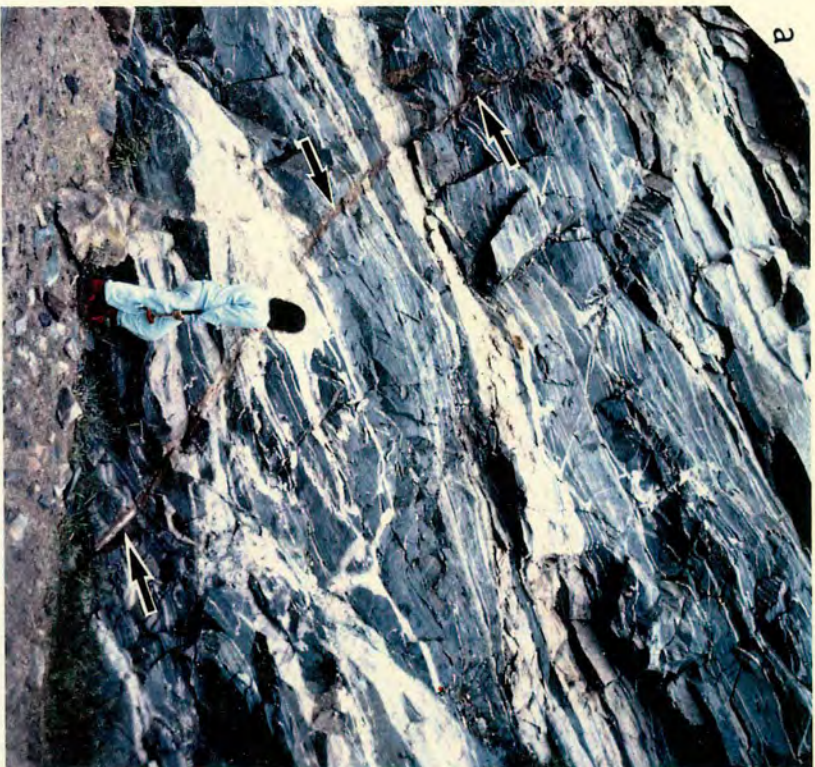


PLATE 13

SAMPLE COLLECTION

A detailed traverse was made along an identical line to that performed by Hart (1964), starting from the eastern contact with an intrusive spur on the northeast side of the stock (see Figure 1.11). Here the contact between monzonite and amphibolites of the Early Gneiss Complex is very sharp (Plate 13b) and reasonably regular, clearly cutting the foliation and associated sub-parallel leucocratic-seams and Late-Stage biotite-pegmatites within the country-rocks. Rusty-weathering mineralised shears occur along some sections of the contact. Samples of both amphibolitic/gneissic and late stage pegmatitic rock were collected at intervals of approximately: 1-2m. (as exposure permitted) within the first 10m., then every 5m. to a distance of 30m., every 25m. to 100m., every 50m. to 280m. and finally approximately every 250m. to 3.5km. away from the contact.

The bulk mineralogical and textural properties of the rocks close to and at distance from the contact remain fairly constant at outcrop-scale, with no obvious modifications which can be clearly related to intrusion of the stock.

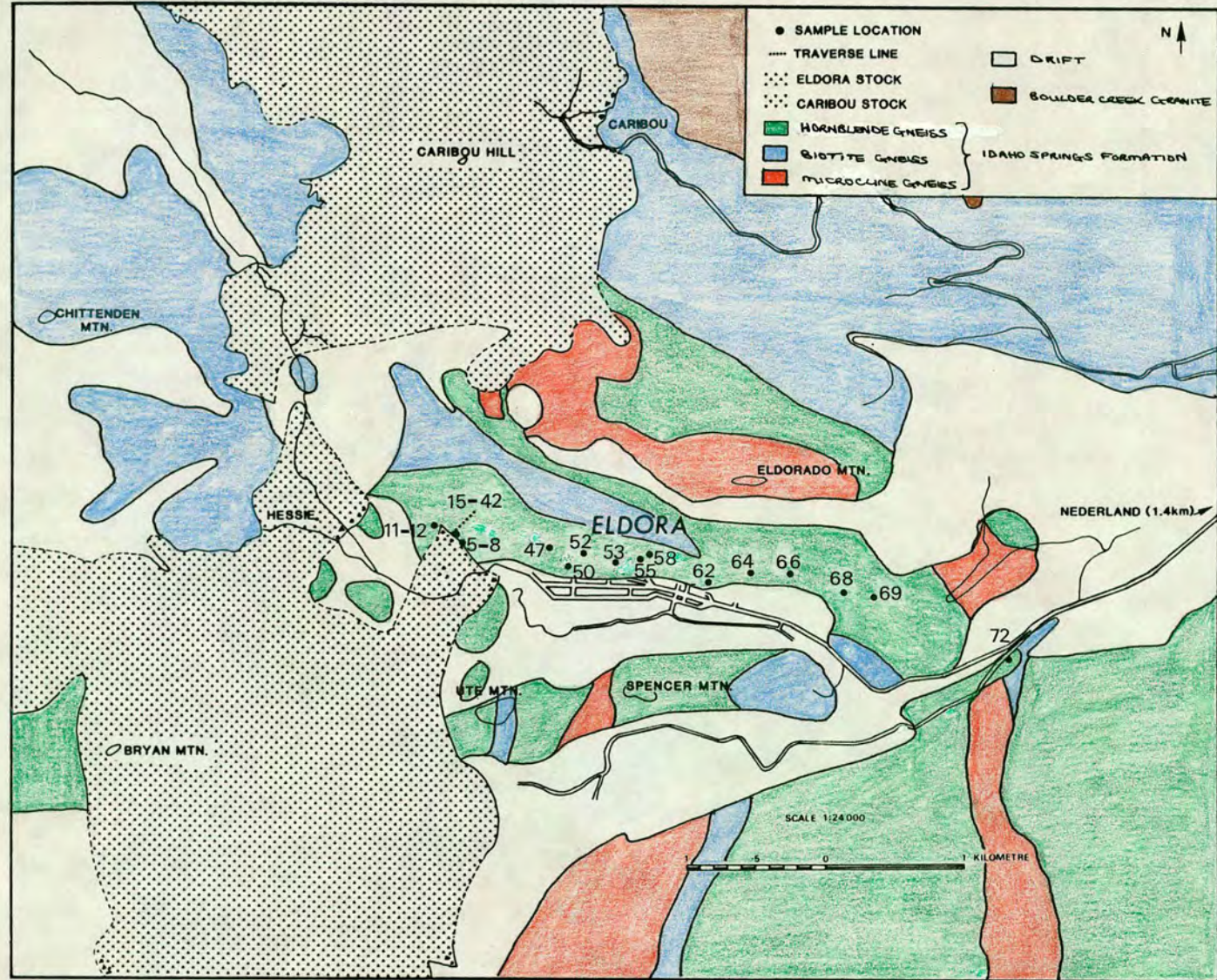


FIG 1.11. Location of sample points within the Eldora Aureole.
AMPHIBOLITIC ROCK NUMBERS ARE SHOWN; TABLE 4.1 LISTS
THEIR DISTANCES FROM THE STOCK CONTACT.

1.3. RESEARCH APPRAISAL

The field and preliminary laboratory-based investigations of the four areas allowed further consideration of their suitability for detailed studies. The Snowbank Lake Aureole rocks were considered to be too texturally and modally variable in their pre-metamorphic petrography to enable ready comparison of any variation either in partial reaction and/or zoning of mineral chemistries. The Christmas Lake Aureole is similarly complicated with country-rock comprising two different rock-types, gneisses only exposed close to the contact and amphibolites at distances beyond 74m. The rock-types themselves are otherwise fairly constant, both texturally and mineralogically, and as such would be appropriate for consideration. However the surrounding geology is rather poorly constrained and the geochronological studies indicated a very narrow aureole. For these reasons the Snowbank Lake and Christmas Lake Aureoles were given low priorities and attention was focussed on the Giant's Range and Eldora Aureoles which are discussed further below.

1.3.1 THE GIANT'S RANGE AUREOLE

The Giant's Range Granite suite initially appeared to be the ideal setting for continued study with its largely quite simple and relatively constant mineralogical and textural properties throughout. Field observations particularly highlighted the widespread occurrence of euhedral amphiboles as inclusions within feldspar phenocrysts. Conceptually these were considered to be closest to an ideal "simple" situation, with tight grain boundaries set in homogeneous feldspar, from which assessment of diffusion parameters might be established. In such cases any compositional gradient between opposing amphibole-feldspar interfaces will be equal. Any zoning at the margins of the amphibole inclusions, which was the result of increasing temperature associated with intrusion of the Duluth Gabbro, might be expected to have developed by volume diffusion and should be symmetrically disposed within the inclusion. Thus the multi-component diffusion occurring within these inclusions potentially provided a good control against which the more complicated situations involving amphibole crystals in the groundmass of the rock could be examined.

Thin-section studies of the Giant's Range rock's revealed that recrystallisation (with the formation of new grains) of the original amphibole grains in the rock matrix had occurred. Many of the smaller amphibole crystals situated within the groundmass of the rock are completely replaced by an

aggregate of fine-grained biotite crystals and many of the larger amphibole grains display core and mantle textures; original amphibole cores are rimmed by fine-grained biotite crystals. These recrystallising matrix amphiboles would clearly be difficult to interpret with respect to grain-scale diffusion processes due to the destruction of the original amphibole and the extensive movement of their grain-boundaries. Furthermore, the relative timing of the thermal and recrystallising events is unknown. Field observations of increased recrystallisation within 2km. of the contact suggest that much of the recrystallisation could be largely a result of contact metamorphism, but this does not eliminate the possibility of some of the alteration having occurred during primary igneous cooling.

The included amphiboles with their predominantly sharply-bounded, euhedral habits are apparently unaffected by recrystallisation processes and electron microprobe data revealed them to contain encouraging zonation patterns, though it was again uncertain to what extent this might be igneous. Unfortunately the average probe-slide contained very few of these included amphiboles and as a result little information on any modification in the zonation widths and plateau concentrations with distance from the contact was obtained. To overcome such sample preparation problems it was considered necessary to serially-section several carefully chosen samples. Although further determinations were considered to be potentially interesting the time devoted to the Eldora study has made this impossible.

1.3.2 THE ELDORA AUREOLE

The rocks of the Eldora Aureole though once again not perfect, due to their complex regional history and "lack of constant pre-metamorphic characteristics" (Hart, 1964), were considered suitable for further examination. Although, as outlined in section 1.2.4, the amphibolites are heterogeneous in composition (varying mineralogically from amphibole \pm plagioclase to amphibole \pm plagioclase \pm pyroxene to amphibole \pm plagioclase \pm biotite-rich rocks) it was possible to select groups of rocks with relatively uniform textural and modal characteristics across a considerable distance from the contact. Furthermore, the studies of Hart and subsequent workers had established evidence of an aureole within which zoned mineral composition had developed. The sequence of intrusive/migmatitic events outlined in section 1.2.4. indicate that the Eldora rocks have had a complex geological history. Hart (1964) assumed all the phases to have achieved constant regional compositions during PreCambrian equilibration prior to the much younger contact event.

Thin-section examination of the ferromagnesian minerals within the Eldora rock-types indicated the amphiboles to be the least altered and/or recrystallised phase present; the pyroxenes are largely heavily altered to actinolite, the biotites display recrystallisation along their rims and, within the amphibolitic rock types of the early gneiss complex, are chemically unzoned. Preliminary microprobe investigations of original, unrecrystallised amphibole grains detected discrete chemical zonations along their grain boundaries and it was considered appropriate therefore to concentrate upon establishing mobility variations with increasing distance from the intrusive contact within amphibole crystals.

In order to be able to compare elemental mobilities within grains from different rocks it was necessary to devise a grain selection and classification procedure scheme. Since the initial emphasis was upon volume diffusion effects, it was initially considered important to carefully select those grains which appeared to be the freshest, generally lacking recrystallisation and if possible displaying evidence of smooth, texturally equilibrated grain boundaries. Amphiboles included within plagioclase feldspar crystals, as seen in the Giant's Range Aureole, were, where possible preferentially selected for reasons given in section 1.3.1 Other situations involving the study of matrix amphiboles were also considered; these were grouped, for ease of comparison, into particular "environments" using the grain classification scheme outlined in Figure 1.12. In order to make careful comparisons within similar rock-types, it was necessary to sub-divide the country-rocks so that zonations within mineralogically similar rock-types could then be compared with one another.

CLASSIFICATION SCHEMES FOR ELDORA ROCKS

A: ROCK-TYPE

Depending essentially on the present mineralogy. For the amphibolites of the Early Gneiss Complex (the first three cases) this is related to the composition of the original rocks prior to regional metamorphism. The fourth case represents pegmatites from the 'Late-Stage Biotite Pegmatites', intruded during regional metamorphism.

- (a) AMPHIBOLITES:- amphibole + feldspar + quartz \pm minor pyroxene \pm occasional biotite flake + accessories.
- (b) BIOTITE AMPHIBOLITES:- amphibole + essential biotite foliation + feldspar \pm minor pyroxene + quartz + accessories.
- (c) PYROXENE AMPHIBOLITES:- amphibole + abundant pyroxene + feldspar + quartz + accessories.
- (d) BIOTITE PEGMATITES:- encompasses the abundant pegmatite veins noted in the field to cut the above rock-types but pre-date the contact intrusive event. These basically consist of biotite, feldspar and quartz + accessories.

B: GRAIN SITUATION

Devised as a means of expressing the 'environment' within which a grain occurs. Four main groups have been defined-

- (a) GROUP I:- amphibole grains which occur as inclusions within feldspars.
- (b) GROUP II:- amphibole grains which form part of the rock matrix and are in mutual contact with other amphiboles and feldspars only.
- (c) GROUP III:- amphibole grains which form part of the rock matrix but are in mutual contact only with other feldspar grains.
- (d) GROUP IV:- other individual situations such as amphibole-biotite or amphibole-pyroxene interfaces.

C: GRAIN-SIZE

Each studied grain was carefully measured (using a calibrated eye-piece graticule) to determine if grain-size influenced the type or amount of diffusion occurring.

FIGURE 1.12. Rock and grain characterisation scheme devised as a basis in which to compare elemental mobilities discovered.

1.4. RESUME OF THESIS CONTENT

Following the investigations reported in this chapter, a thorough optical, geochemical and geochronological investigation of samples ranging between approximately 0.15cm. and 3km. from the Eldora Stock Contact has been made. It will be shown in the following chapters that the nature of the amphibole alterations in the vicinity of Eldora is of a much more complicated nature than that of simple diffusion control along and from grain boundaries, and that the extent of the alteration is not regularly related to distance from the intrusive contact. In broad terms the following four objectives are pursued:

- (i) To highlight the apparent sporadic development of much of the secondary amphibole found around and within original hornblende crystals (at the mineral grain-scale).
- (ii) To describe the larger scale distribution of the hornblende alteration and document the presence of rock-penetrative alteration zones with which the development of secondary amphibole is intimately associated. In conjunction with (i), the nature of the amphibole alteration is discussed.
- (iii) To consider to what extent the mineral alterations are the result of regional as opposed to contact-related events.
- (iv) To report ^{40}Ar - ^{39}Ar ages from individual amphibole grains and K-Ar ages from mineral separates in the light of this new petrological information and reappraise the "reduced age aureole" reported by Hart (1964).

A guide to the contents of the remaining chapters in this thesis is given below:

- (i) Chapter two outlines the principles of both diffusion theory and the closure temperature concept and gives a review of the current knowledge of the Amphibole Mineral Group.
- (ii) Chapter three discusses the technical aspects of each method used to obtain information presented in subsequent chapters.
- (iii) Chapter four presents details of the petrographic studies made from which the different types of amphibole alterations have been identified and related to geological events.

- (iv) Chapter five reports the results of the geochemical data obtained which, combined with (iii), enabled conclusions concerning the types and processes by which the original amphibole crystals have altered to be deduced.
- (v) Chapter six presents a summary of the alteration history of the amphibolites based on the optical, B.S.E. and microprobe investigations undertaken during this research. It attempts to delineate the complex sequence of events which have contributed to the alteration patterns visible in the rocks today by way of a complex collation diagram.
- (vi) Chapter seven discusses the isotopic age determinations made on both hornblende mineral separates (as Hart, 1964) and single mineral grains (involving laser microprobe single spot analysis) and re-assesses the original work of Hart (1964).
- (vii) Chapter eight outlines the major conclusions of this research and suggests areas where future research might be focussed.

CHAPTER 2. THEORETICAL BACKGROUND

2.1. DIFFUSION

2.1.1. PRINCIPLES OF DIFFUSION

Diffusion is a physical process involving the mobility and migration of atomic particles. It is a fundamental phenomenon within solid, liquid and gaseous systems and is often the rate limiting mechanism by which physical or chemical change can take place. Within a geological context it has a control on the rates of nucleation, crystal growth, exsolution and the structural and chemical modifications of minerals that occur under the broad heading "metamorphic processes".

Most minerals comprising solid solution series' may form compositionally zoned crystals as they grow. Subsequent diffusion within the crystal, either during or after growth, may remove such zoning. Conversely, a homogeneous crystal can become zoned by diffusion if the composition imposed on the edge of the crystal, by equilibrating with other phases (including fluids), differs from the existing composition within the crystal (Loomis, 1983). Diffusion therefore acts in two ways

- (i) It eliminates 'growth zoning' produced due to natural fractionation processes.
- (ii) It creates 'diffusion profiles' within originally homogeneous crystals.

Both of the above processes occur with the aim of achieving equilibrium, and thus constant compositions of minimum free energy.

An extensive literature exists on almost every conceivable aspect of diffusion, the two most significant of which are the reference works of Crank (1975) and Carslaw and Jaeger (1959). A brief resume of those aspects considered relevant to this study are outlined below, more complete explanations to which may be found either in the above texts or in the further references cited.

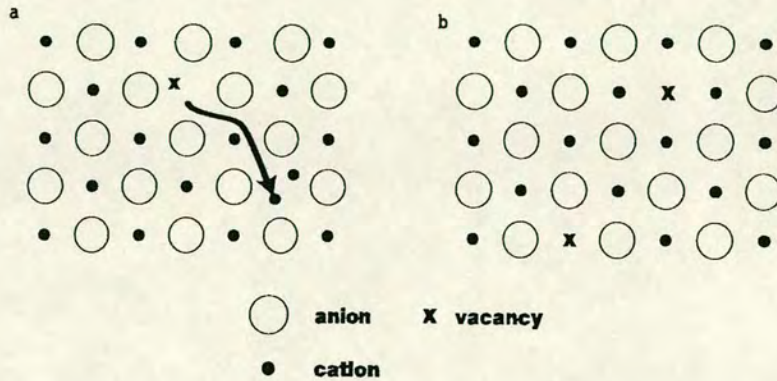
All crystalline solids consist of regular periodic arrangements of atoms or molecules. These ordered lattices allow diffusion mechanisms to be described in relatively precise terms (*c.f.* gases and liquids where atoms are randomly



arranged). Departures from atomic regularity in crystal structures are known as 'defects'; the two most significant of which are:

(i) Point Defects (see Brophy, Rose and Wulff, 1964)

involving one single atom or molecule including Frenkel⁴ and Schottky⁵ imperfections:



POINT DEFECTS WITHIN CRYSTAL LATTICES (Vernon, 1976)

(a) Frenkel imperfections: interstitial cation and vacancy

(b) Schottky imperfection: vacant lattice sites.

(ii) Line Defects (see Manning, 1968)

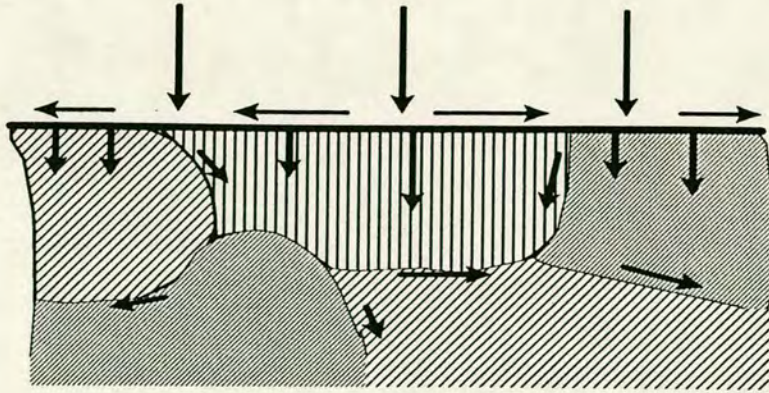
extended 2- and 3-dimensional departures from regularity in crystals including cleavages, cracks, grain-boundaries, crystal surfaces. At an atomic level dislocations⁶ may also be considered under this broad heading.

Diffusion in all crystalline materials takes place by the movement of point or line defects within the crystal structure. Conventionally diffusion is generally thought of as occurring in one of three main ways; *volume diffusion* takes place by movement of point defects within the crystal lattice, *grain boundary* and *surface diffusion* taking place through movement of line or surface defects. The following sketch depicts the three different types:

⁴ A vacant lattice site with an associated interstitial atom (i.e. one not in its normal lattice position).

⁵ A vacant lattice point.

⁶ Introduction of planes of atoms within crystals, often related to stacking faults. These involve both screw and edge dislocations.

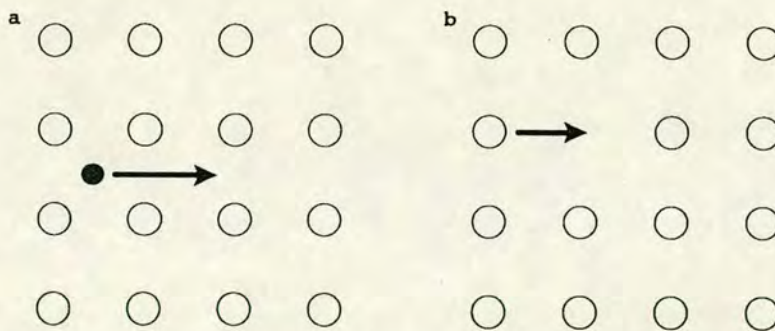


ROUTES TAKEN BY VOLUME, GRAIN-BOUNDARY AND SURFACE DIFFUSION (Manning, 1974).

More recent studies undertaken using modern S.E.M. and T.E.M. techniques (*e.g.* Worden *et al.*, 1990; Hacker and Christie, 1991) are increasingly highlighting the presence of previously unknown microstructures such as channel-ways, micropores and complex dislocation patterns within natural crystals; these appear to provide far easier routes along which diffusion may occur than some of the more conventional varieties.

Similar principles and mathematical relationships are thought to control diffusion in many situations; further discussion here is made in the regular context of volume diffusion.

Migration through a crystal (*i.e.* volume diffusion) occurs by the periodic jumping of atoms between energetically favourable lattice sites, the most frequently encountered types of elementary jump being the interstitial and vacancy mechanisms:



ELEMENTARY JUMPS WITHIN CRYSTAL LATTICES (Manning, 1974).
 (a) The Interstitial Mechanism: atoms jump from one interstitial site to another.
 (b) The Vacancy Mechanism: atoms exchange with vacancies within the lattice.

When interstitial atoms are present within the lattice, jumps may be made directly from one interstitial site to another (*i.e.* the "interstitial" mechanism) An atom may also move through the crystal by making a series of exchanges with

vacancies⁷ (the vacancy mechanism). Such elementary jumps are often obstructed by neighbouring atoms; in order for an atom to break away and jump to a new position within the crystal structure it must surmount this restraining energy barrier. An increase in temperature increases the motion of atoms about their atomic sites and thereby considerably helps to provide enough kinetic energy to enable diffusion to take place. As a consequence volume diffusion is strongly temperature dependant, being difficult at low temperatures where the ions of the lattice form tight impenetratable masses and becoming more important with higher metamorphic grades. The temperature dependence of diffusion is best represented by the Arrhenius Relationship:

$$D = D_0 \exp(-E/RT)$$

D = Diffusion Coefficient
 E = Activation Energy
 R = Gas Constant
 T = Absolute Temperature
 D₀ = Constant of Proportionality

Assuming diffusion to have taken place by a single mechanism only, a plot of logD versus 1/T (known as the "Arrhenius plot") will yield a straight line graph whose slope is proportional to E and whose y-axis intercept gives D₀.

Individual atomic jumps will occur in random directions within the lattice but the frequency of jumps will change with chemical potential⁸; where a chemical potential gradient is operating there will be a greater tendency for more atoms to go one way (down gradient) than the other. The net result is displacement of matter (of flux, J⁹).

The diffusion (or rate) coefficient, D, is defined as being the constant of proportionality between the flux of material (J) and the "driving force¹⁰" (such as a compositional gradient ($\partial C/\partial x$); more specifically a chemical potential gradient ($\partial \mu/\partial x$), or temperature gradient ($\partial T/\partial x$)). This relationship was discovered empirically with respect to composition and is expressed as:

$$J = - D \frac{\partial C}{\partial x} \qquad \text{FICK'S FIRST LAW}$$

Thus the law states that the rate of flow ("flux") is proportional to the concentration gradient; the minus sign indicating a flux toward lower concentrations. This is the situation for steady state conditions. In most

⁷ Any crystal at a temperature above absolute zero contains a certain number of vacant lattice sites.

⁸ Caused by a pressure-, temperature- or composition-gradient.

⁹ Defined as the amount of material passing through unit area normal to the flux direction per unit time (Vernon, 1976).

¹⁰ Any influence which makes the jump frequency for a jump in one direction between two given sites differ from that for a jump in the opposite direction between these same two sites (Manning, 1968).

processes the concentration of the diffusing species actually changes with time (t). Under transient conditions the compositional gradient and therefore the flux will change with the progression of time. The change in composition is expressed:

$$\frac{\partial C}{\partial t} = \frac{\partial(D\frac{\partial C}{\partial x})}{\partial x}$$

If D is assumed to be independent of concentration, and hence x, this becomes :

$$\frac{\partial C}{\partial t} = D \frac{\partial^2 C}{\partial x^2} \quad \text{FICK'S SECOND LAW}$$

Experimentally the change in the composition gradient with the progression of time is recorded such that the concentration at a given place and time, C(x,t), becomes a function of both distance from some boundary, (x), and time, (t). To apply Fick's Laws the equations must be solved for the experimental conditions in question; such a solution is displayed below¹¹:

$$C(x,t) = \frac{(C_1+C_2)}{2} + \frac{(C_1-C_2)\text{erf } x}{2(Dt)^2}$$

From this a more general relationship has been derived:

$$x = \sqrt{Dt}$$

which allows an approximation of the distance over which diffusion is likely to operate in time, t, to be made without the need to solve Fick's Second Law. In order to make such approximations, however, it is still necessary to have knowledge of diffusion coefficients (D).

There is a paucity of reliable diffusion data on natural minerals within the literature. Most experimental studies to date have been beset by the difficulties involved in investigating complex silicate systems (*c.f.* simple metallic systems where significant advances have been achieved). Early results published within the geological literature tend to concentrate on tracer¹² and self diffusion¹³ (*e.g.* Sneeringer and Hart, 1978; McCallister et al. , 1979) of single species within synthetic crystals as opposed to the more complex situation of multicomponent diffusion within natural minerals. The significance of diffusion as perhaps the single most important rate limiting process active within most geological situations (*e.g.* mineral equilibria and zoning, exsolution, spinoidal decomposition, crystal growth *etc.*, *etc.*) highlights the need for a better

¹¹ Where "erf" denotes a mathematical function found in some solutions of Fick's Second Law, existing by agreed definition as do sines and cosines (Brophy, Rose and Wulff, 1964). C1&C2=initial and final concentrations.

¹² Tracer Diffusion - transport of ions present in 'trace' quantities (Freer, 1981).

¹³ Self Diffusion - movement of the host's own species through itself (Freer, 1981).

understanding of both diffusion processes themselves and reliable estimates of likely diffusion rates and coefficients. Freer (1981) provides a thorough compilation of the data obtained on silicates and glasses up to the 1980's. Foremost amongst these works are those of Smith (1974) on feldspars, Barrer (1978) on zeolites, Hofman (1980) on glasses, Freer (1980) on oxides and Giletti (1974) on geochronological nuclides. More recent studies of oxygen diffusion in quartz and feldspar utilising secondary ion mass spectrometry (S.I.M.S.) depth profiling techniques (Giletti *et al.*, 1978; Freer and Dennis, 1982; Dennis, 1984; Giletti and Yund, 1984; Elphick *et al.*, 1986, 1988; Fortier and Giletti, 1991) have enabled diffusivities to be measured with much more precision than has previously been attainable. Most studies of cation diffusion within natural minerals have tended to concentrate on the simpler structures, such as quartz, olivine, feldspar and garnet (Lin and Yund, 1972; Buening and Buseck, 1973; Misener, 1974; Freer, 1979; Hart, 1981; Elphick *et al.*, 1981, 1985; Giletti, 1991). Some attempts have also been made at establishing diffusion data in the more complex structures such as sheet and chain silicates (Giletti, 1974; McCallister *et al.*, 1979). Very little data has been obtained on diffusion in amphiboles. As amphiboles are commonly used for obtaining K-Ar/Ar-Ar ages numerous attempts have been made at obtaining estimates of both their Ar diffusion parameters and possible diffusion mechanisms. The first such investigations were performed by Amirkhanoff *et al.* (1959) and Gerling *et al.* (1965) and more recently vacuum step heating (*e.g.* Berger, 1975; Berger and York, 1981), hydrothermal-isothermal treatment (*e.g.* Harrison, 1981; Harrison *et al.* 1985) and geological heating (*e.g.* Hart, 1964; Harrison and McDougall, 1980b) techniques have all been utilized with some success. Harrison and McDougall (*op.cit.*) examined $^{40}\text{Ar}/^{39}\text{Ar}$ age spectrum analyses of hornblendes collected at varying distances from an intrusive granite heat source (in an approach identical to Hart's (1964)) and estimated the diffusivity of Ar in hornblende ($D_{\text{Ar}}=10^3 \exp(-60/RT)$). Subsequent isothermal-hydrothermal studies (see Giletti, 1974b for details) by Harrison (1981) suggested hornblende to be unstable during vacuum heating, ^{with} argon transport more likely reflecting a response to phase changes rather than volume diffusion [$D_{\text{Ar}}=0.061 \exp(-66.1/RT)$]. Detailed studies by Harrison and FitzGerald (1986), Onstott and Peacock (1987), Gaber *et al.* (1988), Baldwin *et al.* (1990), Lee *et al.* (1990) and Wartho *et al.* (1991) seem to confirm that in many situations Ar diffusion in amphiboles is probably being controlled by phyllosilicate intergrowths and/or microstructures such as exsolution lamellae within the crystals; these supply 'easier' pathways along which argon can escape without the need to invoke volume diffusive processes. In vacuo $^{40}\text{Ar}/^{39}\text{Ar}$ release spectra obtained from amphiboles during step-heating investigations

(Gaber *et al.*, 1988; Wartho *et al.*, 1991) appear to correlate with complex sequences of "decomposition events" between 750-1300°C [hornblende → oxyhornblende → clinopyroxene structured phase → fine-grained reaction products → glasses (Wartho *et al.*, 1991)] rather than reflecting volume diffusion as was originally believed. This suggests that the mechanisms of argon release in vacuo operate in a quite different way to those within natural metamorphic environments.

To the authors knowledge no data has yet been obtained for cationic diffusion within the amphiboles. However studies of pyroxenes have made considerable progress over the last ten years and given the similarity of crystalline structure these may give some rough guide to amphibole diffusion rates. The following table summarises some of the most recent pyroxene diffusion measurements published.

SUMMARY OF PYROXENE DIFFUSION DATA.

AUTHOR	YEAR	STUDY	D Cm ² S ⁻¹	E kcal/mol	D ₀ Cm ² S ⁻¹	T °C
Seitz	1973	Al in diopside	6x10 ⁻¹²	-	-	1240
Wood & Hemming	1978	Al in diopside	2x10 ⁻¹³	-	-	1280
McCallister <i>et al.</i>	1979	Ca in diopside	1.9x10 ⁻¹¹ to 7.7x10 ⁻¹²	~50-100	-	1300
Freer <i>et al.</i>	1982	Al+Fe in diopside Ca+Mg in diopside	< 4x10 ⁻¹⁴ < 7x10 ⁻¹⁴	~60 "	- -	1200 1250
Brady & McCallister	1983	Ca-Mg in diopside		86.25	3.89 x10 ⁻³	1150-1250
Brady & McCallister	1983	Ca-Fe in diopside	<10 ⁻¹³	-	-	1300
Sneeringer <i>et al.</i>	1984	Sr-Sm in diopside		97	54	1100-1300
Sautter <i>et al.</i>	1988	Al in diopside	-	-	0.32±0.07 x10 ⁻¹⁶	1180

D=diffusion coefficient

E=activation energy

D₀=pre-exponential coefficient

T=temperature

As further advances are made using S.I.M.S. and other techniques it will be possible to build upon the data already obtained, not only enhancing our knowledge of diffusion processes as a whole but also generating a reliable data

base from which diffusion coefficients may be obtained. Once an appreciation of both tracer and interdiffusion coefficients for the major rock forming minerals are known over a range of P-T environments it should be plausible to view rock textures with greater insight into the rates at which relevant processes took place.

2.1.2. THE CLOSURE TEMPERATURE CONCEPT.

As temperature decreases the effects of diffusion become more and more restricted until eventually a temperature is reached at which the atoms no longer have the necessary energy to jump from site to site with sufficient frequency to cause significant change of chemical composition. This temperature, known as the *closure temperature*, has been thoroughly examined in a series of theoretical papers by Dodson (1973, 1976, 1979 and 1986), and Dodson & McClelland-Brown (1985). In these works Dodson concentrates predominantly upon radiogenic element populations within minerals, outlining closure temperatures as "the temperatures at which various systems start to retain their radiogenic daughter products" (Dodson, 1979). Dodson (1973) defines the term "closure temperature" as:

"the temperature of the system at the time represented by its apparent age".

This definition is illustrated in Figure 2.1; the closure temperature (T_c) falls within the time period during which the radiogenic mineral system is partially closed to escape of the daughter product. It is clear from Figure 2.1 that daughter products do not become "frozen" within minerals at sharply defined temperatures, but rather over a transitional temperature-time range to which the closure temperature equates. When a rock mass cools steadily a transition will therefore occur from a state of "continuous equilibrium" (where all radiogenic daughter products are lost (Dodson, 1979)) to a state of "false equilibrium" (where the daughter product is quantitatively retained, (Dodson, 1979)) This change from continuous to false equilibrium takes place in the neighbourhood of the closure temperature (Dodson, 1976). Slower rates of cooling provide longer time intervals within which total or partial loss of daughter product may occur resulting in lower apparent ages and corresponding closure temperatures.

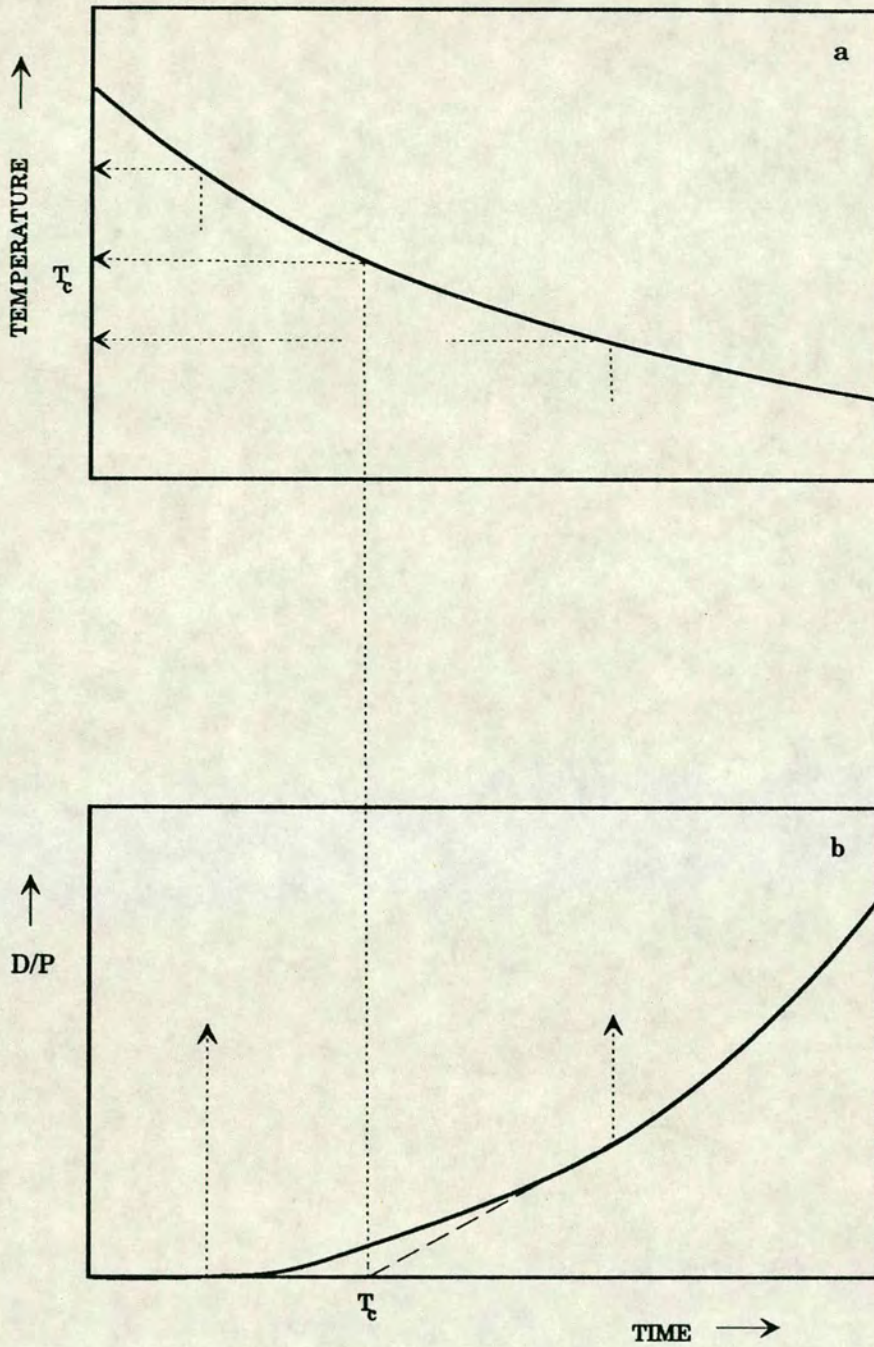


FIG. 2.1. Graphical definition of the closure temperature concept (from Dodson, 1979).

(a) Cooling curve.

(b) Ratio of daughter to parent (D/P) isotope retained with time/decreasing temperature.

The closure temperature (T_c) is approximated from the temperature of the system at the time where all radiogenic daughter is retained within the crystal (linear extrapolation of D/P curve to zero).

The age of a rock or mineral thus *ideally* represents a point in time at which a completely mobile daughter product becomes immobile (Dodson, 1979). Early works assumed this point in time to be related to either primary igneous crystallisation or recrystallisation during peak metamorphic conditions. Detailed isotopic investigations since the late 1960's have documented inconsistencies in the ages of rocks within both regional and contact metamorphic terrains, *e.g.* The Dalradian Supergroup (Harper, 1967; Dewey and Pankhurst, 1970; Dempster, 1985) and the Eldora Aureole (Hart, 1964). Age measurements performed upon different minerals within the same rocks often established that a range of ages existed. Clearly the "age of the rock" was not simply recording the age of igneous crystallisation or peak metamorphism and often could not be equated with any known series of metamorphic events. There is now a wealth of evidence indicating that radiogenic systems remain mobile in minerals at temperatures well below those of crystallisation, or have become remobilised by a thermal pulse. Differences in the closure temperatures of isotopic systems within different minerals enables a range of "ages" to be obtained from minerals/rocks whose geological histories are otherwise identical.

Dodson (1979) suggests isotopic elements may "leave" minerals using one of two main mechanisms:

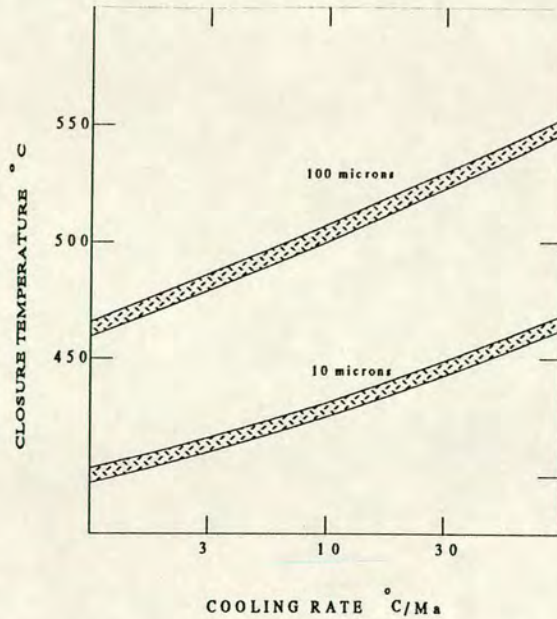
(i) "First Order Loss".

occurs when daughter products are removed at an identical rate to which they are generated, *i.e.* they do not accumulate within the mineral. This loss-mechanism is independent of grain geometry.

(ii) "Loss by volume diffusion".

the more likely of the two mechanisms is dependant upon grain geometry, reflecting either the size of the whole grain or some smaller volume (known as the "effective grain size").

The effective grain-size concept is fundamental to age determination studies, the length of the diffusion path from the diffusing species' origin to it's position of minimum concentration being of extreme importance (Cliff, 1985). In studies where the path length equals the grain radius different ages will be retained by different sized grains (assuming all other considerations remain constant). Cliff (1985) shows how T_c for Ar diffusion in hornblende varies with both different grain-size and cooling rate (using data from Harrison, 1981):



VARIATIONS IN THE CLOSURE TEMPERATURE OF ARGON AS A FUNCTION OF BOTH GRAIN-SIZE AND COOLING RATE

(modified from Cliff, 1985) *the widths of the stripled bands corresponds to the uncertainty in activation energy for diffusion.*

It is crucial to any closure temperature calculation to consider all possible kinetic processes, grain geometries and cooling histories. In earlier works Dodson (1973, 1976, 1979) derived a relationship between the effective closure temperature of the system, the diffusion parameters and rate of cooling which he expresses:

$$E/RTc(x) = \ln(\tau D_0/a^2) + G(x) \quad \text{(Dodson, 1986)}$$

- where
- E is the activation energy
 - τ is the cooling time constant; the time taken for D to diminish by a factor e
 - a is the linear grain-size, the radius or half-thickness of the system
 - G(x) is the closure function, a function of the shape of the grain and the position within it.¹⁴
 - T_c the closure temperature
 - D₀ the pre-exponential constant

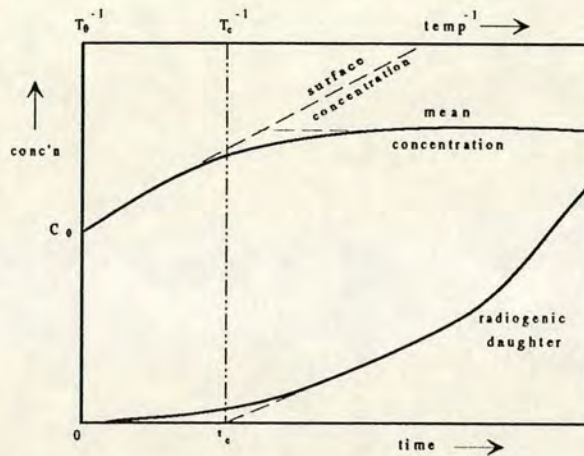
In these formulations Dodson assumes the diffusing component is present at low concentrations within the grain which is in contact with an infinite, well-mixed reservoir. He also assumes that over the transitional T_c-interval 1/T and C_s¹⁵ change uniformly with time. An important assumption made in closure temperature theory involves consideration of the grain-boundary situation. Here the diffusing species is required to continue to move with sufficient ease to

¹⁴ Incorporating the previously used term 'A' for diffusion across grain geometries such as spheres, plane sheets and infinite cylinders.

¹⁵ The concentration at the surface of the grain.

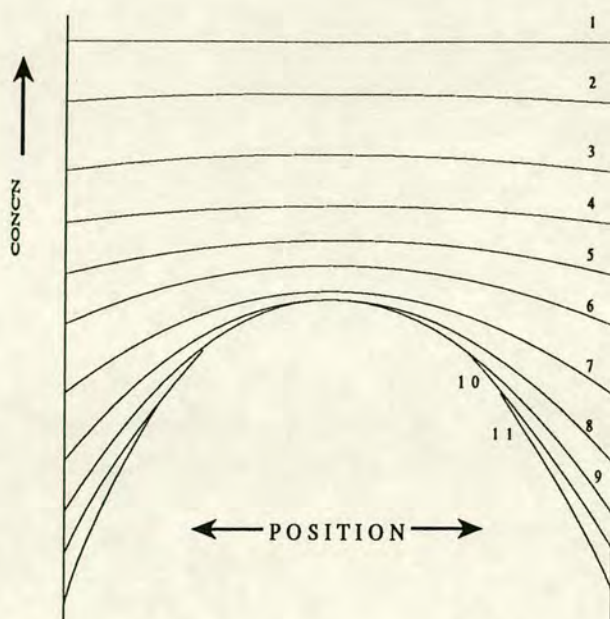
enable the concentration there to remain effectively zero. Little is known of grain-boundary diffusion in rocks but microtextural studies indicate that grain-boundaries are more likely to be regions packed and knotted with dislocations and imperfections. Grain-boundaries therefore provide much faster diffusive pathways than those of volume diffusion. Cliff (1985) suggests there are indications from geochronological studies that grain-boundaries may not always provide such easy pathways.

Dodson (1973, 1976) discusses the similarity between geochronological closure temperatures and those recorded by "frozen" geochemical systems. Here the closure temperature relates to the temperature required to produce the observed concentration at thermodynamic equilibrium. The following Figure displays the relationship between geochemical and geochronological closure:



RELATIONSHIP BETWEEN GEOCHEMICAL AND GEOCHRONOLOGICAL CLOSURE (Dodson, 1973).
[assuming $1/T$ increases linearly with time]

At high temperatures the concentration of the mobile component follows its equilibrium value for the P-T concerned. This is analogous to the total loss of daughter product in a geochronological system. With cooling element mobility diminishes until a static state is reached from which the closure temperature can be inferred (Dodson, 1979). This static state, and the cooling interval over which element mobility changes from an open to a closed system, is preserved in rocks as "stranded" diffusion profiles, the changing mobility of the element generating zoned mineral compositions. Dodson (1986) discusses how rapid diffusion in the early stages of cooling maintains equilibrium concentrations and how as temperature decreases the diffusion occurring within grain interiors slows with respect to that occurring at the surface until eventually the system effectively closes producing a "closure profile". This concept is illustrated below:



SUCCESSIVE CONCENTRATION PROFILES ACROSS A COOLING BODY WITH CHANGING EQUILIBRIUM CONDITIONS (Dodson, 1986).

1: equilibrium maintained - grain unzoned.

2-11: grain progressively closes from core to rim preserving "stranded" diffusion profiles.

Different ages obtained from minerals within the same rock suggest that closure is controlled by properties specific to each phase (which one would expect assuming diffusivities vary from phase to phase). As the T_c of a particular isotopic system allows an estimate to be made of the temperature of the host rock at a certain instant in time, knowledge of T_c using several systems in different minerals will enable a more complete idea of the rocks thermal history to be built up. In terms of 'closure' this allows elucidation of the cooling histories of both regional metamorphic terrains and igneous bodies. Amongst the first works of this type were investigations carried out on the rocks of the Swiss Alps (Jager *et al.*, 1967; Purdy and Jager, 1976), here Rb-Sr and K-Ar ages of biotites, K-Ar ages of muscovites and U-fission tracks in apatites allowed a clear and consistent picture of cooling history to be obtained. Numerous subsequent studies along these lines, notably Dempster (1985), van-Breeman *et al* (1979), Dallmeyer (1974) and Elias *et al.* (1988) combined with laboratory based experimental investigations (*e.g.* Hofmann *et al.*, 1974) and studies made in contact aureoles, discussed below, have enabled a fairly reliable picture of the closure temperature ranges of different isotopic systems within a host of commonly dated minerals to be established. These have been summarised in Figure 2.2, from Dodson and McClelland-Brown (1985).

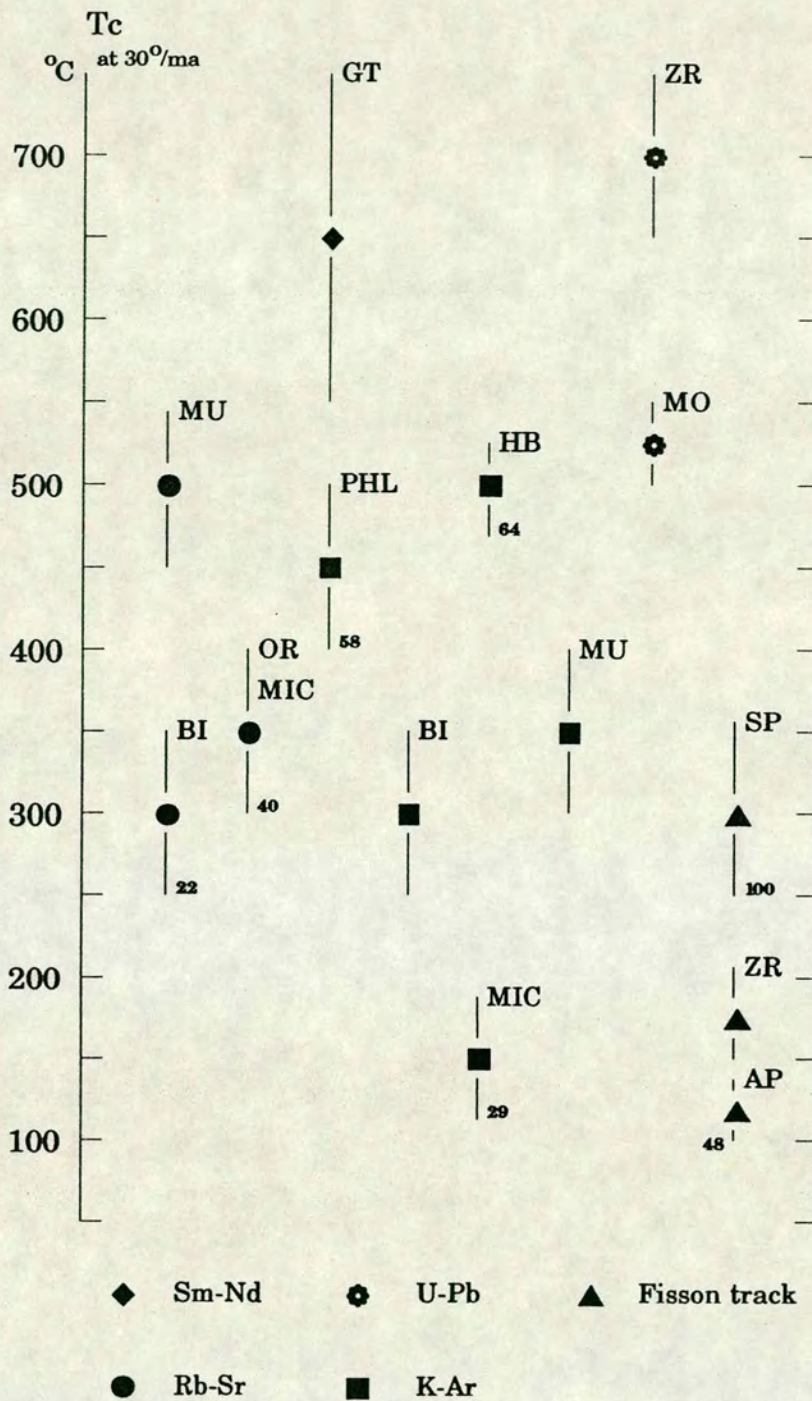


FIG. 2.2. Estimates of mineral closure temperatures (standardised to cooling rates of 30°C/Ma where possible) From Dodson and McClelland Brown, 1985.

Small numbers in bold are activation energies (Kcal/mol).

Mineral abbreviations:

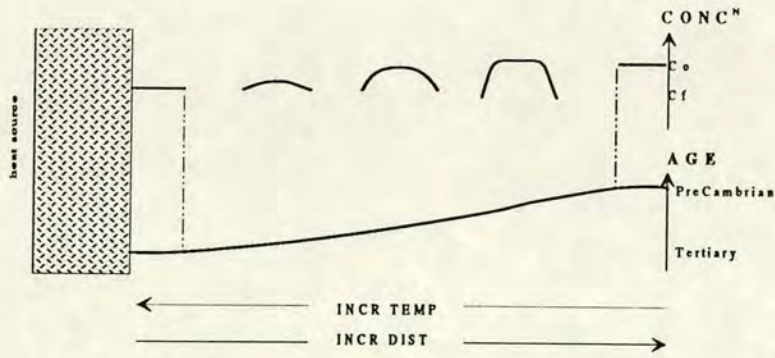
MU-muscovite	BI-biotite	GT-garnet	HB-hornblende	ZR-zircon	MIC-microcline
AP-apatite	SP-sphene	OR-orthoclase	MO-monazite	PHL-phlogopite.	

The closure temperature for Ar diffusion, particularly in hornblendes, has been thoroughly investigated by both traditional K-Ar and $^{39}\text{Ar}/^{40}\text{Ar}$ step heating techniques (Harrison, 1981; Berger and York, 1981; Elias ^{et al.} 1988). These suggest hornblende to be one of the most Ar-retentive of phases, with estimates for its closure temperature averaging around 550°C. For this reason hornblende is generally thought of as providing amongst the most reliable K-Ar/Ar-Ar ages in a rock.

The re-opening of a geochronological or geochemical system due to a thermal pulse has been studied with similar treatment by numerous workers. Here the term "blocking temperature" is preferred, referring to the temperature *above* which geologically significant diffusion *can* occur (*c.f.* "closure" referring to the temperature *below* which significant diffusion *does not* occur). In the simplest situations originally unzoned grains exposed to increased temperatures (associated with re-heating) gain enough kinetic-energy to enable elemental reconfiguration through diffusion. In many studies blocking and closure temperatures are assumed to be identical, seen as equal but opposite phenomena. It seems more reasonable to assume that they differ especially when one considers the sensitivity of kinetic processes to heating/cooling rates (Cliff, 1985). Cliff (1985) even goes as far as to suggest that different processes may dominate during heating and cooling events.

Unlike most regional studies, the temperature history of contact aureoles can, at least in theory, be quite accurately determined. Estimates of the likely temperature of the intrusion allows a model of the thermal gradient activated within the aureole to be developed¹⁶. The country-rock closest to the intrusion experiences the greatest increase in temperature; if this is within or above the appropriate T_c range, isotopic and elemental diffusion may occur creating both 'closure' and 'geochemical' profiles within the minerals (as discussed in terms of cooling systems). In an ideal situation the ages recorded by the mineral species and the widths of any geochemical zonation will closely reflect their position within the aureole. In the following sketch the sample closest to the intrusion is able to ^{undergo the most} diffusion resulting in both a total re-setting of the mineral ages and establishing chemical plateaus representing equilibrium concentrations within the new P-T environment. The sample furthest from the intrusion is unaffected by the re-heating and retains its original geochemical and geochronological plateaux.

¹⁶ Assuming conduction to be the mechanism by which heat is being transported.



GEOCHEMICAL AND GEOCHRONOLOGICAL PROFILES WITH DISTANCE/TEMPERATURE FROM A HEAT SOURCE.

C_o =original concentration C_f =final concentration.
 concentration profiles are across individual mineral grains

Any detailed examination of either isotopic or elemental variation with distance, and hence temperature, from the contact should enable an estimate of T_c to be made. Many useful quantitative results of the T_c of minerals have come from such investigations and these are incorporated into Figure 2.2 (Dodson & McClelland-Brown, 1985).

The study of compositional profiles within minerals has been independently investigated by metamorphic petrologists with the aim of enhancing our knowledge of the mathematics of both inter- and multi-component diffusion (*e.g.* Lasaga *et al.*, 1977; Saxena, 1972; Lasaga, 1983; Loomis, 1983; Chakraborty and Ganguly, 1990). Their treatment involves the derivation and solution of complex expressions for the boundary condition between two phases which have exchanged components but not reached equilibrium, and has close similarities to the mathematical treatment of T_c . The reader is referred to the original texts for the detailed aspects of solutions to the diffusion equations for zoned minerals. In essence the shapes of the 'frozen' composition profiles enable the P-T-t history of the assemblage to be determined. Garnets have been particularly well documented in these terms (Hollister, 1966; Harte and Henley, 1966; Anderson and Buckley, 1973; Loomis, 1975, 1977, 1978(a) & (b), 1983; Cygan and Lasaga, 1982; Dempster, 1985; Chakraborty and Ganguly, 1990; Spear, 1991); their physical resistance, stability within a range of bulk compositions over a diversity of P-T space in addition to their relatively simple exchange mechanisms and limited diffusion rates enable them to readily retain zoning which preserves evidence of the samples equilibration history. Lasaga, Richardson and Holland (1977) discuss Mg-Fe exchange between co-existing garnet-cordierite pairs in response to falling temperature (associated with the waning stages of an orogeny) and use the compositional profiles to reconstruct the thermal history of the rock. Lasaga (1983) takes the principal one step further

and relates the P-T-t history of the assemblage to the kinetic response within the mineral over T-t. Lasaga (1983) refers to aspects of these studies as "geospeedometry". Like closure temperature theory geospeedometry involves consideration of grain-size, cooling rate, activation energy, temperature and diffusion rates.

Lasaga (1983) expresses the diffusion equation as:

$$\frac{\partial c}{\partial t} = D_0 \frac{\partial^2 c}{\partial x^2} \quad (1)$$

where c =concentration
 x =distance from boundary
 t '=dimensionless time
 D_0 =the initial diffusivity, (D), at $t=0, T=T_0$

To solve equation (1) Lasaga (1983) introduces the dimensionless parameters t'_r and x'_r , reducing the problem to constant-D diffusion equation:

$$\frac{\partial c}{\partial t'_r} = \frac{\partial^2 c}{\partial x'^2_r} \quad (2)$$

where $t'_r = D_0 a^2 / t'$
 a =crystal diameter
 $x'_r = x/a$

which is independent of the boundary conditions. The solution to equation (2) is as follows:

$$c(x'_r, t'_r) = \sum_{n=0}^{\infty} \exp \left[-\frac{(2n+1)^2 \pi^2 t'_r}{4} \right] A_n \sin \left[\frac{(2n+1)\pi x'_r}{2} \right] \quad (3)$$

$$\text{where } A_n = \frac{(2n+1)\pi e^{\alpha_n} c_{1A}}{\gamma'} \int_{1-\gamma' t'_r}^1 e^{-\alpha_n u} u^{\beta/\gamma} du + \frac{4}{(2n+1)\pi} c_{1A}$$

$$\alpha_n = \frac{(2n+1)^2 \pi^2}{4\gamma'} \quad u = t' \frac{D_0}{a^2} \quad c_{1A} = \text{initial concentration of component 1 in phase A.}$$

Equation (3) can be solved provided the values of γ' and β/γ are known:

$$\gamma' = \frac{E_a s a^2}{D_0 R T_0^2}$$

E_a =activation energy
 s =initial cooling rate
 R =gas constant
 T_0 =initial temperature

$$\beta/\gamma = \frac{\Delta H}{E_a} \frac{\sqrt{(D_B^0/D_A^0)}}{[\sqrt{D_B^0/D_A^0} \{1 + (c_{1A}^1/c_{1A}^2)\} + (c_{1A}^1/c_{1B}^2) + (c_{1A}^1/c_{2B}^2)]}$$

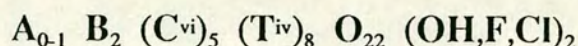
where A and B are phases
 C1 and C2 are components
 D_A^0 = initial diffusivity of phase A for component 1-2 exchange.
 c_{1A}^1 = initial concentration of component 1 in phase A.
 ΔH = enthalpy of change for reaction.

Given $c(x_r)$ when $t_r = 1/\gamma'$, each set of β/γ and γ' parameters will define a curve (a "Lasaga curve") from which estimates of the other parameters can be obtained. The successful fit of a Lasaga curve to a chemical profile (*e.g.* an electron microprobe traverse) enables values of β/γ and γ' to be determined directly. Knowledge of these parameters allows the cooling history of the mineral to be determined.

2.2. THE AMPHIBOLE GROUP

Amphiboles are amongst the most complex of the commonly encountered silicate minerals. Their notoriety as "mineralogical sharks in a sea of unsuspecting elements" (Robinson *et al.*, 1982) combined with their crystal-chemical flexibility (Hawthorne, 1981) allows a host of cationic substitutions to take place generating an enormous range of possible chemical compositions. As a consequence amphiboles occur in a diverse range of P-T environments, being encountered within rocks of sedimentary, igneous and metamorphic origins. They are particularly abundant minerals within metamorphic rocks where they are stable from greenschist to lower granulite facies.

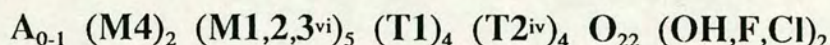
The standard amphibole formula is generally written



where

A = Na, K C = Mg, Fe²⁺, Mn, Al, Fe³⁺, Ti
 T = Si, Al B = Na, Li, Ca, Mn, Fe²⁺, Mg

or in crystallographic terms (Robinson *et al.*, 1982)



likely site occupancies are displayed in the following table:

NORMAL CATION SITE-ALLOCATIONS IN AMPHIBOLES

CATION	A	M(4)	M(1), M(2), M(3)	T(1), T(2)
Si				
Al				
Fe ³⁺				
Ti				
Fe ²⁺				
Mn				
Mg				
Li				
Ca	—			
Na	—			
K	—			

(from Hawthorne, 1981)

2.2.1 (i). STRUCTURE

The structure of amphiboles has been comprehensively documented by Hawthorne (1981, 1983), a brief resume is given below.

Amphiboles are characterised by a double chain of linked Si-O tetrahedra which extend infinitely in one direction, having the general stoichiometry $(T_4O_{11})_\infty$ (Hawthorne, 1983). The z axis of the amphibole cell is defined from the direction of 'infinite polymerization' of the double chain; the repeat distance in the z direction reflecting the c dimension within the unit cell. Oxygen atoms lie in two planes approximately parallel to the chain direction; two types are distinguished by Hawthorne (*op.cit.*):

- a: Basal oxygens - those lying in the same plane as the bonds between adjacent tetrahedra.
- b: Apical oxygens - those which lie in the other plane.

Oxygens which bond to two tetrahedrally coordinated cations are called "**bridging oxygens**", *i.e.* they link two TO_4 tetrahedra together. Oxygens which bond to one tetrahedrally coordinated cation are called "**non-bridging oxygens**". Basal oxygens are thus comprised of both bridging and non-bridging types whereas apical oxygens are non-bridging types only (see Figure 2.3). T1 cations are linked to three bridging oxygens and one non-bridging oxygen. T2 cations are those which are linked to two non-bridging and two bridging oxygens; these are depicted in Figure 2.3.

Non-bridging anions are bonded to di- and tri-valent cations and these link the $(T_4O_{11})_\infty$ chains together. There are three types of interchain linkages:

- 1: Di- and Tri-valent cations located between two layers of apical oxygen atoms belonging to double chains.

Apical oxygens of adjacent chains assume a pseudo-octagonal arrangement around each of the linking cations. An additional monovalent anion (*i.e.* F,OH,Cl) is located within the centre of this strip to complete the coordination of the cations. Adjacent double chains become tightly bonded together forming I-beam units (Hawthorne, 1983). Figure 2.3 illustrates the I-beam unit of the C2/m amphiboles (viewed down z).

- 2: Linkages between I-beam units.

Di and tri-valent cations at the edges of I-beam units link laterally to non-bridging basal oxygens of adjacent I-beams to create three-dimensional arrays.

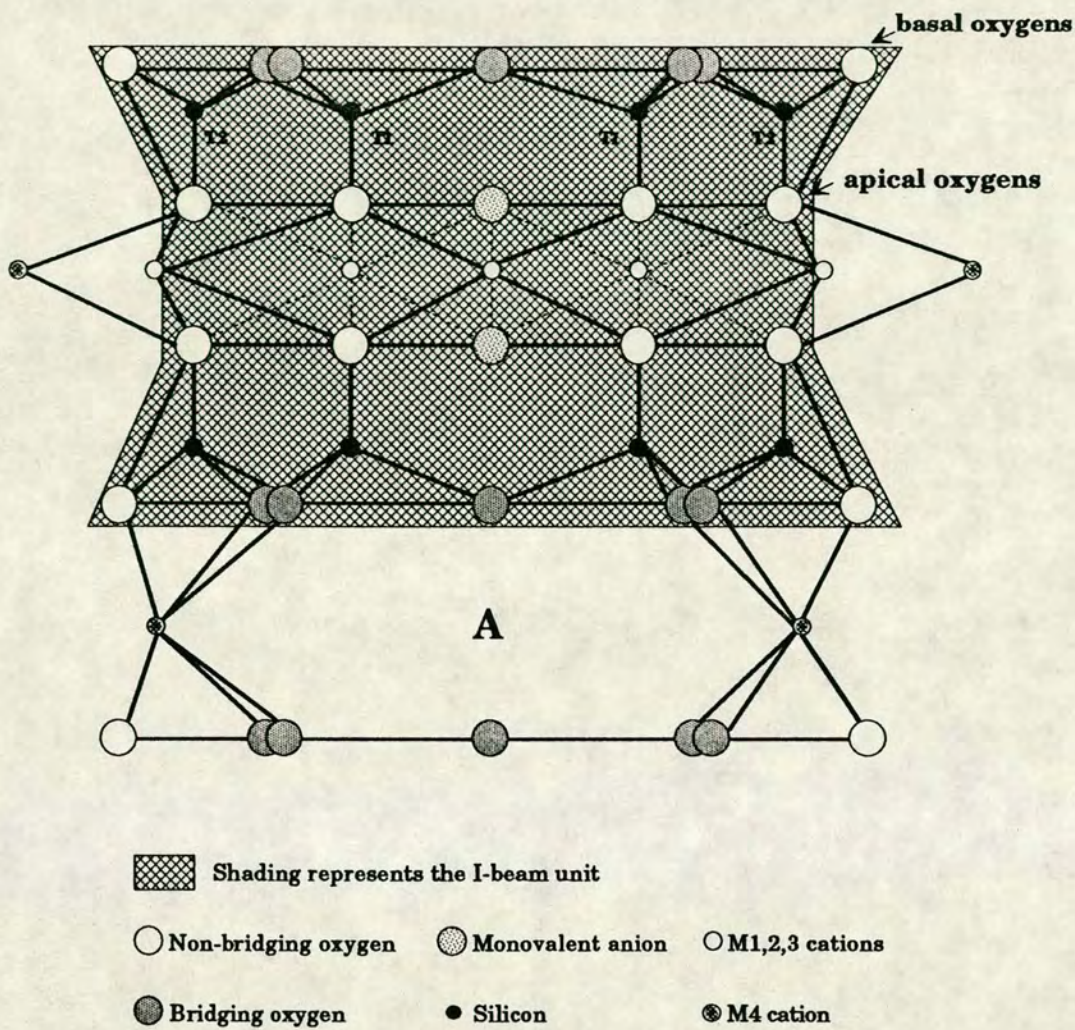


FIG. 2.3. The I-beam unit of the C2/m amphibole; viewed down z (modified from Hawthorne, 1983).

3: Additional linkages provided by A and B cations.

B-type (M4) cations are located toward the margins of I-beam strips, bonding to both non-bridging and bridging anions (*c.f.* C-type (M1-3) cations which bond only to non-bridging anions). They supply additional linkages both within and between I-beams. Between the back-to-back double chains is a large cavity surrounded by bridging oxygen atoms, it is here that the A-cations are located, providing further linkage between adjacent double chains.

The amphiboles have been characterised as belonging to at least five major crystallographic space groups (Hawthorne, 1983). Of these the C2/m is the most common of the structure-types observed. Hawthorne (*op.cit.*) reviews the numerous site-nomenclature schemes that have been previously used, ^{and} it is his terminology, now the most widely accepted version, which has been used in this section.

Figure 2.4 illustrates a 1/4 of the tremolite unit cell, distinguishing the positions of the various crystallographic sites. Here O₇ is a bridging anion, O₃ the monovalent anion, M_{1,4} the locations of the major cations and A the A-site, in this case vacant.

2.2.1 (ii). CLASSIFICATION AND NOMENCLATURE

Leake (1978) established the much needed and fairly rigorous method of standardising amphibole nomenclature, largely based on crystal chemistry, which has been adopted in this thesis. A general outline follows.

Leake (*op.cit.*) sub-divides the amphiboles into four main groups on the basis of their B-Site occupancy:

1: Fe-Mg-Mn Group	$(Ca+Na)_B < 1.34$
2: Calcic Amphibole Group	$(Ca+Na)_B \geq 1.34$ $Na_B < 0.67$
3: Sodic-Calcic Amphibole Group	$(Ca+Na)_B \geq 1.34$ $0.67 \leq Na_B < 1.34$
4: Alkali Amphibole Group	$Na_B \geq 1.34$

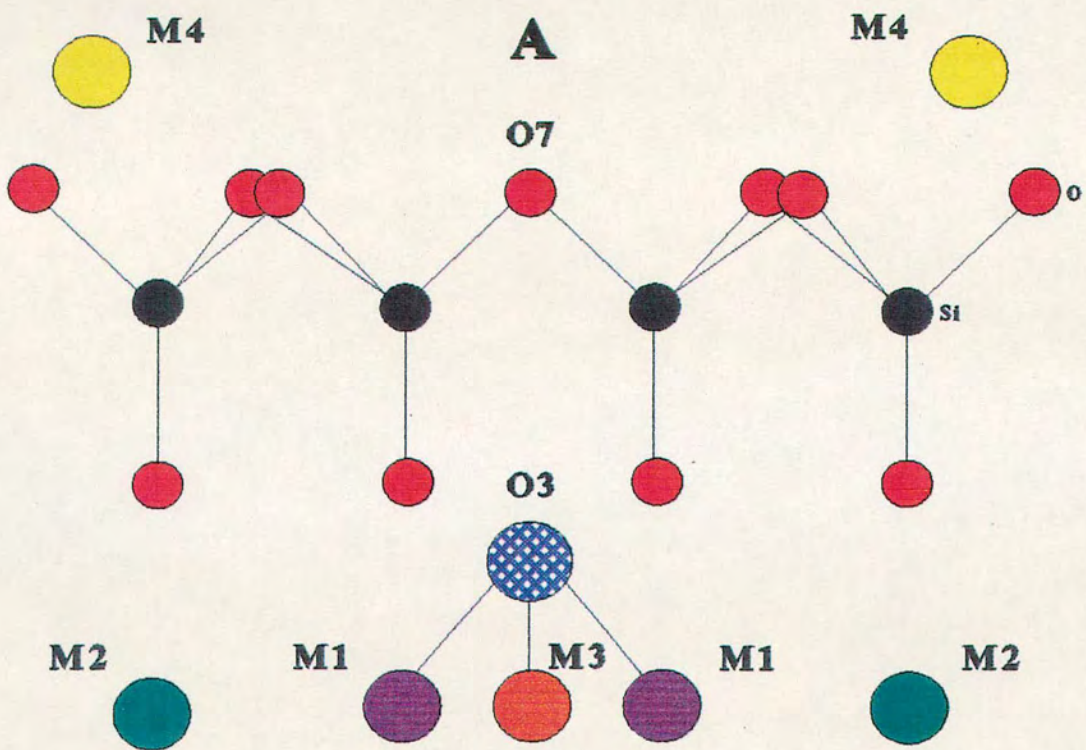


FIG. 2.4. 1/4 OF THE TREMOLITE UNIT CELL DEPICTING THE POSITIONS OF THE MAJOR CATION SITES (Troll and Gilbert, 1972).

The amphiboles investigated in the course of this research fall compositionally within the 'calcic amphibole' group, a guide to their nomenclature is now given; the reader is referred to Leake (1978) for greater discussion of both these and the other groups.

The end-member formulae of the calcic amphiboles are displayed in the following table, the stoichiometric limits on the use of each name are displayed in Figure 2.5.

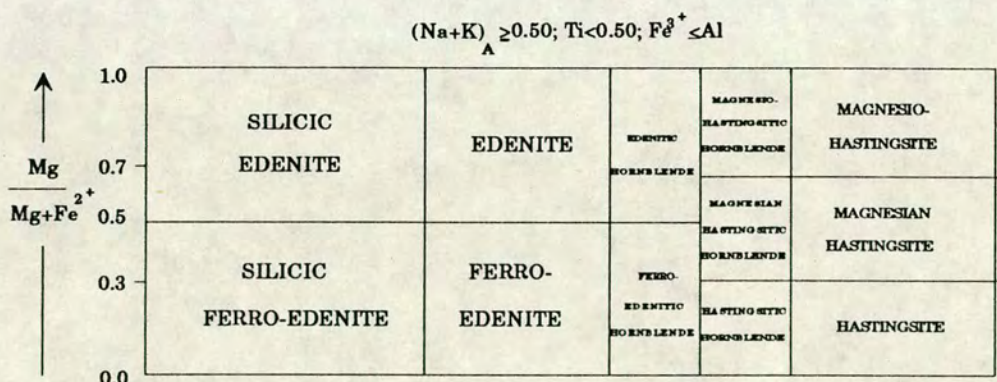
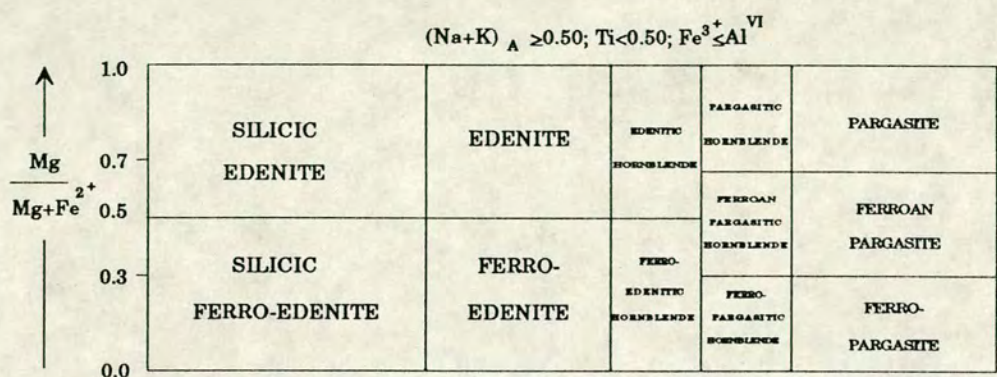
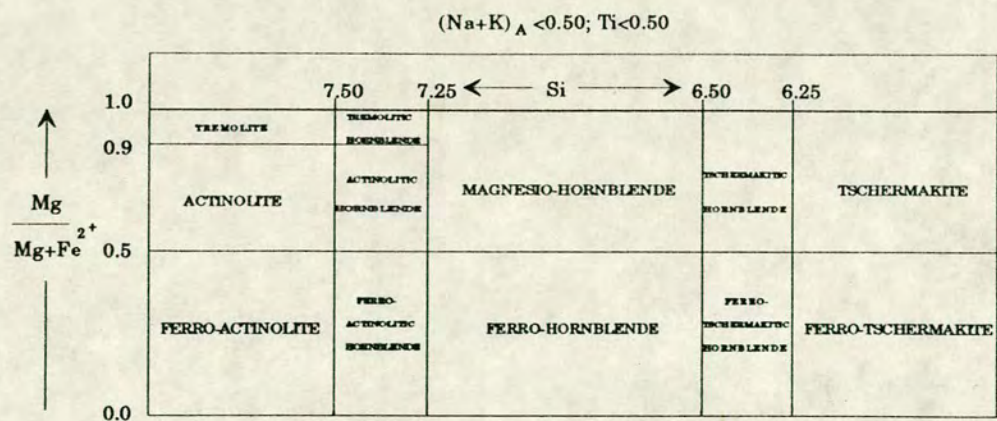
THE CALCIC AMPHIBOLES: END-MEMBER NAMES AND FORMULAE

<u>END MEMBER</u>	<u>FORMULA</u>
Tremolite	$\text{Ca}_2\text{Mg}_5\text{Si}_8\text{O}_{22}(\text{OH})_2$
Ferro-actinolite	$\text{Ca}_2(\text{Fe}^{2+})_5\text{Si}_8\text{O}_{22}(\text{OH})_2$
Edenite	$\text{NaCa}_2\text{Mg}_5\text{Si}_7\text{AlO}_{22}(\text{OH})_2$
Ferro-edenite	$\text{NaCa}_2(\text{Fe}^{2+})_5\text{Si}_8\text{O}_{22}(\text{OH})_2$
Pargasite	$\text{NaCa}_2\text{Mg}_4\text{AlSi}_6\text{Al}_2\text{O}_{22}(\text{OH})_2$
Ferro-pargasite	$\text{NaCa}_2(\text{Fe}^{2+})_4\text{AlSi}_6\text{Al}_2\text{O}_{22}(\text{OH})_2$
Hastingsite	$\text{NaCa}_2(\text{Fe}^{2+})_4\text{Fe}^{3+}\text{Si}_6\text{Al}_2\text{O}_{22}(\text{OH})_2$
Magnesian-hastingsite	$\text{NaCa}_2\text{Mg}_4\text{Fe}^{3+}\text{Si}_6\text{Al}_2\text{O}_{22}(\text{OH})_2$
Alumino-tschemmakite	$\text{Ca}_2\text{Mg}_3\text{Al}_2\text{Si}_6\text{Al}_2\text{O}_{22}(\text{OH})_2$
Ferro-alumino-tschemmakite	$\text{Ca}_2(\text{Fe}^{2+})_3\text{Al}_2\text{Si}_6\text{Al}_2\text{O}_{22}(\text{OH})_2$
Ferri-tschemmakite	$\text{Ca}_2(\text{Fe}^{2+})_3(\text{Fe}^{3+})_2\text{Si}_6\text{Al}_2\text{O}_{22}(\text{OH})_2$
Alumino-magnesian-hornblende	$\text{Ca}_2\text{Mg}_4\text{AlSi}_7\text{AlO}_{22}(\text{OH})_2$
Alumino-ferro-hornblende	$\text{Ca}_2(\text{Fe}^{2+})_4\text{AlSi}_7\text{AlO}_{22}(\text{OH})_2$
Kaersutite	$\text{NaCa}_2\text{Mg}_4\text{TiSi}_6\text{Al}_2(\text{O}+\text{OH})_{24}$
Ferro-kaersutite	$\text{NaCa}_2(\text{Fe}^{2+})_4\text{TiSi}_6\text{Al}_2(\text{O}+\text{OH})_{24}$

Prefixes specific to calcic amphiboles

Alumino	viAl	≥	1.00	
Sodian	Na	≥	1.00	
Subcalcic	Ca	<	1.50	
Silicic	Si	>	7.25	$(\text{Na}+\text{K})^A \geq 0.50$

(from Leake, 1978)



Ti ≥ 0.50

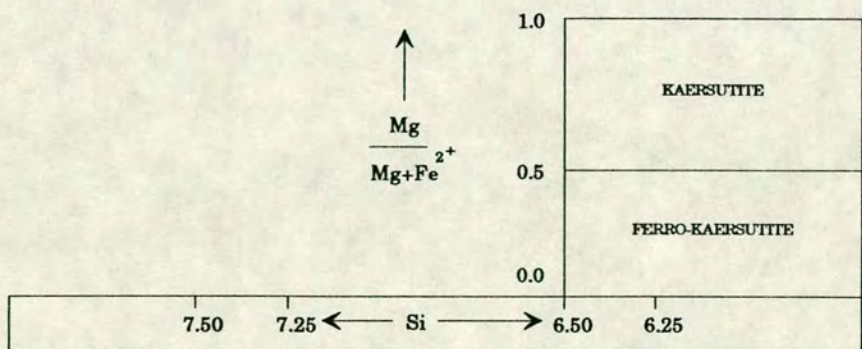


FIG. 2.5. The nomenclature of the calcic amphiboles (from Leake, 1978).

Classification is based on the chemical contents of a standard amphibole obtained, in this thesis, on the basis of electron-microprobe data recalculated to cation proportions using both the 23(O) and average of the 13-CNK and 15-NK methods (see Robinson *et al.*, 1982). The 23(O) recalculation introduced by Miyashiro (1957) is the most commonly used method of recalculating electron microprobe analyses of amphiboles. It compensates for poorly determined H₂O, F and Cl, assuming 22 oxygens and 2(OH,F,Cl) in the formula, calculating the cations to 23(O). The 13-CNK method assumes the sum of C and T-type cations is 13 and excludes Fe²⁺, Mg and Mn from the B(M4) site. Ca, Na and K cations and vacancies do not occupy T(1,2) or M(1,2,3) sites. The 15-NK method assumes B+C+T=15, thereby excluding Na, K from the B(M4) site and Ca from the A-site. In all methods the cations are assigned to sites using the method described by Robinson *et al.* (1982).

The pro's and con's of the numerous methods of recalculating amphibole formulae have been extensively discussed by Robinson *et al.* (1982) and Hawthorne (1981, 1983), to which the reader is referred for thoughtful consideration. Recalculations based on the average of the 13-CNK and 15-NK method (see chapter 5, Table 5.1) were made using AMPHIBOL - a compiled computer program written by Richard and Clarke (Am.Min.,1990) which recalculates chemical analyses of amphiboles into their structural formulae and classifies them according to current IMA guidelines. This program is particularly useful as it determines the Fe³⁺ content of the amphibole on the basis of the charge-balance method described by Stout (1972) and Robinson *et al.* (1982). This calculates the Fe³⁺/Fe²⁺ ratio by normalising both the anions and cations to fixed numbers and then adjusting the ratio until electro-neutrality is obtained. It is emphasised that these calculations only provide limiting bounds and have been performed to give one possible *estimate* of the likely Fe³⁺ content.

2.2.2. SUBSTITUTIONS AND MINERAL REACTIONS

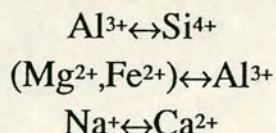
The flexibility of the amphibole structure permits a multitude of ionic substitutions to take place. There are two basic types (Welch, 1987):

a: Monatomic Substitutions

Involving simple substitutions such as $Mg^{2+} \leftrightarrow Fe^{2+}$ which preserve neutrality within the crystal.

b: Coupled Substitutions

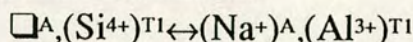
Involving more complex substitutions such as



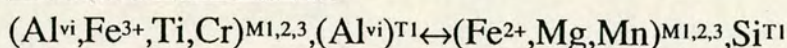
Here more than one substitution must occur within the crystal in order to maintain charge balance.

There are five major coupled substitutions which commonly take place within the amphiboles from which the entire compositional range can be generated. Most of these are also observed within solid solution series of other silicate phases:

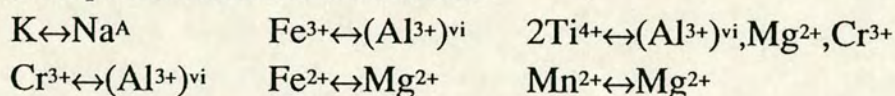
1: Edenite Substitution.*



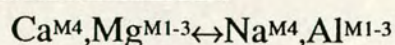
2: Tschermaks Substitution.



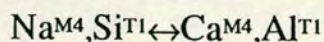
where simple substitutions are combined:



3: Jadeite Substitution.



4: Plagioclase Substitution.



5: $Al^{M1-3}, \square^A \leftrightarrow Na^A, Mg^{M1-3}$

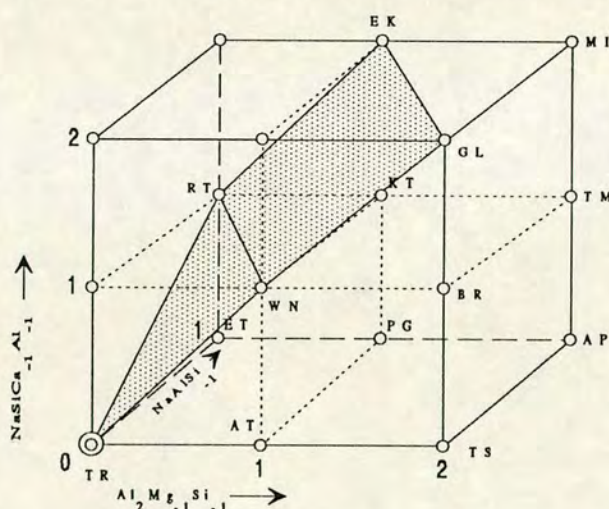
These are more eloquently dealt with in terms of the vector notation of Thompson *et al.* (1982). The "vector" is assigned a chemical formula using

* \square represents a vacancy.

positive subscripts to indicate 'atoms in' and negative subscripts for 'atoms out' (Thompson *et al.* 1982). The main substitutions and their vector notations are displayed below:

SUBSTITUTION	VECTOR NOTATION
EDENITE	NaAlSi_1
TSCHERMAKS	$\text{AlAlMg}_{-1}\text{Si}_{-1}$
JADEITE	$\text{NaAlCa}_1\text{Mg}_{-1}$
PLAGIOCLASE	$\text{NaSiCa}_1\text{Al}_{-1}$
$\text{Al}^{\text{M}1-3}\square^{\text{A}} \leftrightarrow \text{Na}^{\text{A}}\text{Mg}^{\text{M}1-3}$	$\text{AlNa}_1\text{Mg}_{-1}$

In this way the compositional field of all the Na-Ca amphiboles can be represented graphically, starting with a composition of $\text{Ca}_2\text{Mg}_5\text{Si}_8\text{O}_{22}(\text{OH})_2$ (*i.e.* the Tremolite end-member) making additions via three independent coupled exchange vectors, the tschermak, plagioclase and edenite substitutions:



COMPOSITIONAL SPACE OF THE Na-Ca AMPHIBOLES
(Thompson *et al.* 1982).

Idealised compositions:

TR:tremolite

BR:barroisite

PG:pargasite

TM:taramite

AT: $\text{Ca}_2\text{Mg}_4\text{Al}_2\text{Si}_7\text{O}_{22}(\text{OH})_2$

AP: $\text{Na}_3\text{Mg}_3\text{Al}_5\text{O}_{22}(\text{OH})_2$

MI: $\text{Na}_3\text{Mg}_5\text{AlSi}_7\text{O}_{22}(\text{OH})_2$

TS:tschermakite

GL:glaucophane

RT:richterite

EK:ekermanite

WN:winchite

ET:edenite

KT:kataphorite

Compositions above the shaded area are not accessible to clinoamphiboles.

Once the principal exchange vectors have been recognised it is possible to express mineral reactions in terms of either "exchange reactions" or "net transfer reactions". Exchange reactions are those which can be written entirely on the

basis of vectors. Net transfer reactions are those that involve two or more additive components (Thompson *et al.*, 1982). Examples of both types are described in the following section.

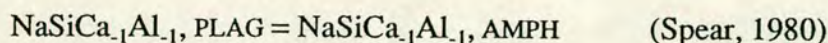
2.2.3. AMPHIBOLE EQUILIBRIA AND PHASE RELATIONS

AMPHIBOLE EQUILIBRIA

Amphibole-plagioclase associations are amongst the most commonly encountered mineralogies within metamorphosed mafic rock-types. Their use as a means to define P-T-t paths is still enigmatic, however, due to their apparently continuous as opposed to discontinuous (*c.f.* pelitic rocks) modal and chemical variations with increasing grade of metamorphism. This continuous compositional variation has been the subject of numerous previous works (Graham, 1974; Grapes, 1975; Harte and Graham, 1975; Grapes and Graham, 1978; Holland and Richardson, 1979; Spear, 1980, 1981; Laird and Albee, 1981; Haynes, 1982; Blundy and Holland, 1990;). In general amphibole becomes more NaAl-rich and plagioclase more calcic with increasing metamorphic grade. However, due to complex solid solution the change has been difficult to document (see Robinson *et al.* (1982) for in depth discussion). The works of Spear (1980, 1981) amongst others (notably Graham, 1974) have shown that equilibrium between plagioclase, amphibole and quartz can be described in terms of three reactions:

- 1: 2(ALBITE-ANORTHITE) = GLAUCOPHANE + TSCHERMAKITE
- 2: 28TREMOLITE + 14GLAUCOPHANE = 28EDENITE + 6CUMMINGTONITE
- 3: EDENITE + 4QUARTZ = ALBITE + TREMOLITE

Equation (1) is an exchange reaction with an exchange-vector $\text{NaSiCa}_1\text{Al}_1$, it may be re-written using vector notation (Thompson *et al.* 1982) as:



This governs the variation of plagioclase composition with M4 site occupancy in amphiboles.

Equations (2) and (3) are "net transfer reactions" (Thompson *et al.*, 1982), resulting in changes in the modal proportions of the amphibole, plagioclase and

quartz in addition to changes in the edenitic component of the amphibole (Spear, 1980). The third equation controls the variation in A-site occupancy between the amphibole and the plagioclase.

On the basis of equations 1 and 3 Spear (1980, 1981) has outlined a possible method of classifying "mafic schists" in terms of their metamorphic grade and facies. However, these equilibria have yet to be unequivocally proven experimentally (Greenwood, 1979; Gilbert *et al.*, 1982; Graham and Novrotsky, 1986).

Calcic-amphibole equilibria have more recently been investigated in the hope of founding reliable thermobarometers on the basis of Al contents (Hammarstrom and Zen, 1986; Hollister *et al.*, 1987; Johnson and Rutherford, 1989; Rutter *et al.*, 1989; Blundy and Holland, 1990; Vyhnal *et al.*, 1991). In their study of hornblendes from calc-alkaline plutonic rocks Hammarstrom and Zen (1986) established a linear relationship between total Al (Al_{TOT}) content and pressure (P) of crystallisation (for low (2kbar) and high (8kbar) situations):

$$P(\pm 3\text{kbar}) = -3.92 + 5.03Al_{TOT} \quad r^2=0.80\#$$

this relationship assumes the final consolidation pressure corresponds to the pressure of crystallisation of the 'hornblende'.

Hollister *et al.* (1987) confirm this calibration and with additional data extend the relationship to include intermediate pressures (4-6kbar) obtaining a very similar equation but with a significantly improved correlation coefficient, and hence decreased uncertainty:

$$P(\pm 1\text{kBar}) = -4.76 + 5.64Al_{TOT} \quad r^2=0.97$$

The use of both Hammarstrom and Zen's (1986) and Hollister *et al.*'s. (1987) barometers is specifically restricted to calc-alkaline rocks containing the assemblage quartz + plagioclase + alkali-feldspar + hornblende + biotite + titanite + magnetite/ilmenite; both rely on indirect estimates of total pressure, obtaining their equations from the best fit lines to plots of P versus Al_{TOT} (where P is an estimate taken from literature).

r^2 is the multiple correlation coefficient; a statistical term describing the fit of data from more than two variables to a straight line. 0=no fit; 1.0=straight line/perfect fit.

Experiments by Johnson and Rutherford (1989) were undertaken in an attempt to test and further calibrate the proposed geobarometer. The specified assemblage within natural samples of both volcanic and plutonic rocks were equilibrated over the pressure range 2-8kbar at 740-780°C. This data confirmed the linear relationship but yielded a different equation for the regressed line:

$$P(\pm 0.5\text{kBar}) = -3.46(\pm 0.24) + 4.23(\pm 0.13)Al_{\text{TOT}} \quad r^2=0.99$$

Blundy and Holland (1990) critically review these early methods and suggest they are "subject to appreciable uncertainty and commonly fail to produce reliable results" (see also Barnes, 1987). From both new and published experimental studies of amphibole stability they conclude the Al^{iv} content of amphibole co-existing with plagioclase in silica saturated rocks to be a function of temperature and propose the relationship:

$$T = \frac{0.677P - 48.98 + Y}{-0.0429 - 0.008314 \ln K}$$

where Si= number of atoms per formula unit in amphiboles
 Y represents plagioclase non-ideality from DQF¹⁷
 P in kbar T in °K $K = \frac{Si-4}{8-Si}$

with which they obtain apparently quite good estimates of temperature (assuming a prior knowledge of pressure) for both greenschist to granulite facies metamorphic rocks and a variety of igneous rocks. They report their thermometer as having a sensitivity of $\pm 75^\circ\text{C}$ for the temperature of equilibration for hornblende-plagioclase pairs in rocks equilibrated in the range 500-1100°C, where plagioclase is less calcic than An_{92} and amphibole containing less than 7.8 Si atoms p.f.u.

PHASE RELATIONS

Co-existing and intergrown calcic amphiboles have been widely reported in the literature (Cooper, 1972; Graham, 1974; Hietanen, 1974; Misch and Rice, 1975; Sampson and Fawcett, 1977; Grapes *et al.*, 1977; Allen and Goldie, 1978; Laird and Albee, 1981; Kimball, 1988; Smelik *et al.*, (submitted)) and much discussion has focussed on evidence for miscibility within the amphibole solid solution series' as a whole. Whilst it has been clearly established that a miscibility gap exists between monoclinic and orthorhombic amphiboles through

¹⁷ DQF-Darken's Quadratic Formalism; Y=0 for $X_{Ab} > 0.5$.

investigation of exsolution lamellae of cummingtonite or grunerite in hornblende and gedrite in anthophyllite (Ross *et al.*, 1969; Robinson *et al.*, 1969; Stout, 1972; Gittos *et al.*, 1974, 1976; Harrison and FitzGerald, 1986), far less information is available on the relationships amongst the calcic amphiboles. A compositional miscibility gap between actinolite and hornblende has been suggested by many authors (Hallimond, 1943; Klein, 1969; Cooper and Lovering, 1970; Brady, 1974; Misch and Rice, 1975; Oba, 1980; Oba and Yogi, 1987). However, studies by Graham (1974), Grapes (1975), Grapes and Graham (1978), Moody *et al.* (1983) and Jenkins (1988), favour the explanation of such gaps as being related to rapid but continuous amphibole compositional changes combined with abrupt mineral reactions associated with the actinolite-hornblende transition. The review by Grapes and Graham (1978) provides an excellent, unbiased discussion of the arguments both for and against the presence of any miscibility gap and suggests that only evidence of either exsolution or co-existing, homogeneous grains of actinolite/hornblende will suffice in attempts to confirm its existence. To date only the study of Klein (1969) has reported the presence of homogeneous grains of both hornblende and actinolite within the same rock, whether this is the result of particularly unusual P-T conditions or reflects the presence of a true solvus remains to be resolved (Grapes and Graham, 1978).

Smelik, Nyman and Veblen (submitted to *Am.Mineral.*) report finding pervasive actinolitic lamellae with host hornblendes. Their T.E.M./A.E.M. study distinguishes a fine-scale, tweed-textured exsolution microstructure composed of 5-15 μ m. thick lamellae almost parallel to (132) and ($\bar{1}\bar{3}2$). These results and those of Klein (1969) are the most convincing evidence for a crystal-chemically controlled miscibility gap presented thus far.

Of particular interest to this study due to their relationship with hydrothermal solutions, are reports of co-existing and variably zoned amphiboles associated with porphyry-copper mineralization (Czamanske and Wones, 1973; Mason, 1978; Chivas, 1981; Hendry *et al.*, 1985; Pe-Piper, 1988). In all of these investigations the amphiboles are reported as displaying irregular core to rim zoning (although outermost rims of some crystals were more often actinolitic hornblende). Most amphiboles contained patchy compositional domains ranging from hornblende to actinolite. Chivas (1981) and Hendry *et al.* (1985) interpreted the actinolitic hornblende as having crystallised under subsolidus conditions in the presence of a fluid. Chivas (1978, 1981) clearly showed actinolite to occur as a hydrothermal alteration product.

2.2.4. AMPHIBOLE DEFORMATION AND RECRYSTALLISATION MECHANISMS.

Amphiboles are in general rather poorly documented in terms of both their mechanical behaviour and recrystallisation phenomena. The few experimental studies made to date have largely focussed on characterising deformation mechanisms within experimentally deformed hornblendes (Dollinger and Blacic, 1975; Rooney, Riecker and Ross, 1970; Rooney, Riecker and Gavaski, 1975; Morrison-Smith, 1976). These studies suggest mechanical twinning on (101) to be the most common mode of deformation. Rooney, Riecker and Gavaski (1975) report that twinning is not present above 800°C (at any pressure); Morrison-Smith (1976) observes that they contain high proportions of dislocation densities. Dollinger and Blacic (1975), Rooney, Riecker and Gavaski (1975) and Morrison-Smith (1976) all conclude a major slip system to be active along (100)[001]. Dollinger and Blacic (*op.cit.*) suggest this glide results in a clustering of kink bands about [001].

Twinning on (101) has not been reported in naturally deformed monoclinic amphiboles except in those situations characterised by very high strain rates (Chao, 1967). Biermann (1981) reports (100) deformation and growth twins from naturally deformed hornblende crystals. Carter and Raleigh (1969) observed that amphiboles in tectonites rarely displayed signs of plastic deformation. Brodie and Rutter (1985) examined amphibolites from the Ivrea Zone, Northern Italy using a T.E.M. They discovered dislocations to play an important role in amphibole deformation; walls, stacks and dissociated dislocations were distinguished, often forming sub-grains suggesting dynamic recrystallisation via sub-grain rotation. Cumbest *et al.* (1989) describe mylonitic amphibolites from Norway which also exhibit microstructures characteristic of dynamic recrystallisation. Brittle failure has been observed in some situations (Rooney *et al.*, 1974), this probably reflecting lower temperature strain accommodation (Brodie and Rutter, 1985).

CHAPTER 3. TECHNIQUES

This chapter describes the analytical procedures and techniques used to gather information presented in the subsequent chapters of this thesis.

3.1.1. TRANSMITTED LIGHT

Petrographic observations were made using a James Swift optical microscope with dual reflected and transmitted light facilities. A 10mm/100 part graticule inserted into the righthand eyepiece enabled accurate grain-size determinations to be made. Modal abundances were made by visual estimation during microscopic observations using charts of modal proportions in Best (1982).

3.2. CHEMICAL PETROGRAPHY

3.2.1. ELECTRON MICROPROBE

Geochemical analyses of major and minor element concentrations within all rock-forming phases were made using Edinburgh University's Cameca Camebax Electron Microprobe equipped with both a four-spectrometer wavelength-dispersive system and an energy-dispersive system. Operating conditions were maintained at an accelerating voltage of 20kV and a beam current of approximately 20nA. An average beam-size of $\approx 1\text{-}2\mu\text{m}$ was used in all spot analyses. Counts for F, Na, Mg, Al, Si, K, Ca, Ti, Fe, Mn and Cr were collected for 30 seconds (at peak positions) and 15 seconds (at background positions), corrections to weight percent oxides being made via the on-line ZAF-correction procedure¹⁸ (see Sweatman & Long, 1969 or Reed, 1975 for further details). All four spectrometers were used to minimise the overall analysis-time; 4 crystals: 2 TAP's, 1 PET and 1 LiF enabled all 11 elements to be measured and corrected within 5 minutes. A list of crystals, elements and standards is given in the following table.

¹⁸ PAP correction procedure installed in 1990.

ELEMENTS, STANDARDS AND CRYSTALS

ELEMENT	LINE	PEAK POSN	MINERAL STANDARD	CRYSTAL*	B-G OFFSET
F	K α	71258	MAGNESIUM FLUORIDE	TAP	750
Na	K α	46344	JADEITE	TAP	750
Mg	K α	38496	PERICLASE	TAP	1250
Al	K α	32465	CORUNDUM	TAP	750
Si	K α	27750	WOLLASTONITE	TAP	750
K	K α	42693	ORTHOCLASE	PET	1000
Ca	K α	38374	WOLLASTONITE	PET	750
Ti	K α	31407	RUTILE	PET	1000
Fe	K α	48092	METAL	LiF	1000
Mn	K α	52197	METAL	LiF	1000
Cr	K α	56863	METAL	LiF	1000

* TAP-THALLIUM HYDROGEN (ACID) PHTHALATE PET-PENTA-ERYTHRITOL LiF-LITHIUM FLUORIDE.

The detection and precision limits for each oxide vary slightly from phase to phase, the following table summarises these values based on representative analyses of amphibole, plagioclase, pyroxene and biotite compositions.

MINERAL DETECTION AND PRECISION LIMITS

ELEMENT	AMPHIBOLE		PLAGIOCLASE		PYROXENE		BIOTITE	
	D.L. wt%	σ	D.L.	σ	D.L.	σ	D.L.	σ
F	0.22	0.11	-	-	-	-	0.23	0.12
Na	0.03	0.03	0.03	0.05	0.03	0.02	0.03	0.02
Mg	0.02	0.06	0.02	0.01	0.02	0.06	0.02	0.06
Al	0.02	0.05	0.02	0.07	0.02	0.02	0.02	0.06
Si	0.03	0.10	0.03	0.11	0.03	0.10	0.03	0.09
K	0.02	0.02	0.01	0.01	-	-	0.02	0.05
Ca	0.02	0.05	0.02	0.05	0.02	0.07	0.02	0.01
Ti	0.02	0.02	0.02	0.01	0.02	0.01	0.02	0.03
Fe	0.03	0.09	0.03	0.02	0.03	0.07	0.03	0.10
Mn	0.03	0.02	-	-	0.03	0.02	0.03	0.02
Cr	0.03	0.02	-	-	0.03	0.02	0.03	0.02

DETECTION LIMIT (D.L.) = $3/m\sqrt{[R_b/T_b]}$

m- counts above background ($S^{-1}wt\%^{-1}$)

R_b - background count rate (S^{-1})

T_b - time on background (S^{-1})

PRECISION LIMIT $\sigma^* = 100/(\sqrt{T_p}[\sqrt{R_p}-\sqrt{R_b}]) \%$

T_p - time on peak (S^{-1})

R_p - peak counts (sec)

R_b - background counts (sec)

* expressed as a percentage of the weight percent oxide

Closely-spaced (1-40 μm .) fully automated analytical traverses were utilised to document elemental variation across individual crystals. These, in addition to individual spot analyses, enabled a data-base in excess of 10,000 analyses to be obtained. Plagioclase and pyroxene analyses were recalculated into cation proportions on the anhydrous basis of 8 and 6 oxygens per formula unit (p.f.u.) respectively; biotite and amphibole on the anhydrous basis of 22 and 23 oxygens p.f.u. The amphiboles have additionally been subjected to more rigorous recalculation procedures which were outlined in chapter 2.

The great majority of detailed electron-microprobe traverses made were performed with step-intervals of *c.*5-10 μm . This enabled any chemical differences to be documented relatively rapidly. Additionally the spacing of analysis points was sufficiently great to prevent incremental overlap occurring between successive points. Once the types of secondary amphibole and their interfaces against their host hornblende crystals had been more fully characterised closer-spaced traverses (*c.*1-2 μm .) were performed. Since the microprobe beam-size averages \sim 1-2 μm . it is likely that successive analysis points did overlap to a certain extent resulting in a spatial averaging of the concentration profile across the interface between the original and secondary amphiboles. The true nature of the interface (i.e. gradual/abrupt) was determined from B.S.E. images.

3.2.2. BACK-SCATTERED-ELECTRON IMAGERY

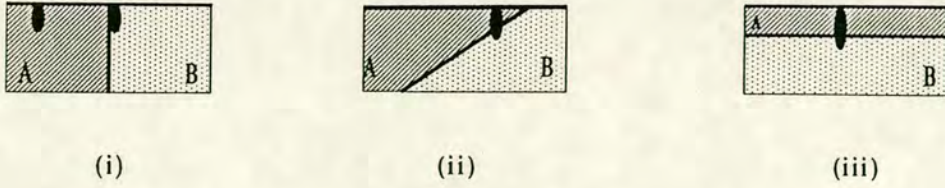
Variations in mean atomic number (*Z*) within compositionally zoned crystals may be imaged with a cathode ray tube (C.R.T.) attached to either a scanning electron microscope (S.E.M.) or conventional electron microprobe. A beam of electrons emitted from an electron gun focus' at a point on the sample surface where they interact with a discrete pear-shaped volume of the sample generating a number of different emission signals (Lloyd, 1987). Inelastic electrostatic interactions between the primary electrons and the specimen result in secondary electron emissions; it is these which are used to produce 'topographical' images of rough surfaces, such as fossils within limestones, with which most geologists are familiar. Predominantly elastic interactions, however, result in "backscattered electron emissions" (B.S.E.) from 'within' the specimen which have the potential of providing images reflecting both composition and crystal structure (Lloyd, 1987). This composition-variation imagery technique has been used to great effect in this study and it is this aspect of B.S.E. emission

and detection with which further discussion is concerned. Fuller details of these along with other aspects of B.S.E. techniques are reviewed by Lloyd (1987).

The highest quality B.S.E. images are obtained from flat specimens, thus it is imperative to ensure that all samples have been highly polished either through conventional electron microprobe preparation processes or by syton polishing (where continual mechanical abrasion in a silica slurry removes layers of atoms until a sufficient polish has developed). Samples should then be thoroughly washed before being carbon coated and loaded into the specimen chamber. The fraction (η) of incident electrons which reappear as B.S.E. depends, in this instance, on the specimen's mean atomic number (Z). The Z -contrast image is generated from a synchronization of C.R.T. scans with the passage of the electron beam over the specimen, in this way each point on the specimen will correspond to a pixel on the C.R.T. screen. The intensity of the image is governed by the number of electrons emitted at each point and the contrast is a function of the difference in intensity from pixel to pixel (Lloyd, 1987). In homogeneous grains Z will be constant and the resulting image will comprise a uniform intensity with no contrast. In both polyphase and heterogeneous grains, however, there will be a variation in Z , in these cases areas with higher Z 's will reflect more electrons and hence appear brighter (Lloyd and Hall, 1981). An increased Z will increase the energy of the B.S.E., decrease the volume of the interacted region and thereby provide better spatial resolutions. Hall and Lloyd (1981) were able to detect contrasts as low as $0.1Z$. Lloyd (1987) suggests that it is possible to resolve variations of $0.01Z$.

An important consideration in such studies is the nature of the contact between adjacent grains. Beam penetrations are generally shallow, being approximately on the order of atomic lattice widths. Most images thus supply direct information upon any Z variations at the surfaces of specific grains. Complications such as inclined contacts, hidden underlying phases or emissions from a volume incorporating adjacent phases, may all result in B.S.E. patterns which reflect emissions from more than one source (see figure below, from Lloyd, 1987). It is important to combine all B.S.E examinations with detailed optical observations in order to establish the extent to which any of these situations apply. In this study most images obtained were from grains which had already been extensively characterised both optically and chemically, ^{and,} except for one particular rock (E5), few situations were encountered where a visibly altered grain (via B.S.E.) did not prove to represent a true variation in Z .

GRAIN-BOUNDARY EFFECTS IN B.S.E. IMAGES



● = Interacted volume

- (i) Interacted volume isolated within phase 'A' generates B.S.E.'s reflecting Z contrast. Interacted volume overlapping phases 'A' and 'B' produces an image representing emissions from both phases.
- (ii) Inclined phase boundary's results in combined emissions from phases 'A' and 'B'.
- (iii) Interacted volume penetrates the thin layer of phase 'A' generating additional B.S.E.'s from underlying phase 'B'.

Most imaging was carried out using a combination of Edinburgh University's Cambridge Stereoscan 250S S.E.M. (based in the Botany department) and a C.R.T. attachment to the Camebax Electron Microprobe. In order to be sure that maximum Z-contrast resolution was being achieved several of the most discretely zoned samples were re-examined using Leeds University's high resolution Cambridge Camscan Instrument. The author was satisfied that all three machines were capable of resolving the Z variations present. Considerable time was spent optimising the optical resolution of each machine. Variations in the acceleration voltage, beam size and beam current control the depth of penetration, size and shape of the interacted volume. Once these have been optimised maximum Z-contrast, *may* in some instances, be improved by varying the distance between the B.S.E. detector and the sample (the working distance, W.D.). Shorter W.D.'s of ≈ 10 mm. (obtained on the Leeds S.E.M.) were not found to significantly improve resolution in this study, and as a result most observations were made at 20mm.

In this study maximum sensitivity was achieved working with the operating conditions summarised in the following table:

COMPARISON OF OPERATING CONDITIONS

CATHODE	BEAM-SIZE	ACCN VOLTAGE	BEAM CURRENT	WORKING DISTANCE
Camscan				
tungsten	≈1μm	20-25kV	3-6nA	10-20mm
250S				
tungsten	size 3-5	15-20kV	≈4nA	17-20mm
Camebax				
tungsten	≈1μm	20kV	20nA	c. 10mm

In order to visualise the often subtle Z variations occurring within the amphiboles ($\geq 0.1-0.2 Z$) it was necessary to bias the contrast and intensity settings to such an extent that most other phases (i.e. plagioclase, biotite and pyroxene) were 'blackened-out' (Plate 14a). The resulting images predominantly reflect Mg-Fe and Al-Si variation within the amphiboles. Figure 3.1 displays a typical situation; here the darker, lower Z rim correlates chemically with an increase in Mg/Si and decrease in Fe/Al concentrations. The use of such extreme contrasts makes observations at grain edges particularly difficult. Here, in addition to any grain-boundary effect, there is a tendency for a 'shadow' effect to occur; the blackened phase (feldspar) results in a 'diffuse' edge to the brighter (higher Z) phase (amphibole) particularly where grain edges are aligned 90° to the C.R.T. scan direction (compare Plate 14a & b). In order not to misinterpret such effects as true diffusely zoned edges (or to over-estimate the width of a zone) it is necessary to image the grain edge in several orientations; both parallel to and at 90° to the scan direction. If the edge is zoned the Z-pattern should be distinguishable in both situations. A similar effect may be observed adjacent to grains which are opaque in transmitted light (appearing as white, bright grains in B.S.E. images due to their high Z); here if the contrast setting is very high a blurr of 'white' will occur, again in an orientation depending on the scan direction (Plate 14c). These shadow and blurring effects seem to be particularly problematic whilst working at high contrasts; they can be minimised through image integration (discussed below). Both the Cameca C.R.T. and Leeds Camscan S.E.M. displayed some blurring adjacent to opaques; this was minimised by working at slightly lower contrasts and enhancing the image (see discussion below). The Cambridge 250S seemed to be largely unaffected by such problems. In all cases it is possible to distinguish between any 'edge effects' and true Z-variations through careful B.S.E. investigation combined with detailed optical and chemical information.

Both the Leeds S.E.M. and Camebax C.R.T. have 'image enhancers' which enable parts of the B.S.E. signal to be preferentially treated at the expense of the rest (Lloyd, 1987). Edinburgh's Camebax C.R.T. allows image enhancement to be made through an intensity-modulation (γ correction) process. The Leeds Camscan framestore and image processor enables the C.R.T. signal-noise ratio to be considerably improved by integrating superimposed images over several minutes. A similar enhancer is available within the Links An10000 image analyser attached to Edinburgh's Cameca Microprobe (here it is known as the "electron signal processing (esp)" facility). Images downloaded from the C.R.T. may be integrated and further "improved" by colour-enhancement within 'digipad'. In colour-enhanced images bright, high Z areas of normal B.S.E. studies are represented by pale colours near the "blue" end (ultimately white) of the colour spectrum, whilst lower Z areas appear increasingly "red", ultimately black.

3.2.3. ION MICROPROBE

Trace and rare-earth-element measurements were carried out using Edinburgh University's Cameca Ims-4F Ion Microprobe. A primary beam of ^{16}O ions with beam diameter averaging approximately 15-20 μm . and current of ~2-10nA were accelerated across a voltage of 10kV within the primary column to impact the specimen and generate positive secondary ions. These secondary ions are accelerated along a secondary column, through an energy sector and into a mass spectrometer where they are separated ideally into individual ions. An estimate of the proportion of each ion species emitted may then be determined using either an electron-multiplier (<10⁶ counts per second) or faraday cup (>10⁴ counts per second) detection system. It is imperative to ensure the primary and secondary columns have been accurately aligned and the instrument is 'on mass' before low mass resolution measurements may be made.

Specially prepared 1" round ion-probe slides were gold coated and loaded into the sample chamber. Working with an energy offset of 75-77 volts, mass surveys, spot analyses and automatic step-scans were performed upon specific amphibole grains which had already been extensively investigated optically using a microscope and geochemically using the electron-probe. Since standards were not used only the relative trace-element variations within individual crystals were obtained. Counts for ^{26}Mg , ^{27}Al , ^{30}Si , ^{39}K , ^{47}Ti , ^{56}Fe , ^{85}Rb & ^{87}Rb , ^{88}Sr , ^{89}Y , ^{90}Zr , ^{93}Nb , ^{138}Ba , ^{139}La , ^{140}Ce , ^{142}Nd & ^{146}Nd , ^{149}Sm & ^{152}Sm and ^{151}Eu & ^{153}Eu were measured for between 5-15 seconds each; overall analysis time ranging from 20-

30 minutes. Step-scans were performed with step intervals ranging between 2 and 15 μm . (depending on the beam-size); here a 60 second wait time preceded each analysis to enable the beam to burn through the gold-coat at every point.

Edinburgh's Ion-Probe has two imaging facilities; a Scanning Ion Beam Unit and a Resistive Anode Encoder (R.A.E.). The integrated 'Scanning Ion Beam Unit' operates in an identical manner to S.E.M.'s, rastering the primary beam over a small area of the sample's surface generating a pixel for pixel image reflecting variations in ionic concentrations. Resolutions of $\sim 10\mu\text{m}$. can be achieved when working with suitably small beam-sizes. The R.A.E. uses a multiple channel plate to convert ionic concentrations to electronic signals (1 ion $\approx 10^6$ electrons); a digitised image reflecting variations in concentration is obtained. The quality of the image is controlled by the optical configuration of the apparatus; the crispest images are achieved with the smallest apertures. Spatial resolution is in the region of approximately 5 μm . More detailed explanations of S.I.M.S. imagery are given by Elphick *et al.*,(1991).

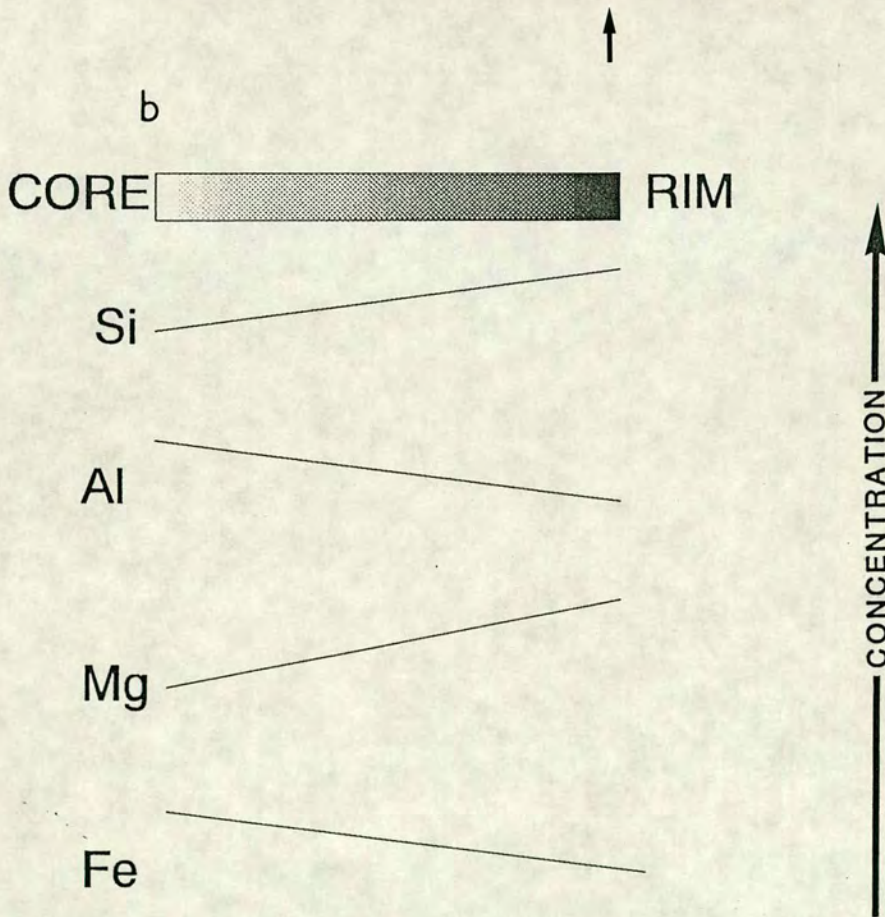
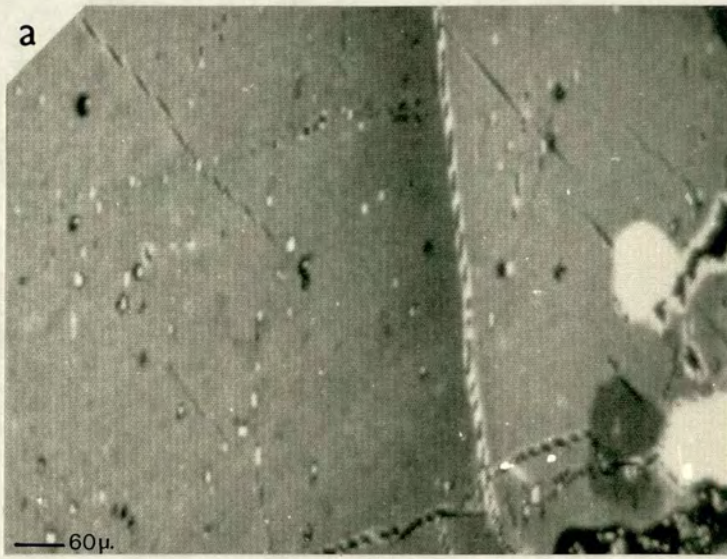


FIG. 3.1.(a) Digitised image of a zoned amphibole grain; pale grey core ($Z \approx 13.3$) contrasts with darker grey rim ($Z \approx 13.1$). (b) Idealised sketch diagram indicating the changes in Si, Al, Mg, Fe concentration producing the core-rim Z variation in (a).

PLATE 14 B.S.E. IMAGERY.

(a) A typical B.S.E. image of a hornblende (grey) with internal secondary amphibole patches visible as darker grey patches (arrowed 1). The hornblende is surrounded by feldspar which has been "blacked out" to throw maximum contrast onto the amphibole.

Note small spots correspond to electron microprobe analysis points.

Compare the locations and widths of the darker-grey patches (arrowed 1) with those of (b).

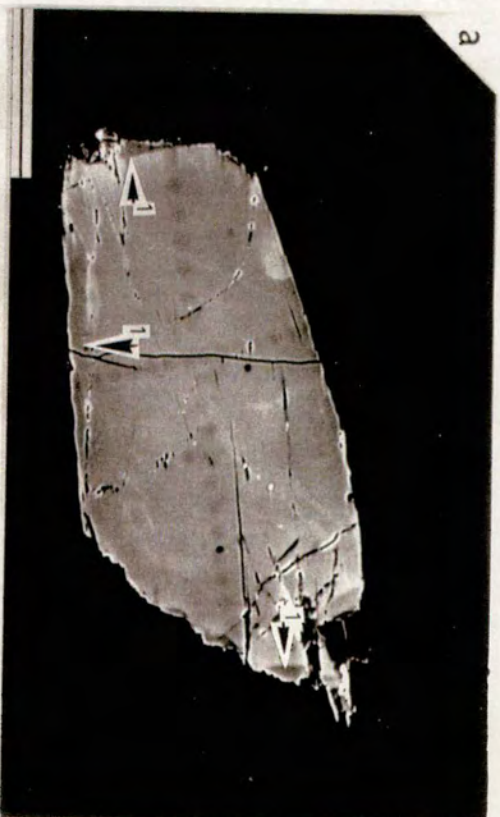
Scan direction from left to right.

(b) B.S.E. image of hornblende grain as (a) but rotated $c.90^\circ$ to illustrate the 'shadow effect' created along amphibole grain edges orientated at 90° to the scan direction of the C.R.T. The secondary amphibole patch indicated by the large arrow in (a) is considerably darker and slightly wider in (b).

Scan direction from left to right.

(c) B.S.E. image of "opaque" grain (white; OP), amphibole (pale grey-white; AM) and darker feldspar (F). A blurr of white can be seen adjacent to the "opaque" (arrow).

All scales: $100\mu\text{m}$.



3.3. ISOTOPIC ANALYSIS

3.3.1. K-Ar AGE DETERMINATIONS FROM MINERAL SEPARATES

THEORETICAL BASIS

There are three naturally occurring isotopes of potassium: ^{39}K (93.2581%), ^{40}K (0.01167%) and ^{41}K (6.7302%). Approximately 11.2% of the ^{40}K atoms decay to ^{40}Ar via electron capture and positron emission; the remaining 88.8% of the ^{40}K atoms decaying to ^{40}Ca by negatron emission (see Faure, 1986 for further details). The branching decay of ^{40}K is expressed:

$$^{40}\text{Ar}^* + ^{40}\text{Ca}^* = ^{40}\text{K}(e^{\lambda t} - 1) \quad (1)$$

where $^{40}\text{Ar}^*$ =radiogenic argon-40
 $^{40}\text{Ca}^*$ =radiogenic calcium-40
 λ =total decay constant for ^{40}K
 t =time in years (*i.e.* age)

the total decay constant (λ) is the product of the decay constants for each branch of the decay *i.e.*:

$$\lambda = \lambda_e + \lambda_\beta \quad (2)$$

where λ =total decay constant for ^{40}K ($5.543 \times 10^{-10}\text{y}^{-1}$)
 λ_e =decay constant for ^{40}K to $^{40}\text{Ar}^*$ ($0.581 \times 10^{-10}\text{y}^{-1}$)
 λ_β =decay constant for ^{40}K to $^{40}\text{Ca}^*$ ($4.962 \times 10^{-10}\text{y}^{-1}$)
 The values of the decay constants quoted are those recommended by the IUGS Subcommission on Geochronology (Steiger and Jager, 1977)

The K-Ar dating technique concentrates upon the decay of ^{40}K to $^{40}\text{Ar}^*$. The decay of ^{40}K to $^{40}\text{Ar}^*$ in a K-bearing rock or mineral can be expressed as follows:

$$^{40}\text{Ar}^* = \frac{\lambda_e}{\lambda} ^{40}\text{K}(e^{\lambda t} - 1) \quad (3)$$

from which an estimate of the age of the rock can be determined by solving in terms of t . The resulting "age equation" is usually expressed as follows:

$$t = \frac{1}{\lambda} \ln \left[\frac{^{40}\text{Ar}^*}{^{40}\text{K}} \left(\frac{\lambda}{\lambda_e} \right) + 1 \right] \quad \text{THE AGE EQUATION} \quad (4)$$

The age of the rock/mineral determined in this way is based on the following assumptions (Faure, 1986):

- 1: No $^{40}\text{Ar}^*$ is present in the mineral at the time of it's formation.

- 2: The mineral became closed to both K and $^{40}\text{Ar}^*$ soon after it's formation. All the radiogenic argon produced by the decay of ^{40}K is thus retained within the mineral and neither K nor Ar have been "lost" since formation.
- 4: No $^{40}\text{Ar}^*$ has been incorporated into the mineral either at the time of it's formation or during a later metamorphic event.
- 5: A correction is made to eliminate atmospheric $^{40}\text{Ar}^*$.
- 6: The concentrations of $^{40}\text{Ar}^*$ and K within the mineral/rock are accurately known.

To date a K-bearing mineral/rock the potassium concentration and $^{40}\text{Ar}^*$ content must be accurately determined. Potassium concentrations may be measured using a variety of different methods of which flame photometry is perhaps the most widely used. Details of this technique are discussed by Dalrymple and Lanphere (1969). The $^{40}\text{Ar}^*$ content of the rock/mineral is most commonly determined using a process known as isotope dilution. "Isotope dilution" involves the mixing of a known amount of argon enriched in ^{38}Ar (known as the "spike") to gasses released from the sample (discussed below). The mixture of spike and sample gasses are admitted to a mass spectrometer where the ratios of $^{40}\text{Ar}/^{38}\text{Ar}$ and $^{38}\text{Ar}/^{36}\text{Ar}$ are measured. The measured value of $^{38}\text{Ar}/^{36}\text{Ar}$ enables a correction to be performed for the presence of atmospheric argon in the sample. Since the ratio of $^{40}\text{Ar}^*/^{38}\text{Ar}$ in the spike is known it is possible to determine the amount of $^{40}\text{Ar}^*$ in the sample (using a complex equation described by Dalrymple and Lanphere, 1969; Faure, 1986).

Once the amount of $^{40}\text{Ar}^*$ and concentration of K have been measured their ratio can be determined using the following equation:

$$\frac{^{40}\text{Ar}^*}{^{40}\text{K}} = \frac{^{40}\text{Ar}(\text{ppm}) (\text{AT.WT.K}) (A)}{\text{K}(\text{ppm}) (\text{AB. } ^{40}\text{K}) (\text{AT.WT.}^{40}\text{Ar})(A)} \quad (5)$$

where $^{40}\text{Ar}(\text{ppm})$ =amount of argon-40 in parts per million
 AT.WT.K=the atomic weight of potassium (39.098304)
 A=Avogadro's number (6.022045×10^{23})
 K(ppm)=the concentration of potassium in parts per million (weight percent $\times 10^4$)
 AB. ^{40}K =abundance of ^{40}K atoms (0.0001167 atoms)
 AT.WT. ^{40}Ar =the atomic weight of argon-40 (39.9623)

Once the ratio of $^{40}\text{Ar}^*:^{40}\text{K}$ is known it can be substituted directly into the age equation (presented above) and thus the absolute age of the mineral/rock can be calculated. Further details of this technique can be found in Faure (1986).

EXPERIMENTAL PROCEDURE

High purity (~99%) hornblende mineral separates were prepared from crushed and carefully sized rock fragments using conventional heavy liquid and magnetic separation techniques (see Figure 3.2). The effect of any stray impurity (largely pyroxene or plagioclase crystals) on the apparent K-Ar age is considered to be negligible.

K-Ar ages were determined by Dave Rex at the K-Ar Laboratory at Leeds University, using the decay constants and isotopic abundances recommended by the I.U.G.S. Subcommittee on Geochronology (Steiger and Jager, 1977). Potassium concentrations were determined from ~0.05g hornblende splits using a Flame Photometer with a Li internal standard. Three solutions of each sample were prepared upon which K concentrations were determined four times (calibration continually checked by comparisons with standard solutions). The coefficient of variation obtained for the K determinations on each sample ranged between 0.2-1%, well within the acceptable standard of accuracy associated with such measurements.

Argon was extracted from 0.14-0.20g fractions of the hornblende separates placed within copper boats and heated by a radio-frequency (RF) source (450 kcycles per second) within a molybdenum crucible. With a silica blank acting as an extra flux the crucible was heated to *c.* 1200°C and the system left to outgas overnight. The argon generated was then purified in a titanium sponge, removing reactive gasses, before it's concentration was measured statistically by the isotope dilution technique in an AEI MS-10 mass spectrometer with ³⁸Ar as spike. A computer program written by Philip Guise (Leeds University) then calculated and corrected the radiogenic argon (⁴⁰Ar*) content using the measured ratios of argon 38:40, 38:36 and 40:36 and the apparent K-Ar age of the sample was obtained.

MINERAL SEPARATION PROCEDURE

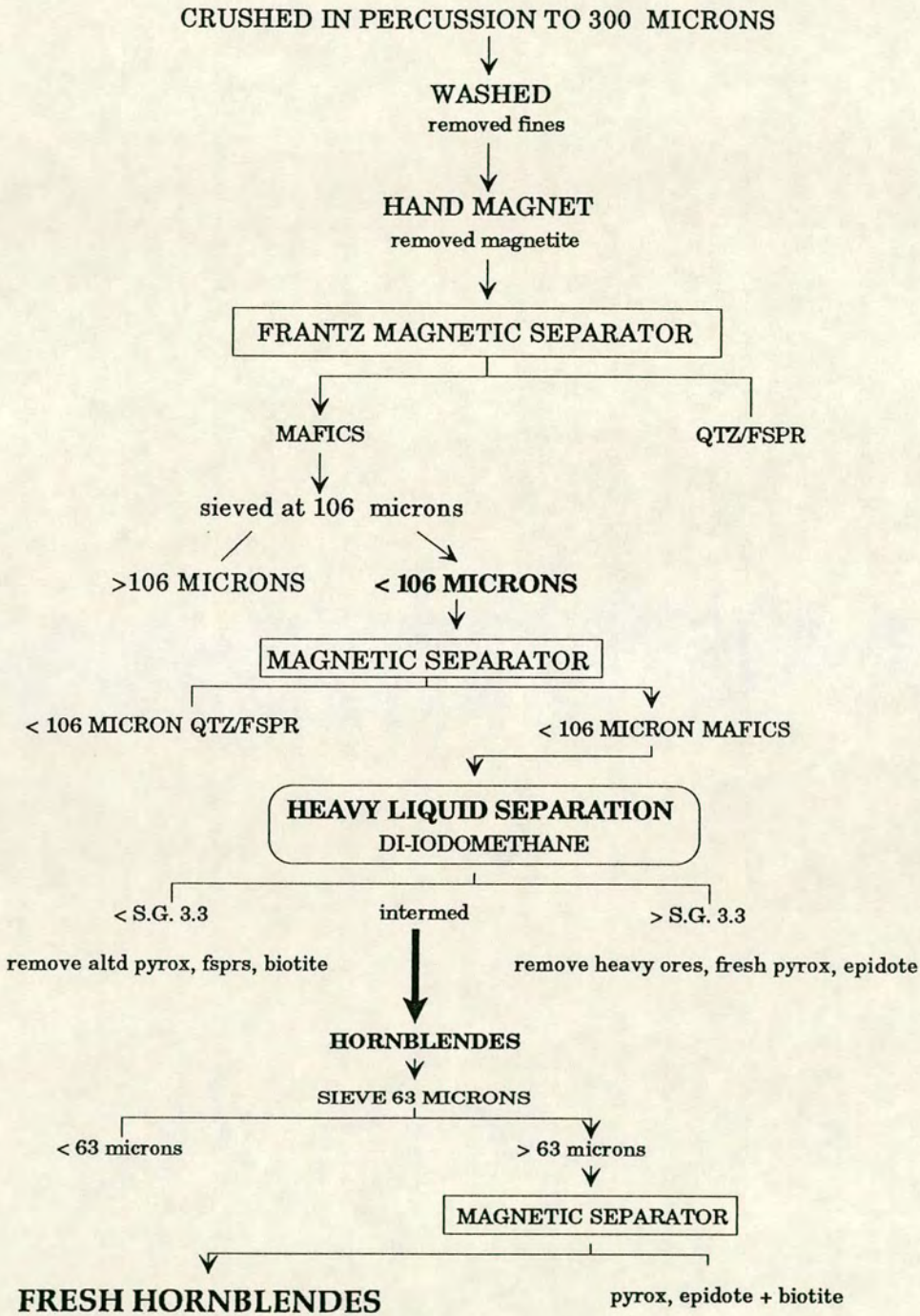


FIG. 3.2. Flow diagram illustrating the various stages involved in producing fresh hornblende separates.

3.3.2. $^{40}\text{Ar}^*/^{39}\text{Ar}$ LASER SPOT AGE DETERMINATIONS

THEORETICAL BASIS

$^{40}\text{Ar}^*$ - ^{39}Ar age determinations are based on the production of ^{39}Ar atoms during the irradiation of K-bearing samples within a nuclear reactor. When a K-bearing sample is bombarded with neutrons in a reactor isotopes of argon (particularly ^{36}Ar , ^{37}Ar , ^{38}Ar and ^{39}Ar) are formed through a combination of radiogenic reactions involving K, Ca and Cl elements within the sample. ^{39}K decays to ^{39}Ar by combined negatron-positron emission. The number of ^{39}Ar atoms formed during the irradiation can be calculated using an equation derived by Mitchell (1968):

$$^{39}\text{Ar} = ^{39}\text{K} \Delta T \int \varphi(\epsilon) \sigma(\epsilon) d\epsilon \quad (6)$$

where ^{39}K =number of ^{39}K atoms in the sample
 ΔT =the irradiation time
 $\varphi(\epsilon)$ =the neutron flux density at energy (ϵ)
 $\sigma(\epsilon)$ =the capture cross-section of ^{39}K for neutrons having energy (ϵ)

The number of radiogenic ^{40}Ar atoms in the sample, resulting from the natural decay of ^{40}K atoms (as discussed in 3.3.1), is given by equation (3). The $^{40}\text{Ar}^*/^{39}\text{Ar}$ ratio is thus obtained by dividing equation (3) by equation (6) resulting in equation (7):

$$\frac{^{40}\text{Ar}^*}{^{39}\text{Ar}} = \frac{\lambda_c}{\lambda} \frac{^{40}\text{K}}{^{39}\text{K} \Delta T} \frac{1 - e^{-\lambda t}}{\int \varphi(\epsilon) \sigma(\epsilon) d\epsilon} \quad (7)$$

To simplify equation (7) a parameter, known as the J value, is introduced. J is defined as:

$$J = \frac{\lambda_c}{\lambda} \frac{^{39}\text{K} \Delta T}{^{40}\text{K}} \int \varphi(\epsilon) \sigma(\epsilon) d\epsilon \quad (8)$$

Substitution of equation (8) into equation (7) gives equation (9):

$$\frac{^{40}\text{Ar}^*}{^{39}\text{Ar}} = \frac{e^{-\lambda t} - 1}{J} \quad (9)$$

To solve equation (9) a value for J must be determined. The easiest way to evaluate J is to irradiate a sample of known age (a "flux monitor") simultaneously with the samples of unknown age. The $^{40}\text{Ar}^*/^{39}\text{Ar}$ ratio of the monitor is measured by mass spectrometry and the J value can be calculated using equation (10):

$$J = \frac{e^{-\lambda t_m} - 1}{^{40}\text{Ar}^*/^{39}\text{Ar}} \quad (10)$$

where t_m = the known age of the flux monitor
 $^{40}\text{Ar}^*/^{39}\text{Ar}$ = the measured $^{40}\text{Ar}^*/^{39}\text{Ar}$ ratio of the monitor

To determine the age of a sample its $^{40}\text{Ar}^*/^{39}\text{Ar}$ ratio is measured in a mass spectrometer. Assuming:

- 1: Ar has not been either lost or incorporated into the mineral since formation.
- 2: All ^{40}Ar in the sample is either atmospheric or radiogenic
- 3: All ^{36}Ar is atmospheric
- 4: ^{39}Ar is produced only by the reaction $^{39}\text{K}(n,p)^{39}\text{Ar}$.

then the ratio between $^{40}\text{Ar}^*$ and ^{39}Ar is given by equation (11):

$$\frac{^{40}\text{Ar}^*}{^{39}\text{Ar}} = \left(\frac{^{40}\text{Ar}}{^{39}\text{Ar}} \right)_m - 295.5 \left(\frac{^{36}\text{Ar}}{^{39}\text{Ar}} \right)_m \quad (11)$$

where m = measured values
 $295.5 = ^{40}\text{Ar}^* : ^{36}\text{Ar}$ ratio of atmospheric argon

The age of the sample can then be calculated using equation (12):

$$t = \frac{1}{\lambda} \ln \left(\frac{^{40}\text{Ar}^*}{^{39}\text{Ar}} J + 1 \right) \quad (12)$$

The dates obtained in this way are referred to as "total argon release ages".

In most instances the argon isotopes present in the sample (i.e. ^{36}Ar , ^{37}Ar , ^{38}Ar and ^{39}Ar) are the combined result of the radioactive decay of naturally occurring isotopes of Ca, K and Cl within each sample. A table depicting the relevant element types, their isotopes and the Ar isotopes they produce as a result of their radioactive decays is given below. Some of the argon isotopes produced are themselves unstable and decay further; these are also shown in the table.

CALCIUM, POTASSIUM, CHLORINE AND ARGON DECAYS PRODUCED DURING
IRRADIATION OF K-BEARING SAMPLES.

ARGON PRODUCED	CALCIUM	POTASSIUM	ARGON	CHLORINE
^{36}Ar	^{40}Ca	-	-	-
^{37}Ar	^{40}Ca	^{39}K	^{36}Ar	-
^{38}Ar	^{42}Ca	^{39}K ^{41}K	^{40}Ar	^{37}Cl
^{39}Ar	^{42}Ca ^{43}Ca	^{39}K ^{40}K	^{38}Ar ^{40}Ar	-
^{40}Ar	^{43}Ca ^{44}Ca	^{40}K ^{41}K	-	-

modified from Faure, 1986

To obtain the precise age of the sample it is necessary to perform a series of corrections for each of the interfering reactions. Detailed discussions of these corrections are given by Dalrymple and Lanphere (1971) and an outline of some of the more important interfering reactions is given in Faure (1986).

TYPES OF $^{40}\text{Ar}^*/^{39}\text{Ar}$ ANALYSIS

There are two principle methods by which the $^{40}\text{Ar}^*/^{39}\text{Ar}$ age of a sample can be determined

- (i) The incremental or step heating technique
- (ii) Laser microprobe analysis.

In step heating experiments, measurements of the $^{40}\text{Ar}^*/^{39}\text{Ar}$ ratios of *multi-crystal* samples are obtained for argon released over a range of successively increasing temperatures. If the sample has ^{not} been disturbed since 'closure'/initial cooling the $^{40}\text{Ar}^*/^{39}\text{Ar}$ ratios calculated at each temperature interval should be constant. If the sample has been disturbed by, for example, a re-heating event, and argon loss has taken place from some sites within the individual crystals the $^{40}\text{Ar}^*/^{39}\text{Ar}$ ratios of the gas released at different temperatures may be different. Step heating analysis has not been performed during this research.

Laser microprobe analysis utilises a finely focussed laser beam to release gasses from small selected volumes within *individual mineral grains*. Both pulsed and continuous-type laser beams can be used to volatilise certain parts of mineral grains enabling the argon released to be measured in a mass spectrometer. The new $^{40}\text{Ar}^*/^{39}\text{Ar}$ information presented in this thesis was obtained using laser microprobe techniques which are discussed in detail below.

LASER MICROPROBE ANALYSIS: EXPERIMENTAL PROCEDURE

Seven doubly polished rock slivers with an average size of $\sim 14 \times 14 \times 0.1$ mm. were made from the same seven rocks from which the hornblende separates were obtained. Each sample was thoroughly investigated using B.S.E. imagery techniques; amphibole alterations were again clearly distinguishable due to their variations in mean atomic number, as described in section 3.2. Once an appreciation of the type (see chapter 4) and extent of the amphibole alterations within each sample had been gained, between three and nine areas within each rock were selected and a series of B.S.E. photographic collage maps were made (Plate 15a & b). Where possible areas containing both

altered and unaltered amphibole grains were selected. The same areas were then re-photographed in PPL and a similar set of photographic maps were produced. The thickness of the slivers meant optical recognition of the amphibole alterations was not possible and as a result no extensive optical investigations were made. The original rock chips used to produce the doubly polished slivers were those from which the thin-sections were made and it seems reasonable to assume that at least broad comparisons can be made between the two. Both B.S.E. and PPL photographic maps were used to relocate the specific areas within the samples once they had been loaded into the sample chamber; B.S.E. maps were essential when it came to positioning the beam on certain zones within individual amphibole grains.

The rock slivers were then ultrasonically washed in methanol, wrapped in aluminium foil and irradiated in the core of the Herald Reactor A.W.R.E. Aldermaston. The samples were irradiated for ~6 hours with a total reactor flux of $\sim 10^{17} \text{ncm}^{-2}$. Flux levels were monitored using the Hb3gr hornblende standard (Roddick, 1983); J values were calculated to be ~ 0.003 . The samples were left to cool for a period of approximately 5 months before analysis took place.

Laser 'spot' dates were obtained on amphibole, biotite and plagioclase feldspar grains within the rock slivers by Dr. R. Burgess at the Laser Microprobe Laboratory, Scottish Universities Research and Reactor Centre (S.U.R.R.C.), East Kilbride. Laser extractions were performed by narrowly focusing a pulsed Nd-YAG laser beam (wavelength $\sim 1\mu\text{m}$.) at the required point on the specimen and volatilizing a small volume of the mineral grain. The exact volumes volatilized are not known. However, studies performed by Lee *et al.* (1990) suggest the volumes to be no greater than the diameter of the pits. The Nd-YAG laser beam was accurately centred and focused using a companion He-Ne laser beam; the working Nd-YAG laser beam diameter was approximately $20\mu\text{m}$. and the resulting extraction pit sizes ranged between 50μ and $100\mu\text{m}$. The gases evolved were purified in a Zr/Al SAES GP10 getter run at 400°C ; reactive gases were removed over a time interval of ~ 5 minutes and the remaining inert gases were then admitted into a Mass Analyser Products 215 mass spectrometer equipped with an electron multiplier detector. Argon isotope peaks 35-41 inclusive were measured by magnetically controlled peak switching operated by an online computer. Argon peak scans were repeated 11 times for each individual analysis; the overall analysis time was approximately 20-25 minutes. The system was continually monitored by performing "blank" analyses after every second sample analysis. A computer program written by Dr. Burgess (S.U.R.R.C.) determined

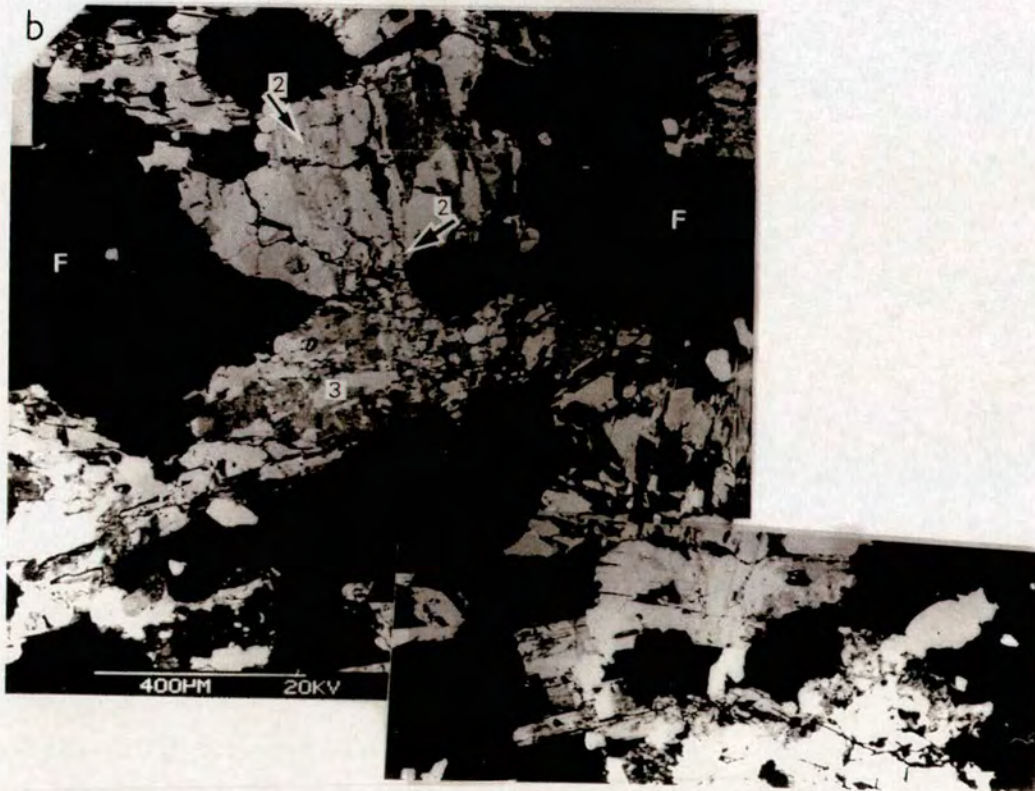
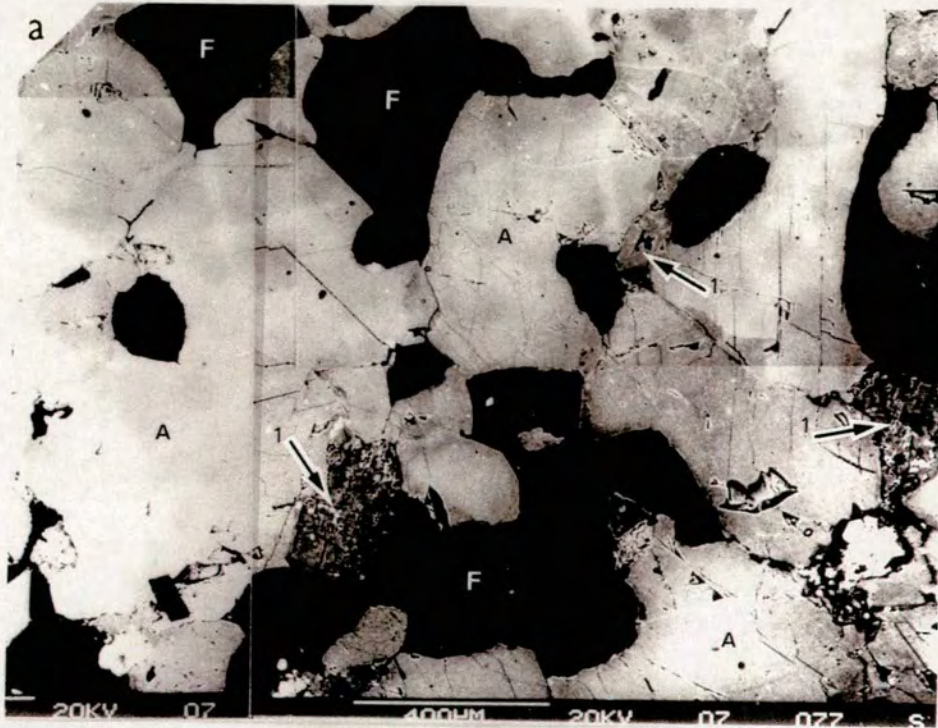
and corrected each peak intensity from which the $^{40}\text{Ar}^*/^{39}\text{Ar}$ age of the spot was obtained. I.U.G.S. decay constants and abundances were used in all calculations.

Electron microprobe analyses of amphibole grains from these rocks indicate the K-concentrations of the unaltered parts of amphibole grains vary between 1 and 1.5wt% and often $\ll 0.5\text{wt}\%$ for altered parts of the grains. Such low K-concentrations were found to produce very small volumes of gas in single laser volatilizations; these would result in gross errors to any ages obtained. In order to generate enough gas to measure with any acceptable degree of accuracy it was necessary to fire several (c.3-10) laser pulses within and/or around the required position.

PLATE 15. LASER PROBE ANALYSIS.

(a) & (b) Low power B.S.E. image collage maps of rock slivers depicting location of secondary amphibole patches and microveins within original amphiboles (pale-dark grey;A). Feldspars (black); opaques (white); pyroxenes (arrowed 1).

Note microveins in (b) (arrowed 2) can be linked to extensive intragranular alterations (3).



CHAPTER 4. PETROGRAPHY AND SPATIAL DISTRIBUTIONS OF MINERAL ALTERATIONS WITHIN THE ELDORA AMPHIBOLITES

This research has concentrated specifically upon the characterisation of amphibole alteration within the Early Gneiss Complex amphibolites of Eldora, Colorado. This chapter outlines the types and distributions of the alteration phenomena observed and considers the wider aspects of their implications in terms of the geological events affecting the amphibolites. In order to establish the overall effect imposed on the country rocks by their geological history reference will additionally be made to alteration occurring within co-existing phases.

4.1. PETROGRAPHY

4.1.1. TERMINOLOGY

This chapter draws on observations made on scales ranging from individual crystals within thin-sections to rock outcrops. It is important therefore to establish a nomenclature which expresses this in a clear, concise manner.

The term "*alteration*" is used here to indicate phenomena which result in the modification of original mineral compositions. This may occur either with or without change in the mineral-type in question. Alterations involving no change in the mineral-type (*e.g.* amphibole-amphibole alterations) can take place either with or without the growth of new crystals. Changes brought about through diffusive processes alone do not involve the growth of new crystals. "*Recrystallisation*" is used in the more restricted sense (as Cox, Price and Harte, 1974) referring to the structural and chemical reconstitution of original grains resulting in the development of new crystals of a similar mineral-type with or without a different optic orientation to that of the host. Alterations which do involve a change in the mineral type can only take place with the growth of new crystals. "*Neomineralisation*" refers to the formation and subsequent growth of nuclei of a chemically and structurally different phase (*e.g.* pyroxene altering to actinolite). "*Crystallisation*" refers to any process of mineral growth (*i.e.* recrystallisation or neomineralisation).

"*Replacement*" occurs when an original mineral has been partially or completely changed to a new composition and/or mineral. With respect to an

original single mineral grain, this term is used to signify part of the volume of an original grain which has been converted to a new phase composition. In contrast to this use of 'replacement' for single crystals, the term "*overgrowth*" refers to situations in which a new mineral growth is added to the surface of a pre-existing phase. Overgrowths thus result in an increase in volume, whereas replacements take place in a way which retains the volume of an original crystal.

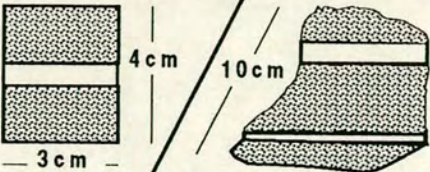
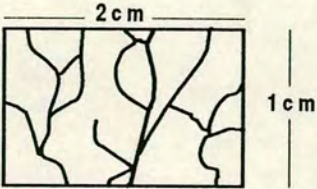
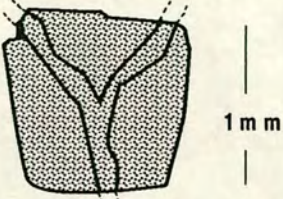
Replacements and overgrowths often involve "*epitaxial growth*" - the orientated growth of one mineral phase in optical continuity with another due to structural similarities between the two phases (Barker, 1990). It is kinetically speaking much easier to modify the existing crystal via such epitaxial growths than by processes involving widespread nucleation; this is extensively shown by the amphibole alterations observed in the Eldora amphibolites.

The term '*microfracture*' has been adopted to describe narrow fractures which are often only clearly visible under the microscope. A '*microvein*' is defined as a narrow vein of material which appears to have filled a microfracture.

Microfractures are often seen to have been rock penetrative *i.e.* their existence may be traced across a series of mineral grains by the presence of fine-cracks, streams of fine inclusions or alteration and/or microveins. Microveins of a particular mineral composition (*e.g.* actinolite) are mostly confined to host mineral grains of similar composition (*e.g.* hornblende), although this is not necessarily always the case. The microfractures themselves are indistinguishable without recognition of their associated wall-rock alteration.

The crystallisation of secondary amphibole material whether it be by replacement, overgrowth or microvein formation, is commonly spatially associated with microfracture patterns. It is important to distinguish microfracture patterns, and the microveins associated with them, from large scale (>1mm.) leucocratic seams which developed during the major regional metamorphism and migmatitisation of PreCambrian age. These seams may be parallel or cross-cutting to the rock foliation.

The following table summarises this information:

term	scale	example
LEUCOCRATIC SEAMS	THIN-SECTION TO ROCK-SCALE	
MICROFRACTURES	THIN-SECTION	
MICROVEINS	THIN-SECTION TO GRAIN-SCALE	

4.1.2. ELDORA ROCK TYPES

The rock types at Eldora have been classified, according to the classification scheme presented in section 1.3.2., as being divisible into four types:-

- (i) Amphibolites
- (ii) Pyroxene Amphibolites
- (iii) Biotite Amphibolites
- (iv) Biotite Pegmatites

The three amphibolite 'facies' are very similar, predominantly being composed of homogeneous intergrowths of fine-medium-grained hornblende prisms and xenoblastic plagioclase with interstitial biotite and/or pyroxene. In the following descriptions the amphibolites are considered together as one group, the variations between each type being indicated where appropriate. The Biotite Pegmatites have been briefly examined petrographically and some preliminary probe work completed, however, this investigation was more a cursory study

rather than an attempt at gaining detailed information. Large (c.1cm. diameter) biotites within the Biotite-Pegmatites were discovered to be very subtly zoned in Na (a change of $\leq 0.2\text{wt}\%$ NaO over a distance of c.1000 μm .) and occasionally Ti ($\leq 0.6\text{wt}\%$ TiO₂ over 500 μm .) and Fe ($\leq 0.7\text{wt}\%$ FeO over 900 μm .). Most flakes are recrystallised along their grain edges. Hart (1964), Steiger and Hart (1967) and Wright (1967) investigated the transition from orthoclase to microcline alkali-feldspars within the Biotite Pegmatites. Hart (1964) reported the change to occur approximately 300m. from the Stock contact. This transition has also been optically identified in thin-section examinations of the pegmatite samples collected by the author, ^{and} takes place between 230 and 280m. from the contact.

The amphibolitic rocks, upon which subsequent research was concentrated, display a marked similarity in texture throughout and beyond the vicinity of the intrusive stock. In order to relate the range of textures and alteration phenomena observed within the amphibolites, four rocks are first described in detail. Although the rocks selected for detailed description are successively closer to the Stock-contact, the types and distributions of the alterations do *not* entirely reflect the proximity of the igneous contact. A summary and suitable terminology for subsequent discussion is established in section 4.2.

4.1.3. DETAILED ROCK DESCRIPTIONS

E52 (663m.)

HAND-SPECIMEN DESCRIPTION

A fine-medium-grained, mesocratic rock composed of homogeneous, granoblastic intergrowths of mafic and feldspar grains with an average grain-size of ~1mm. A solitary (hairline) fracture associated with a greenish discolouration of 1.5mm. width penetrates the specimen (Plate 16a).

THIN-SECTION DESCRIPTION

Selected as representing one of the more pristine of the amphibolites collected, this rock is predominantly composed of sub-idioblastic amphibole and xenoblastic plagioclase with minor pyroxene, magnetite, pyrite, epidote, chlorite and apatite. Though the rock is largely composed of fresh crystals which exhibit many grain-boundaries and triple junctions indicative of textural equilibrium,

several rock penetrative microfractures are also observed adjacent to which the minerals display varying degrees of secondary alteration. The most prominent microfractures run approximately centrally through the thin-section (Plate 16b).

The original amphiboles (c.40-50% mode) occur as pleochroic yellow-green/brown, sub-idioblastic grains ranging in size from 20-1400 μm . in length. The majority of crystals appear very regular, lacking undulose extinction with straight grain boundaries, crisp intragranular cleavage planes and few inclusions. The amphibole grain boundaries are either smooth and clean or rather ragged with patches and fringes of tiny crystals (<1-20 μm) nucleating along their edges (Plate 22c). These tiny crystals have a different optic orientation to the host amphibole and are composed of mixtures of pleochroic dark green/brown biotite, colourless amphibole and irregular, microcrystalline aggregates of secondary epidote (see below). The width of these fringes of new growth varies between ≤ 5 and 80 μm . with many of the crystals actually falling within the thickness of the slide.

More detailed investigations of specific interfaces reveals that amphibole-amphibole interfaces are usually (~95%) rather clean and straight reflecting a gradual approach toward minimum interfacial energy configurations; a small minority (c. 4-5%) are more irregular reflecting the development of the new growth amphibole/biotite fringes. Amphibole-plagioclase interfaces are also characterised by both smooth, even grain-boundaries (c.10%) and more irregular types (c.90%) associated with crystal nucleation; here many of the tiny crystals are epidote (Plate 24d).

Adjacent to the microfractures within the rock (Plate 37) the original yellow-green/brown amphibole grain boundaries display an optical zonation from the original pale-green to a more blue-green colour. Here continuous edges ("rims") and discrete portions ("patches") of some of the amphibole grain boundaries are visibly altered to a blue-green coloured amphibole (Plate 28c). This blue-green coloured amphibole can additionally be observed as intragranular spots, segments and microveins within some original crystals (Plate 27d). In most instances the blue-green coloured amphibole is in optical continuity with and displays a similar birefringence to the host crystal; both extinguish at the same angle (*i.e.* they are epitaxial growths).

PLATE 16 HANDSPECIMEN/ THIN-SECTION PHOTOGRAPHS OF E52

(a) Handspecimen of E52; a penetrative fracture with an alteration haloe c.0.5cm. wide is clearly visible on the cut-rock surface (arrow 1). Note also discrete fracture (arrow 2).

Scale bar: centimetre squares.

(b) Thin-section photograph of E52; a zone of rock penetrative microfractures can just be distinguished (arrowed).

Scale : approximately 2cm. diameter.

THE THIN SECTION ILLUSTRATED COMES FROM A PART OF THE ROCK AWAY FROM THE OBVIOUS FRACTURES SHOWN IN (a).

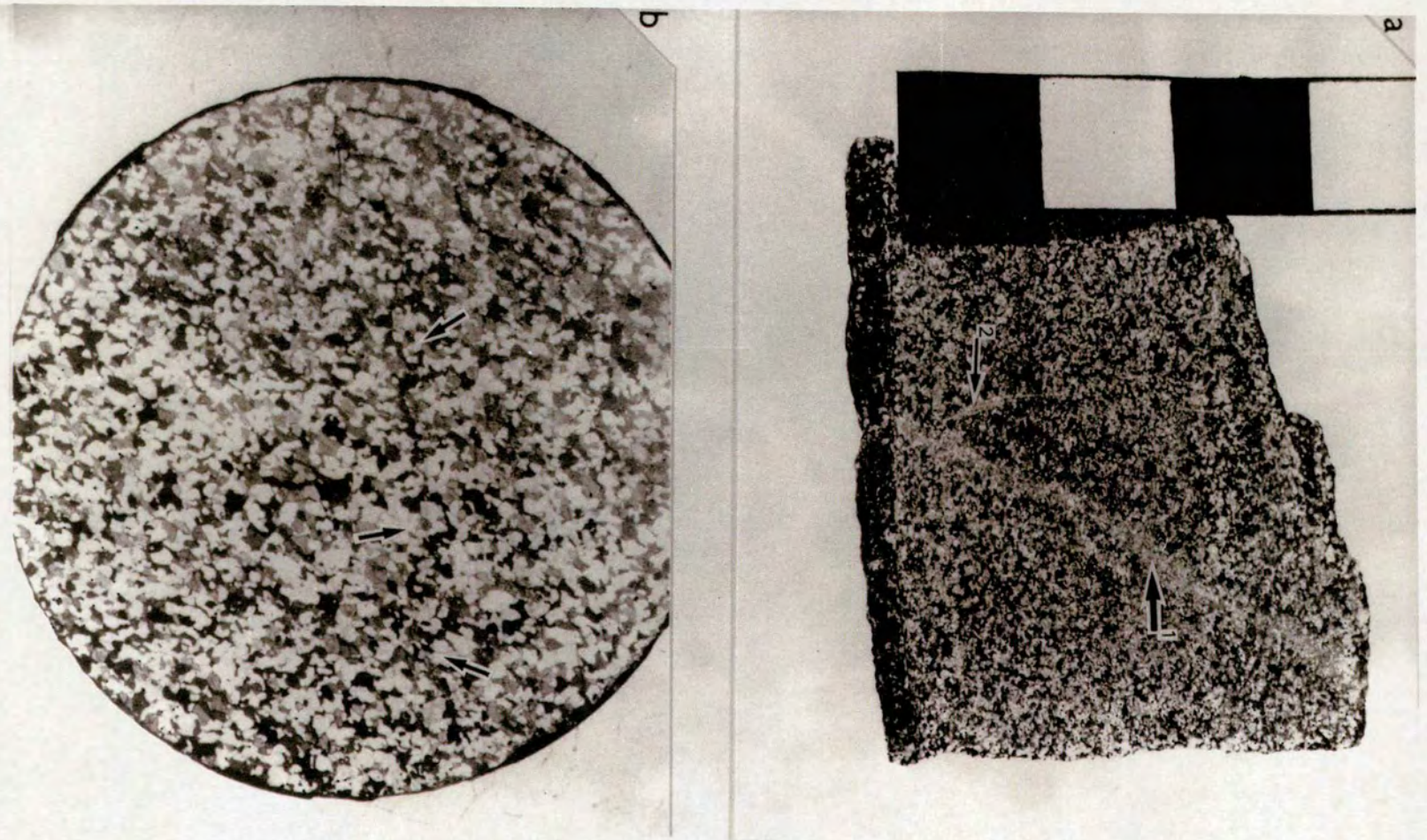


PLATE 16

Interfaces between blue-green coloured amphibole and host grains occur as either continuous or more abrupt colour variations. In many cases no distinct grain-boundary or Becke line is visible between the original yellow-green/brown and blue-green amphibole. Thus the blue-green amphibole does not usually occur as separate grains. Blue-green coloured amphibole patches and rims are sporadically developed along both amphibole-amphibole and amphibole-plagioclase interfaces (in addition to some interfaces associated with other minor phases). They occur along both crisp, straight grain-boundaries and ragged irregular grain-boundaries upon which the new growth nucleation described above has taken place. Although they are variable in size they predominantly appear to be less than 20 μm . in width. Blue-green coloured spots and segments developed within some of the original amphibole crystals (both with and without patches and rims along grain-edges) are occasionally observed adjacent to regions of intragranular cleavage planes/cracks and as irregular portions of some grains. They often coincide with the presence of an increased abundance of inclusions of magnetite and/or pyrite within the host crystal. In places the blue-green coloured alteration and opaque inclusions define discrete microveins which pervade the original amphibole crystal; these either irregularly traverse the crystals linking blue-green spots, segments and opaques to form rather indistinct microveins or they occur as quite sharply bounded, obviously cross-cutting features of *c.*10 μm . width, again associated with an increased abundance of opaque inclusions and tiny opaque specks (Plates 31a and 37b). Many of these blue-green coloured microveins contain small crystals of highly birefringent epidote and some contain larger *c.*200 μm . often elongate inclusions of pyrite, magnetite and feldspar. Trails of tiny inclusions traverse many of the amphiboles. In addition to the blue-green coloured amphibole zonations already described, a small minority of the original amphibole crystals exhibit a pale-green coloured alteration to chlorite; here the altered rim or portion of the original amphibole affected exhibits the low first order, anomalous blue birefringence characteristic of chlorite and a Becke line may often be seen between the chlorite and unaltered amphibole.

The plagioclase feldspars (*c.*30-40% mode) comprise xenoblastic to subidioblastic grains ranging in size from 60-1100 μm . Many crystals appear relatively pristine; in PPL the grains are quite clean colourless and largely featureless crystals. In XPL the first order grey coloured feldspars appear more variable, some crystals exhibit sharp multiple twinning others have either strained, wedge-shaped twins, no twins or combinations of multiple, lamellar twins and strain-induced twins. In both twinned and untwinned situations the

crystals often have weakly-moderately undulose extinctions. The freshest crystals display smooth, lobate-curved feldspar-feldspar grain-boundaries whilst those within the more altered areas of thin-sections may additionally exhibit a brownish coloured alteration with less crisp grain-boundaries along which tiny crystals of epidote or secondary alteration to clay minerals may be observed (Plate 24d). In addition to these grain-boundary alterations some of the feldspars within the more altered areas of the rock display intragranular alterations in the form of either irregularly developed or crack associated patches of clay minerals and/or epidote or as distinct microveins within which clay mineralisation and tiny opaque grains may be observed (Plates 31a and 37b). These microveins can be traced through adjacent feldspars linking with the blue-green amphibole microveins previously described. Discrete colourless inclusion trails are present within some of the feldspars in the altered areas of the rock, the inclusions are largely $<1\mu\text{m}$ in size with ovoid, slightly elongated outlines. Occasionally a tiny bubble is observed suggesting them to be fluid filled. Those within which bubbles are not observed may be either solid inclusions or micropores such as those described within the Klokken Syenites (Worden *et al.*, 1990).

Clinopyroxene (*c.*3-5% mode) is quite difficult to identify in this rock due to its commonly rather altered appearance. Approximately 1% remains unaltered; these have a high relief and a weakly pleochroic green colour. Most grains are xenoblastic, ranging in size from 10-700 μm . with curved grain edges along which tiny crystal fringes similar to those already described can again be observed. Intragranular cracks are quite common and several of the larger crystals exhibit very fine, sub-micron scale exsolution lamellae within their cores. The remaining, *c.*2-4% mode, of the pyroxenes fall within the generally more altered areas of the rock, these are seen in various stages of secondary alteration; most are lightly cleaved with a very pale-yellow-greenish colour in PPL and an abundance of small opaque and colourless inclusions within their cores. Much of the original pyroxene has been replaced by an aggregate of either chlorite and/or blue-green amphibole, however an occasional remnant of the original pyroxene can often still be distinguished within the largely xenoblastic aggregates. Interfaces between altered pyroxene and plagioclase crystals tend to be occupied by microcrystalline aggregates of epidote and those between altered pyroxene and original amphibole can be either sharp and relatively straight both with and without blue-green rims within the amphibole, or less distinct but again with no consistent correlation to the presence of a blue-green amphibole rim/patch.

Epidote (*c.*7-10% mode) occurs as irregular aggregates of pleochroic pale-yellow-green coloured, strongly birefringent (2nd-3rd order) xenoblasts, ranging in size from $<1\mu\text{m}$. crystals nucleating along plagioclase grain-boundaries to 40-400 μm . composite grains (Plate 24d) interstitially scattered throughout the more altered horizons (adjacent to the microfractures) within the rock. The composite epidote masses often incorporate crystals of pyrite, magnetite and chlorite (Plate 37b).

The 'opaques' within the rock appear to have a distinctly bimodal distribution. In fresher areas the opaques are magnetites (*c.*1%) with typical high relief, cubic-octahedral habits and with characteristic brownish-grey, isotropic properties in reflected light. The average grain-size is approximately 100-200 μm . In the more altered areas of the rock there is an increased abundance of opaques (3-5%); these occur as both discrete grains of magnetite and pyrite (white with a yellow tint in reflected light; ranging in size from 20-400 μm .) and as specks (*c.*1 μm .) and inclusions within the other phases. Within these more altered areas the opaques may be seen in both sub-idioblastic to idioblastic (cubic-octahedral) habits and as more xenoblastic crystals; occasionally an elongate pyrite crystal can be seen within a blue-green amphibole microvein. Pyrite grains are often observed within and adjacent to composite epidote masses.

Apatite ($<1\%$ mode) occurs as small (*c.*10-20 μm .), high relief, low birefringence needles and prismatic crystals within both the fresh and more altered areas of the rock. It is not considered to be a product of alteration.

E5 (15m.)

HAND-SPECIMEN DESCRIPTION

A fine-medium-grained, meso-melanocratic, granular rock comprised of a sub-idioblastic, homogeneous groundmass of mafic and feldspar grains. Patches of coarser-grained (*c.*2mm.) quartz and feldspar containing an occasional crystal of epidote, sphene and amphibole are visible on the cut rock surface; these correspond to the presence of a ~1cm. thick leucocratic seam on adjacent surfaces. A hairline fracture, causing clouding of the feldspars and having a slightly greenish halo, penetrates part of the rock. This fracture appears to terminate adjacent to the leucocratic seam (Plate 17a).

PLATE 17 HANDSPECIMEN/THIN-SECTION PHOTOGRAPHS OF E5

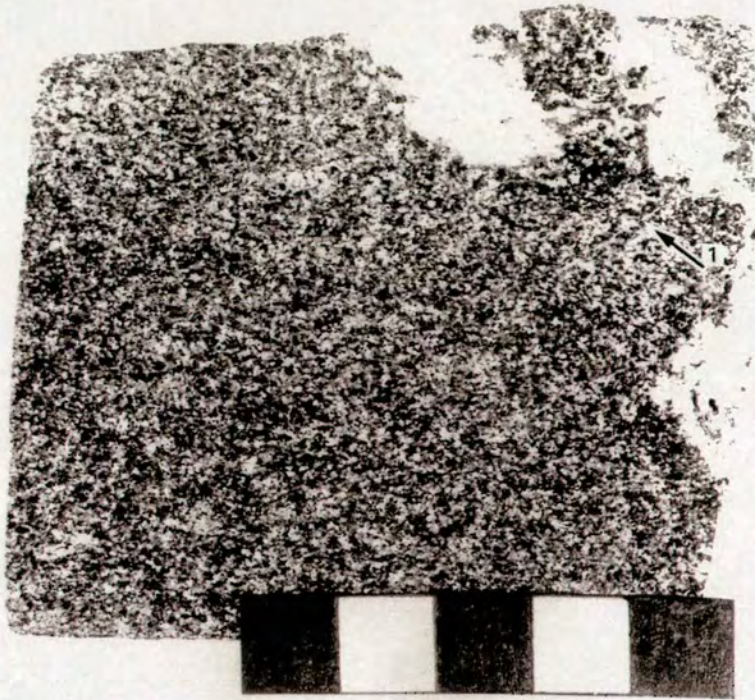
(a) Handspecimen of E5; patches of quartz-feldspar (upper right) are part of a leucocratic seam. Arrow 1 points to a discrete fracture which apparently dies out toward the margin of the quartz-feldspar seam.

Scale bar: centimetre squares.

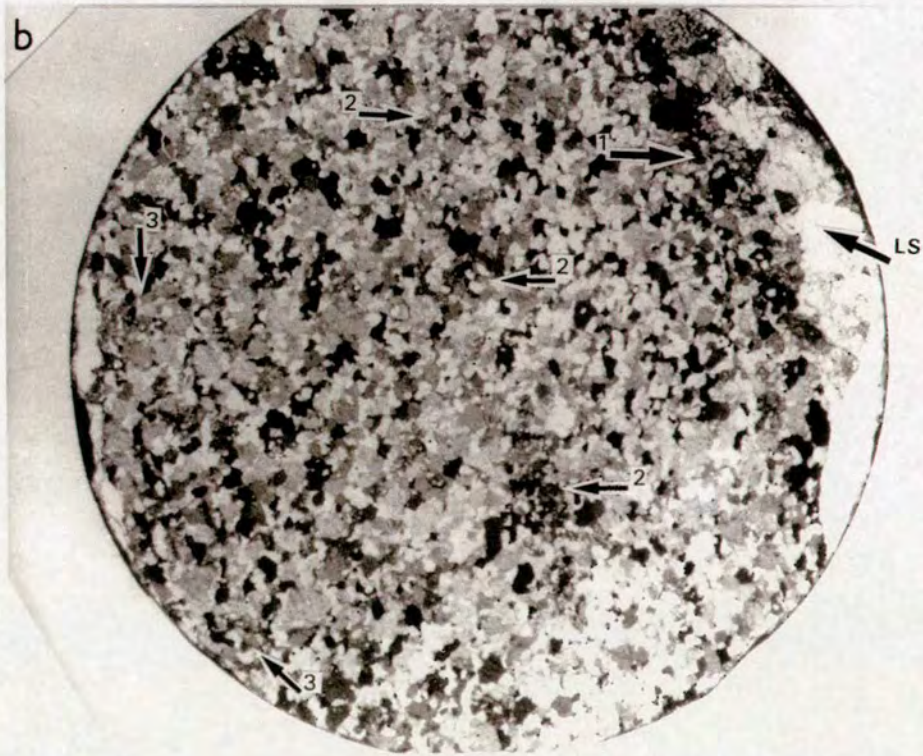
(b) Thin-section photograph of E5 depicting the spatial locations of the three irregular zones of greater alteration (arrowed 1-3). Leucocratic seam arrowed LS.

Scale: approximately 2cm. diameter.

a



b



THIN-SECTION DESCRIPTION

Texturally E5 is similar to E52 although it is classed as a pyroxene amphibolite because it has a greater modal abundance of pyroxene. It consists of amphibole, plagioclase, pyroxene, magnetite, pyrite and minor epidote and apatite. Although much of the rock remains quite pristine three discrete, sub-parallel (though somewhat irregular) bands can be distinguished within which the minerals are preferentially altered (Plate 17b). The bands are not as sharply bounded as the penetrative microfractures seen in E52; in this rock the mineral alterations occur within linear though rather diffusely bounded physical zones. The mineral alterations are most particularly picked out by the preferential alteration exhibited by clinopyroxene and plagioclase crystals. Towards one edge of the thin-section part of a quartz-feldspar-rich, leucocratic seam has been intersected along the margin of which a band of greater alteration occurs. The following description relates specifically to the amphibolitic rock.

The amphiboles (*c.*55% mode) are a pleochroic straw yellow-green-brown colour in PPL with crystal sizes ranging between 20 μ and 1600 μ m. in length. Most grains are sub-idioblastic with clean, smooth grain boundaries; some edges are thinned/shallowly sloping due to thin-sectioning effects and a minority, *c.*1%, display a fringe of colourless crystals of new growth amphibole similar to those described in E52. In this rock the fringes do not contain epidote and are far less prominent, being predominantly <10 μ m. in width. The great majority of the amphiboles appear relatively unaltered with crisp cleavage traces, cracks and few inclusions. Where alteration has occurred (*c.*5%) the amphiboles again display irregular optical zonations with blue-green coloured rims and patches (Plate 26d) occurring along grain edges and occasionally intragranular blue-green spots. These blue-green coloured, epitaxial amphibole growths are very similar but often much more subtle and less common than those seen in E52. Blue-green coloured amphibole rims and patches are most prevalent in a region running approximately centrally through, and small areas towards the outer edges of the thin-section (Plate 17b); these are associated with an increased abundance of pyrite and magnetite grains and a generally greater degree of alteration amongst the other phases (Plate 38 and Figure 4.1), particularly pyroxene (described below). Within the central altered region the original amphibole cores are often still pristine, lacking evidence of alteration, devoid of inclusions of opaques and blue-green spots and segments; optical zonations are predominantly confined to small (*c.*10 μ m.) patches along grain edges. Most of the intragranular blue-green coloured amphibole occurs in the small areas towards the edges of the thin-

section (Plate 17b). Here the amphiboles exhibit an increased abundance of inclusions of both tiny specks and opaque grains, discrete inclusions trails are common. The occasional blue-green microvein is also observed though these are not abundant and tend to be less sharply bounded than those described in E52. In this rock the few microveins observed have limited penetrations, apparently being restricted to individual crystals; it is not possible to trace blue-green amphibole microveins into adjacent amphibole or plagioclase crystals.

The plagioclase feldspars (*c.*20% mode) form xenoblastic-sub-idioblastic crystals with a range in size between ~100 and 1400 μm . The most pristine grains are colourless, rather featureless crystals with some intragranular cracking. In XPL the feldspars exhibit either multiple, lamellar twinning or are devoid of twins; wedge-shaped twins are restricted to a very small minority of crystals. Both twinned and untwinned crystals have sharp to weakly undulose extinctions. Alteration within the "greater alteration bands" is expressed by the presence of intracrystalline clay particles along cracks and sometimes as patches throughout the crystals as well as occurring along plagioclase grain edges (Plate 25b). Occasionally rather diffusely defined alteration microveins (*c.*5-10 μm . in width), characterised by preferential clay mineralisation and abundant colourless inclusions (similar though less sharply bounded than those seen in E52), are observed. The more altered plagioclase feldspar crystals are also either untwinned or multiply twinned with sharp to undulose extinctions.

The clinopyroxenes (*c.*15% mode) are generally much fresher and more readily identifiable than those of E52 (Plate 38). Within the most pristine regions of the rock the clinopyroxenes appear as xenoblastic, high relief, pleochroic pale green coloured grains with a high second order birefringence and size range of ~60 to 1000 μm . Most have smooth and relatively crisp grain boundaries; intracrystalline cracks are common. A few cores of the larger grains exhibit the fine exsolution texture noted in E52. The less pristine pyroxenes occur both within and adjacent to "bands of greater alteration" within the rock. Secondary alteration of these pyroxene crystals is evident through the development of intragranular aggregates of blue-green amphibole, tiny black specks (<1 μm .) and opaque grains (<10 μm .), see Plate 25b. The intragranular amphibole is a pleochroic dark-blue-green colour comprising xenoblastic, very irregularly shaped crystals typically less than 10 μm . in size. The degree to which alteration has occurred is quite variable; in places the pyroxene crystals display only a limited amount of amphibole neomineralisation with much of the original grain remaining unaffected. In the more extensively altered areas of the rock, such as

the zone running approximately centrally through the thin-section and toward the edge of the quartz-feldspar-rich leucocratic vein, the pyroxenes are more substantially affected, occasionally completely replaced by an irregular aggregate of blue-green coloured amphibole crystals. The more altered pyroxenes often have irregular shapes to their grain boundaries reflecting this new growth nucleation, which in some instances appears to also replace part of the adjacent amphibole crystal.

The opaques (*c.*3% mode) within the rock predominantly consist of xenoblastic-sub-idioblastic pyrite (<5-240 μ m) and sub-idioblastic magnetite (<5-100 μ m) grains (Plates 24a, 26d, 25b). Again a bimodal distribution is apparent; the more pristine areas of the rock contain <1% sub-idioblastic magnetites (Plate 38). This contrasts with the more altered areas of the rock; the alteration zone running approximately centrally through the thin-section contains an abundance of pyrite crystals, the altered patches within the rocks as a whole display a significantly increased number of both inter and intra-granular magnetite and pyrite grains.

Both epidote and apatite are present in very minor amounts (<1% mode). Epidote occurs as discrete weakly pleochroic pale yellow crystals and aggregates (<50 μ m) in close proximity to the pyrite crystals within the altered band running through the centre of the thin-section. It is far less abundant than seen in E52.

E21 (8.70m.)

HAND-SPECIMEN DESCRIPTION

A fine-medium-grained, mesocratic rock comprising a homogeneous matrix of granular mafic and feldspar grains with an average grain-size of 0.75mm. The specimen is cut by a 0.6cm. thick quartz-feldspar-rich leucocratic seam within which the occasional biotite and pyrite crystal can be seen. Small, <1mm. to 2mm. thick, fractures are also visible within the rock; these result in a dusty, white alteration of the feldspars. Tiny specks of ore can be distinguished both adjacent to and within some of the fracture zones. The fractures are not present within, or show continuity, across the leucocratic seam (Plate 18a).

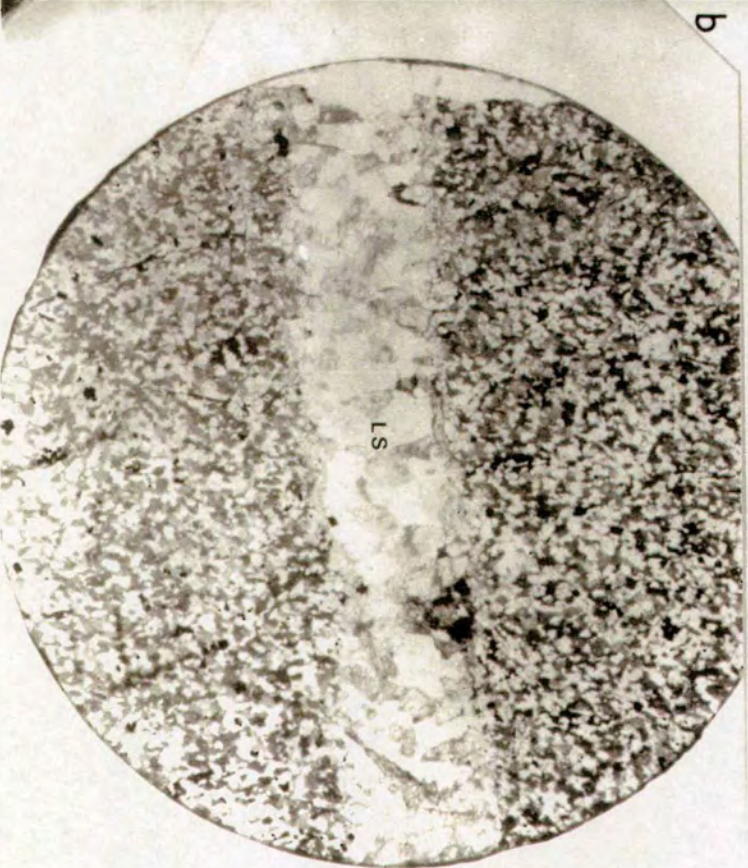
PLATE 18 HANDSPECIMEN/ THIN-SECTION PHOTOGRAPHS OF E21

(a) Handspecimen of E21 cut by a leucocratic, quartz-feldspar rich seam (arrow 1). Note also the presence of bifurcating fracture networks within the amphibolitic rock - identified due to the preferential dusty-white alteration of the feldspars (arrowed 2). Fractures do not clearly cross-cut the leucocratic seam.

Scale bar: centimetre squares.

(b) Thin-section photograph of E21; the leucocratic seam (LS) runs through the centre of the slide but no obvious zones of greater alteration can be distinguished.

Scale : approximately 2cm. diameter.



THIN-SECTION DESCRIPTION

This rock, classified as a Biotite Amphibolite, was selected as representing one of the more altered of the rocks collected. It is dominated by the presence of xenoblastic-idioblastic grains of amphibole, plagioclase, biotite, quartz, chlorite, pyrite, magnetite and sphene with minor chalcopyrite, apatite and epidote. The minerals define a weak preferred orientation within the rock. The quartz-feldspar-rich leucocratic seam described in hand specimen above runs approximately through the centre of the thin-section (Plate 18b). Mineral alterations are observed throughout the thin-section; there is no obvious localisation to the alterations such as those described in E52/E5.

The amphiboles (*c.*50% mode) typically occur as yellow-green/brown coloured, sub-idioblastic, often prismatic crystals ranging in length from 40-800 μ m. Approximately 90% of the amphiboles display evidence of alteration; intragranular opaque inclusions and tiny black specks are ubiquitous. Though many of the original amphiboles retain relatively smooth-curved grain boundaries the overall crisp, pristine nature of the crystals is no longer present. Some (*c.*10%) crystals display embayed-lobate grain margins and a minority (*c.*3%) are shallowly sloping and thinned due to thin-sectioning cut effects. Tiny microcrystalline new growth fringes may be observed adjacent to approximately 1% of both the smoothly curved and more lobate original amphibole grain-boundaries. *C.*5% of the amphiboles contain intragranular aggregates and occasionally single crystals of $\leq 200\mu$ m. biotite flakes which nucleate along cleavage traces and cracks within the amphiboles. Pleochroic pale-green-yellow regions observed along some (*c.*3%) amphibole grain boundaries and occasionally adjacent to the intragranular biotite aggregates represent secondary chloritic alteration. These have distinctly anomalous blue or first order birefringence contrasting with the blue-green coloured amphibole zonations which have a similar or higher birefringence than the original, unaltered, yellow-green/brown amphibole crystal. It is often quite difficult to clearly distinguish between these two alteration phenomena, but especially difficult where the altered grain margin is particularly shallowly sloping due to the cut orientation of the thin-section.

Original yellow-green/brown amphiboles are optically zoned, both along grain margins and intragranularly, to a blue-green colour. *C.*80% of the alterations observed are epitaxial growths of blue-green coloured amphibole occurring as rims and patches within the original amphiboles. The rims and

patches are very sporadically developed with highly irregular sizes and shapes. There appears to be no consistent correlation between the nature of the grain boundary or adjacent phase and the development of a blue-green coloured zone. Intragranular alterations (*c.*20%) occur as epitaxial, blue-green coloured spots and segments adjacent to cracks and cleavage planes within the crystal; these sometimes link with one another outlining the passage of a microvein. Few sharply bounded, cross-cutting microveins similar to those described in E52 can be seen. The nature of the contact between the blue-green amphibole and the unaltered host is variable; in some instances the colour change is clearly gradational and no interface can be distinguished between the two, in many other situations however the interface is much sharper (a Becke is sometimes though not always present).

The plagioclase feldspars (*c.*25% mode) form xenoblastic crystals ranging in size from 100-600 μm . Most have either curved or lobate grain-boundaries and all display secondary alteration in the form of many inclusions of clay particles. Both colourless inclusions and opaque specks are also present. In PPL the crystals are colourless except for the liberal brownish dusting of the clay particles; these are present at both feldspar grain-boundaries and intragranularly along cracks and within microveins. In XPL the plagioclases are seen to be both twinned and untwinned with most having a moderate to strongly undulose extinction. Wedge-shaped twins are present within some crystals. Inclusion of prismatic apatite crystals (<80 μm .) occur within the cores of many grains.

Quartz (*c.*7% mode) occurs as colourless, xenoblastic crystals in PPL ranging in size between 20 μ and 500 μm .; their slightly higher relief and lack of brownish alteration distinguishing them from the feldspars. Most quartz crystals have noticeably cusped grain-boundaries. In XPL the quartz grains exhibit low first order grey-buff/orange birefringence (due to the slightly overthick nature of the thin-section). Most crystals have undulose extinctions which delimit intragranular substructures such as deformation bands, kink bands and occasionally irregularly distributed subgrains. Tiny (<2 μm .), often almost sub-microscopic, fluid inclusions occur within groups along planes that either cross-cut crystals or parallel intragranular fractures.

Biotite mica (*c.*5-10% mode) is present as <200-1000 μm . sized subidioblastic, pleochroic pale yellow to dark brown coloured grains with characteristically high second to third order birefringence and straight, twinkling extinction. Biotite occurs as both larger grains within the rock matrix and tiny

crystals nucleating within and adjacent to some amphibole crystals (as previously described). Most biotite crystals have a lath shaped habit with either smooth or cusped-embayed grain edges and a prominent cleavage parallel to the length of the grain. Several of the larger grains are xenoblastic with very irregular grain boundaries and no visible cleavage (these probably represent crystals which were cut perpendicular to the c-axis orientation). Most of the biotite grain-boundaries appear rather ragged; fragmentation of the outer edges of the original crystal is common. These 'fragments' remain in optical continuity with the host grain and are not believed to represent new growth crystals. Whilst many biotite flakes appear relatively pristine others, most particularly those adjacent to the leucocratic seam, exhibit chloritisation adjacent to cleavage planes. Several of the larger flakes show quite extensive alteration to very pale pleochroic-green chlorite with an anomalous birefringence.

The opaque grains present within the rock (*c.*5% mode) are composed of xenoblastic-sub-idioblastic magnetite crystals (*c.*94%) with sizes ranging between 2 and 600 μ m. (brown with pinkish tint and isotropic in reflected light); sub-idioblastic pyrite (5%) ranging in size from <2 to 400 μ m. (white with a yellow tint in reflected light) and xenoblastic chalcopyrite (*c.*1%) ranging in size from <2 to 200 μ m. (brass yellow in reflected light). Both pyrite and chalcopyrite crystals are commonly surrounded by an oxidised rim (bluish colour in reflected light; red in PPL). Magnetites are commonly rimmed by aggregates of sphene (see below) suggesting they may be titaniferous in composition. Opaques are liberally scattered throughout the thin-section.

Sphene (*c.*1% mode) occurs as highly irregularly shaped, xenoblastic crystals with a high relief and pale pinkish-brown colour in PPL; sizes range between 20 μ m. and 800 μ m. In XPL the crystals retain their pinkish-brown colours and many grains do not display complete extinction. Most are observed in close proximity to or as rims around magnetite crystals.

E15 (0.15m)

HAND-SPECIMEN DESCRIPTION

A fine-grained, mesocratic rock consisting of a granular, sub-idioblastic and fairly homogeneous matrix of mafic and feldspar grains with an average grain-size of approximately 0.5mm. A slight preferred orientation of the mineral grains is observed. A 1mm. thick leucocratic seam is evident on the orangy-

brown coloured, weathered rock surface. Broad orangy-brown coloured bands (c.0.5cm. thick) and narrow fractures (c.1-1.5mm. thick) within and adjacent to which the feldspars are more highly altered can just be distinguished on the cut rock surface (Plate 19a).

THIN-SECTION DESCRIPTION

The rock essentially comprises an intergrowth of amphibole, plagioclase, quartz and magnetite crystals with minor pyrite, apatite, chlorite and sphene. It was selected to outline the extreme degree to which alteration has occurred and is the closest sample to the intrusive contact collected. As is evident from the hand-specimen description distinct regions again exist within which the minerals display evidence of secondary alteration. Three discrete bands and a fourth more irregular area can be seen in thin-section (Plate 19b) within which greater alteration has occurred. The three discrete bands are approximately 2mm. in width, are sub-parallel to one another and cross the rock at $c.50^\circ$ to its foliation.

The amphiboles (c.45% mode) occur predominantly as sub-idioblastic, pleochroic straw yellow to dark-green to dark-brown coloured grains with a range in length between 60 and 1800 μ m. Within the three "greater alteration bands" the original amphiboles have been extensively and occasionally completely recrystallised to an aggregate of deep blue-green coloured amphibole needles/crystals, an occasional biotite flake and abundant inclusions of magnetite, pyrite, zircon, sphene and rutile are associated (Plate 38b). These aggregate grains typically have embayed and very irregular grain boundaries however the overall-shape of the original crystal has often been partly preserved. Isolated aggregates and occasionally individual laths of blue-green coloured amphibole needles which do not appear to have replaced any pre-existing amphibole are also evident within these three bands (Plate 34d).

Beyond the three "greater alteration bands" the rock is more but by no means entirely pristine. Most amphibole grain-boundaries remain relatively straight-curved; some are quite clean and crisp whilst others are more irregular (cusped), sometimes shallowly sloping and thinned and occasionally the sites of fringes of colourless new growth crystals (<1 μ m.). Amphiboles show a range of alteration states; in some areas grains remain unaltered or display optical zonations in the form of occasional epitaxial, blue-green coloured amphibole patches, rims or intracrystalline spots or segments adjacent to cracks/cleavages within the crystal.

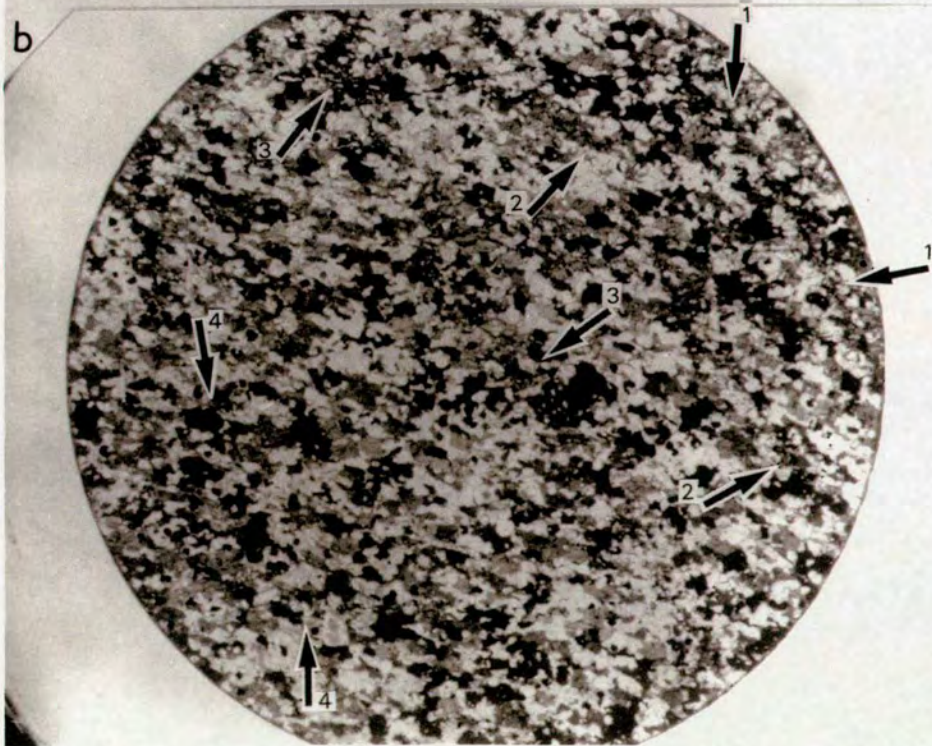
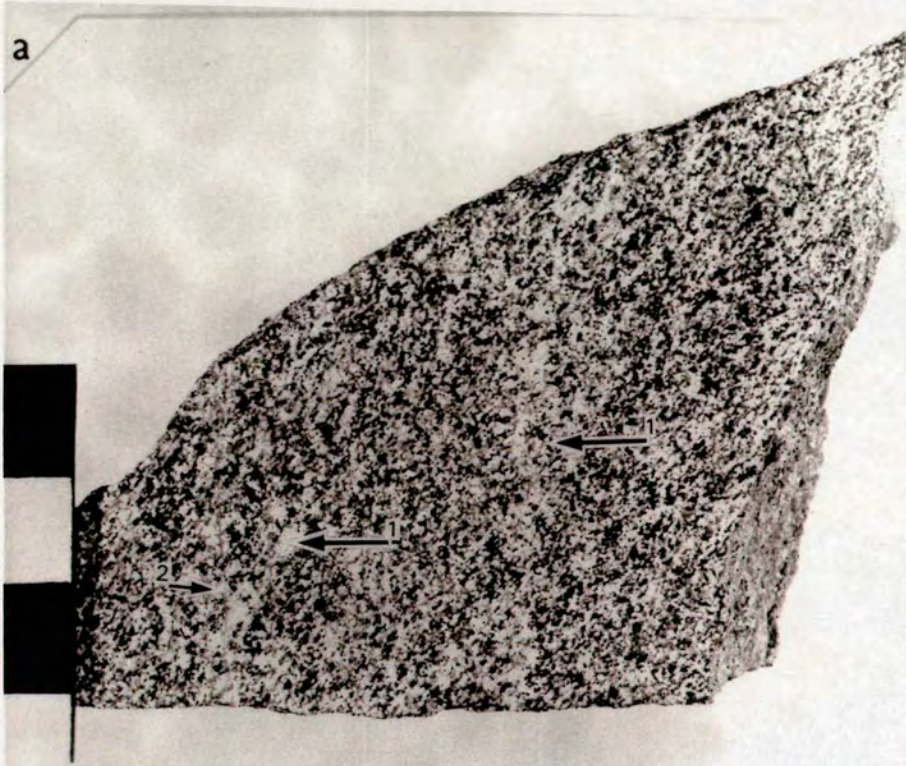
PLATE 19 HANDSPECIMEN/ THIN-SECTION PHOTOGRAPHS OF E15

(a) Handspecimen of E15. Alteration zones are only just distinguishable (arrowed 1). Note also the fracture (arrow 2).

Scale bar: centimetre squares.

(b) Thin-section photograph of E15; three sub-parallel zones of extensive recrystallisation (arrowed 1-3) and a fourth region (arrowed 4) of extensive microveining and epitaxial growth are visible.

Scale : approximately 2cm. diameter.



Those grains within which intracrystalline blue-green coloured amphibole epitaxial growths occur tend also to be riddled with inclusions of both tiny colourless, very high relief and highly birefringent ($<10\mu\text{m}.$) crystals of zircon, colourless inclusions ($<1\mu\text{m}.$) and larger opaque grains (magnetite; *c.*10-100 $\mu\text{m}.$). Often the tiny inclusions form penetrative 'trails' within the amphiboles; these may also be associated with some blue-green coloured alteration within the host amphibole. An occasional sharply bounded blue-green coloured microvein is observed. The majority of blue-green coloured epitaxial growths (*c.*90%) have quite abrupt interfaces with the host amphibole and a Becke line does not exist. In a few instances a continuous optical colour change has also been observed.

The blue-green coloured amphibole alterations described in the preceding paragraphs are similar to those seen in the other rocks, occurring as restricted portions to otherwise unaltered original host amphibole grains. In addition to these commonly encountered types a fourth region within the thin-section contains amphibole crystals within which far more extensive ($<800\times 800\mu\text{m}.$) intragranular segments of the original crystal have been "replaced" by a deep blue-green coloured amphibole. In these amphiboles large blue-green coloured, almost "pseudomorph"-like, epitaxial growths occur in portions of the original crystals adjacent to or bounded by cleavage planes/cracks (Plates 30c, 32a,b,d, 34ab, 35a). Large sections and occasionally ends of individual grains are altered. The blue-green-amphibole involved is identical to that described previously; blue-green and host amphiboles retaining optical continuity (Plate 33c,d). The interface between the blue-green coloured and original amphibole crystal is always very abrupt. Small, colourless zircon crystals with a very high relief are scattered throughout the blue-green coloured amphibole (Plate 34b) and both inter and intragranular opaques of magnetite and pyrite are abundant. One particular crystal displays a reddish discolouration indicative of oxidisation/iron-staining. A network of sharply bounded microfractures with sizes ranging $\sim 1-100\mu\text{m}.$ width can be traced through the area (Plate 19b). The microfractures result in deep blue-green coloured microveins within the original amphiboles (Plates 35a, 30c) which can be clearly linked to one another via similarly distinct microveins within intervening phases (Plate 31d). Within the amphiboles the microveins often bifurcate and either continue within an adjacent amphibole crystal or link with a more extensive blue-green coloured intragranular segment. The microveins are bordered by and often contain abundant tiny inclusions; both blue-green coloured microvein amphibole and host amphibole are in optical continuity. In a few situations the blue-green coloured microvein amphibole can be traced beyond the limits of the host amphibole, clearly

overgrowing a neighbouring feldspar crystal (Plate 46a). The extensive epitaxial growths and microveins described here do not exclusively involve the formation of many tiny crystals of blue-green amphibole; alteration has occurred in a way which preserves the original amphibole structure (Plate 33c,d).

In addition to the complex range of amphibole alterations already described some amphibole grains (3%) also exhibit small flakes of biotite within their cores, very similar to those described in E21, here, however, much of the biotite has itself been replaced by chlorite. Some (*c.*2%) amphibole crystals exhibit partial chloritisation, distinguishable from the blue-green amphibole via its paler green colour and anomalous first order birefringence.

Plagioclase feldspars (*c.*33% mode) occur as xenoblastic crystals ranging in size from 100-1200 μ m.; these have curved to lobate grain-boundaries along which tiny (*c.*1 μ m.) clay particles, other numerous microcrystalline inclusions and Fe staining are common, whether within the relatively pristine or more altered areas of the rock. In XPL the feldspars exhibit either first order grey or slightly orangy-buff coloured birefringence (due to slightly overthick thin-section). Feldspars within the relatively pristine areas of the rock are readily distinguishable from those of the more altered areas due to their far less abundant intragranular alteration. Relatively pristine crystals either display sharp lamellar twinning or no twinning and have weakly-moderately undulose extinctions; occasionally intragranular alteration is observed adjacent to cracks or in the form of 10-40 μ m. thick microveins within which clay particles and other inclusions occur. Within the three sub-parallel "greater alteration bands" and the fourth region of the thin-section (within which the amphiboles exhibit more extensive epitaxial growths) the feldspars are variably effected though generally display a significantly higher degree of intragranular alteration; often complete cores have been altered to aggregates of brownish clay particles and contain numerous other inclusions, microveins are common. In a few instances preferential alteration appears to have occurred along specific twin planes. Within the more altered regions of the rock as a whole the feldspars are often less sharply twinned, commonly untwinned with moderately-strongly undulose extinctions. Amongst the tiny microcrystalline inclusions epidote and fluid inclusions are tentatively identified. The rock-pervasive microfractures which produced the deep-blue-green coloured amphibole microveins described above may in many instances be traced into feldspars where they result in very sharply bounded, colourless, high relief (quartz/feldspar?) microveins (Plate 31d) adjacent to which brownish clay particles are often observed.

Quartz (*c.*10% mode) occurs as xenoblastic blebs and generally rather irregularly shaped grains. Most grains are colourless, largely featureless crystals in PPL though cracks and inclusions are quite abundant. In XPL the quartz grains exhibit buff/orange-pink/mauve birefringence colours (again reflecting the slightly overthick nature of this particular thin-section). Crystals range in size from 60-500 μ m. Most grains have either sharp or weakly undulose extinctions. The abundant intragranular inclusions observed are predominantly comprised of elongate, less frequently necked, fluid inclusions (average *c.*2 μ m. length); these occur either irregularly throughout the body of the grain or as discrete inclusion trails adjacent the cracks. A daughter product may rarely be seen within several of the larger (*c.*4 μ m.) fluid inclusions.

The opaque grains (*c.*10% mode) within the thin-section (identified using reflected light microscopy) are predominantly composed of magnetite and pyrite crystals. Though liberally scattered throughout most of the thin-section there again seems to be an increased abundance of both intra and intergranular opaques within the more altered parts of the rock (Plate 38b). Magnetite (97%) forms xenoblastic-sub-idioblastic grains with a range in sizes from 2-800 μ m. Several of the larger crystals exhibit <10 μ m. width lamellae of ilmenite (brown with pink tint; strongly anisotropic); oxidation of some crystals is indicated by the presence of white lamellae of haematite. In reflected light some magnetite/ilmenite crystals are rimmed by a dull grey, low reflectivity phase, believed to be sphene (see below). The ilmenite lamellae contain abundant inclusions. The pyrite crystals present (*c.*3%) appear to preferentially occur within the three sub-parallel alteration bands in the rock. Most have irregular, xenoblastic habits and are frequently either partially or completely oxidised to FeOOH; appearing reddish in PPL, in reflected light as distinct pale bluish coloured haloes to pyrite cores or isolated grains where complete oxidisation has occurred. Crystal sizes range from *c.*4-800 μ m.

Sphene (*c.*2% mode) occurs both as haloes to some magnetite grains and as inter and intragranular inclusions (5-50 μ m.) within the more extensively altered amphiboles (both the pervasively altered and those within the three sub-parallel alteration bands). The small inclusions often have a flattened lozenge habit distinguishing them from the more granular appearing zircons.

PLATE 20: PRISTINE ROCK TEXTURES.

(a) General view of predominantly pristine rock. Note the smooth, regular grain-boundaries (arrow) and the crisp, fresh amphiboles, plagioclase feldspars and clinopyroxenes.

Scale bar: 0.3mm. (E34:PPL).

(b),(c) Smooth, straight amphibole-amphibole interfaces and triple junctions indicative of textural equilibrium. Note lack of recrystallisation.

Scale bars: 0.1mm. (E34:PPL).

(d) Sub-idioblastic biotite mica lath with mostly smooth grain-boundaries.

Scale bar: 0.2mm. (E16:PPL).

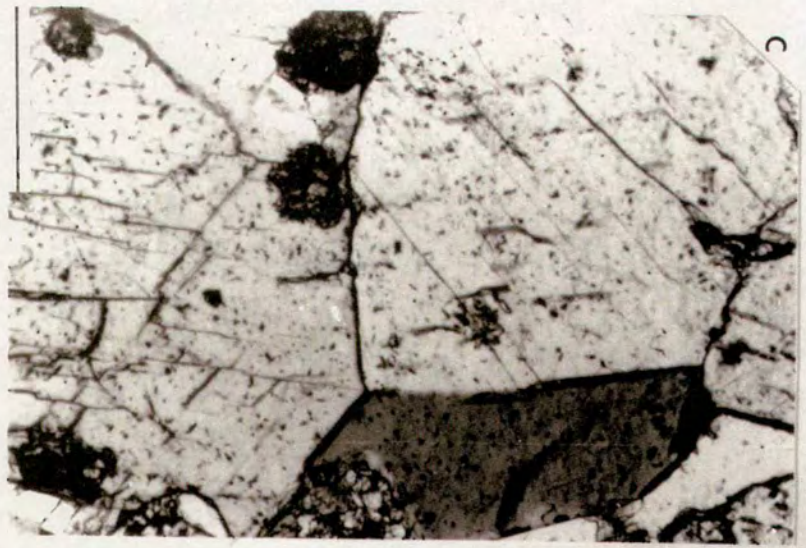
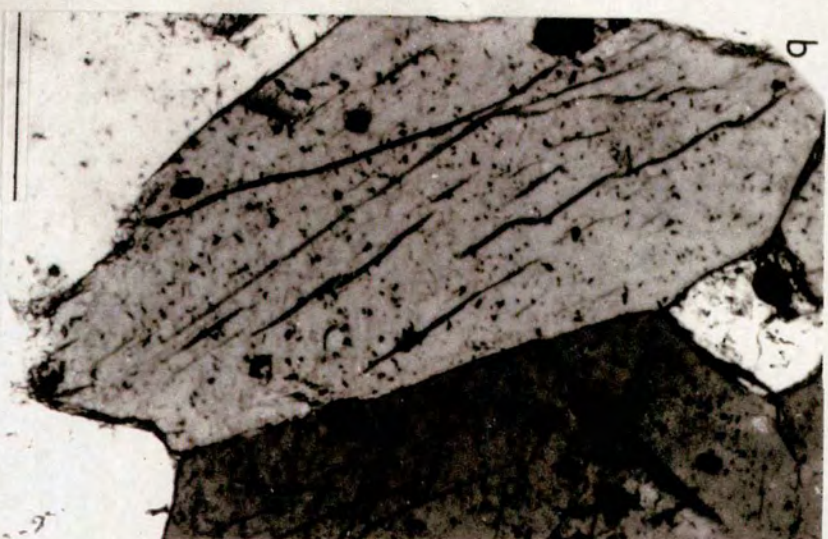


PLATE 20

PLATE 21: PRISTINE ROCK TEXTURES.

(a) Fresh, sub-idioblastic clinopyroxene crystal. Note fine-scale exsolution lamellae within the core (see b).

Scale bar: 0.1mm. (E34:PPL).

(b) Higher magnification photograph of exsolution lamellae within the core of (a).

Scale bar: 0.05mm. (E34:PPL).

(c) Texturally equilibrated amphibole grain boundaries along which recrystallisation has taken place. Pristine textures preserved in less pristine areas of the rock.

Scale bar: 0.1mm. (E34:PPL).

(d) Amphibole crystals surrounded by fresh plagioclase feldspar. Some slight recrystallisation to colourless amphibole crystals has occurred along several grain edges (arrowed).

Scale bar: 0.1mm. (E34:PPL).

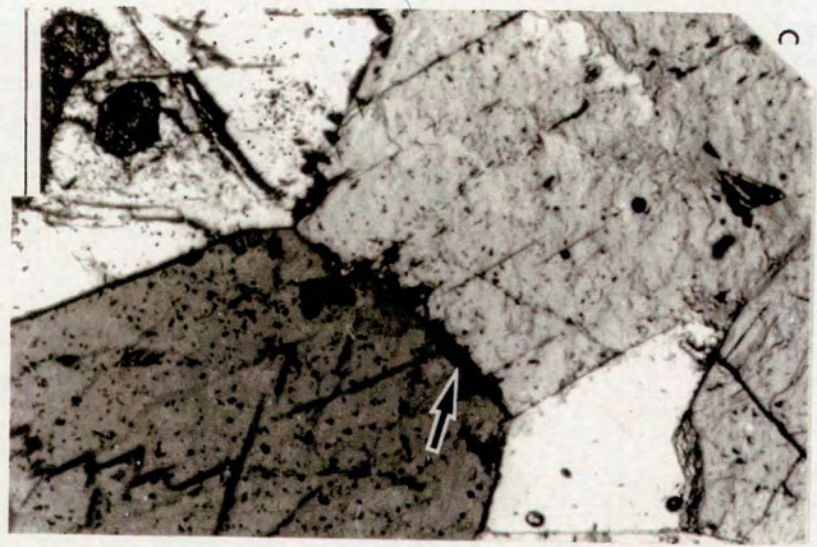
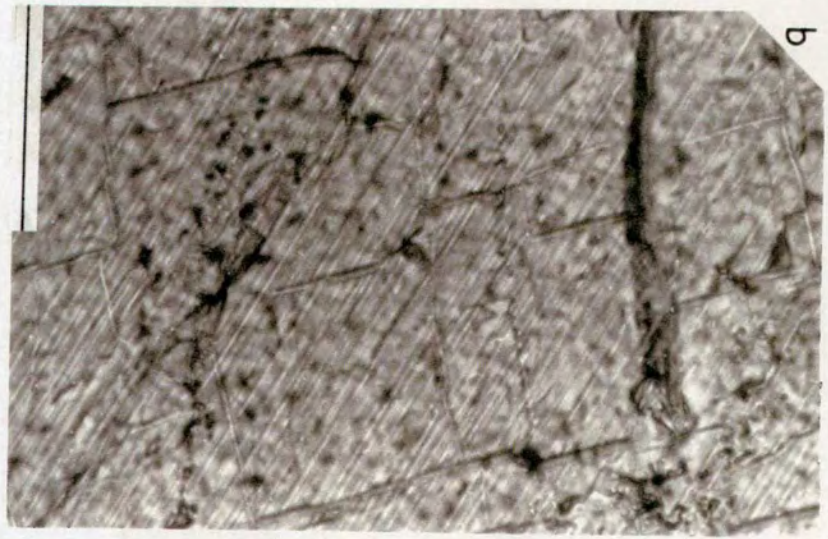
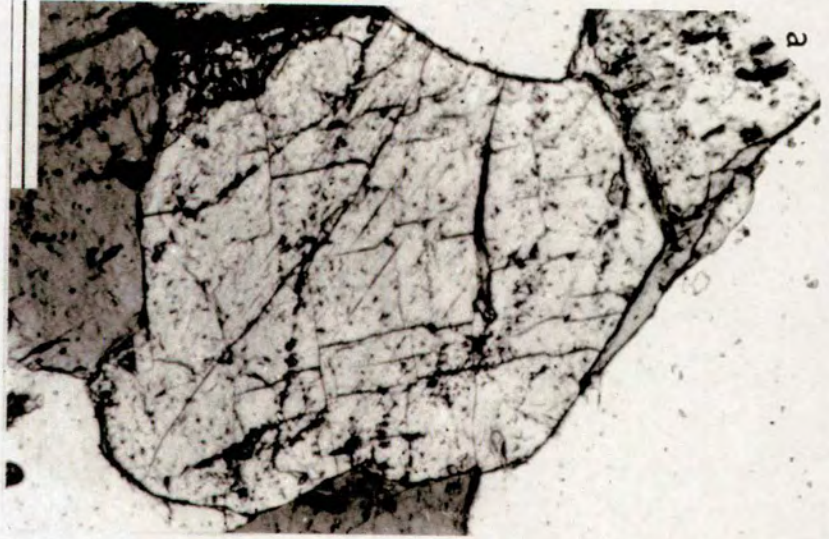


PLATE 22: ALTERED ROCK TEXTURES.

(a) General view of a more altered area of rock. Amphiboles have a scruffy appearance; some have recrystallised rims. Feldspars are altered to clay minerals.

Scale bar: 0.2mm. (ELD6:PPL).

(b) Higher magnification photograph of an altered amphibole crystal with heavily cleaved and inclusion-rich core.

Scale bar: 0.7mm. (E42:PPL).

(c) Relatively pristine original amphibole crystal whose core is unaltered but whose rim (arrow) has recrystallised/neomineralised to a fringe of tiny, colourless amphibole crystals and biotite flakes. The tiny crystals within the fringe have a different optic orientation to the host grain.

Scale bar: 0.2mm. (E52:PPL).

(d) Original amphibole crystal completely recrystallised to an aggregate of new, blue-green coloured amphibole crystals.

Scale bar: 0.08mm. (E11:PPL).

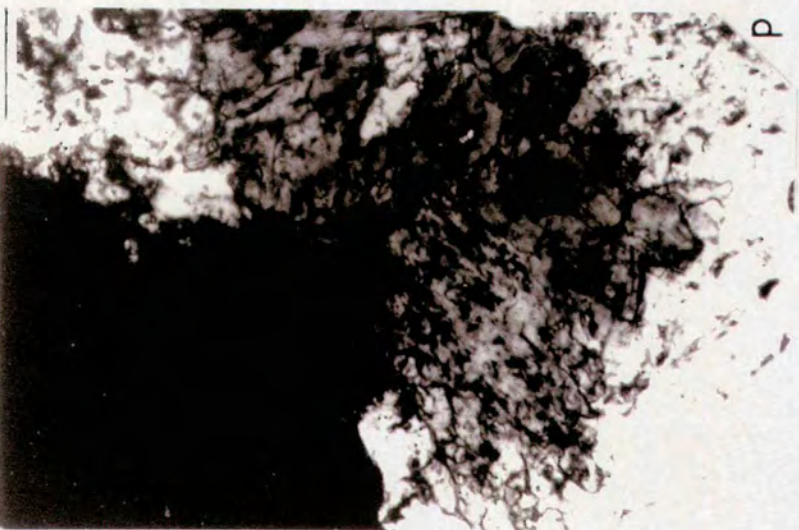
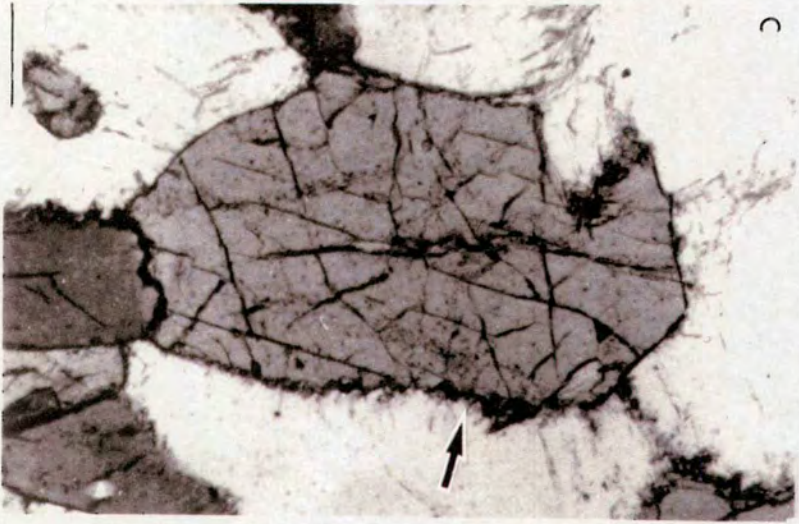
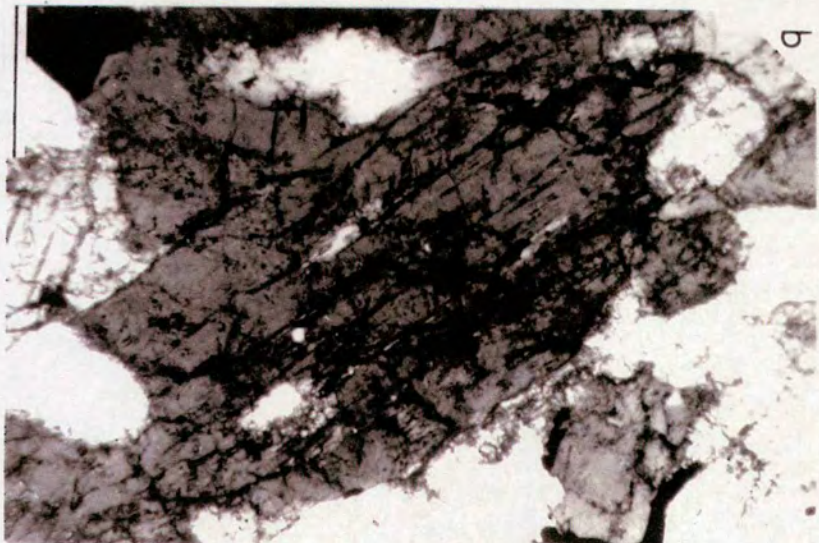
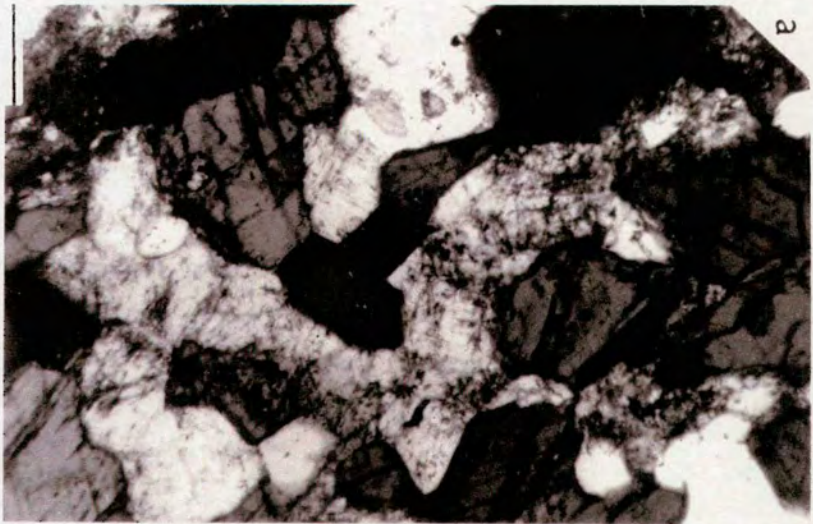


PLATE 23: ALTERED ROCK TEXTURES.

(a) and (b) Tiny crystals of colourless, new growth amphibole nucleating along the margins of original amphibole crystals (arrowed 1). Note fluid inclusions within the plagioclase (arrow 2) in (a).

Scale bars (a):0.05mm. (E34:PPL).

(b):0.08mm. (E34:PPL).

(c) Opaque and colourless inclusions within an amphibole crystal. Note fluid inclusions within the feldspar (arrow 1) and sharply bounded secondary amphibole (arrow 2).

Scale bar: 0.08mm. (E11:PPL).

(d) Irregular shaped opaque located adjacent to amphibole grain-boundaries.

Scale bar: 0.2mm. (E28:PPL).

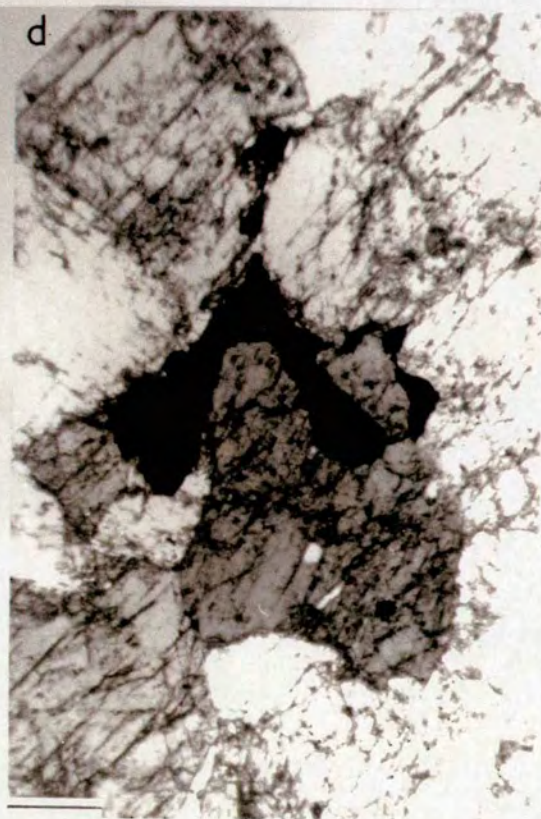
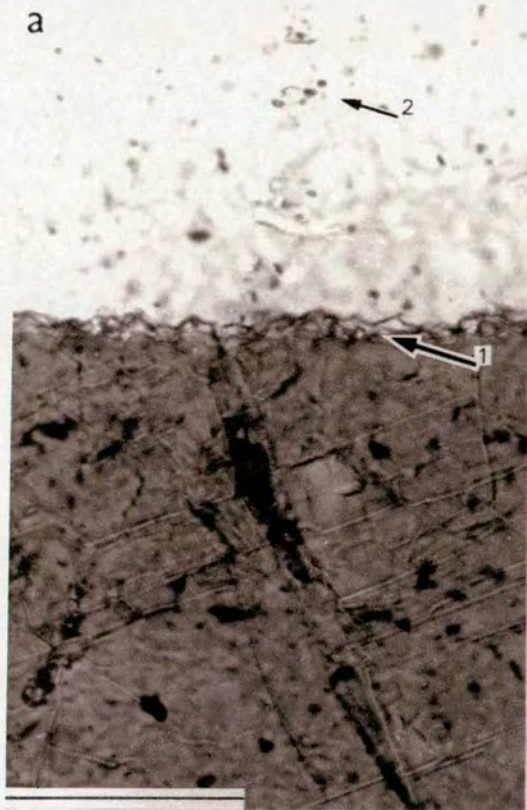


PLATE 24: ALTERED ROCK TEXTURES.

(a) Elongate pyrite grain between two amphibole crystals. Note alteration within the feldspar and some marginal amphibole recrystallisation.

Scale bar: 0.1mm. (E5:PPL).

(b) Sub-idioblastic opaque rimmed by sphene (arrow).

Scale bar: 0.2mm. (E16:PPL).

(c) Alteration of plagioclase feldspar crystals to clay particles. Note preferential alteration (arrowed) defines the passage of a microfracture.

Scale bar: 0.2mm. (ELD6:PPL).

(d) Xenoblastic aggregates of epidotised plagioclase feldspar (arrow).

Scale bar: 0.2mm. (E52:PPL).

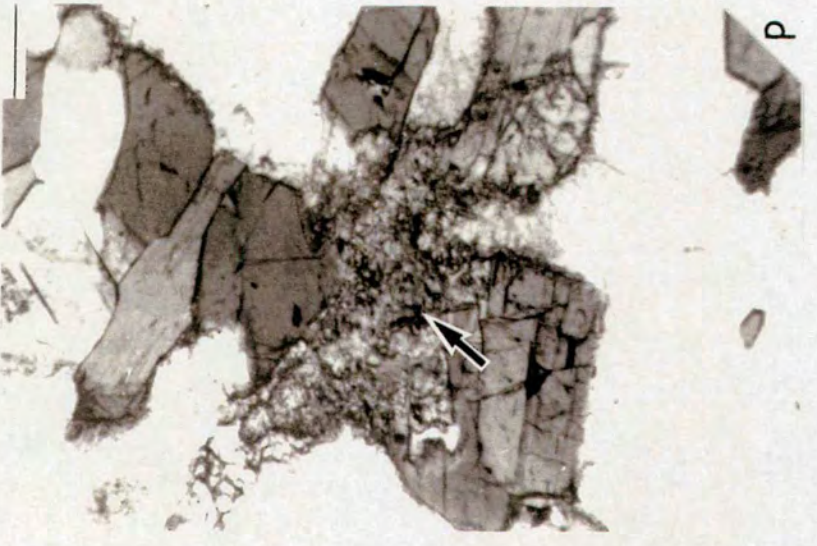
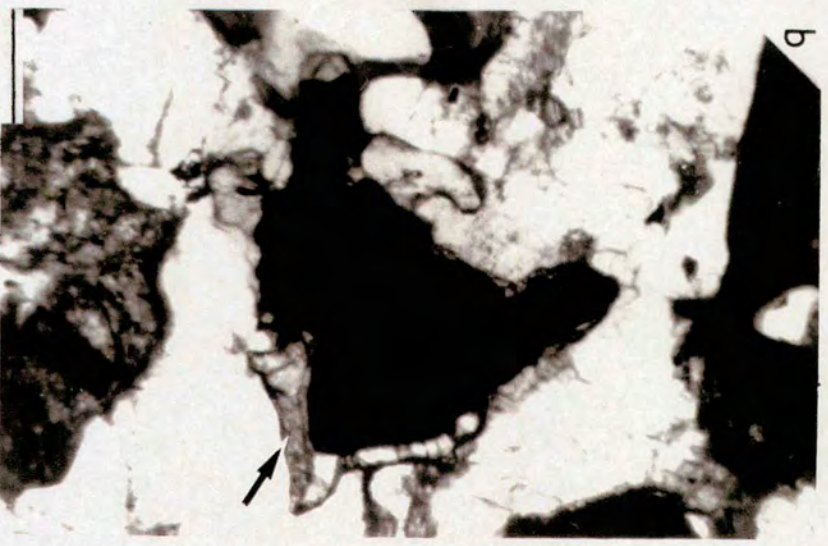
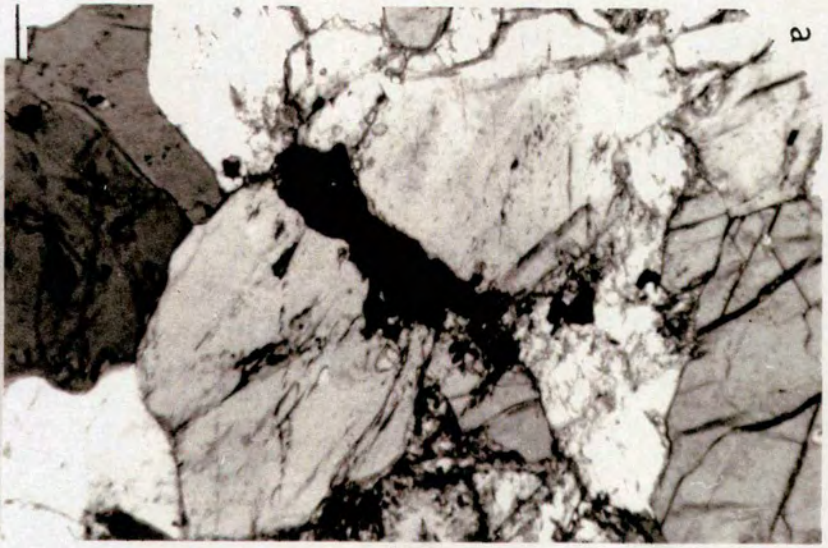


PLATE 25: ALTERED ROCK TEXTURES.

(a) Slightly altered original clinopyroxene crystal: colourless inclusions (arrowed 1) and occasional secondary amphibole crystals (arrowed 2) occur within the core.

Scale bar: 0.05mm. (E34:PPL).

(b) Almost completely neomineralised clinopyroxenes (large arrow): original crystals have been altered to secondary amphibole. Note the increased abundance of both intra- and inter-granular opaques (pyrite; arrowed PY) and the alteration of the plagioclase.

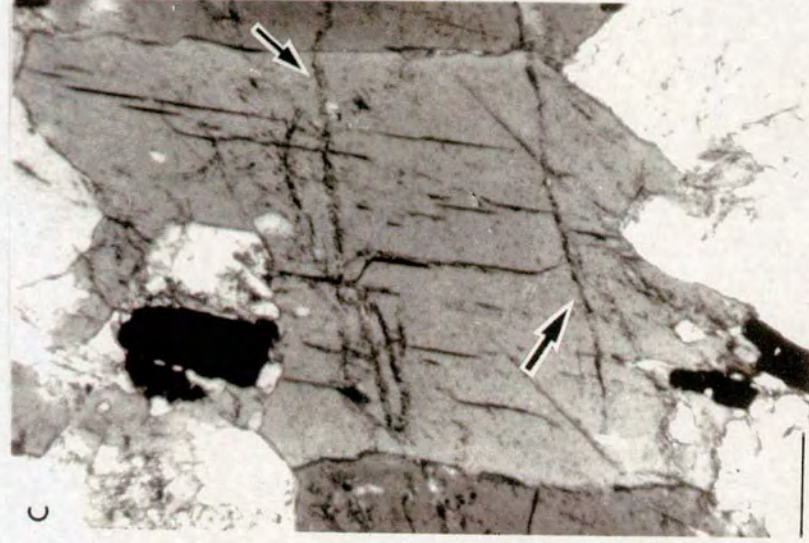
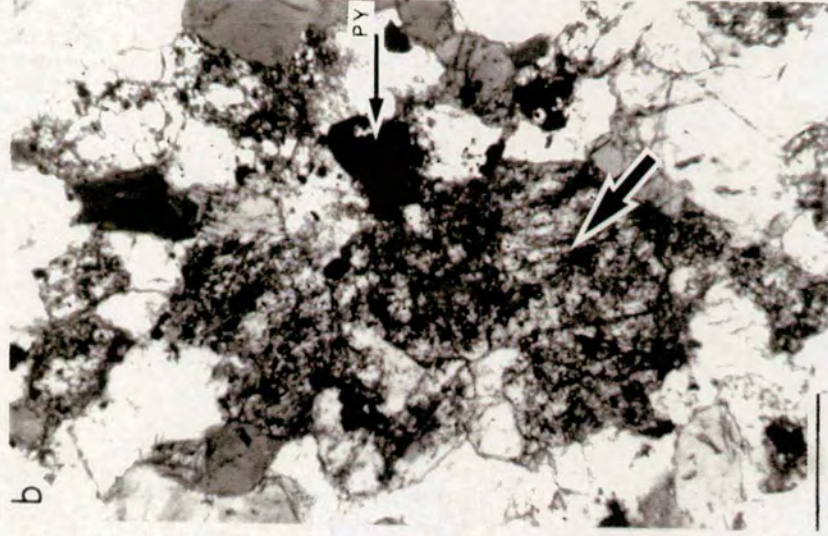
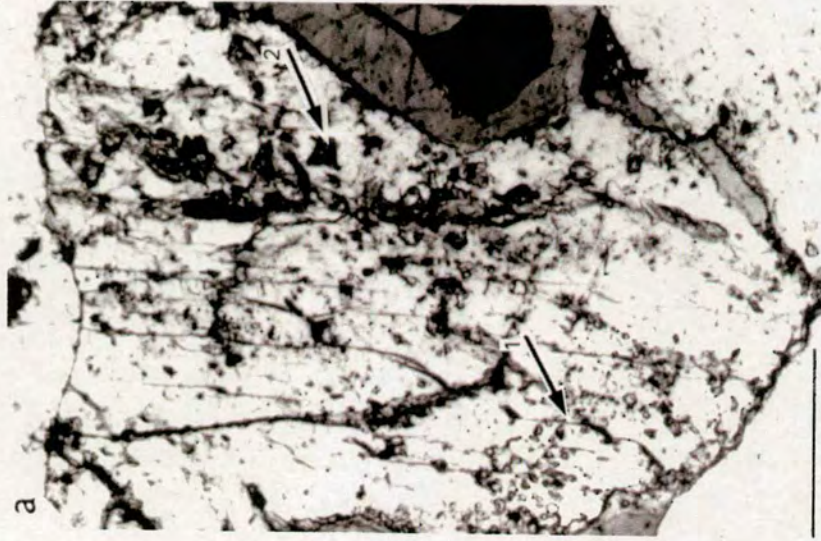
Scale bar: 0.4mm. (E5:PPL).

(c) Relatively pristine original amphibole crystals traversed by inclusion trails.

Scale bar: 0.2mm. (E29:PPL).

(d) Original biotite crystal (arrowed 1) replaced by chlorite (arrowed 2). Note the alteration coincides with a microfracture (arrow 3).

Scale bar: 0.2mm. (E16:PPL).



4.2. SUMMARY OF THE ALTERATION PHENOMENA OBSERVED

The rock descriptions presented in section 4.1.3. were specifically selected to enable the reader to gain an impression of the types and relative distributions of the optically visible mineral zonations, replacements, recrystallisation, crystallisation and neomineralisation phenomena seen within both individual thin-sections and spatially within the amphibolites at Eldora. Thin-section observations indicate that the mineral alterations are heterogeneously distributed on all scales; all rocks, irrespective of their distances from the intrusive contact comprise distinct areas within which the minerals either remain pristine/unaltered or display a variable degree of secondary alteration. In order to be quite clear of the distinctions between the pristine and less pristine/altered regions of the rocks a brief summary is now given.

4.2.1. PRISTINE REGIONS OF AMPHIBOLITIC ROCK

Pristine amphibolitic regions of the rocks are composed of optically homogeneous, crisp, clean crystals with regular, smooth grain boundaries; most minerals are relatively lacking in intragranular inclusions. Intergranular opaque grains are sub-idioblastic magnetite crystals. Amphibole grain boundaries are sharp and 'straight' where controlled by rational 'faces' or smoothly curving; no epitaxial growths of blue-green coloured amphibole, replacement, recrystallisation or crystallisation phenomena are observed. Pyroxene, biotite and feldspar crystals, where present, also occur as fresh, unaltered grains.

Plates 20 and 21 display some of the typical features observed within the pristine regions of the amphibolites.

4.2.2. ALTERED/LESS PRISTINE REGIONS OF AMPHIBOLITIC ROCK

The less pristine amphibolitic regions of the rocks exhibit similar original grain shapes but the optical homogeneity of *all* the crystals is no longer apparent. Original amphibole crystals show the development of the following secondary minerals:

- (i) Blue-green coloured amphibole alterations (discussed below).
- (ii) Recrystallised fringes of colourless, new growth amphibole (<1 μ m. in size) nucleating along some original amphibole grain-edges.
- (iii) Replacement by pale greenish coloured chlorite.
- (iv) Replacement by biotite.

The recrystallised fringes of 'colourless' amphibole crystals are probably the same as the blue-green coloured amphibole; they appear colourless because they are such tiny crystals (< the thickness of the thin-section). In the following descriptions the two amphibole types (*i.e.* both colourless and blue-green) are considered as blue-green coloured/secondary amphibole.

In addition to these amphibole alterations there is an increased abundance of both inter and intra-granular magnetite with the variable introduction of pyrite, chalcopyrite and zircon; titaniferous-magnetite (within which an occasional ilmenite lamellae can be seen) is often partially rimmed by sphene. The plagioclase feldspar crystals display partial alterations to clay particles and/or epidote. Clinopyroxene crystals commonly act as sites of alteration and neomineralisation and are occasionally completely replaced by tiny, blue-green coloured amphibole crystals and pale-green coloured chlorite; they contain numerous colourless inclusions. Inclusion trails are ubiquitous; most quartz crystals and some plagioclase feldspar crystals are riddled with fluid inclusions. Original biotite crystals are variably replaced by chlorite.

Plates 22-25 exhibit the most commonly observed textures and mineral alterations within the less pristine regions of thin-sections.

TYPES OF SECONDARY AMPHIBOLE ALTERATION

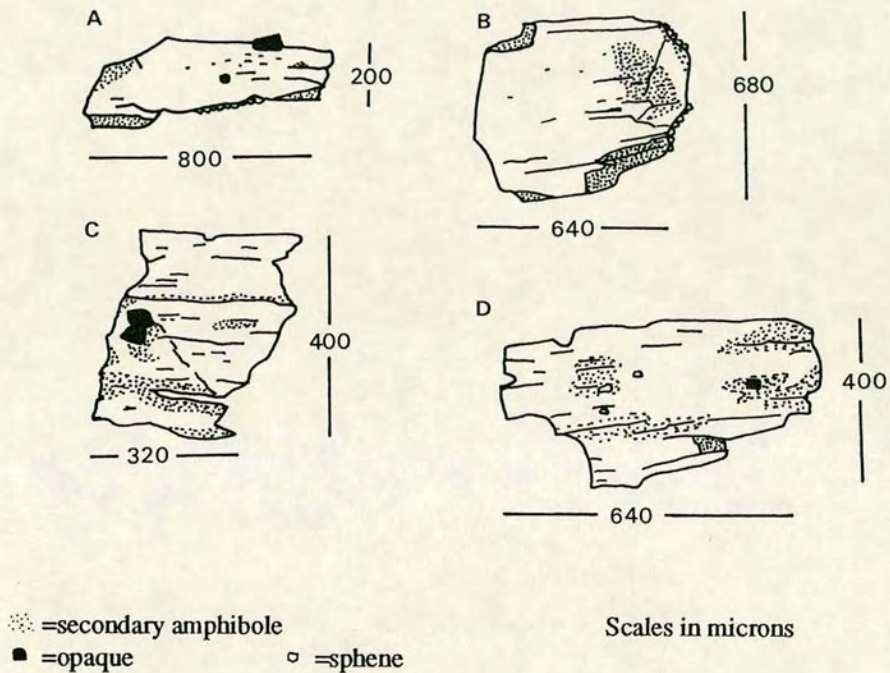
The blue-green coloured amphibole alterations observed have been subdivided into four principle types:

- (a) Boundary alterations.
- (b) Microvein alterations.
- (c) Extensive single crystal alterations.
- (d) Extensive multi-crystal alterations.

These are discussed and illustrated in turn in the following pages.

(a) *Boundary alterations*

This type represents the epitaxial growths observed along pre-existing line and surface defects of crystals, and includes both grain-boundary alterations and those observed adjacent to cleavage traces and cracks within the minerals. Of the amphibole alterations described these include blue-green coloured amphibole rims and patches adjacent to original amphibole grain edges and blue-green coloured spots and restricted segments adjacent to cleavage planes and cracks within the crystal. The following sketches depict typical boundary alterations within four different amphibole grains.



Plates 26-29 display some of the most frequently observed situations.

PLATE 26: BOUNDARY ALTERATIONS.

a,b,c,d Secondary amphibole (pale-grey in black/white photographs) at the edges of original amphibole crystals (darker-grey in black/white photographs). Note the non-continuity in their development *i.e.* they do not always occupy entire crystal edges or occur only at interfaces with adjacent amphiboles.

(a) Secondary amphibole patches (arrows) have abrupt interfaces with the dark-grey host. Note fluid inclusions (arrowed FL) and alteration within adjacent feldspars.

Scale bar: 0.08mm. (E11:PPL).

(b) Less abruptly bounded patch of secondary amphibole (arrow). Note lack of Becke line.

Scale bar: 0.08mm. (E11:PPL).

(c) Sharply bounded patches of secondary amphibole adjacent to an original amphibole grain-boundary. Note the lack of recrystallisation at 1a but recrystallisation at 1b. Note also the pale grey coloured, secondary amphibole microvein within the crystal (arrowed MV).

Scale bar: 0.08mm. (E11:PPL).

(d) Patches of secondary amphibole (pale grey) within original amphibole crystals (arrowed) coincide with pyrite (arrowed PY), heavily altered clinopyroxene (CPX) and plagioclase alteration (F). The mineral alterations and pyrite crystals define the route taken by a microfracture within the rock.

Scale bar: 0.2mm. (E5:PPL).

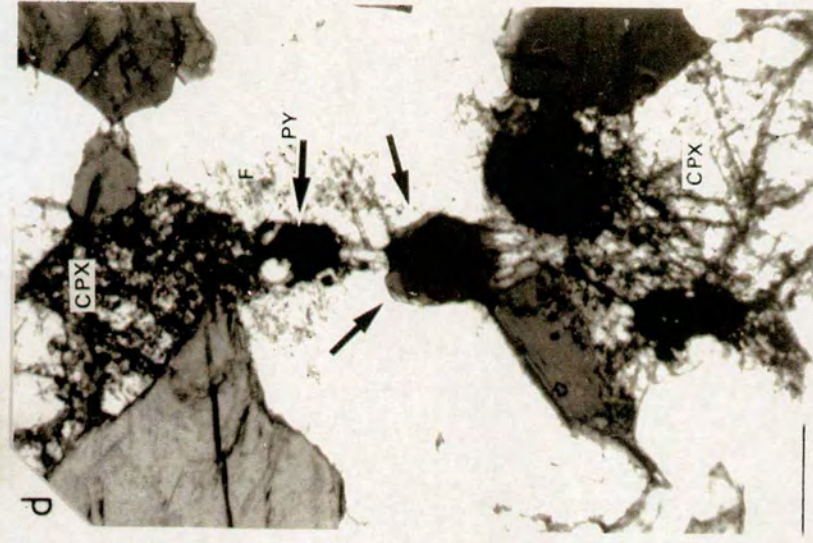
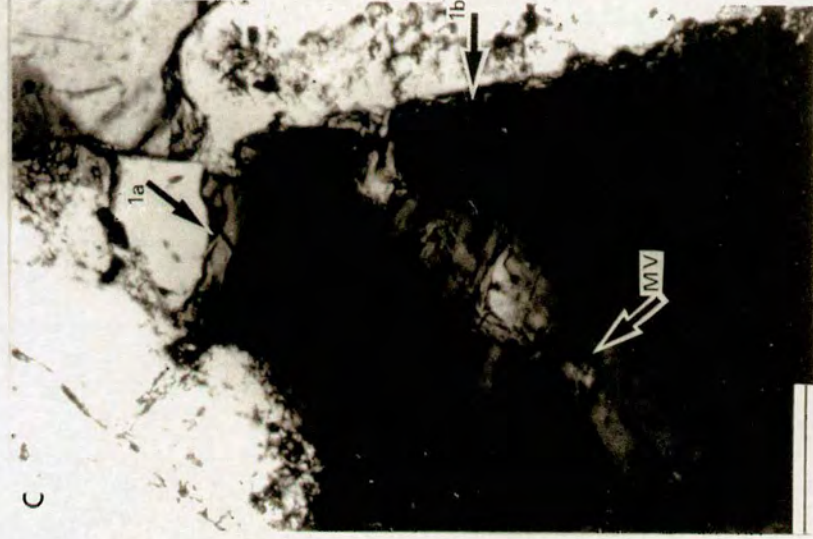
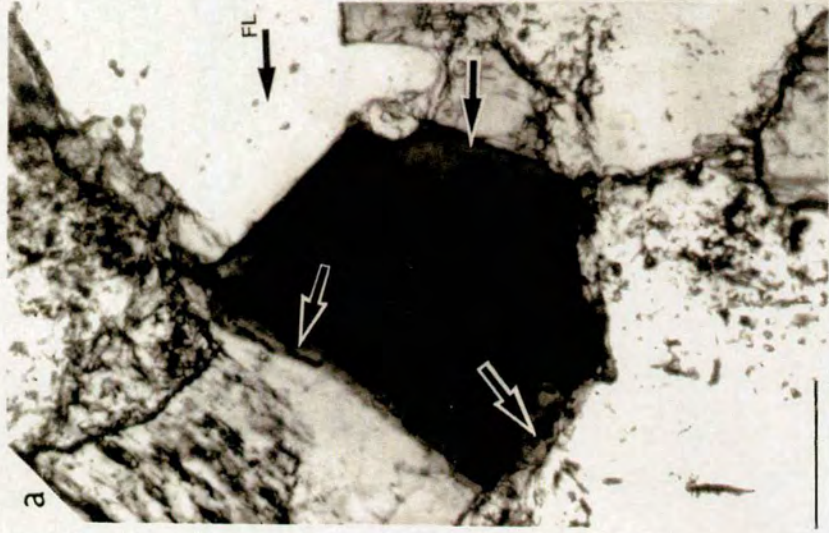


PLATE 27: BOUNDARY ALTERATIONS.

(a) Secondary amphibole (pale-grey) located at an amphibole-amphibole triple-junction. Note part of the secondary amphibole appears to have a distinct grain-boundary (arrow).

Scale bar: 0.08mm. (E11:PPL).

(b) Abruptly bounded secondary amphibole (pale-grey) bordering cleavage planes within an original amphibole crystal (dark-grey).

Scale bar: 0.08mm. (E29:PPL).

(c) Small, patch of secondary amphibole (arrowed 1) at an amphibole-amphibole triple junction. Some alteration is also evident within the core of the crystal (arrowed 2).

Scale bar: 0.2mm. (E16:PPL).

(d) Blue-green coloured alteration and abundant inclusions adjacent to cracks/microfractures within an original amphibole. Note epidote (E).

Scale bar: 0.2mm. (E52:PPL).

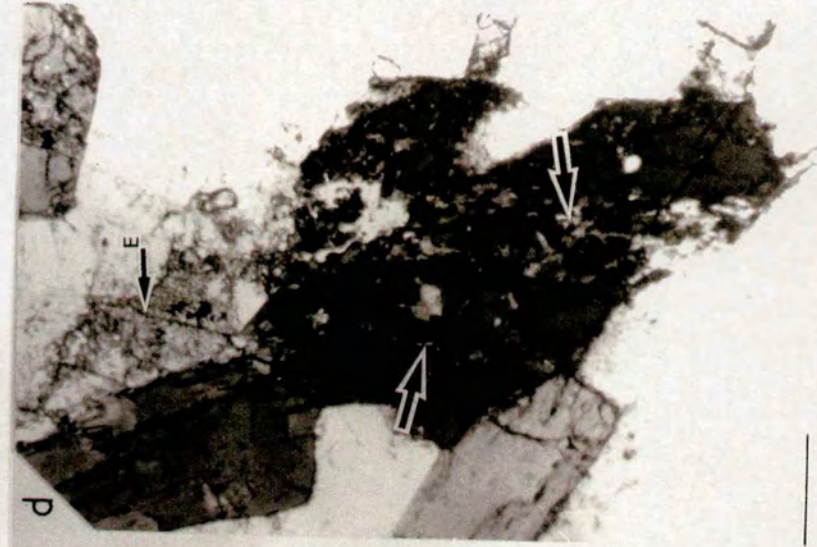
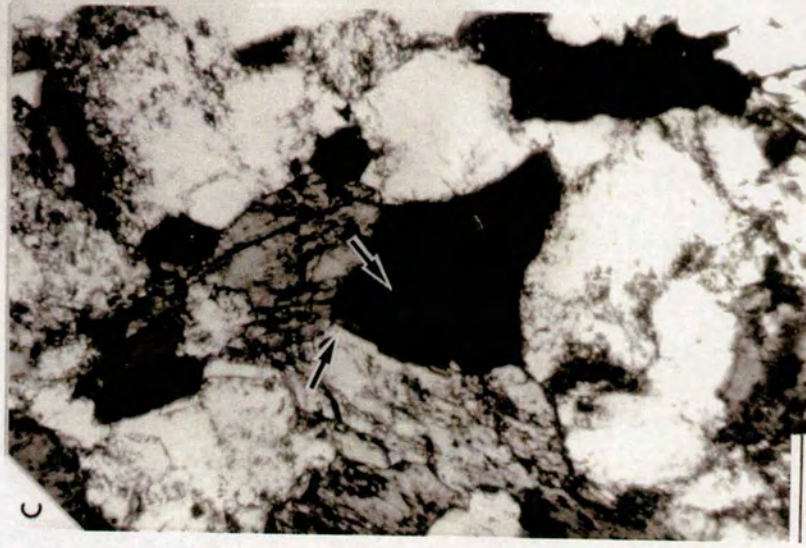
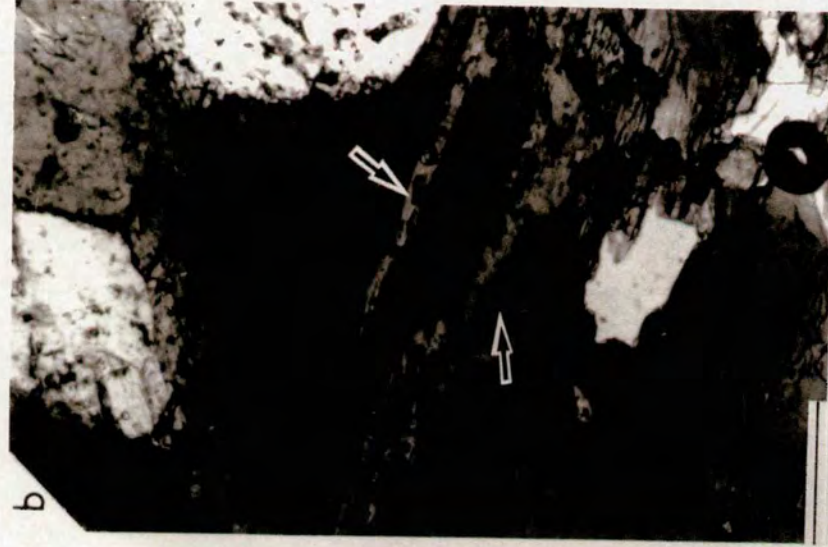


PLATE 28: BOUNDARY ALTERATIONS.

(a) Slightly bluer-green coloured secondary amphibole patches (arrowed) along the margin of an original green-brown coloured amphibole. Note that the interface between original and blue-green coloured amphibole does not coincide with either a grain-boundary or a Becke line.

Scale bar: 0.2mm. (E18:PPL).

(b) Blue-green coloured amphibole (arrowed 1a) has an abrupt interface with the host crystal but no grain-boundary or Becke line is distinct. Compare with blue-green coloured amphibole (arrowed 1b) which shows a gradational change in colour from brown/green host to bluer-green rim.

Scale bar: 0.2mm. (E42:PPL).

(c) and (d) Abrupt interfaces between blue-green and host amphiboles (arrowed). Note more subtle change in colour at arrow 1.

Scale bar in (c): 0.2mm. (E52:PPL).

(d): 0.15mm. (E18:PPL).

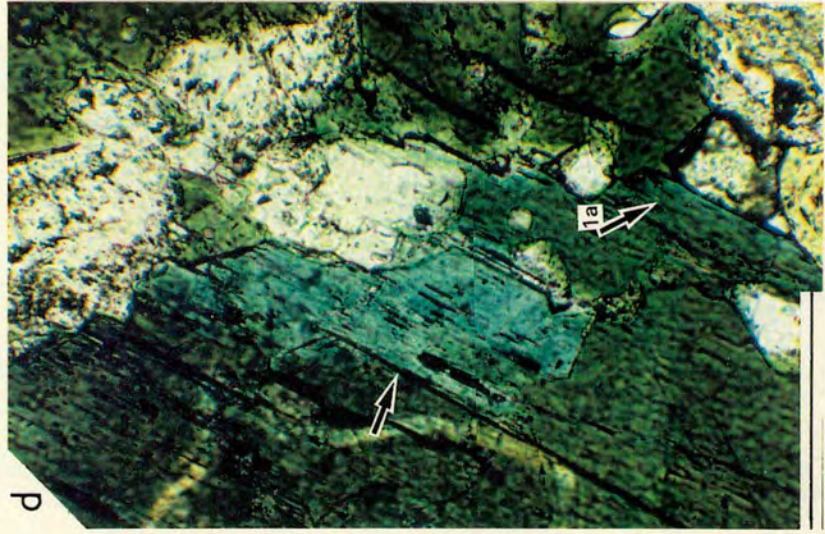
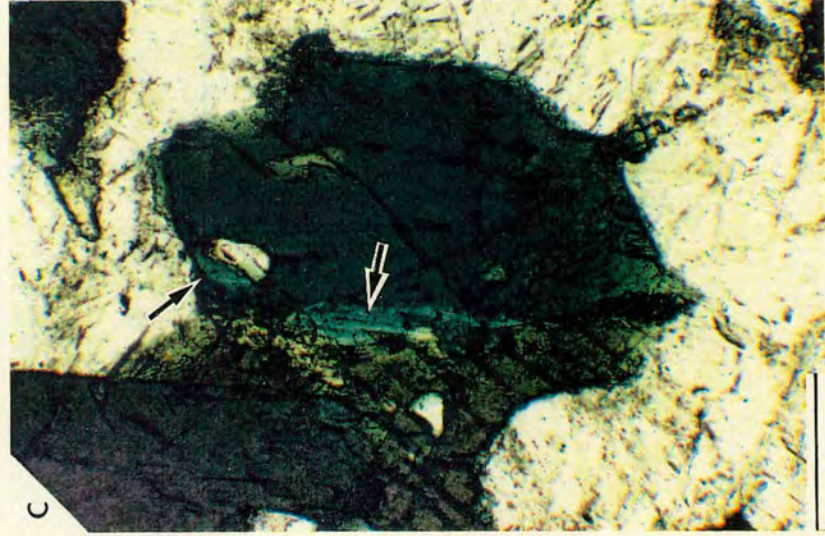
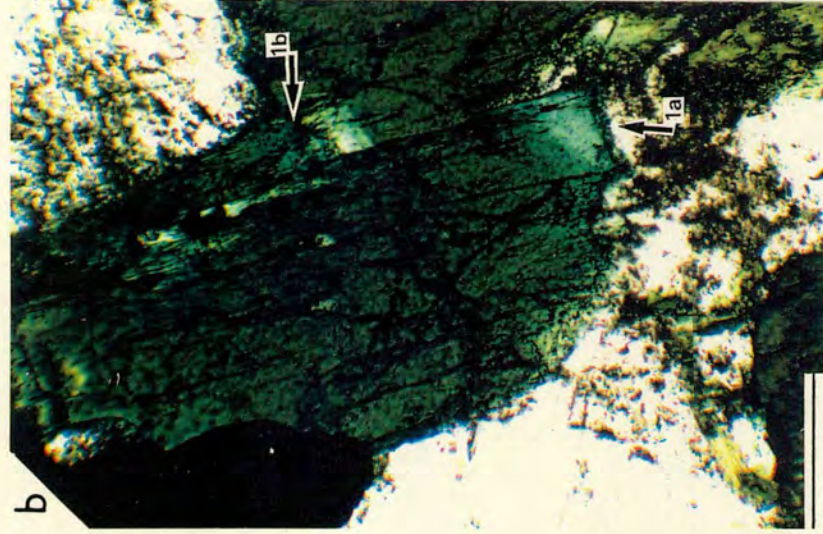
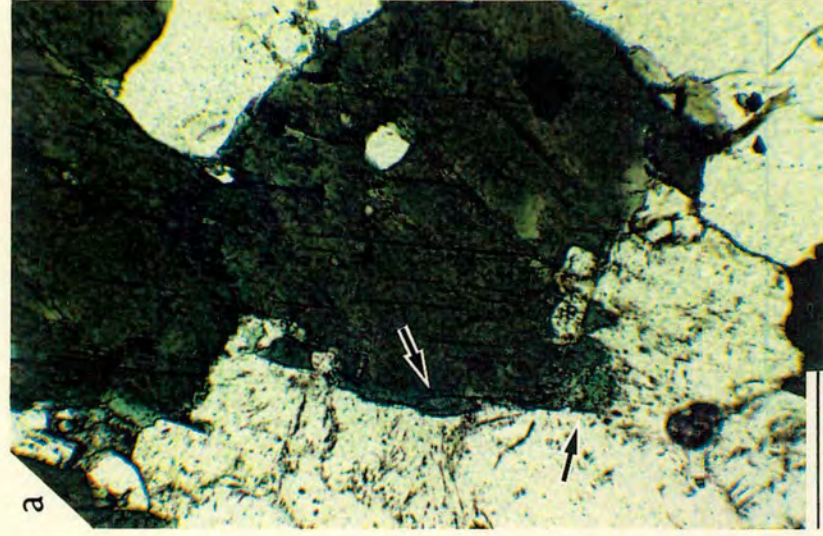


PLATE 29: BOUNDARY ALTERATIONS.

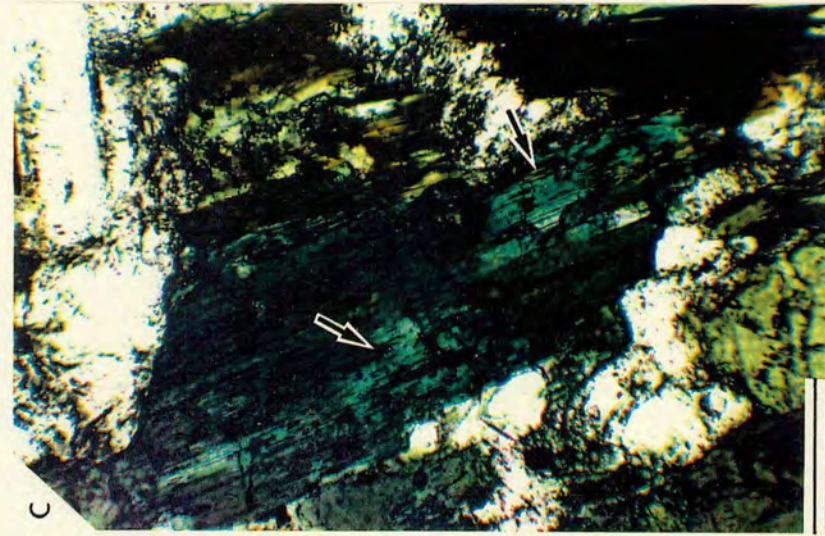
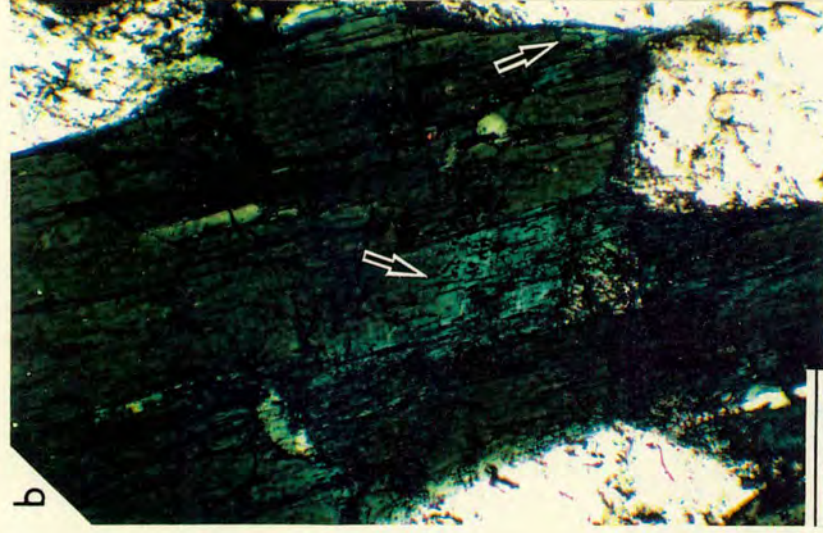
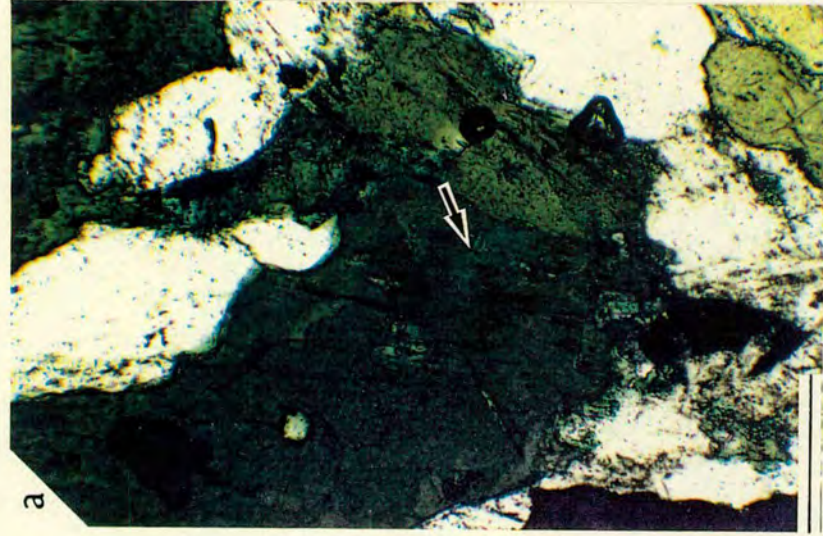
(a) Tiny spots of blue-green coloured amphibole adjacent to cleavage planes within an original amphibole (arrowed but look really hard!).

Scale bar: 0.2mm. (E18:PPL).

(b),(c) and (d): Segments of particularly well cleaved original amphibole crystals are altered to a bluer-green coloured amphibole.

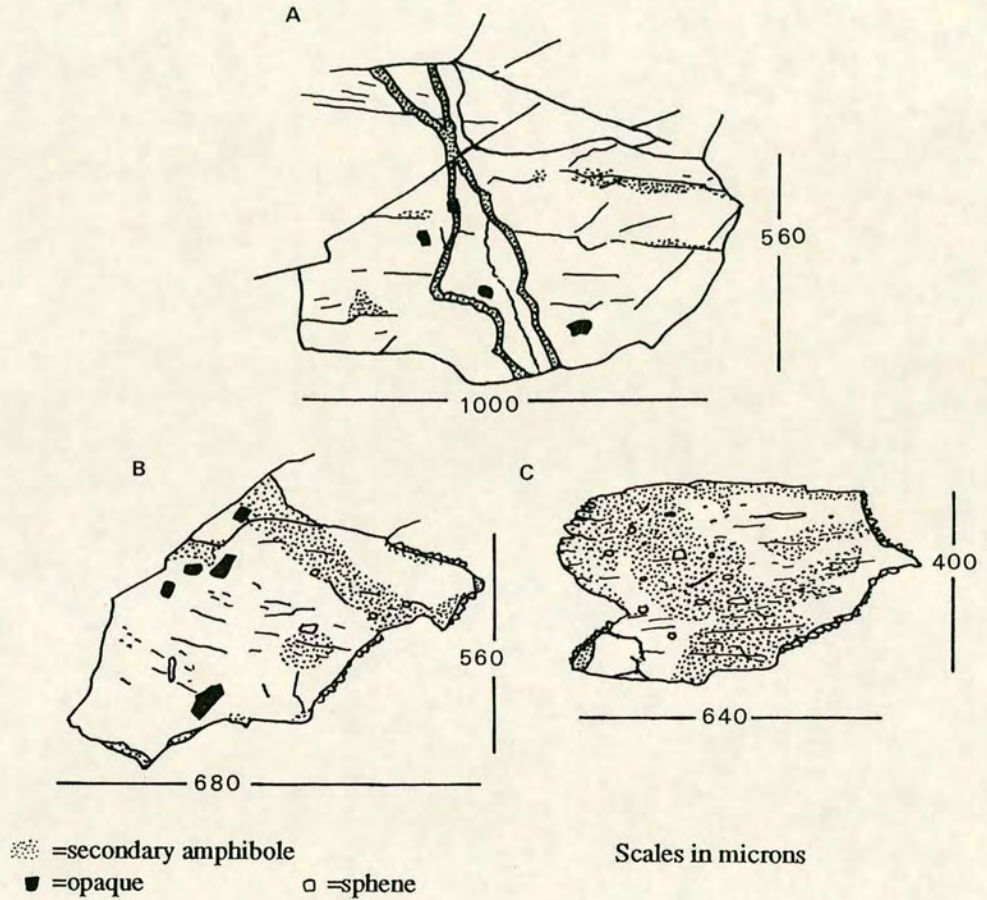
Scale bars: (b) 0.2mm. (E42:PPL).

(c),(d) 0.2mm. (E16:PPL).



(b) *Microvein alterations*

This type represents the cross-cutting mineral alterations observed, included are the intragranular, blue-green coloured, epitaxial amphibole microveins. The microveins may be either sharply bounded (Plate 30a,b,c) or more diffusely bounded features (Plate 30d). The following sketches depict several of the most commonly observed varieties. A photograph of the microveins in sketch A is presented in Plate 30a.



Plates 30-31 (see also Plates 33a,b and 35a) display microveins within the amphiboles, Plates 31c,d and 36d additionally exhibit examples of the types of microveins seen within the feldspars.

PLATE 30: MICROVEIN ALTERATIONS.

a,b,c,d: original amphibole crystals (dark-grey in black/white photographs) are traversed by blue-green coloured secondary amphibole microveins (pale-grey in black/white photographs).

(a) Sharply bounded, secondary amphibole microveins (arrowed 1) can be traced into the feldspar (arrow 2). Some secondary amphibole has overgrown the feldspar (arrow 3).

Scale bar: 0.2mm. (E29:PPL).

(b) High magnification view of secondary amphibole microveins. Note the sharpness of the contact between microvein and original amphiboles.

Scale bar: 0.006mm. (E29:PPL).

(c) A more complicated situation: a secondary amphibole microvein (arrow 1) cuts an original amphibole (dark-grey; arrow 2). Note also the extensive secondary amphibole alteration (arrowed 3) and the abundance of opaques.

Scale bar: 0.2mm. (E15:PPL).

(d) Diffusely bounded secondary amphibole microvein (arrowed) traversing original amphibole crystals. Note opaques.

Scale bar: 0.2mm. (E18:PPL).

PLATE 30

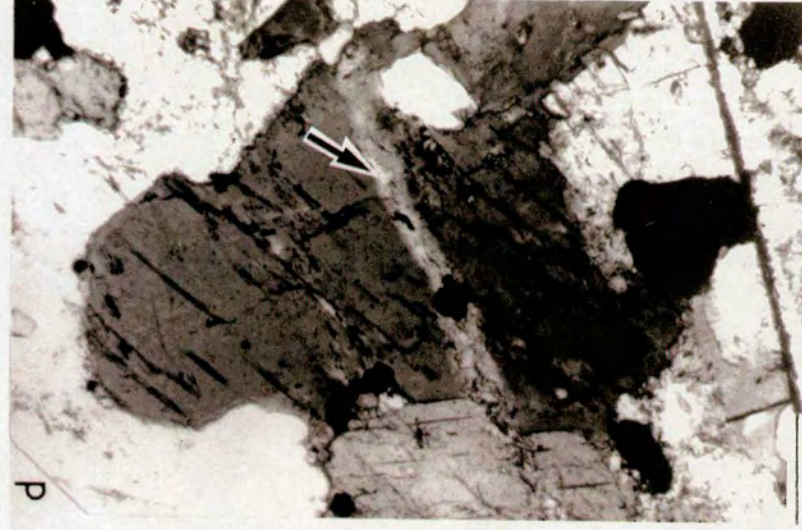
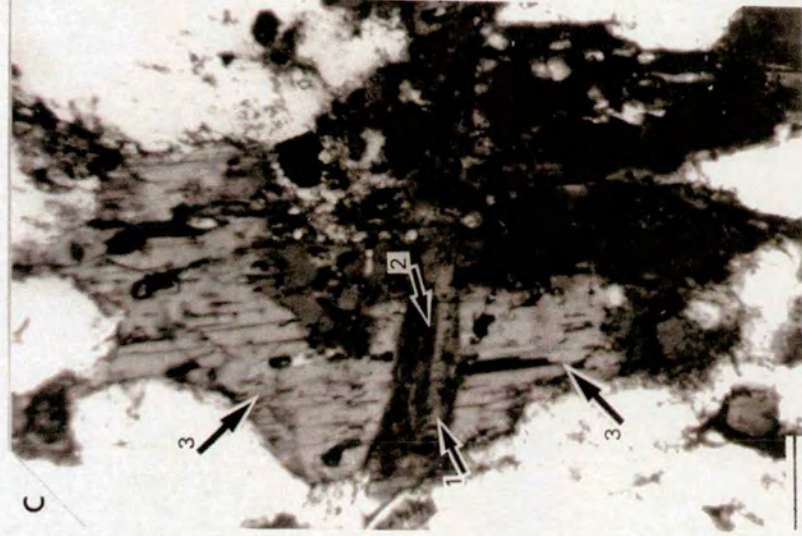
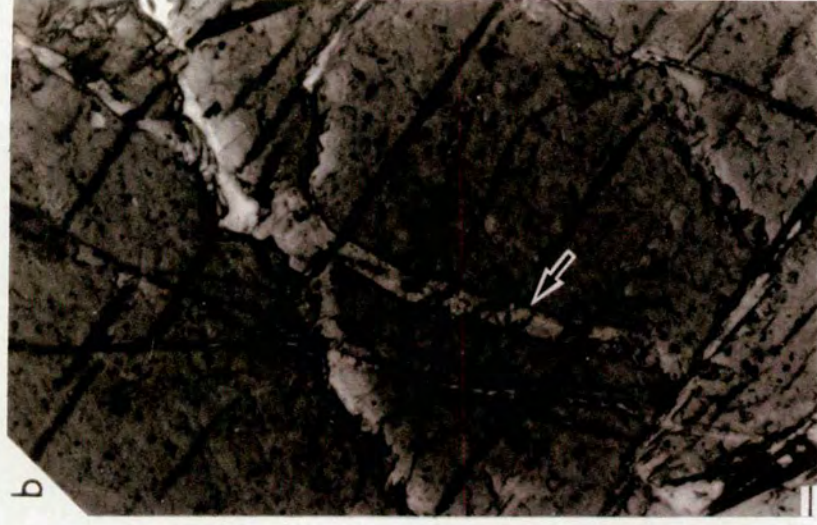
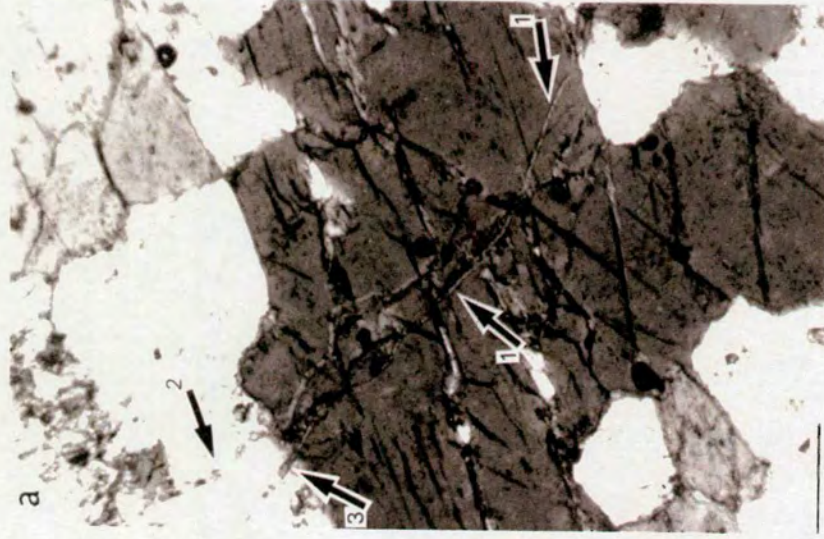


PLATE 31: MICROVEIN ALTERATIONS.

(a) Diffusely bounded alteration microveins within the feldspar (arrow 1) link with blue-green coloured, inclusion rich secondary amphibole microveins (arrow 2).

Scale bar: 0.4mm. (E52:PPL).

(b) Trails of small opaque inclusions (arrow 1) cutting across an amphibole crystal (no blue-green coloured alteration is observed in this instance). These trails link with similar inclusion trails within adjacent feldspar crystals (arrow 2) and a neomineralised pyroxene (arrow 3).

Scale bar: 0.2mm. (E29:PPL).

(c) Discretely bounded microveins cutting through feldspar.

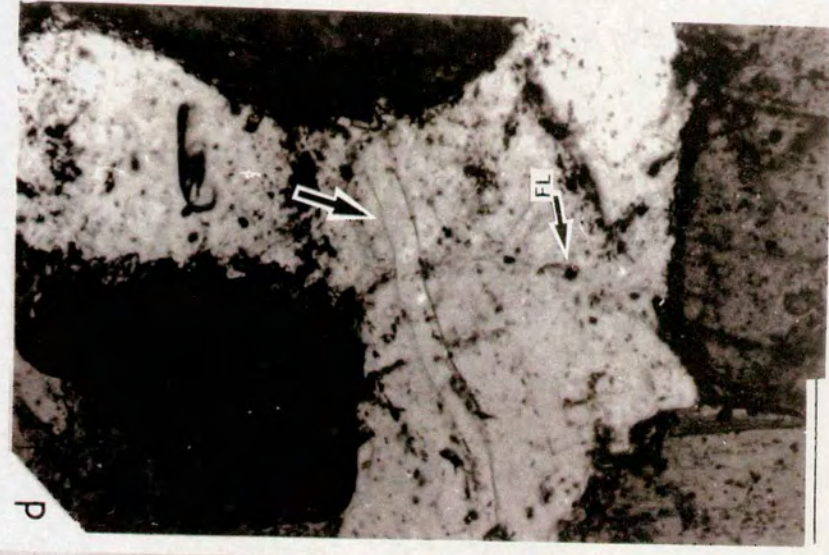
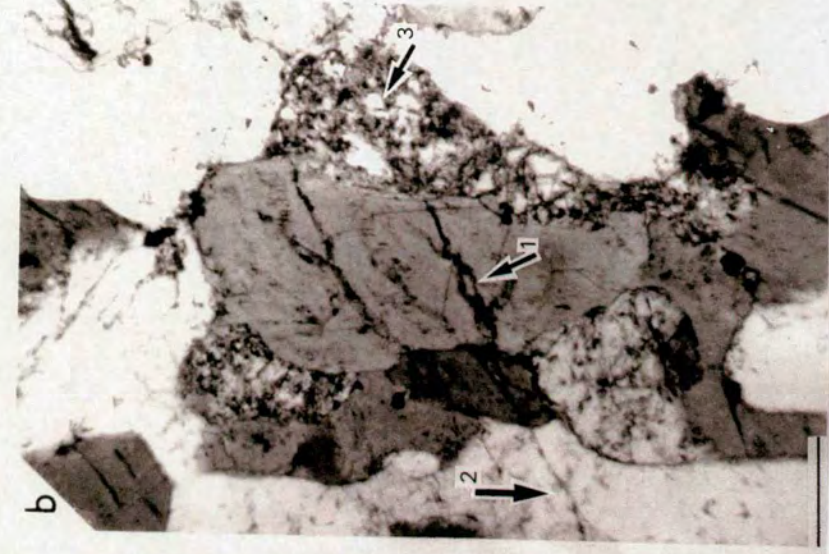
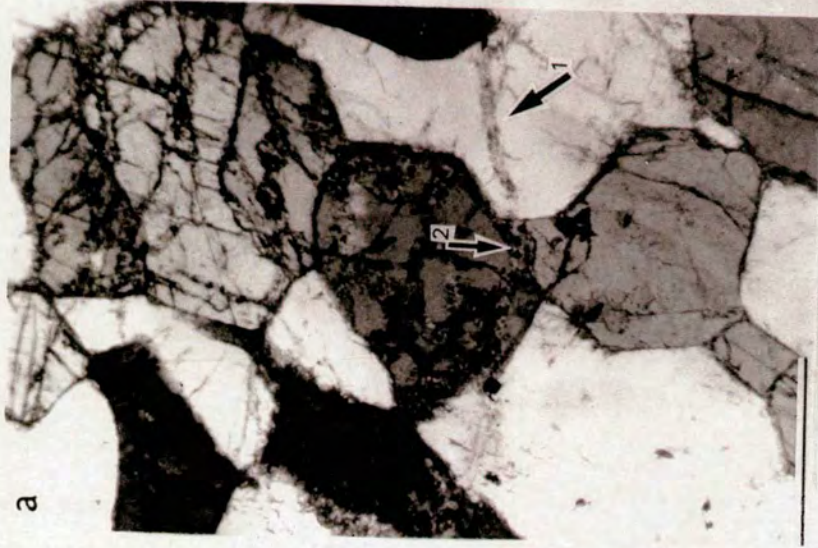
Scale bar: 0.25mm. (E29:PPL).

(d) Sharply bounded feldspar microvein (arrowed) cutting a host feldspar crystal.

Note fluid inclusions (arrowed FI).

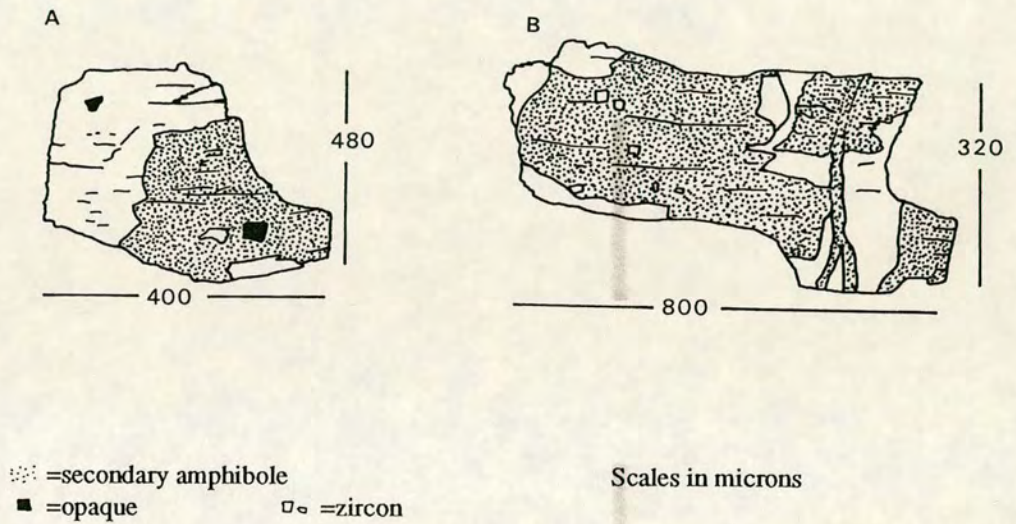
Scale bar: 0.1mm. (E29:PPL).

PLATE 31



(c) *Extensive single crystal alterations*

This type represents the more extreme alterations observed. This includes the more extensive epitaxial growths observed (seen in E16, E7, E8 *etc.* but overlapping to some degree with the boundary alterations previously described) in addition to the blue-green coloured, "pseudomorph-like" amphibole alterations described in E15. The following two sketches depict two grains within which large epitaxial growths are seen. A photograph of the altered amphibole illustrated in sketch B is presented in Plate 33c.



Plates 32, 33c,d, 34a,b and 35a show some of the more extensively altered amphibole crystals.

PLATE 32: EXTENSIVE SINGLE CRYSTAL ALTERATIONS.

a,b,c,d: Large segments adjacent to cracks and cleavage planes within original amphibole crystals (dark-grey in b/w plate) are altered to a blue-green coloured amphibole (pale-grey in b/w pictures). The secondary amphibole is a single crystal in optical continuity with the host. The interface between secondary and host amphiboles is abrupt. Note the abundance of opaque grains.

Scale bars: (a),(b),(d) 0.2mm. (E15:PPL).

(c) 0.2mm. (E18:PPL).

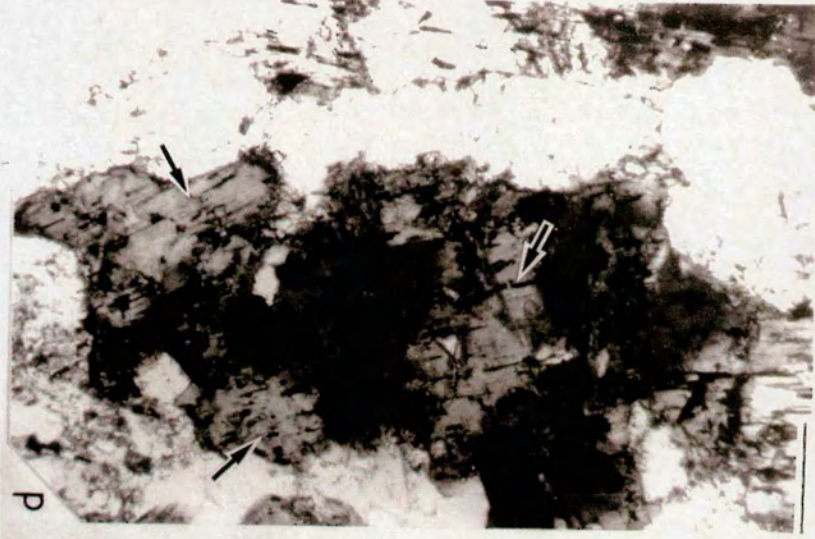
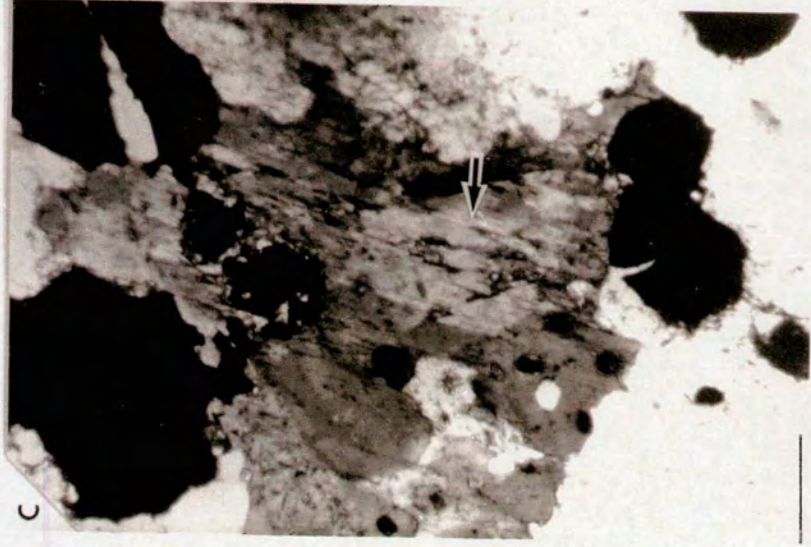
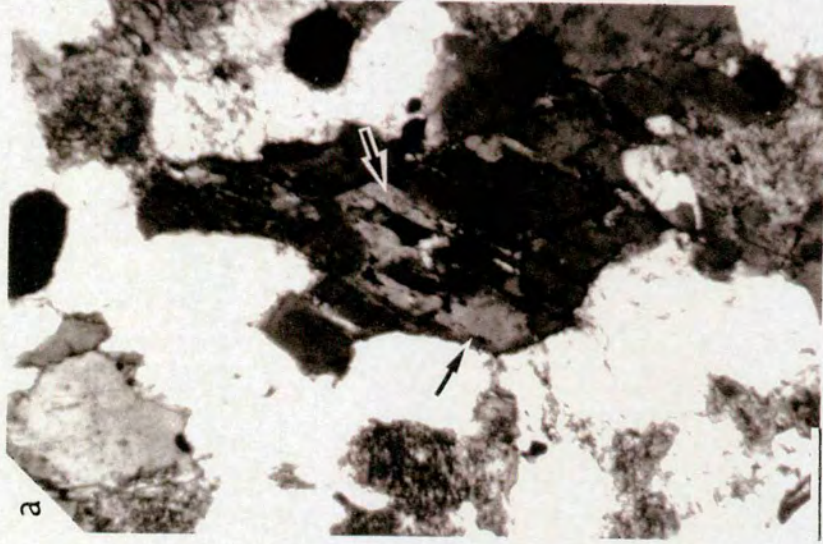


PLATE 33: MICROVEIN ALTERATIONS.

(a) Sharply bounded, blue-green coloured amphibole microveins traversing an original crystal. Note bifurcations and sinewy route taken. Note also microvein continues into feldspar (arrow).

Scale bar: 0.15mm. (E29:PPL).

(b) Both sharply bounded (arrowed 1) and more diffusely bounded secondary amphibole microveins (arrowed 2) within an original crystal.

Scale bar: 0.15mm. (E29:PPL).

EXTENSIVE SINGLE CRYSTAL ALTERATIONS

(c) Extensive, pseudomorph-like, blue-green coloured amphibole (arrow 1); few areas of the original, unaltered, dark-brown coloured amphibole remain (arrowed 2).

Scale bar: 0.2mm. (E15:PPL).

(d) XPL photograph of (c) note both blue-green coloured and host amphibole extinguish at the same angle.

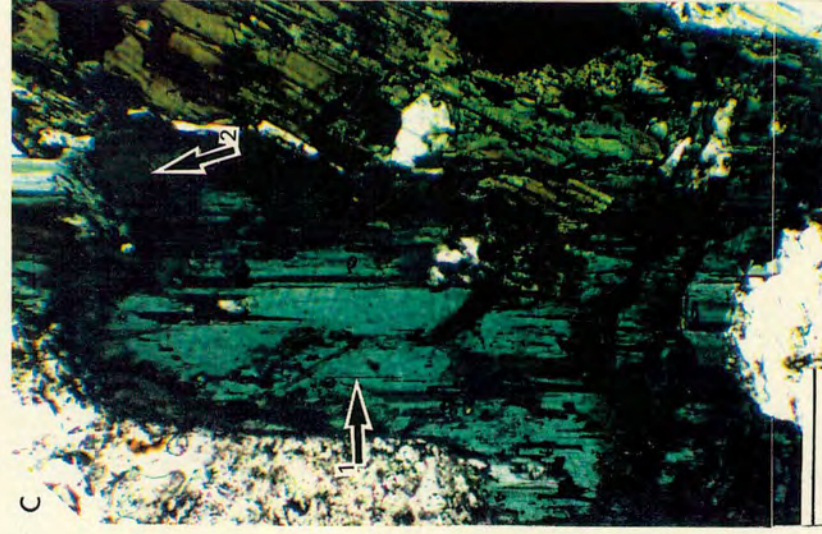
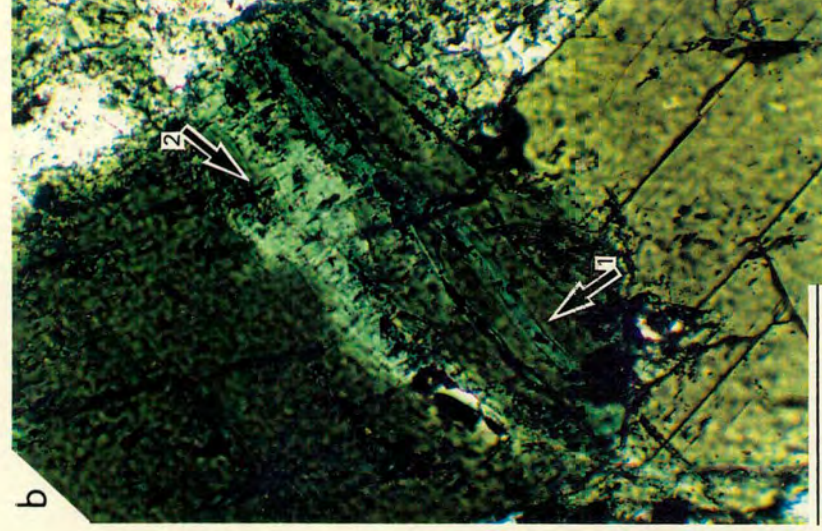


PLATE 34: EXTENSIVE SINGLE AND MULTI-CRYSTAL ALTERATIONS.

(a) and (b) Secondary amphibole (arrowed 1) has almost "pseudomorphed" the original amphibole (arrowed 2). Note the presence of small crystals of zircon within the secondary amphibole in b (arrowed 3).

Scale bars (a): 0.35mm. (E15:PPL).

(b): 0.4mm. (E15:PPL).

(c) Original amphibole grain is recrystallised to small, deep-blue-green coloured amphibole crystals (dark-grey in b/w photo; arrowed). New growth crystals have a different optic orientation to the host.

Scale bar: 0.08mm. (E11:PPL).

(d) Individual prism of secondary amphibole (arrow 1) along side an aggregate of secondary amphibole needles (arrow 2). The aggregate probably represents a completely recrystallised original amphibole grain.

Scale bar: 0.2mm. (E15:PPL).

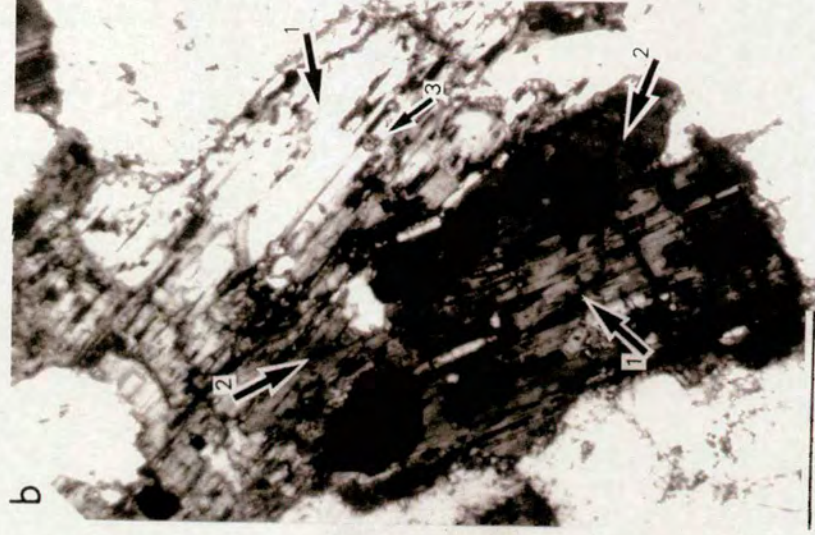


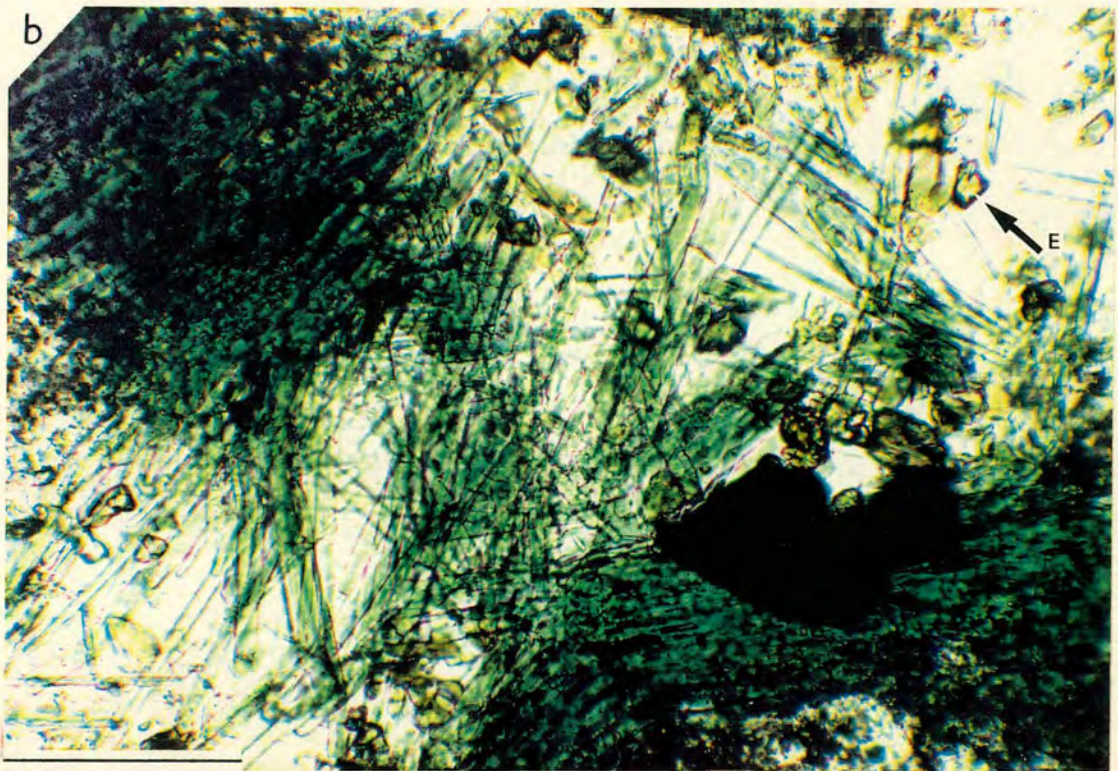
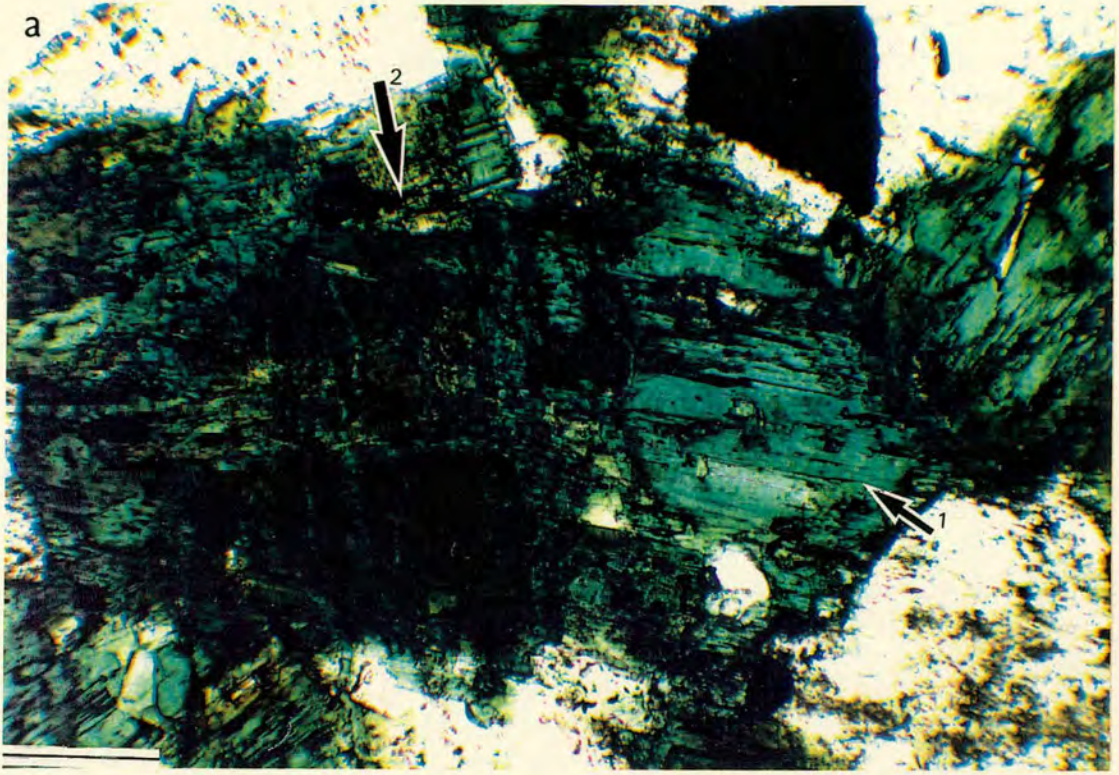
PLATE 35: EXTENSIVE SINGLE AND MULTI-CRYSTAL ALTERATIONS.

(a) Extensively altered original amphibole crystal; large parts of the original grain are 'pseudomorphed' by blue-green coloured amphibole (arrow 1). Note the original darker-brown coloured amphibole (arrow 2) is traversed by a fine network of blue-green coloured amphibole microveins.

Scale bar: 0.2mm. (E15:PPL).

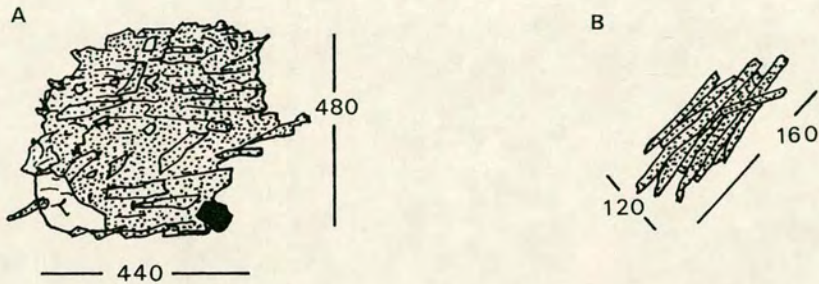
(b) High magnification photograph of blue-green coloured amphibole needles nucleating within a microfracture. Note yellowish crystals of epidote (E) within, and recrystallised amphiboles (R) bordering, the vein.

Scale bar: 0.15mm. (E16:PPL).



(d) *Extensive multi-crystal alterations*

Included within this group are situations within which pre-existing amphibole grains have completely recrystallised to aggregates of blue-green coloured amphibole crystals. Also included are aggregates and solitary laths of blue-green coloured amphibole needles which are apparently unattached to original amphibole grains (*e.g.* E15, E16). In the following sketches (A) is an example of a recrystallised grain, (B) an aggregate of amphiboles needles.



⊙ = secondary amphibole
● = opaque ○ = zircon

Scales in microns

Plate 34c displays a recrystallised grain, Plates 34d, 35b and 36a,b display isolated amphibole prisms and aggregates within the rock.

PLATE 36: EXTENSIVE MULTI-CRYSTAL ALTERATIONS.

(a) and (b) Secondary amphibole needles (arrowed) crystallised in feldspar microveins within the rock. Note epidote crystals (arrow E).

Scale bars (a): 0.3mm. (E16:PPL).

(b): 0.2mm. (E16:PPL).

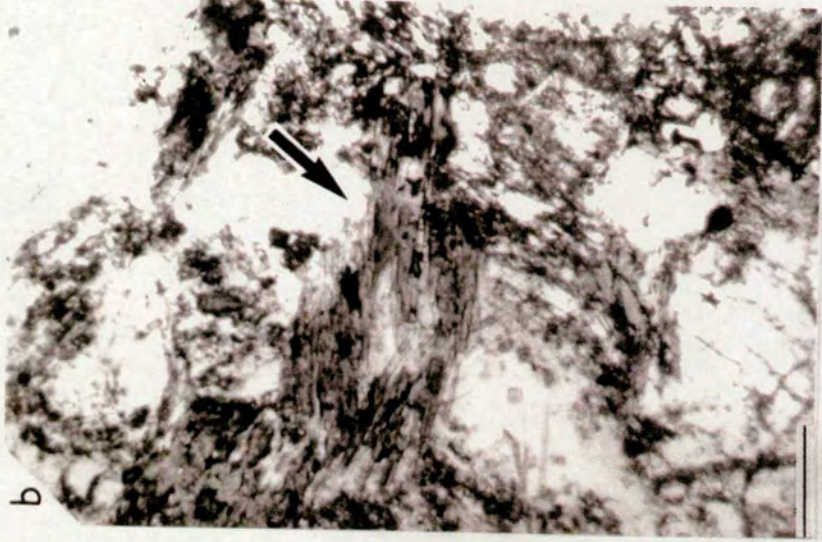
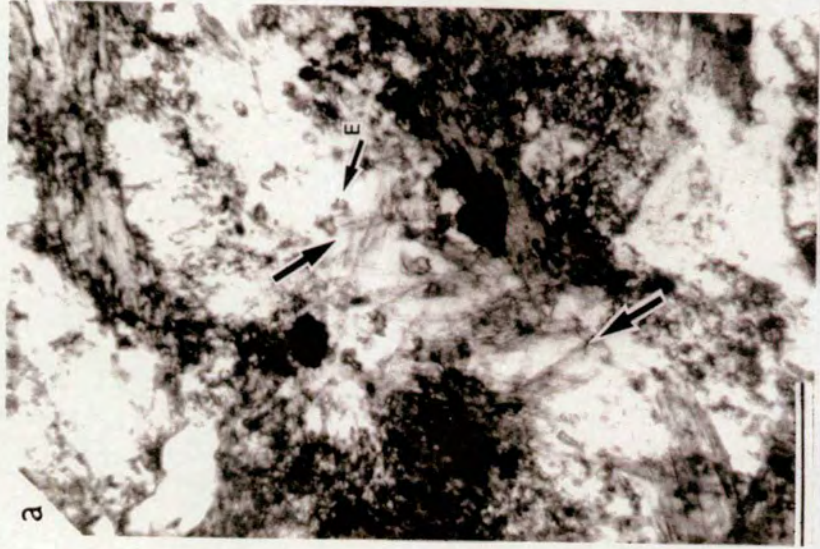
MICROFRACTURE PATTERNS

(c) Rock penetrative microfracture linking blue-green coloured amphibole microveins (arrowed A), neomineralised clinopyroxene (arrowed CPX) and feldspar microveins (arrowed F).

Scale bar: 0.2mm. (E29:PPL).

(d) Higher-magnification of area, arrowed F, in (c) showing the sharply bounded nature of the feldspar microveins. The feldspar microvein links with a microvein of secondary amphibole within an adjacent original amphibole crystal.

Scale bar: 0.06mm. (E11:PPL).



Secondary amphibole microveins and epitaxial growths (both boundary and extensive single crystal types) within individual rocks may occur in either one or a combination of the following two physical forms:

- 1: Those with a gradual interface between original and newly formed amphibole crystals or amphibole microvein margins. Here a continuous change in colour from original yellow-green/brown to blue-green is observed with no apparent discontinuity or grain-boundary between the two regions.
- 2: Those with an abrupt interface between original and newly formed amphibole. In most instances a grain-boundary is not obvious.

In addition to these types a third less commonly encountered situation has also been observed:

- 3: Certain blue-green coloured amphibole interfaces, microvein margins and occasional areas within thin-sections have been observed adjacent to or within which "crystallisation" of a new amphibole has taken place. The new growth amphibole occurs as small, well formed crystals, often needles but its presence is not always reliant upon a reconstitution of an original amphibole (*i.e.* not recrystallisation). Some of these crystals appear to have grown within once fluid-filled voids and/or microfractures adjacent to or within original amphibole crystals within the rocks.

4.3. DISTRIBUTION OF ALTERATIONS WITHIN THE AMPHIBOLITES

4.3.1. DISTRIBUTION WITHIN INDIVIDUAL THIN-SECTIONS

Most of the mineral alterations described in section 4.2. are developed to some degree within every rock examined. Rocks collected at distances between 0.15m. and 3km. from the contact with the quartz monzonite stock show widely variable and irregular effects; some are almost entirely pristine whilst others exhibit large areas within which substantial partial alteration has taken place. Table 4.1. shows the amphibole alteration types distinguished within each of the amphibolitic rocks collected.

The less-pristine regions of thin-sections, within which *all* the mineral alterations (including blue-green-amphibole alteration types a,b,c and d) occur, define the presence of pervasive "*alteration zones*" within the rock. Two main types of "alteration zone" have been distinguished:

- (i) Microfracture networks.
- (ii) Permeation zones.

these are discussed in turn below:

- (i) Microfracture networks (as seen in E52 and E15)

Cross-cutting microfractures can be traced through the rock linking secondary amphibole microveins, alteration microveins within the plagioclases and inclusion trails (Plates 36c,d, 31a,b, 30a).

Microfractures occur as either relatively straight, highly penetrative features (*e.g.* E52) or as more irregular, anastomosing (though still cross-cutting), often bifurcating features (*e.g.* E15).

A discrete physical zone of boundary alterations usually occurs adjacent to microfractures within the rocks; *i.e.* an alteration halo borders individual microfractures.

An increased abundance of "opaques" ± epidote is commonly observed in most regions of rocks which are pervaded by microfractures.

Plate 37 presents both low and high magnification views of a typical microfracture pattern.

TABLE 4.1.AMPHIBOLITIC ROCK ALTERATION DISTRIBUTIONS.

SPEC. N ^o	DIST /m.	ROCK TYPE	ALT ^N TYPE	ALT ^N ZONES	LEUCO SEAM	ORE/% Mt/Py/Cpy
E15	0.15	AMPHIB	a,b,c,d	MF/IPZ	X	9/1/0
E11	0.40	AMPHIB	a,d		✓	8/2/0
E16	1.45	BIO AMPHIB	a,c,d	MF	✓	2/<1/0
E17	2.75	BIO AMPHIB	a,b	MF	✓	5/≥1/tr
E12	4.0	PYROX AMPHIB	a,b	MF	✓	5/?/?
E18	4.1	PYROX AMPHIB	a,b,c	MF	✓	7/tr/0
E20	6.7	AMPHIB	a,b	MF	✓	2/0/0
E21	8.7	BIO AMPHIB	a		✓	6/1/tr
E22	12.7	AMPHIB	a,b	MF	✓	<1/0/0
E25	13.5	AMPHIB	a,b	MF	✓	4/1/0
E5	15	PYROX AMPHIB	a	MF/IPZ	✓	3/<1/tr
E6	15	PYROX AMPHIB	a,b	MF±IPZ	X	3/<1/0
E7	15	PYROX AMPHIB	a,b,c,d	MF	X	9/>1/tr
E8	15	PYROX AMPHIB	a,b,c,d	MF/IPZ	X	8/2/tr
E28	24	AMPHIB	a,b	MF	✓	2/<1/0
E29	27	PYROX AMPHIB	a,b	MF/IPZ	✓	3/<1/0
E30	35	BIO AMPHIB	a		✓	3/tr/0
E33	55	PYROX AMPHIB	a,b	MF	✓	2/tr/0
E34	73	PYROX AMPHIB	a,b	MF/IPZ	✓	3/tr/0
E37	158	PYROX AMPHIB	a	MF	✓	3/<1/0
E40	220	PYROX AMPHIB	a,b	MF	X	6/1/tr
E42	280	AMPHIB	a,b	MF	✓	6/>1/0
E47	437.5	PYROX AMPHIB	a	IPZ	X	5/<1/0
E50	525	AMPHIB	a,b	MF	✓	7/tr/0
E52	662.5	AMPHIB	a,b	MF/IPZ	X	2/1/0
E53	887.5	PYROX AMPHIB	a,b	MF	X	5/1/tr
E55	1075	PYROX AMPHIB	a,b	MF	X	3/tr/0
E58	1137.5	BIO AMPHIB	a,b	MF	✓	1/4/tr
E62	1575	PYROX AMPHIB	a,b	IPZ	✓	4/<1/tr
E64	1887.5	BIO AMPHIB	a,b	MF±IPZ	✓	2/1/tr
E66	2187.5	PYROX AMPHIB	a,b	MF/IPZ	X	2/0/0
E68	2587.5	AMPHIB	a,b		✓	4/tr/0
E69	2800	PYROX AMPHIB	a,b	MF/IPZ	✓	5/>1/tr
E71	2800	PYROX AMPHIB	a,b	MF	✓	3/<1/0

ROCK TYPES:-

AMPHIB=amphibolite.

PYROX AMPHIB=pyroxene amphibolite.

BIO AMPHIB=biotite amphibolite.

ALTERATION TYPES:-

a=boundary alterations.

b=microvein alterations.

c=extensive single crystal alterations.

d=extensive multi-crystal alterations.

ALTERATION ZONES:-

MF=microfracture network.

IPZ=independent permeation zone.

LEUCOCRATIC SEAMS (with border permeation zones):-

✓ denotes presence X denotes absence.

ORE:-

Mt=magnetite Py=pyrite Cpy=chalcopyrite.

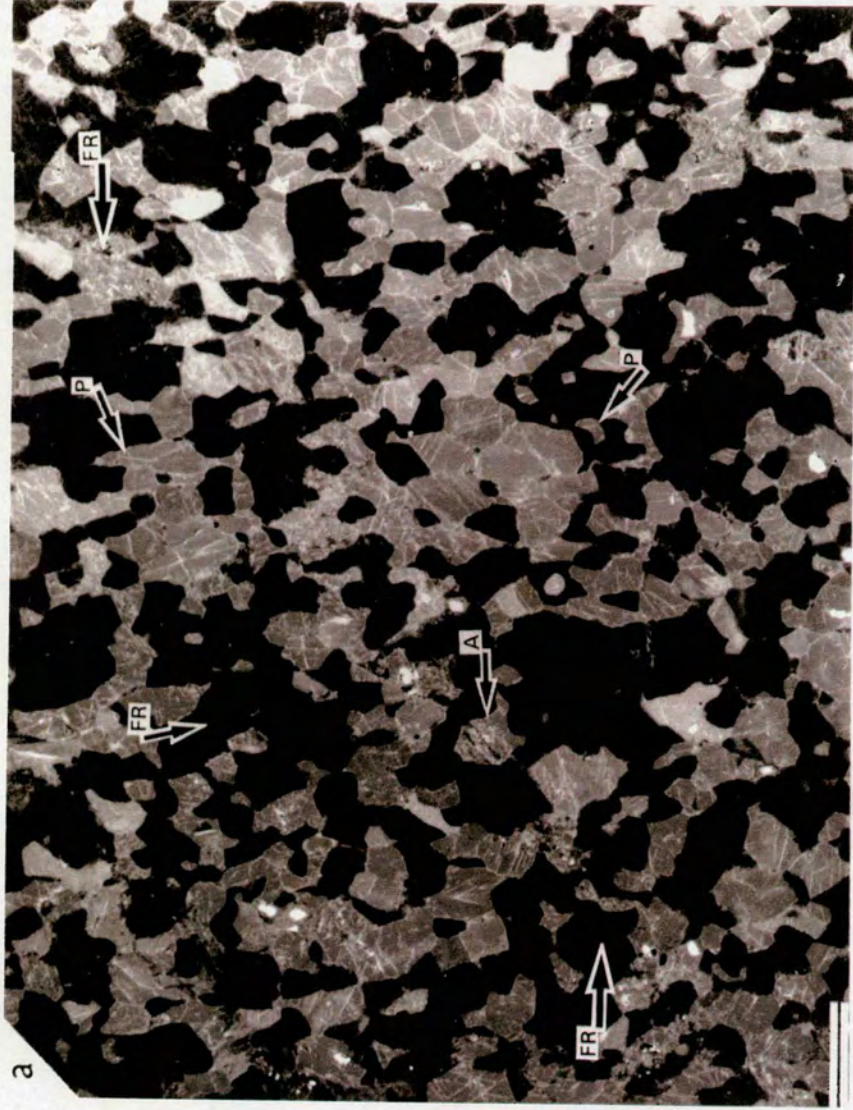
PLATE 37: MICROFRACTURE NETWORKS.

(a) Negative print from thin-section of E52:- amphiboles (grey), feldspar (black), opaques (white). A zone of microfractures (arrowed FR) can be traced from top right to bottom left. Note the increased abundance of opaques, the alteration of crystals close to the microfractures and the pristine textures elsewhere (arrowed P). Arrow A denotes the position of the grain enlarged in (b).

Scale bar: 1mm. (E52).

(b) PPL photograph of grain indicated in (a). The microfractures result in preferential alteration of the feldspars and alteration microveins within the amphibole. Note epidote aggregates (arrow E) and opaques.

Scale bar: 0.25mm. (E52:PPL).



(ii) Permeation zones (as described in E15, E5 and E21)

Definite bands of alteration occur within some rocks without any clear evidence of a central fracture network.

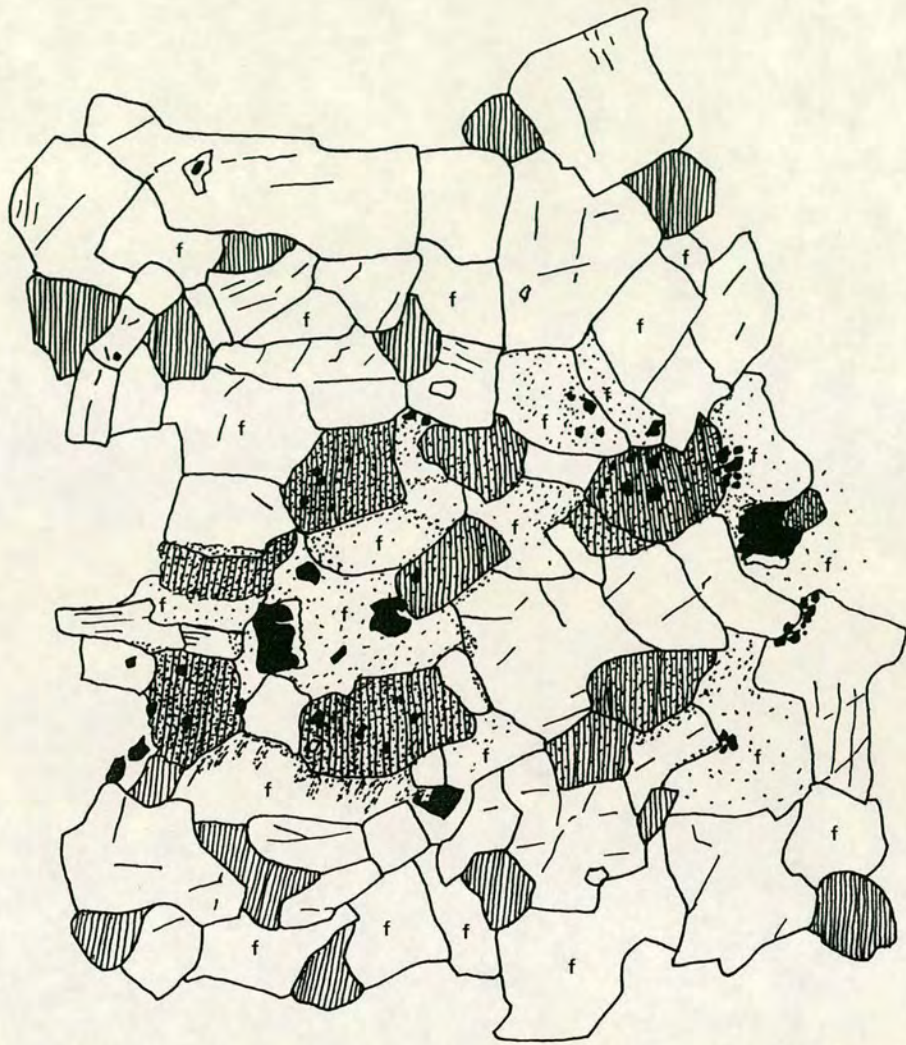
Within the permeation zones the secondary amphibole alteration is either of Boundary or Extensive single/multi-crystal types (or a combination of the two). Frequently the most prominent feature of permeation zones are the preferential neomineralisation and replacement of clinopyroxene crystals falling within them. Individual amphibole crystals within some of the permeation zones occasionally contain a secondary amphibole microvein; these are restricted to specific crystals however rather than linking with microveins within other phases, as is the case of the microfracture networks.

There is often an increase in the abundance of "opaques" ± epidote within the permeation zones.

A sketch of a typical permeation zone is presented in Figure 4.1.

Permeation zones are seen on scales ranging from those clearly visible within thin-sections (*e.g.* E5, E15) to those encompassing the entire thin-section (*e.g.* E21).

Plate 38 presents two negative prints of permeation zones within two of the rocks (E5 and E15) described in section 4.1.3.



1mm.



FIG.4.1. Sketch of a narrow permeation zone (described in E5). Clinopyroxene and plagioclase feldspar crystals are particularly altered, original amphiboles exhibit some secondary amphibole development adjacent to their grain-boundaries. Note the particularly high abundance of opaques (magnetite and pyrite).

PLATE 38: PERMEATION ZONES

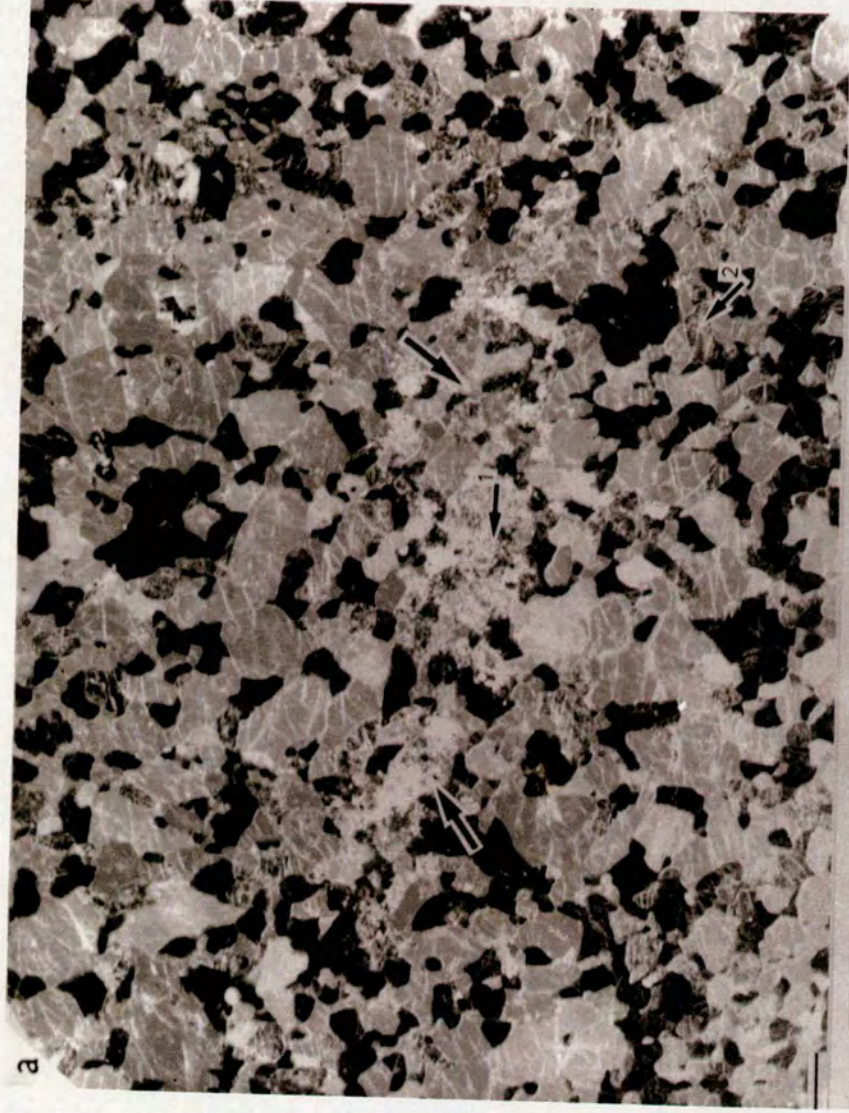
(a) Negative print of rock E5:- amphibole (grey), pyroxene (dark-grey), feldspar (black), opaques (white). A diffusely bounded physical band approximately 2mm wide (arrowed) can be distinguished running from centre left to right. Within this band there is a marked increase in abundance of opaque grains (pyrite and magnetite) and the clinopyroxenes are more highly altered (arrowed 1). Beyond the band the rock is predominantly pristine; clinopyroxenes are fresh (arrowed 2) and there are far fewer opaques.

Scale bar: 1mm. (E5).

(b) Negative print of rock E15:- amphibole (grey-white), feldspar (black) and opaques (white). The physical band of greater alteration (arrowed) runs approximately centre left to bottom right. Within the band the amphiboles are extensively recrystallised; beyond the band of greater alteration the rock is not entirely pristine (as E5) but exhibits generally fresher original crystals.

Scale bar: 1mm. (E15).

PLATE 38



IDENTIFICATION OF ZONES OF ALTERATION WITHIN THE ROCKS

Microfracture network identification is fairly straightforward, since it involves the linking of microveins between adjacent phases. Permeation zones are not so clearly defined since they usually have diffuse margins. Examination of the distribution of the permeation zones shows that they are of two principal types:

- (i) *Independent permeation zones* - those which are unassociated with leucocratic seams.
- (ii) *Border permeation zones* - those which border leucocratic seams.

Independent permeation zones of *Boundary* alterations such as those described in E5 (Plate 38a) are readily identifiable in thin-section (though not hand-specimen), and are seen within numerous additional rocks (e.g. E11, E29, E34, see Table 4.1).

A more difficult situation arises in border permeation zones (such as E21); here *Boundary* amphibole alterations again predominate but no outer limits to the zone is visible within either thin-section or hand-specimen. The widths of these permeation zones are considered to be broader than the width of the thin-section but their absolute widths are not known.

Chapter 1 established the widespread occurrence of leucocratic-seams within the rocks. In thin-section preparation a conscious effort was made to incorporate some portion of these coarser-grained seams; they are therefore commonly encountered within most of the thin-sections available (Table 4.1. indicates the sections within which seams have been incorporated). Of the thin-sections described E5 barely intercepts one edge of a seam adjacent to which *Boundary* amphibole alterations were noted. The thin-section of E21 has a leucocratic-seam running approximately through its centre; adjacent to both sides of the seam the amphibolitic rock again displays an abundance of *Boundary* alterations. This relationship exists in every section within which leucocratic seams have been incorporated; bands of *Boundary* amphibole alterations are therefore believed to usually border the leucocratic seams. With the exception of E15 and E7, all sections (e.g. E52, E6, E53, E66) without leucocratic seams are predominantly pristine. Any optically visible amphibole alterations within rocks lacking leucocratic-seams can be directly related to the presence of either rock penetrative microfractures or independent permeation zones.

As both independent *and* border permeation zones result in alterations of Boundary types it is usually too difficult to be able to delimit any independent permeation zones within permeation zones bordering leucocratic seams. It is also quite difficult to clearly distinguish between alteration haloes adjacent to microfractures and independent permeation zones. Table 4.1 documents the microfractures and independent permeation zones which have been identified in each amphibolitic rock examined. Border permeation zones have been encountered in those rock-section which incorporate some portion of a leucocratic seam.

AGE RELATIONSHIP BETWEEN MICROFRACTURES AND BANDS

Relating the mineral alterations entirely to either microfracture networks and/or permeation zones within the rocks is often quite difficult. Boundary amphibole alterations are observed as both haloes adjacent to microfractures and within permeation zones, this makes it very difficult to establish with any degree of certainty whether a cross-cutting relationship exists. Microfracture networks are often present within some of the border permeation zones, however the large scale (> thin-section) of these bands prevents any relative age relationship to be determined. Independent permeation zones of Boundary amphibole alterations which are visible within thin-sections (E5, E29, E11, E34) have been examined in some detail though no conclusive relationship between these and co-existing microfracture networks within the rock could be determined.

INTERPRETATION OF DISTRIBUTION PATTERNS

Mineral alterations have been comprehensively documented in the preceding sections as having sporadic developments within individual crystals which can be related to microfracture networks and/or permeation zones within the rocks. The presence of such 'zones of alteration' (*i.e.* microfractures and permeation zones), in addition to the sporadic nature of the secondary mineral developments within the alteration zones and the increase in abundance of "opaques" within the rocks, is clearly suggestive of "fluid" activity. Alteration of parts of original minerals has only occurred where fluids have gained access to the crystal. Fluids appear to have primarily invaded the rocks via the networks of microfractures, independent permeation zones and leucocratic seams. Some grain-boundaries within the amphibolitic rocks must have been less tight than others enabling the fluids to also partially "flow" around grain-boundaries adjacent to the major fluid "conduits"; thus resulting in the observation of

alteration haloes to microfractures and alterations within both independent and border permeation zones. The results of this partially penetrative, partially anastomosing fluid activity is quite evident in the alteration patterns distinguished within the original amphibole crystals. Boundary amphibole alterations, and perhaps to some extent microveins, reflect the passage of fluids along pre-existing cracks and cleavages within the crystals. The more clearly cross-cutting microveins and extensive single crystal alterations are believed to be a result of more pervasive fluid activity. In addition to causing the mineral alterations described the fluids introduced magnetite, pyrite and minor chalcopyrite to the rocks.

4.3.2. ALTERATION DISTRIBUTION AT OUTCROP SCALE.

Table 4.1 provides information on the spatial distributions of microfracture networks and independent permeation zones within the amphibolitic rocks. Border permeation zones occur in rocks with leucocratic seams and in effect they occur throughout the area sampled. Microfracture networks and independent permeation zones are also seen to occur at all distances from the igneous contact and no single type can be directly related to a specific position within any "aureole".

Boundary and microvein amphibole alterations (a's and b's in Table 4.1) have a particularly widespread distribution, occurring within nearly every rock. Rocks within ~2m of the contact *additionally* contain a high proportion of extensively altered and recrystallised amphibole grains (c's and d's in Table 4.1). Extensive single and multi-crystal amphibole alterations have only been recognised in one other situation, represented by rocks E7 and E8 collected about 15m. from the contact. A metre-wide mineralised ore-shear (noted in field studies; see chapter 1) occurs immediately adjacent to this sample locality. Similar ore-shears occur intermittently throughout the region but their exact positions in relation to the remaining samples is not known. Plate 13a illustrates one of these ore-shears situated approximately 3km. from the Stock-amphibolite contact. This late-stage mineralisation seems to have taken place in localised zones associated with joint planes or small faults within the rocks. It is interesting to note that a very similar rusty weathering patch can be seen almost immediately adjacent to the Stock-amphibolite contact (Plate 13b), close to which E15 was collected.

MINERALISATION.

Although "opaque" minerals only constitute a small modal percentage of the rocks their relative abundances at both thin-section and outcrop scales is crucial to determining the history of the rocks.

'Zones of alteration' (of all types *i.e.*; microfractures, independent permeation zones and border permeation zones) within individual rocks are usually associated with an increased abundance of "opaques" (magnetite \pm pyrite \pm chalcopyrite). This is in marked contrast with pristine parts of the rock which are devoid of pyrite and chalcopyrite and usually contain <2% magnetite. The relative abundances and distributions of magnetite, pyrite and chalcopyrite within the amphibolites are presented in Table 4.1. Rocks E15 (0.15m.), E11 (0.40m.), E7 (15m.) and E8 (15m.) contain a noticeably greater abundance (*c.*10%) of both magnetite (8-9%) and pyrite (1-2%). Rocks E7 and E8 were collected adjacent to a mineralised ore shear, rocks E15 and E11 were collected close to a distinct mineralised patch adjacent to the Stock contact. Between and beyond the rocks collected adjacent to the contact and the mineralised ore shear the percentages of magnetite, pyrite and chalcopyrite are more irregular, averaging *c.*4% combined.

4.4. CONCLUSIONS/INTERPRETATIONS

Secondary amphibole has developed with a widely variable distribution within all the rocks collected irrespective of their position from the Eldora Stock. The development of secondary amphibole be it of Boundary, Microvein, Extensive single or Extensive multi-crystal types has in every case been linked to pervasive 'zones of alteration' within the rock. The 'zones of alteration' occur in two main types:

- (i) Microfracture networks and their associated alteration haloes.
- and
- (ii) Definite but diffuse permeation zones.

Permeation zones occur both adjacent to leucocratic seams and independently within the rocks (hence border and independent permeation zones). Fluids associated with both microfracture networks and permeation zones are believed to have introduced magnetite \pm pyrite \pm chalcopyrite to the rocks.

In addition to intrusion of the Laramide quartz-monzonite stock at least two major PreCambrian events have affected the rocks (discussed in chapter 1):

- (i) Migmatisation (c.1750my)
with which the leucocratic seams are associated.
- (ii) Retrogressive metamorphism (c.1410my)
Mostly thermal effects associated with the intrusion of the Silver Plume Granite. This resulted in a re-setting of K-Ar ages but otherwise has had unknown affects upon the rocks.

In addition two main mineralisation episodes have occurred:

- (i) PreCambrian mineralisation
including the introduction of pyrite, chalcopyrite and magnetite.
- (ii) Laramide mineralisation
introduction of pyrite, chalcopyrite and magnetite.

The wide-spread occurrence of both Boundary and Microvein amphibole alterations beyond any likely "contact aureole" to the Eldora Stock, and the complex history of the rocks outlined above, and in more detail in chapter 1, suggest that several alteration-events have occurred. Although Hart (1964) was probably correct in assuming that a single re-heating event (associated with Stock

emplacement) had affected the rocks *since* PreCambrian times, he did not elaborate upon the effects produced by the complex PreCambrian events themselves nor upon the post-Cambrian mineralisation events affecting the rocks without obvious reheating.

The border zones of Boundary alterations adjacent to leucocratic seams are most likely to have developed in association with the intrusion and formation of the leucocratic seams. They may have formed either with intrusion of leucosome material or subsequently, perhaps with the expulsion of H₂O associated with the crystallisation of the minerals now constituting the seam. Olsen (1982, 1984) suggests the migmatitic rocks within the Idaho Springs Formation (see chapter 1) developed via infiltration of a water-rich fluid along subparallel channels in the rock. This infiltration led to a metasomatic reaction and partial melting of the wall rocks. The possibility that some mineral alteration zones were present prior to intrusion of the leucocratic seams, or developed from younger fluids which utilised the leucocratic seams as major fluid channelways, cannot be ruled out, however the intimate relationship between leucocratic seams and border permeation zones suggests their formation was probably related. The nature and distribution of the leucocratic seams within the amphibolitic rocks at Eldora was discussed in chapter 1. The often complex cross-cutting and ptymatitic relationships seen in the field (Plates 8b,c, 9a, 12a) suggests that they may have resulted from more than one 'intrusive' episode associated with PreCambrian migmatisation (*c.*1750my).

Independent permeation zones have a generally widespread distribution within the amphibolites at Eldora. Though independent permeation zones are clearly visible in thin-section they are difficult to identify in hand-specimen unless feldspar crystals falling within their bounds have been preferentially epidotised. There is little evidence available from which the relative age relationship between these and the border permeation zones can be conclusively derived, however their widespread distribution suggests a regional as opposed to a localised fluid event.

Microfracture networks occur widely within the amphibolitic rocks at Eldora. In some handspecimens, such as E21 (Plate 18), the microfracture networks show no continuity across nor occur within leucocratic seams which cut the rocks. This and the widespread distribution, suggests that some of the microfractures may be the result of a regional event (or events) which occurred either with the intrusion and/or formation of the leucocratic seams or at a later

date but none-the-less related in some way to the leucocratic seams. A minority of microfracture networks within other rock specimens have been seen which do cross-cut co-existing leucocratic seams and independent permeation zones. This indicates that a microfracture controlled alteration event definitely took place after the formation of both the leucocratic seams (and their border permeation zones) and at least some of the independent permeation zones. In thin-section alteration haloes adjacent to microfracture networks and boundary alterations within the independent permeation zones are identical; cross-cutting relationships cannot be identified with confidence.

The fluids responsible for the formation of microfracture networks within the amphibolites thus seem to have originated from more than one event. Depending on the origin of the fluids, microfractures may have developed from a combination of the following:

- (i) the same fluids which produced the leucocratic seams and their border alteration zones. Thus some microfractures are PreCambrian in age.
- (ii) different fluids to those which created the border alteration zones. In this case the fluids may either: (a) have utilised the leucocratic seams as major pathways from which offshoots into the more competent amphibolitic rock took place thereby enabling microfractures to develop, or (b) have pervaded the rock via grain-boundaries and fissures *etc.* which were entirely unrelated to the leucocratic seams.

In both these cases the fluids forming the microfractures may have been either PreCambrian and/or Laramide in age.

It has not been clearly established whether some the microfracture networks and independent permeation zones are similar in age or not. A small minority of microfractures have been observed in some hand-specimens which cross-cut independent permeation zones. This relationship is not widespread but does suggest that some microfractures are younger than some independent permeation zones. Since microfractures and independent permeation zones have affected the rocks in such different ways it seems likely that they represent different alteration events whose age or ages are not entirely certain.

It has not been possible to convincingly establish the relative ages of the independent permeation zones, border permeation zones and microfracture networks within the rocks. Though border permeation zones are most likely to be PreCambrian, independent permeation zones and microfracture networks probably formed from a combination of both PreCambrian and Laramide events.

CONTACT EFFECTS

A detailed optical examination of rocks originating adjacent to the Eldora Stock contact (*i.e.* E15, E11, E16) revealed a far more extensive alteration (extensive single and multi-crystal amphibole alterations) of the original amphibole crystals and a higher abundance of ore minerals than was seen elsewhere in the amphibolites *other* than rocks E7/E8 collected adjacent to a mineralised ore shear. Since both the Stock and ore shears are known to be Laramide in age (Cree, 1948; Hart, 1964) these distinct alteration and mineralisation phenomena are believed to represent the effects of Laramide events.

The Laramide orogeny is known to span a period of *c.*100my, from Late Cretaceous to Early Eocene times (Tweto and Sims, 1963). The magmatic activity and the related ore deposits which characterise the "mineral belt" (see chapter 1) were not synchronous; the ore deposits are generally thought to be younger than the intrusive porphyries (Tweto and Sims, *op.cit.*). The author observed mineralised shears throughout the sample region and mineralisation was also observed along some portions of the Stock-amphibolite contact. Cree (1948) records mineralised shears both within the Eldora Stock itself and in some portions of the surrounding country-rock. This clearly suggests that the Laramide mineralisation at Eldora occurred after the Stock had been emplaced. The exact relation of mineralisation to the Eldora Stock is uncertain, but the Laramide mineralisation at Eldora may be entirely unrelated to the Eldora Stock itself, perhaps originating from one of the other Laramide porphyries (see Figure 1.9).

Laramide mineralisation (as seen in E7 and E8) has had an unknown effect on the remaining amphibolitic rocks. Samples such as E21, E40, E42 and E50 contain a noticeably higher percentage of magnetite/pyrite (though not as high as in E7/E8 or adjacent to the contact) however they do not exhibit single or multi-crystal amphibole alterations. It is not known whether both PreCambrian and Laramide mineralisation has affected these rocks or not.

Immediately adjacent to the Eldora Stock contact (E15) the extensive epitaxial amphibole growths (single crystal alterations) can be linked to a particularly pervasive microfracture network, suggesting that at least some microfractures are the result of Laramide events. Whether this 'event' is related to fluids emanating from the Laramide Stock or associated with Laramide mineralisation (or both) is uncertain. A distinct rusty weathering patch was noted adjacent to the contact (Plate 13a), and a mineralised ore shear was observed

along some portions of the contact, which suggests that slightly younger Laramide mineralisation fluids may have intruded along or intersected the contact between monzonitic Stock and amphibolitic country-rocks. Whether Stock or ore-shear related, the alteration is clearly associated with mineralising fluids and is not *solely* the result of re-heating adjacent to the contact. Hart himself (1964) recognised metasomatism within 2m. of the contact and suggested it was related to "fluids emanating" from the igneous body itself.

The extensive alteration and mineralisation seen adjacent to the contact may therefore reflect:

- (i) Metasomatism associated with intrusion of the Stock (as Hart, 1964). This may account for the presence of zircon in E15.
- (ii) The passage of slightly later Laramide mineralising fluids along the stock-country-rock interface.
- (iii) The combined effects of both metasomatic and later Laramide mineralisation events.

It seems reasonable to assume that both Laramide metasomatism and mineralisation may have occurred immediately adjacent to the contact and that Laramide mineralisation and its associated mineral alterations have overprinted and perhaps enhanced pre-existing PreCambrian mineralisation and migmatization associated mineral alterations within the rocks. Whatever the relative importance of these different aged events, it is clear from the interrelation of mineral alterations to microfracture networks and permeation zones within the rocks, that the alteration was controlled by fluid infiltration along discrete zones.

CHAPTER 5. MINERAL CHEMISTRY, THERMOBAROMETRY AND DIFFUSION CALCULATIONS

This chapter is split into four main sections numbered 5.1, 5.2, 5.3 and 5.4. Sections 5.1 and 5.2 describe the detailed chemical investigations performed upon the mineral alterations outlined in chapter 4. The combined use of the electron and ion microprobes with B.S.E. imagery, whose methods were described in chapter 3, has enabled the further characterisation of the different aged alteration events identified from optical studies, the conclusions to which are presented in section 4.4.

Section 5.1 presents electron probe, B.S.E. images and ion probe data gathered during the extensive investigations of the amphibole alterations within the Eldora amphibolites. Both the automatic traverse and spot analysis facilities available on the electron microprobe were utilised to provide more detailed information on the amphibole chemistries associated with each of the amphibole alteration types outlined in section 4.2. B.S.E. imagery was extensively used to explore the distribution of the amphibole alterations within the amphibolites. Ion microprobe analysis provided information on the relative partitioning of rare-earth- and trace-elements within the different amphibole chemistries.

Section 5.2 presents the data gathered from the analysis of feldspar, pyroxene and biotite crystals within the amphibolites. These were less comprehensively investigated predominantly using spot analysis facilities on the electron probe and B.S.E imagery.

Section 5.3 gives a brief summary of the major findings of the chemical investigation presented in sections 5.1 and 5.2.

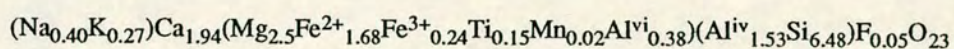
Section 5.4 concerns attempts to constrain the P-T conditions of both regional equilibration and subsequent alteration events based on the compositions of co-existing amphibole-plagioclase crystals within the amphibolites. Simple calculations of the diffusivity of elements within amphiboles are presented, based on the widths of the gradients between original and secondary amphiboles described in section 5.1. Attempts at fitting alteration profiles to both Lasaga and isothermal curves are reviewed and an example of the types of fit observed is given.

5.1. AMPHIBOLE CHEMISTRY

5.1.1. ELECTRON PROBE ANALYSIS AND B.S.E. IMAGES

(i) PRISTINE AMPHIBOLE COMPOSITIONS

Electron microprobe analyses of both the cores and edges of completely pristine amphibole grains and unaltered regions of partially altered amphibole crystals, located both within pristine and less pristine/altered areas of the rocks, have compositions bordering the fields of ferroan-pargasitic and edenitic-hornblendes (nomenclature of Leake, 1978). A typical composition may be written, in terms of cation proportions, as follows:



B.S.E. images of completely pristine amphiboles are a constant light grey colour reflecting their lack of mean atomic number (*Z*) variation. Closely spaced, 3-5 μm , electron microprobe traverses across such grains confirm their lack of chemical variation. An unzoned amphibole image is presented in Plate 39a.

Unaltered portions of amphibole grains examined within rocks originating throughout the area sampled have very similar chemistries; a selection of original amphibole compositions obtained from 5 different localities within the country rocks are presented in Table 5.1. The marked similarity in the pristine hornblende chemistries indicate that amphiboles both close to and at distance from the stock contact originally had quite uniform compositions.

TABLE 5.1 ORIGINAL AMPHIBOLE COMPOSITIONS AT VARIOUS DISTANCES FROM THE CONTACT.

OXIDE	0.15m.	9m.	15m.	663m.	2800m.
SiO ₂	42.452	43.746	43.607	42.986	43.374
Al ₂ O ₃	10.275	10.307	10.524	10.744	9.829
MgO	11.345	11.814	11.915	11.288	10.835
FeO	15.412	14.581	14.894	15.227	16.279
TiO ₂	2.002	1.735	1.223	1.343	1.580
MnO	0.334	0.285	0.209	0.315	0.303
Cr ₂ O ₃	0.006	0.048	0.066	0.000	0.064
CaO	11.716	11.778	11.830	12.008	11.907
K ₂ O	1.368	1.127	1.568	1.379	1.299
Na ₂ O	1.526	1.506	1.403	1.379	1.178
F	0.147	0.273	0.155	0.101	0.180
Total	96.580	97.200	97.390	96.770	96.830
<u>-O=Cl,F</u>	<u>0.060</u>	<u>0.110</u>	<u>0.070</u>	<u>0.040</u>	<u>0.080</u>
TOTAL	96.520	97.090	97.330	96.730	96.750
Si ^{iv}	6.428	6.542	6.512	6.475	6.556
Al ^{iv}	1.572	1.458	1.488	1.525	1.444
Al ^{vi}	0.263	0.359	0.366	0.384	0.309
Cr	0.001	0.006	0.008	0.000	0.008
Fe ³⁺	0.246	0.178	0.248	0.235	0.249
Ti	0.228	0.195	0.137	0.152	0.180
Mg	2.560	2.633	2.652	2.534	2.441
Fe ²⁺	1.681	1.611	1.575	1.675	1.795
Mn	0.021	0.018	0.013	0.020	0.019
BFe ²⁺	0.025	0.035	0.037	0.009	0.014
BMn	0.021	0.018	0.013	0.020	0.019
BCa	1.901	1.887	1.893	1.938	1.928
BNa	0.053	0.060	0.057	0.033	0.038
ANa	0.395	0.376	0.349	0.370	0.307
AK	0.264	0.215	0.299	0.265	0.251
ATOTAL	0.659	0.591	0.648	0.635	0.558
CF	0.070	0.129	0.073	0.048	0.086
SUMCAT	15.696	15.591	15.648	15.635	15.558
SUMOXY	23.000	23.003	23.000	23.000	23.000
Z	13.457	13.311	13.340	13.409	13.285
	F-P-H	E-H	E-H	F-P-H	E-H

Recalculated on the anhydrous basis of 23 oxygens using AMPHIBOL (Am.Min., 1990) selected scheme AV.15-NK* & 13-CNK**

F-P-H = Ferroan-Pargasitic-Hornblende

E-H = Edenitic-Hornblende

* 15NK = Total Number Of Cations=15, excluding sum of Na+K.

** 13CNK = Total Number Of Cations=13, excluding sum of Ca+Na+K.

PLATE 39: B.S.E. IMAGES.

(a) B.S.E. image of an original, unaltered amphibole grain (homogeneous, pale-grey colour). Feldspar is black.

Scale bar: 40 μ m. (E33)

(b) B.S.E. image illustrating spots (arrowed 1) and edges (arrowed 2) of secondary amphibole within an original amphibole crystal. Note the presence of a slight edge effect (arrow 3).

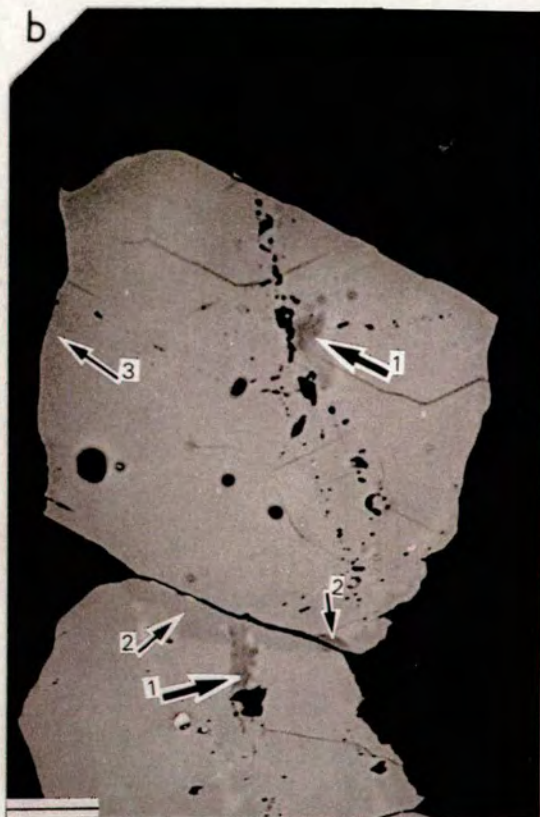
Scale bar: 40 μ m. (E28)

(c) B.S.E. image of secondary amphibole patches adjacent to cracks/microfractures within a crystal (arrowed).

Scale bar: 100 μ m. (E29)

(d) B.S.E. image of marginally disposed patches of secondary amphibole. Note irregular shapes.

Scale bar: 100 μ m. (E15)



(ii) ALTERED AMPHIBOLE COMPOSITIONS

The integrated use of the electron microprobe with B.S.E. images has shown that changes in the original mineral compositions which, based on the original work of Hart (1964), were expected to be at least in some way diffusion controlled are in fact the result of crystal nucleation associated with fluids penetrating along cracks and grain-boundaries within the rocks. The results of this work have quite clearly demonstrated the complex manner by which rocks within the crust strive to maintain equilibrium in a changing physico-chemical environment.

Because the initial orientation of the project was to examine diffusive alteration, much time (c.18 months) was spent analysing minerals using the electron probe in attempts to relate mineral zonations and the widths of these zonations to distance from the intrusive Stock and therefore the heat source responsible for? diffusional compositional change. A substantial bias toward "zonations" occurring adjacent to amphibole grain-boundaries therefore exists in much of the early analytical data obtained. Optical investigations (chapter 4) indicated that the samples closest to the contact (*i.e.* within 2m.) contain a greater abundance of altered grains than often seen elsewhere, however detailed geochemical analysis did not establish the simple, distance related pattern in "zonation" widths expected (following Hart, 1964). Since the mineral alterations no longer appeared to be simply the result of re-heating caused by stock emplacement subsequent research was aimed at identifying the factors controlling the changes in chemistry that have taken place. It was imperative to be able to rapidly identify and characterise altered grains within the rocks. B.S.E. images enable the instantaneous recognition of chemical heterogeneity within minerals and this technique, whose sensitivity has only been relatively recently recognised, proved to be an invaluable tool in later studies. Comparisons of the B.S.E. images of specific grains and their previously obtained, microprobe generated elemental profiles, established that both techniques were equally sensitive to the changes in chemistry involved. Experience enabled the relative grey-levels of altered amphibole B.S.E. images to be equated with likely chemical compositions; spot analyses were performed as a continual monitor. A period of approximately 6 months ensued during which the amphiboles were re-examined visually using B.S.E. imagery; it was during these investigations that the intragranular and microvein alterations were first recognised (though they are now known to also be optically distinct in thin-sections).

In the following pages each of the blue-green coloured amphibole alteration types described in chapter 4 will be considered in turn:

(a) *Boundary Alterations.*

Secondary amphibole observed optically along amphibole grain edges (rims and patches of chapter 4) and blue-green coloured spots and segments adjacent to cleavage planes and cracks within crystals appear as darker shades of grey within black & white B.S.E. images; higher colours in colour enhanced images. Some typical images are presented in Plate 39. The secondary amphibole has been found to comprise a range of possible chemical compositions which vary not only from grain to grain within an individual rock but also from place to place within individual crystals. By far the most common chemical variations detected within the samples examined correspond approximately to the following changes in oxide wt%/cation proportions:

ORIGINAL AMPH CONCN	VARIATION IN OXIDE WT%	RANGE IN CATION PROPORTIONS
c.42wt% SiO ₂	+ 0.3-6.0	6.45-7.20 Si
c.10wt% Al ₂ O ₃	- 0.5-4.5	1.80-1.00 Al
c.12wt% MgO	+ 0.2-2.0	2.50-3.00 Mg
c.15wt% FeO	- 0.2-1.5	2.00-1.80 Fe
c.1.5wt% K ₂ O	- 0.2-1.0	0.26-0.10 K
c.1.5wt% TiO ₂	- 0.02-1.0	0.20-0.03 Ti
c.1.5wt% Na ₂ O	- 0.2-0.7	0.40-0.24 Na
c.12wt% CaO	+ 0.2-0.7	1.90-1.96 Ca

+ represents an increasing concentration -represents a decreasing concentration from original compositions.

representing alteration from original ferroan-pargasitic-hornblendes to secondary amphiboles with edenitic and ultimately magnesio-hornblenditic compositions. Less commonly secondary, actinolitic-hornblende and occasionally actinolite are encountered. A range of typical compositions obtained from spot analyses within secondary amphiboles are presented in Table 5.2. These are from the same amphibole crystals whose unaltered compositions were displayed in Table 5.1. The widths of the secondary amphibole zones or patches were found to be quite variable, ranging from <1µm. to ~120µm. irrespective of distance from the contact. Even within individual rocks the secondary amphibole shows no apparent consistency in either width of development or chemical composition.

Figure 5.1 is an example of one of the more subtle chemical variations whilst Figure 5.2 illustrates the larger variations detected.

NATURE OF INTERFACE BETWEEN AMPHIBOLE TYPES

Secondary amphibole may occur with either sharp or gradual chemical boundaries against the original hornblende. The widths of the gradients between original and secondary amphiboles, studied in detail using automatic traverses on the electron probe, were found to range from ≤ 4 to $\sim 100\mu\text{m}$. The profiles presented in Figure 5.2 display a rapid change in composition between two chemically distinct regions (image presented in Plate 40c). The first $\sim 5\text{--}6\mu\text{m}$ of the traverse represents the original hornblende, a gradient of $4\mu\text{m}$ separates this from the secondary amphibole compositional plateau. Examples of the B.S.E. images of secondary amphibole patches whose interfaces with the original hornblende correspond to discontinuous changes in chemistry of the types just described are presented in Plates 40 and 41. The abrupt interfaces between original and secondary amphibole regions are clearly illustrated in B.S.E. images as visually sharp boundaries. These abruptly bounded secondary amphibole patches account for approximately 90% of all the boundary alterations observed.

In contrast, a minority of the profiles, such as those presented in Figure 5.1 (with the exception of Mg,Fe), display a more gradual, almost continuous change in chemistry from original hornblende cores to secondary amphibole compositional rims. In Figure 5.1 this change occurs over a distance of approximately $100\mu\text{m}$; the original hornblende occupies the central portion of the profile, the rims of the original crystal have been altered to a secondary amphibole composition. B.S.E. images of these continuous type gradients are presented in Plates 42 and 43. The continuous chemical changes involved are seen in B.S.E. images as progressive changes in the grey/colour level of the amphibole image from original, light-grey/white hornblende regions to darker-grey-black/higher-colour areas of secondary amphibole.

Many of the gradual-type profiles obtained appear to retain at least some evidence for the existence of two distinct amphibole compositions (such as those seen in Figure 5.2); the interface between the two amphibole generations is marked by a gradual change in concentrations. The Mg/Fe profiles seen in Figure 5.1 may be interpreted as representing two originally homogeneous domains whose interface has been extensively smoothed. Figures 5.3 and 5.4 present two further examples of apparently continuous gradients occurring

between two chemically distinguishable amphiboles. In Figure 5.3 the original amphibole composition represents the first ~270 μm . of the traverse, the secondary amphibole occupies the final ~40 μm . An approximately 30-40 μm . wide gradient occurs between original and secondary amphibole compositions.

The profiles presented in Figure 5.4 (with the exception of K) show a very gradual and mostly continuous (particularly Al, Si, Fe, Mg, Na) variation over a distance of approximately 40 μm . The K profile of Figure 5.4 suggests again that two discrete amphibole compositions may have originally been present; this compositional difference is indistinguishable in the gradients observed for the other elements.

ADDITIONAL BOUNDARY ALTERATION TYPE

Whilst undertaking B.S.E. investigations a more unusual and again predominantly marginally disposed (occasionally intragranularly located) alteration pattern was discovered. Although the altered crystal margins in question are still identifiable as blue-green coloured patches/rims within thin-sections their true "triangular" or "sawtooth shapes" are only visible in B.S.E. images (see Plates 44 and 45). Interfaces between secondary, triangular-shaped amphibole areas and original hornblende hosts are both chemically and visually (*i.e.* in B.S.E. images) sharp. A closely spaced (*c.* 1 μm . interval) electron-probe traverse across one such triangular-shaped secondary amphibole area is presented in Figure 5.5. The first 3 μm . and final 9 μm . of this traverse represent the original edenitic hornblende composition; these are separated from an approximately 9 μm . wide secondary magnesio-hornblende plateau by gradients of *c.* 5 μm . and 3 μm . width. In other situations the secondary amphibole forming the triangular-shaped area is either actinolitic-hornblende or actinolite. There is no apparent crystallographic control to either the shapes or locations of these secondary amphiboles whose origin remains rather enigmatic.

DEVELOPMENT OF BOUNDARY-TYPE SECONDARY AMPHIBOLE.

A comparison of element profiles obtained from many altered amphibole grains both close to and at successively greater distances from the Stock contact established that:

- 1: the development of secondary amphibole rims/patches and

- 2: both abrupt and gradual gradients between original hornblende and secondary amphibole

bear no relationship to distance from the intrusive heat source and are in fact highly irregular within individual rocks.

A comprehensive B.S.E. study was performed in order to establish whether the *marginally disposed* secondary amphibole rims/patches reflected the host hornblendes inter/intragranular properties. It was considered possible that secondary amphibole may only develop at:

- 1: certain mineral interfaces *e.g.* amphibole-biotite, amphibole-amphibole or amphibole-altered plagioclase *etc.*
- 2: particular grain-boundary types *e.g.* smooth-lobate, open-tight, recrystallised-unrecrystallised *etc.*
- 3: triple-junctions

or be related to the state of strain of the host amphibole and/or its neighbouring phases.

Many altered amphibole grains were imaged and B.S.E. photographs taken to record the precise position of secondary amphibole areas within the original crystals. These B.S.E. photographs were then compared directly with the microscopically visible intra- and inter-granular properties of the amphibole grain. The nature of the adjacent phases, grain-boundary types, state of strain *etc.* were each carefully assessed in relation to the location and shape of the secondary amphibole patch/rim. In all but a minority of situations the B.S.E. image of the secondary amphibole patch coincided with an optical change to a blue-green colour but no other consistent pattern emerged.

SPATIAL DISTRIBUTION

Boundary-type secondary amphiboles have been documented in every rock investigated. Of the two types described, those with abrupt interfaces against the host crystal are by far the most abundant (*c.*90%). Rocks falling within approximately 2m. of the contact and the particularly heavily mineralised samples (*e.g.* E21) contain a noticeably high proportion of these sharply bounded secondary amphibole patches.

Secondary amphiboles with more gradual gradients against the host crystal were only encountered at distances beyond 15m. from the contact

However, this may well be more a consequence of their relative scarcity as opposed to the far more abundant sharply bounded types.

A fuller discussion of the relationships between these two alteration types is given in section 5.1.4.

TABLE 5.2 SECONDARY PATCH AND RIM AMPHIBOLE COMPOSITIONS
(COMPARE WITH THOSE OF TABLE 4.1)

OXIDE	0.15m.	9m	15m.	663m.	2800m.
SiO ₂	45.192	46.341	45.767	44.218	49.577
Al ₂ O ₃	11.669	7.904	8.850	10.951	5.051
MgO	10.572	12.996	12.471	11.230	14.452
FeO	13.407	13.916	14.310	14.528	13.394
TiO ₂	1.698	1.435	1.121	1.466	0.225
MnO	0.300	0.359	0.225	0.269	0.302
Cr ₂ O ₃	0.010	0.045	0.075	0.006	0.044
CaO	11.248	12.058	12.160	11.778	12.486
K ₂ O	1.111	0.836	1.159	1.354	0.425
Na ₂ O	1.853	1.108	1.136	1.186	0.625
F	0.248	0.034	0.243	0.263	0.143
Total	97.310	97.030	97.520	97.250	96.720
<u>-O=Cl,F</u>	<u>0.100</u>	<u>0.010</u>	<u>0.100</u>	<u>0.110</u>	<u>0.060</u>
TOTAL	97.200	97.020	97.410	97.140	96.660
Si ^{iv}	6.764	6.860	6.789	6.607	7.273
Al ^{iv}	1.236	1.140	1.211	1.393	0.727
Al ^{vi}	0.825	0.240	0.337	0.537	0.147
Cr	0.001	0.005	0.009	0.001	0.005
Fe ³⁺	0.000	0.192	0.141	0.116	0.308
Ti	0.191	0.160	0.125	0.165	0.025
Mg	2.358	2.867	2.757	2.501	3.160
Fe ²⁺	1.606	1.513	1.617	1.663	1.335
Mn	0.019	0.022	0.014	0.017	0.020
BFe ²⁺	0.073	0.018	0.017	0.036	0.000
BMn	0.019	0.023	0.014	0.017	0.017
BCa	1.804	1.913	1.933	1.886	1.963
BNa	0.104	0.047	0.036	0.061	0.020
ANa	0.433	0.271	0.291	0.283	0.158
AK	0.212	0.158	0.219	0.258	0.080
ATOTAL	0.646	0.429	0.510	0.541	0.237
CF	0.117	0.016	0.114	0.124	0.066
SUMCAT	15.646	15.429	15.510	15.541	15.237
SUMOXY	23.257	23.000	23.000	23.036	23.000
Z	13.138	13.233	13.260	13.301	13.533
	ED	M-H	ED	E-H	A-H

Recalculated on the anhydrous basis of 23 oxygens using AMPHIBOL (Am.Min., 1990) selected scheme AV.15-NK & 13-CNK

ED=Edenite

M-H=Magnesio-Hornblende

A-H=Actinolitic-hornblende

FIGURE 5.1.

Plot of cation concentration versus distance (in microns) across an altered original hornblende crystal. The subtle change in concentration toward both edges of the grain represent a mostly gradual change from original to secondary amphiboles (discussed in detail in text).

Step intervals $\sim 15\mu\text{m}$. intervals.

KEY: Red curve/crosses correspond to the element plotted on the red axis.

Blue curve/diamonds correspond to the element plotted on the blue axis.

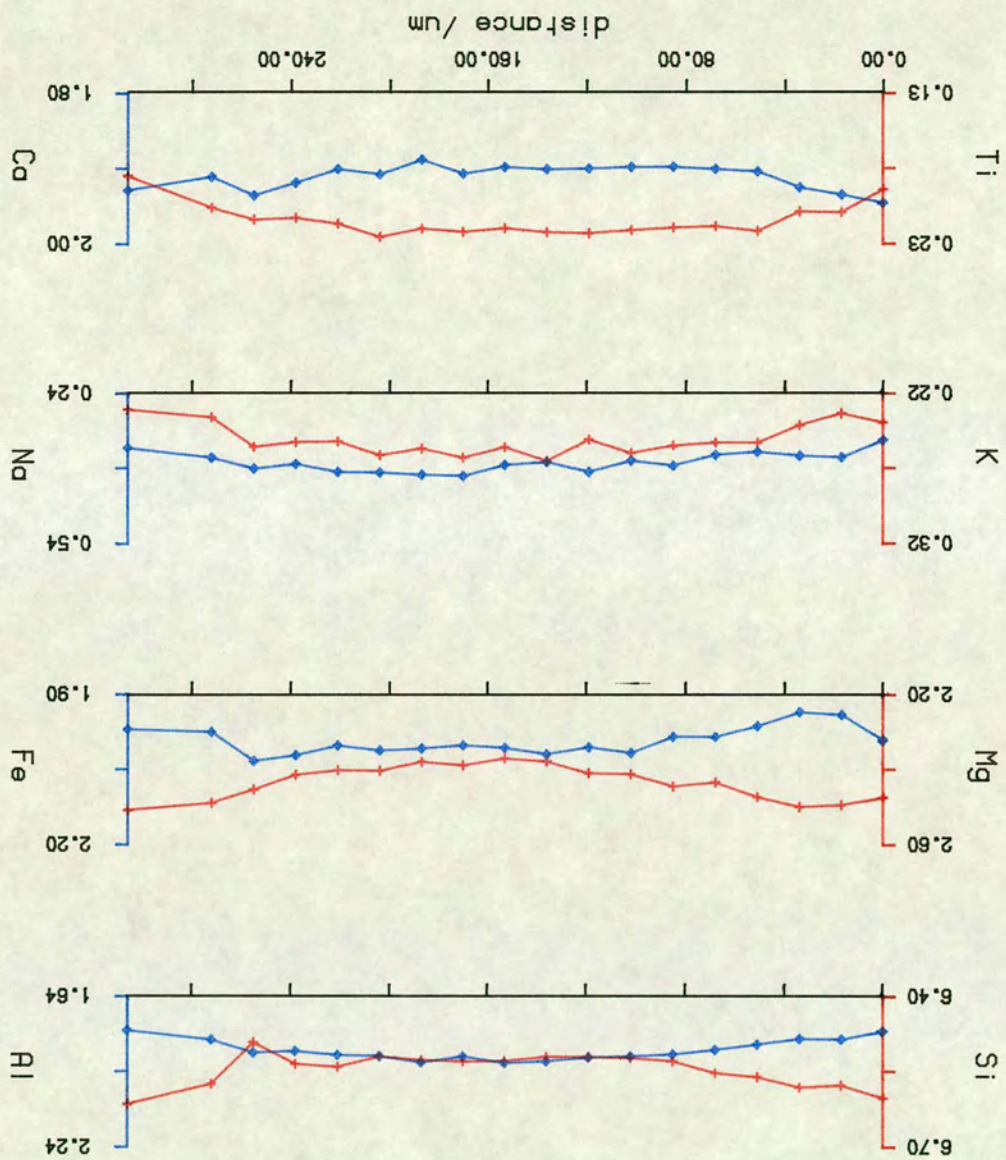


FIGURE 5.2.

Plot of cation concentrations versus distance across a sharply bounded secondary/original amphibole interface. The original hornblende compositional plateau is represented by the first four data points, the secondary amphibole by the final 12 points (B.S.E. image presented in Plate 40c).

Step interval $\sim 2\mu\text{m}$. intervals.

KEY: Red curve/crosses correspond to the element plotted on the red axis.

Blue curve/diamonds correspond to the element plotted on the blue axis.

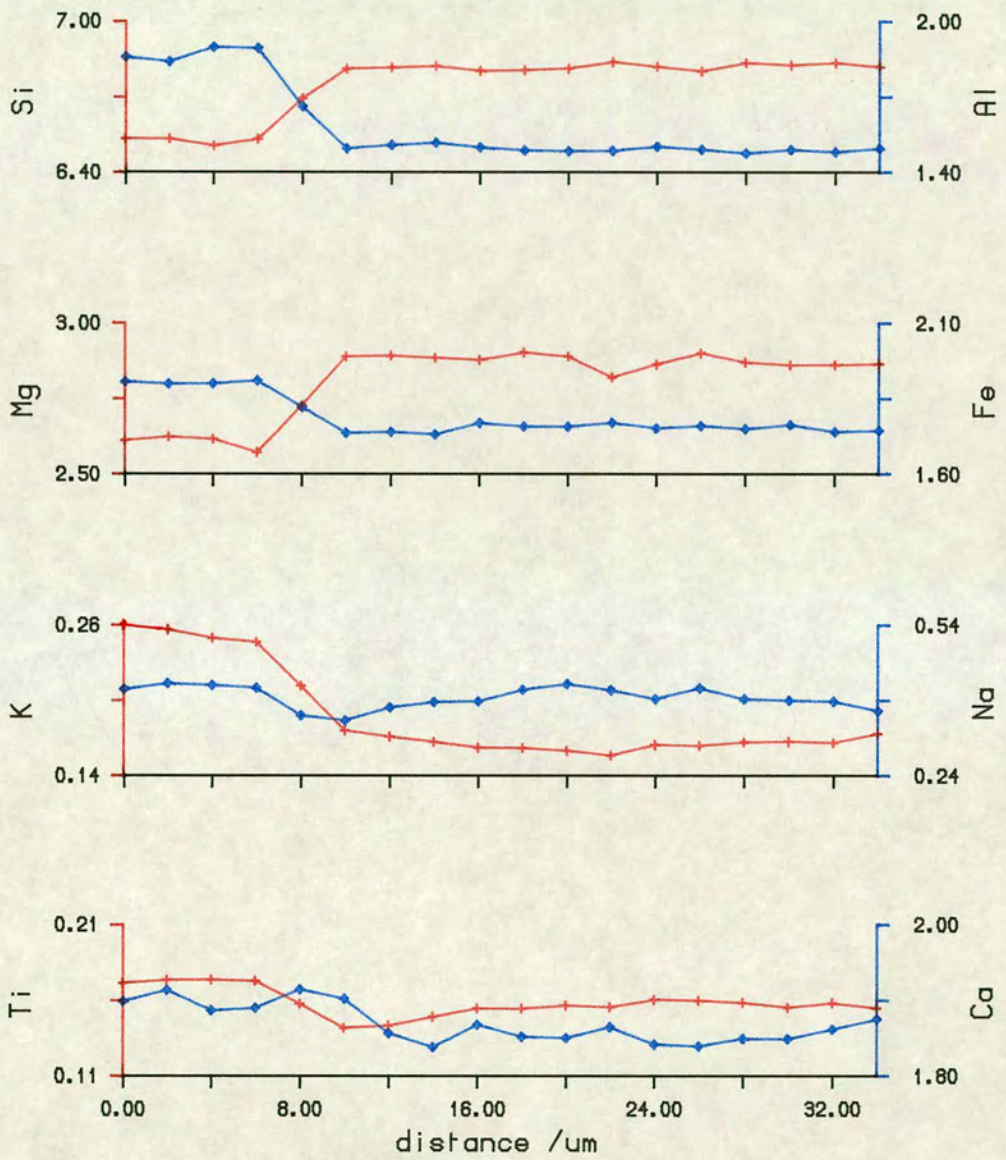


PLATE 40: BOUNDARY ALTERATIONS - Sharply bounded patches.

(a),(b),(c) B.S.E. images of secondary amphibole patches developed along the edges of original amphibole crystals. Note sharpness of interface between altered and unaltered regions of the crystals.

Scale bars (a) 200 μ m. (E12)

(b) 50 μ m. (E15)

(c) 100 μ m. (E5)

(d) Higher magnification B.S.E. image of an original/secondary amphibole interface. Note the sharpness of the interface between original and secondary amphiboles and how the secondary amphibole ends in one grain (arrow 1) and re-appears in the adjacent amphibole (arrow 2). Arrow 3 points to a darker-grey amphibole overprinting a pre-existing rim of secondary amphibole.

Scale bar: 100 μ m. (E50)

PLATE 41: BOUNDARY ALTERATIONS - Sharply-bounded patches.

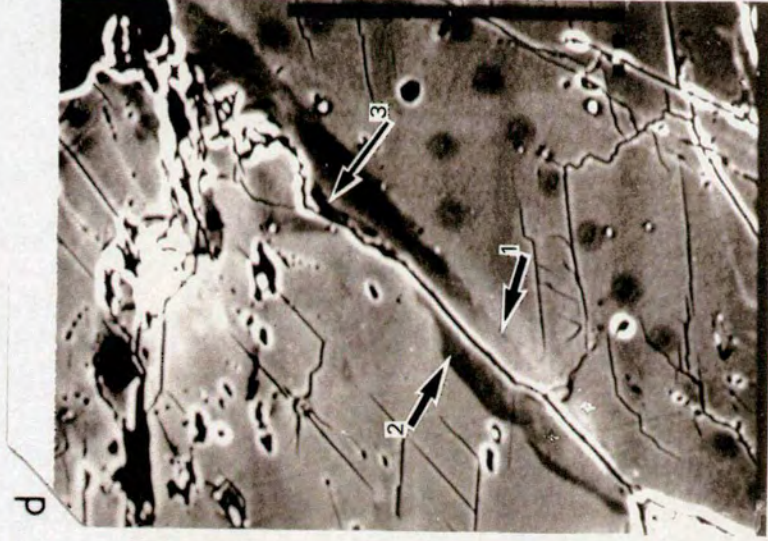
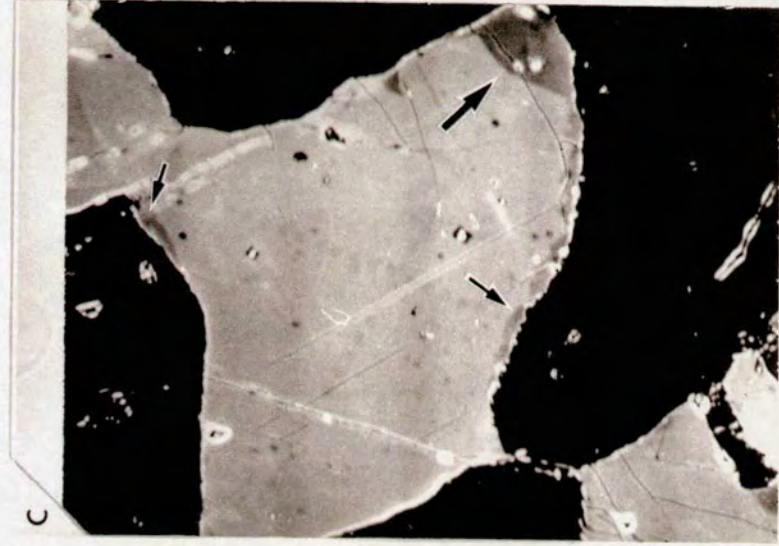
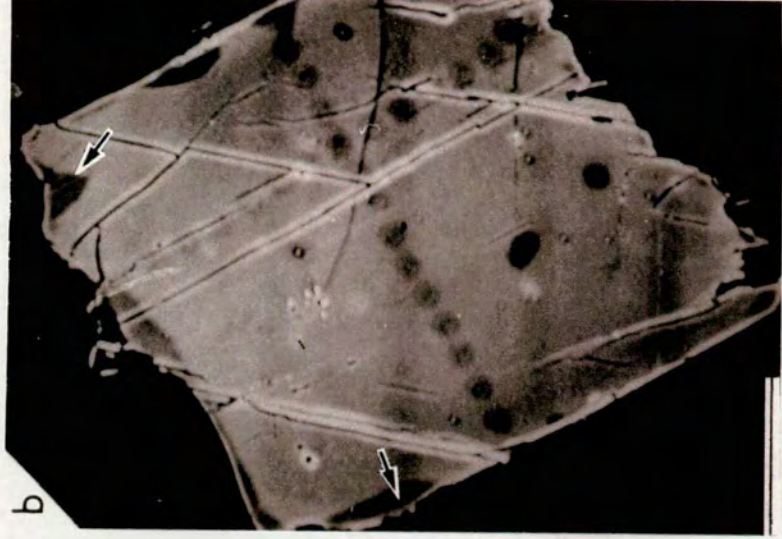
(a),(b),(c) Colour-enhanced images of secondary amphibole patches developed adjacent to rims of original grains. Note again the non-regularity of the secondary amphibole with regards to both development and their shapes. The interfaces between original and secondary amphiboles are all very sharp. Yellow zones in (c) overprint a diffusely-bounded, blue coloured halo (arrow H).

Scale bars: (a) 100 μ m. (E5)

(b) 200 μ m. (E22)

(c) 50 μ m. (E5)

PLATE 40



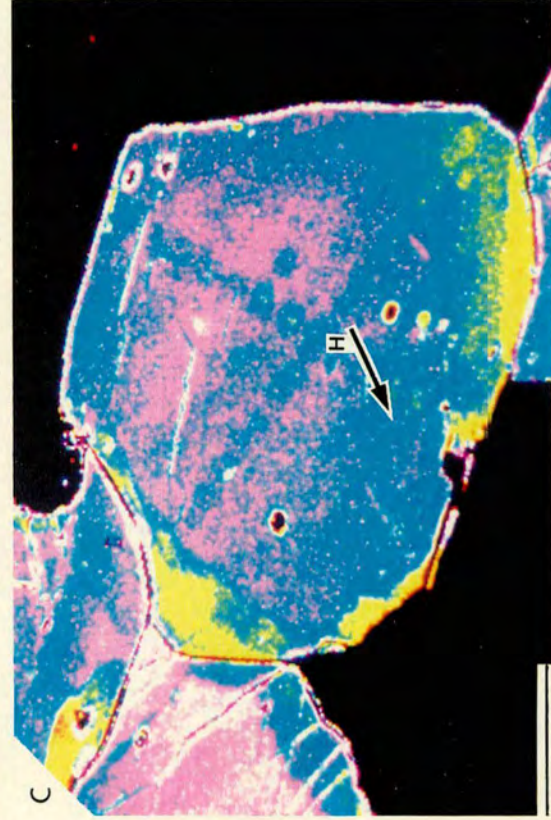
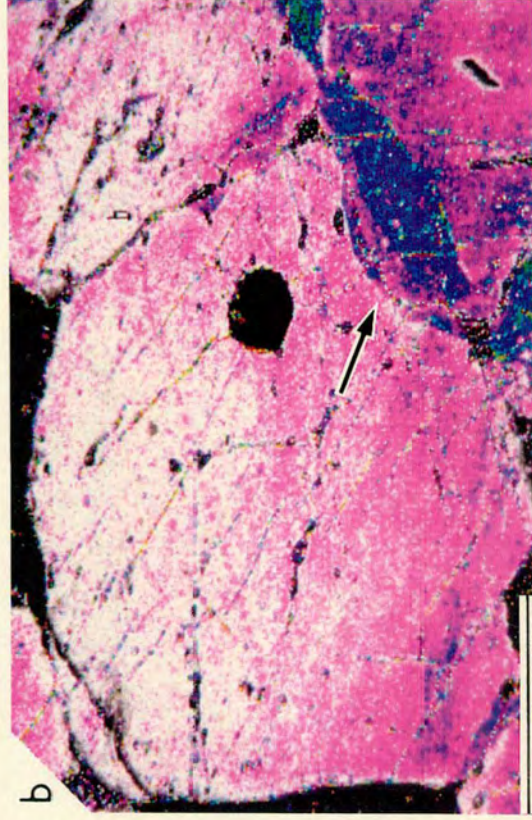
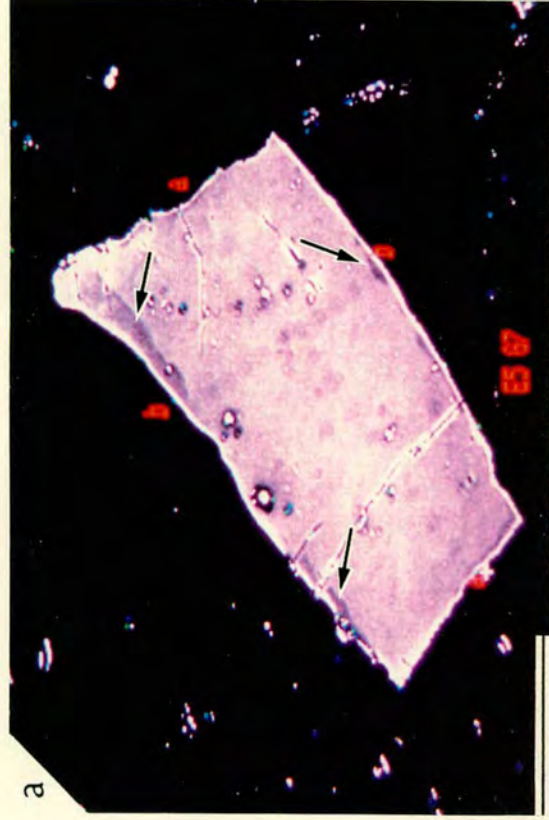


PLATE 42: BOUNDARY ALTERATIONS - Gradational alterations.

(a) B.S.E. image of an original amphibole with smooth, regular grain-boundaries indicative of textural equilibrium. Gradational changes in mean atomic number (light-grey diffusely bounded rims) are pinpointed by arrows (1). Note that the diffuse rim is not continuous (*i.e.* it is only developed along certain edges). Darker-grey, sharply-bounded patches of secondary amphibole (arrowed 2) appear to overprint the diffuse rims.

Scale bar: 100 μ m. (E71)

(b) B.S.E. image of an original amphibole grain within which a halo of slightly darker-grey is apparent (arrow 1). Note biotite (arrow 2).

Scale bar: 100 μ m. (ELD6)

(c) B.S.E. image of a diffuse edge within an original amphibole grain. Note the alteration does not appear to occur as a continuous halo.

Scale bar: 100 μ m. (E21)

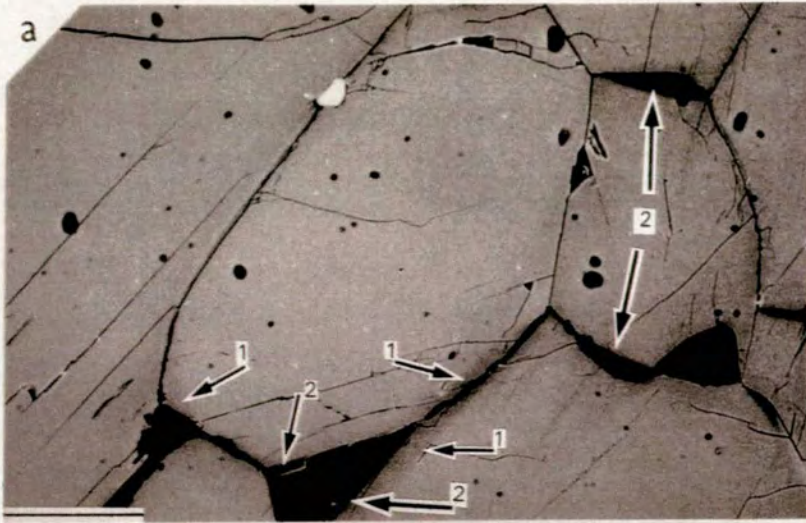


PLATE 43: BOUNDARY ALTERATIONS - Gradational alterations.

(a) Colour-enhanced B.S.E. image of an almost continuous, diffusely-bounded rim (pink) within an original amphibole crystal (white). Note the larger altered area (arrow 1) coincides with a more cracked region of the crystal, adjacent to which the amphibole is apparently unaltered (arrowed 2). Red letter b's relate to an electron microprobe traverse line.

Scale bar: 100 μ m. (E50)

(b) Colour-enhanced B.S.E. image of an amphibole crystal; a gradual decrease in mean atomic number (increase in colour) can be seen toward the edge of the crystal. Note the asymmetry in the width of the diffuse alteration (blue-green colour) and how the alteration dies out where arrowed.

Scale bar: 100 μ m. (ELD5)

(c) Colour-enhanced B.S.E. image of an original amphibole crystal in which both diffuse (arrowed 1) and sharply bounded (arrowed 2) secondary amphiboles can be identified. Note the diffuse alteration (arrow 1a) does not coincide with a similarly diffuse alteration within the adjacent original amphibole crystal (arrow 3). Note also that the crystal interface immediately opposing 1a is unaltered (arrow 4). Sharply bounded patches of secondary amphibole (2a and b) appear to have overprinted a diffuse rim within an adjacent amphibole.

Scale bar: 200 μ m. (E5)

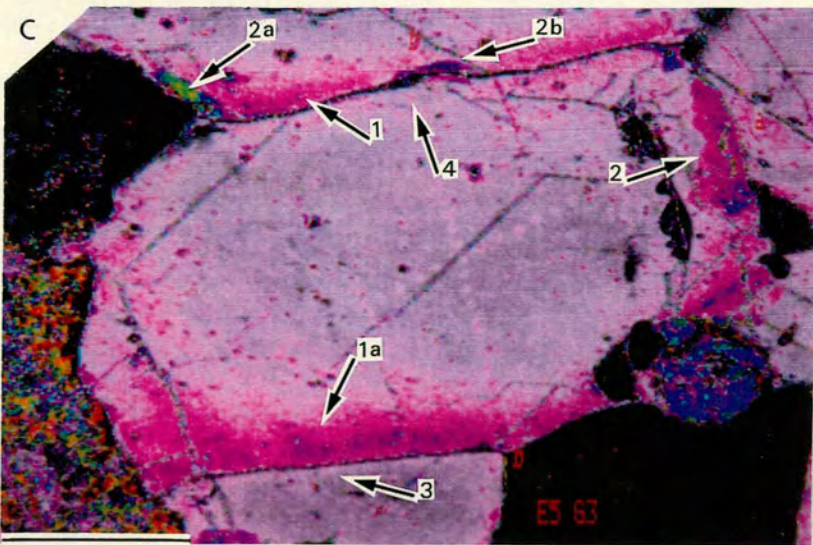
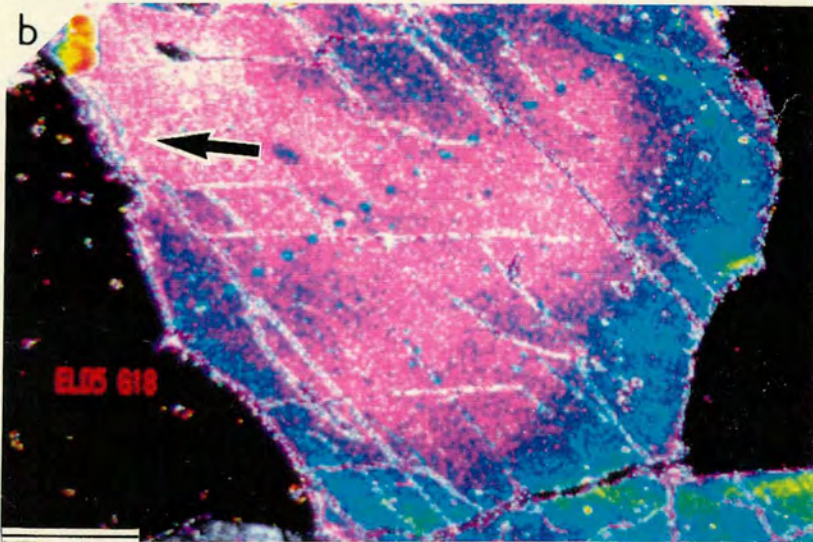
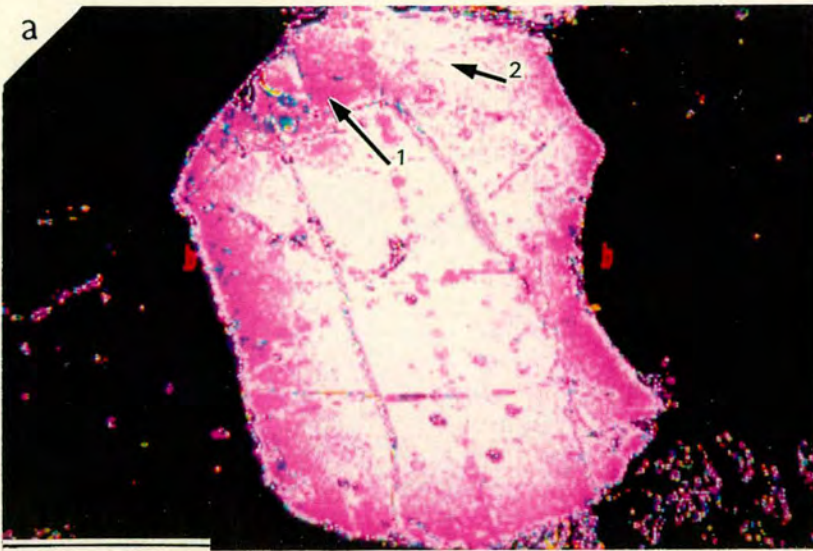


FIGURE 5.3.

Plot of cation concentrations versus distance across an original/secondary amphibole interface. The original hornblende compositional plateau represents approximately the first 28 data points, the secondary amphibole the final four data points. The interface between the two plateaus is marked by a gradual change in concentrations (discussed in text).

Step intervals $\sim 10\mu\text{m}$.

KEY: Red curve/crosses correspond to the element plotted on the red axis.

Blue curve/diamonds correspond to the element plotted on the blue axis.

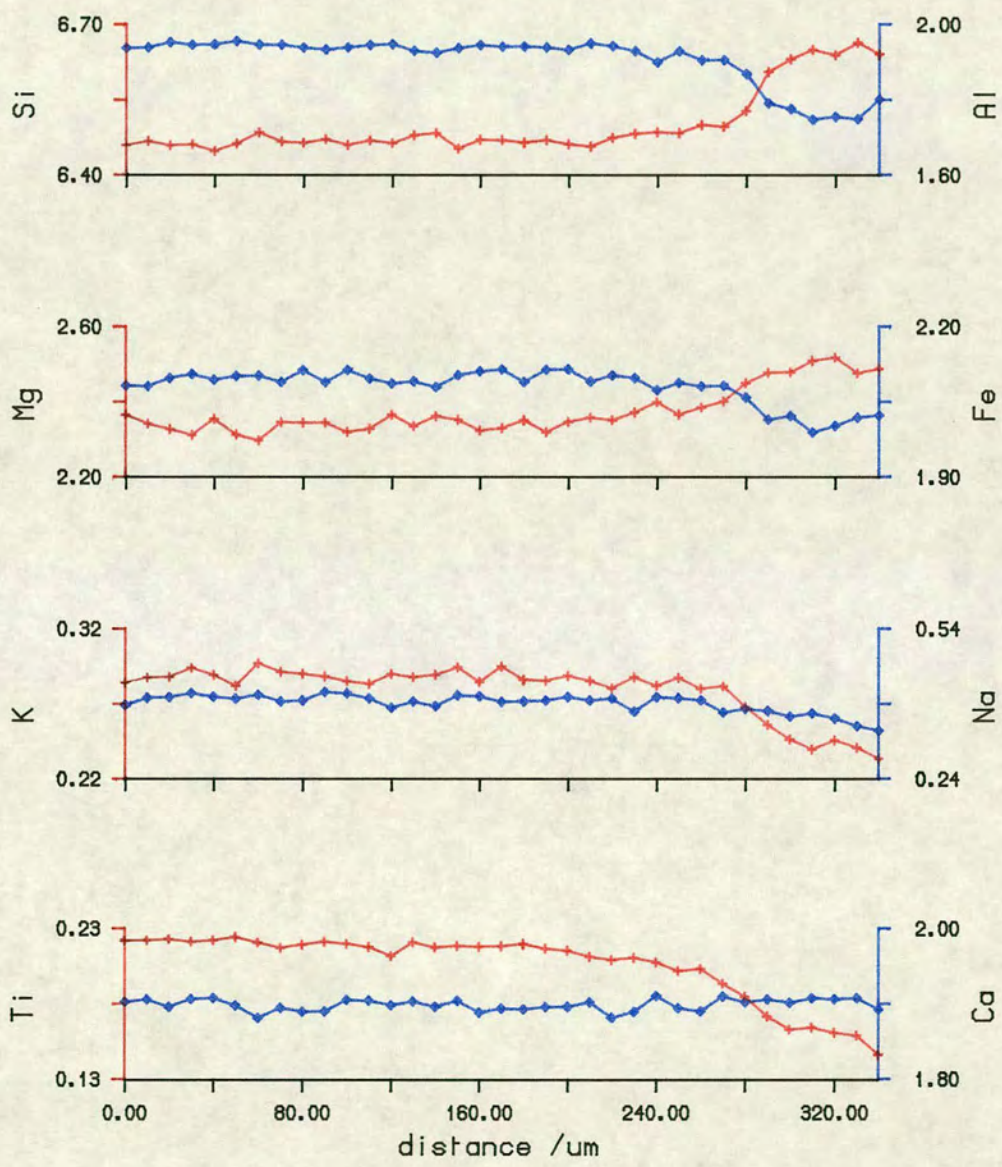


FIGURE 5.4.

Plot of cation concentrations versus distance from original (approximately the first 13 data points) to secondary amphibole compositions. The changes in concentration are almost continuous from core to rim (see text for further discussion).

Step intervals $\sim 3.5\mu\text{m}$.

KEY: Red curve/crosses correspond to the element plotted on the red axis.

Blue curve/diamonds correspond to the element plotted on the blue axis.

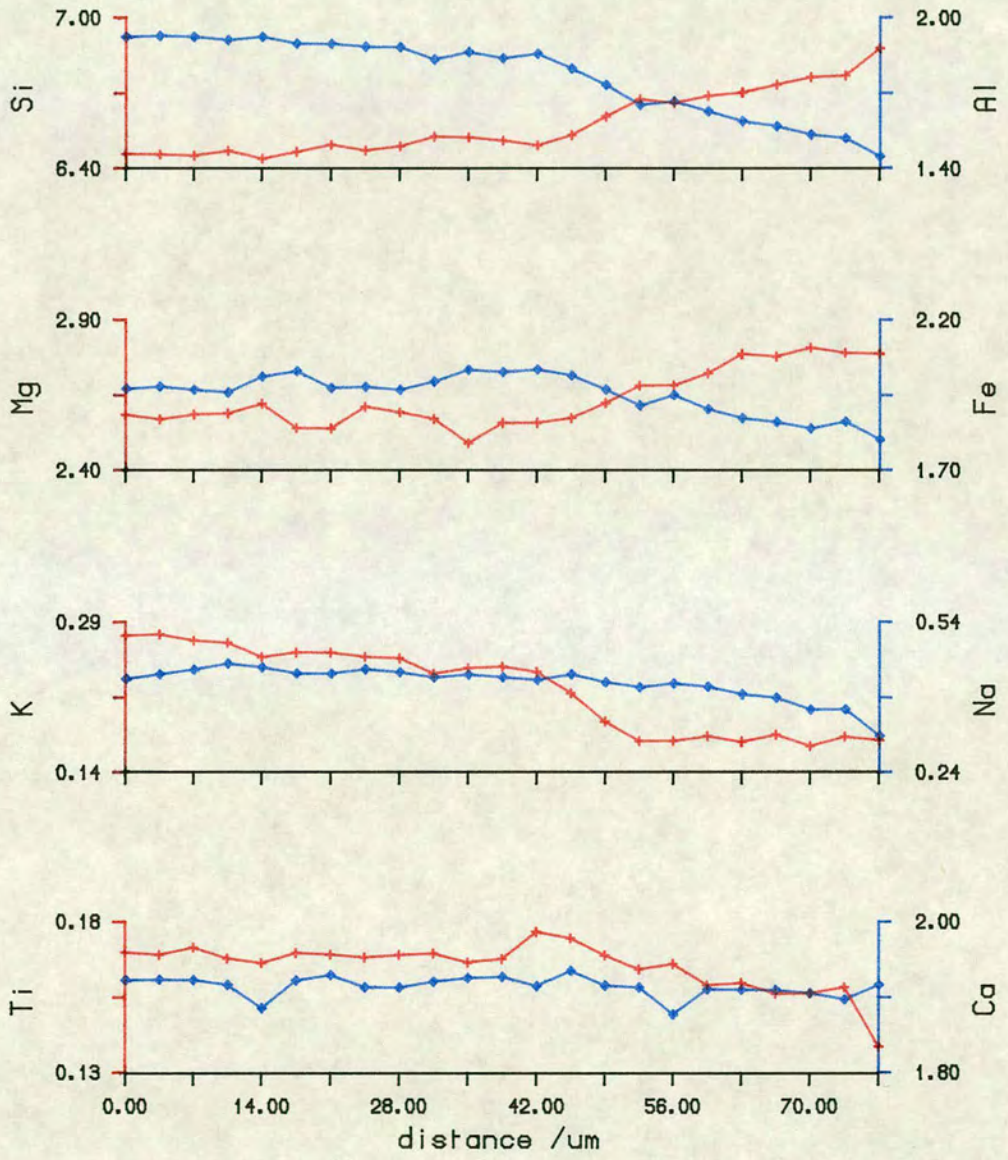


PLATE 44: BOUNDARY ALTERATIONS

Sawtooth/triangular shaped patches.

(a) B.S.E. image depicting the presence of sharply-bounded, triangular-shaped secondary amphibole areas developed at the edge of an original amphibole crystal.

Scale bar: 15 μ m. (ELD4)

(b), (c) B.S.E. images of triangular and sawtooth shaped secondary amphiboles developed adjacent to cracks/cleavage planes within an original amphibole crystal.

Scale bars: (b) 20 μ m. (E21)

(c) 40 μ m. (E21)

(d) B.S.E. image of marginally developed, sawtooth shaped secondary amphiboles (arrowed). Note the lack of alteration along the adjacent interface (arrow 1).

Scale bar: 40 μ m. (E5)

PLATE 44

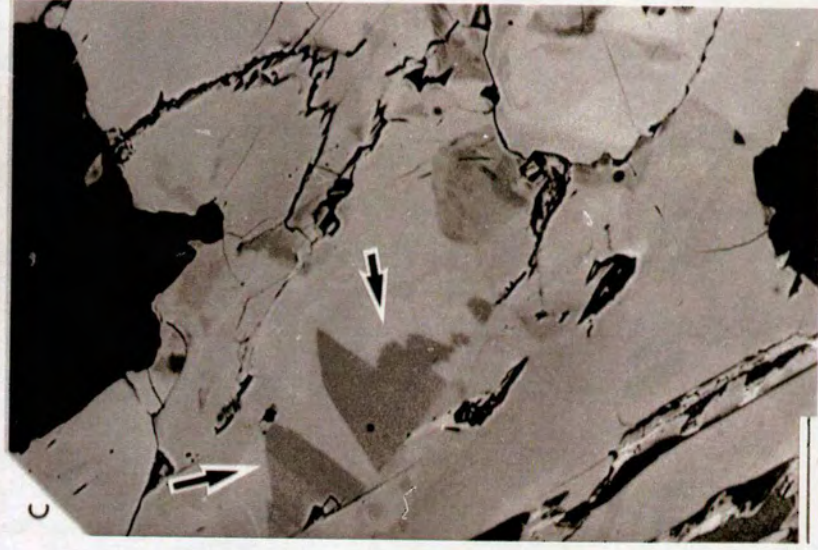
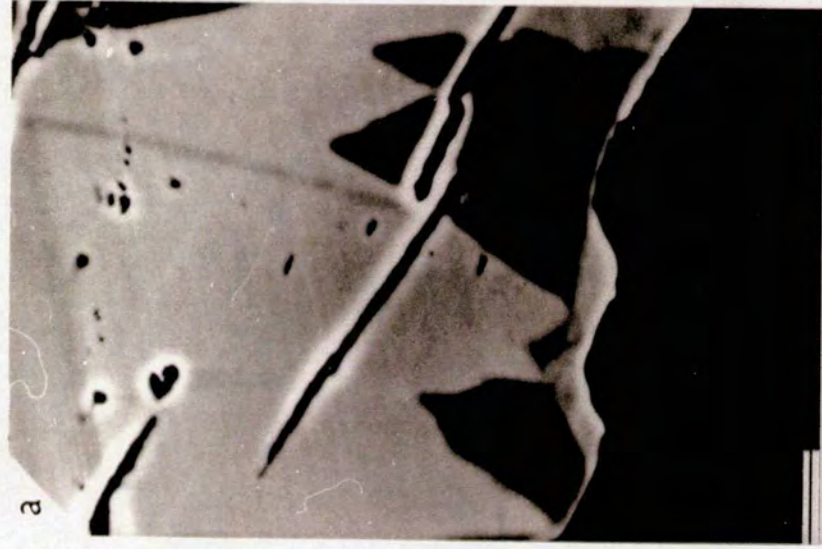


PLATE 45: BOUNDARY ALTERATIONS

Sawtooth-shaped secondary amphiboles.

(a) Colour-enhanced B.S.E. image of an original amphibole crystal (yellow-blue colour) around the rim of which sharply bounded, sawtooth-shaped secondary amphiboles may be seen (red colour).

Scale bar: 100 μ m. (E5)

(b) Colour-enhanced B.S.E. image of an original amphibole crystal (pink-mauve colours; OA) within which both diffuse (blue-green colours; arrowed 1) and sharply bounded, triangular-shaped secondary amphiboles (yellow; arrowed 2) are clearly visible. Note that the diffuse secondary amphibole forms an almost continuous halo within the crystal but is much wider at 1a and 1b than at 1c (all arrowed). The sharply-bounded alterations have quite clearly overprinted the diffuse halo.

Scale bar: 300 μ m. (ELD4)

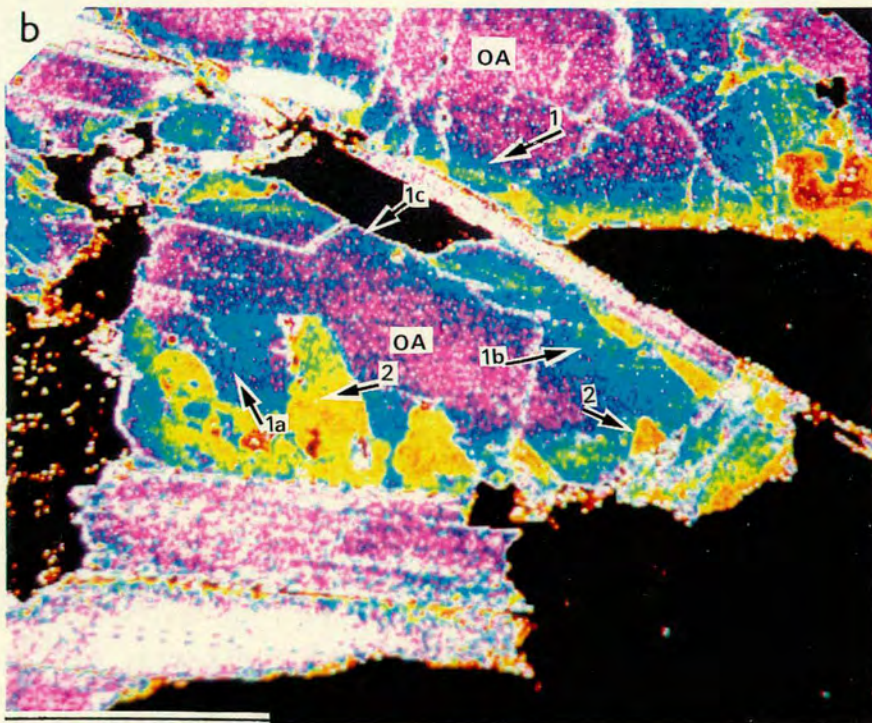
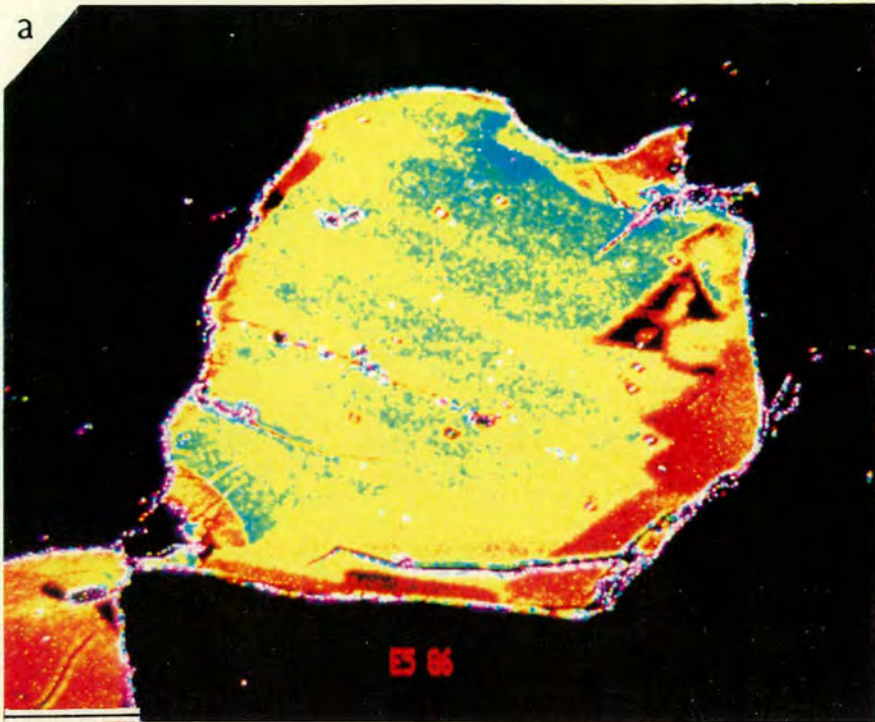


FIGURE 5.5.

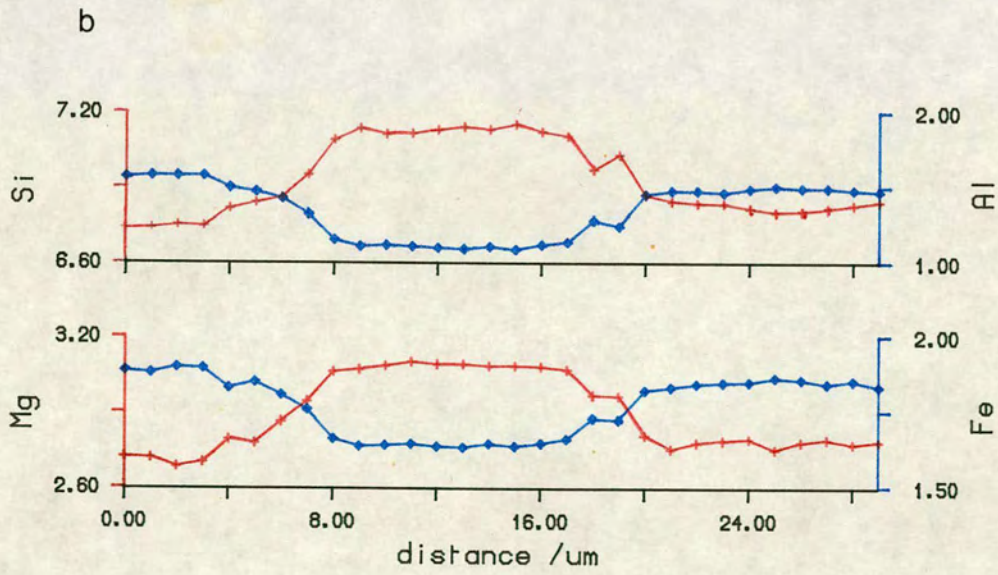
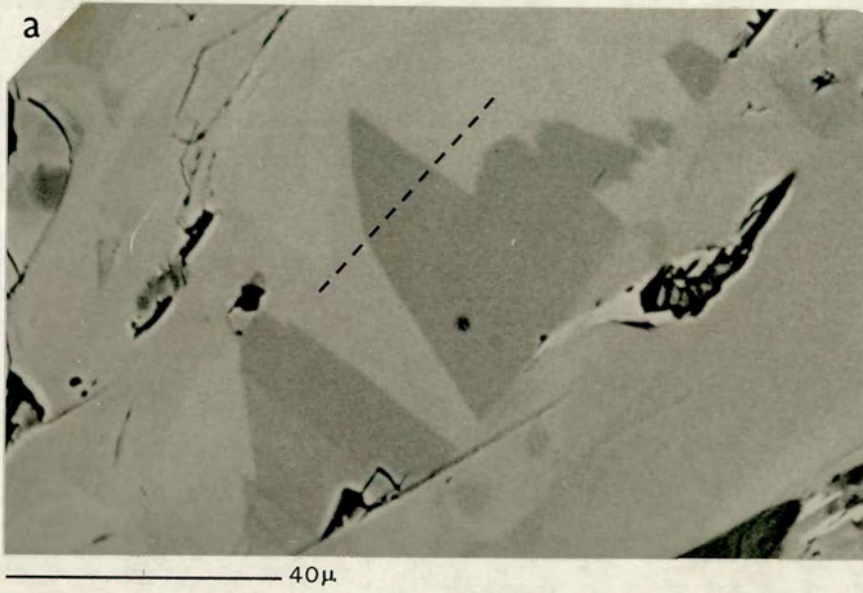
(a) High magnification B.S.E. image of triangular-shaped secondary amphiboles adjacent to cracks within an original hornblende crystal.
The approximate position of the traverse line in (b) is indicated.

(b) Plot of cation concentration versus distance across the secondary amphibole indicated in (a). Note the fairly sharp change in chemistry between original hornblende and secondary magnesio-hornblende (discussed in the text).

Step intervals $\sim 1\mu\text{m}$.

KEY: Red curve/crosses correspond to the element plotted on the red axis.

Blue curve/diamonds correspond to the element plotted on the blue axis.



(b) *Microvein Alterations.*

Cross-cutting amphibole microveins were largely recognised as a consequence of B.S.E. imagery performed using Edinburgh Universities S.E.M. Since no analytical facilities were available on the S.E.M. only a small proportion of the microveins have been analysed in detail during subsequent studies carried out on the electron-probe. Similarities in both the optical properties and B.S.E. images of the microveins suggest that the analyses obtained are representative of the compositions present; these being composed of either actinolitic-hornblende or actinolite. The maximum differences in chemistry involved are:

ORIGINAL AMPH CONCN	VARIATION IN OXIDE WT%	ACTIN.CATION PROPORTIONS
c.42wt% SiO ₂	+ 12	7.85 Si
c.10wt% Al ₂ O ₃	- 9	0.16 Al
c.12wt% MgO	+ 5	3.50 Mg
c.15wt% FeO	- 4	1.40 Fe
c.1.5wt% K ₂ O	- 1.3	0.01 K
c.1.5wt% TiO ₂	- 1.8	0.01 Ti
c.1.5wt% Na ₂ O	- 1.2	0.04 Na
c.12wt% CaO	+ 0.8	2.00 Ca

+ represents an increasing concentration -represents a decreasing concentration from original compositions

A representative microvein composition is presented in Table 5.3. This marked difference in chemical composition corresponds to a large decrease in Z relative to the unaltered host amphibole's Z. As a consequence of this large Z variation the actinolitic veins stand out particularly well in B.S.E. images where they correspond to very dark-grey-black features (Plates 46, 47 and 48). The detailed relationships between microvein and host amphiboles were far easier to distinguish in B.S.E. images than was possible optically; a variety of slightly different microvein types were observed:

TABLE 5.3 EXTENSIVELY ALTERED AND MICROVEIN AMPHIBOLE COMPOSITIONS

OXIDE	0.15m. ⁱ	0.15m. ⁱⁱ	9m. ⁱⁱⁱ	9m. ^{iv}	15m. ^v
SiO ₂	53.875	54.462	53.865	50.115	54.021
Al ₂ O ₃	1.219	0.964	1.914	4.930	1.495
MgO	16.545	16.344	16.198	14.765	16.451
FeO	11.218	11.329	11.809	13.056	11.441
TiO ₂	0.225	0.057	0.127	0.642	0.057
MnO	0.462	0.545	0.551	0.516	0.630
Cr ₂ O ₃	0.035	0.025	0.012	0.028	0.053
CaO	12.447	12.786	12.433	12.169	12.097
K ₂ O	0.075	0.061	0.151	0.470	0.088
Na ₂ O	0.255	0.171	0.322	0.702	0.295
F	0.000	0.000	0.207	0.062	0.122
Total	96.360	96.740	97.590	97.450	96.750
<u>-O=Cl,F</u>	<u>0.000</u>	<u>0.000</u>	<u>0.090</u>	<u>0.030</u>	<u>0.050</u>
TOTAL	96.360	96.740	97.500	97.430	96.700
Si ^{iv}	7.806	7.876	7.743	7.283	7.797
Al ^{iv}	0.192	0.124	0.257	0.717	0.203
Al ^{vi}	0.017	0.040	0.068	0.128	0.051
Cr	0.004	0.003	0.001	0.003	0.006
Fe ³⁺	0.111	0.030	0.137	0.273	0.192
Ti	0.025	0.006	0.014	0.070	0.006
Mg	3.573	3.522	3.470	3.198	3.539
Fe ²⁺	1.243	1.340	1.277	1.296	1.167
Mn	0.028	0.058	0.033	0.032	0.038
BFe ²⁺	0.003	0.000	0.006	0.017	0.022
BMn	0.028	0.009	0.034	0.032	0.039
BCa	1.932	1.981	1.915	1.895	1.871
BNa	0.036	0.010	0.045	0.056	0.041
ANa	0.036	0.038	0.045	0.142	0.041
AK	0.014	0.011	0.028	0.087	0.016
ATOTAL	0.050	0.049	0.073	0.229	0.058
CF	0.000	0.000	0.094	0.028	0.056
SUMCAT	15.049	15.049	15.072	15.229	15.030
SUMOXY	23.000	23.000	23.001	23.000	23.010
Z	12.852	12.876	12.896	13.076	12.857
	ACT	ACT	ACT	A-H	ACT

Recalculated on the anhydrous basis of 23 oxygens using AMPHIBOL (Am.Min., 1990) selected scheme AV.15-NK & 13-CNK

ACT = Actinolite

- i Patch adjacent to hornblende grain boundary.
- ii 100% recrystallisation.
- iii Microvein composition.
- iv Extensively altered hornblende
- v Actinolic patch toward rim of hornblende.

- 1: Sharply bounded and occasionally bifurcating, crystal-pervasive microveins with regular shapes. (Plates 46 and 47ab)

The host amphibole composition immediately adjacent to the microvein margins remains unaltered and the secondary amphibole which constitutes the microvein shows continuity across adjacent phases (both amphibole and plagioclase). Plate 46 (a and b) exhibits examples of actinolitic microveins which can be clearly traced through one original hornblende crystal into an adjacent hornblende; part of the actinolitic microvein can also be traced through an interstitially situated plagioclase crystal. Plate 46c depicts secondary amphibole microveins which can again be traced through adjacent original amphiboles. In this instance the microfracture, with which these secondary amphibole microveins are associated, have caused albitisation within interstitial plagioclase crystals.

As is evident in Plate 46a, the secondary amphibole microveins are also clearly visible optically; the blue-green coloured, actinolitic amphibole forming the microvein is usually a single crystal in optical continuity with the hornblende host. The sharp interfaces between host and microvein amphiboles seen in the B.S.E. images are also optically sharp (Plate 30b).

- 2: Highly irregularly shaped, crystal-penetrative, sharply bounded microveins (Plate 47c,d).

Again no alteration of the host hornblende occurs beyond the margin of the microvein but unlike (1) these microveins do not appear to continue beyond the host amphibole crystal. These have not been identified optically.

PLATE 46: MICROVEIN ALTERATIONS.

(a) PPL photograph of original yellow-brown coloured amphibole grains within which bluer-green coloured secondary amphibole microveins can be distinguished (arrowed 1). Note the blue-green amphibole (arrow 2) 'overgrowing' a plagioclase crystal.

Scale bar: 0.4mm. (E15)

(b) B.S.E. image of (a) within which the blue-green coloured secondary amphibole of (a) is clearly visible as sharply-bounded, darker-grey coloured microveins. Note that the original amphibole immediately adjacent to the microveins (arrowed 1) is not altered. Note also the continuation of the microveins from one crystal into another and the overgrowths (arrowed 2).

Scale bar: 0.4mm. (E15)

(c) B.S.E. image in which white is original amphibole (A), grey is feldspar (F). Secondary amphibole microveins within the original amphibole (arrow 1) can be traced through the feldspars (arrow 2) where they produce a darker-grey coloured alteration (arrow 2).

Scale bar: 200 μ m. (E29)

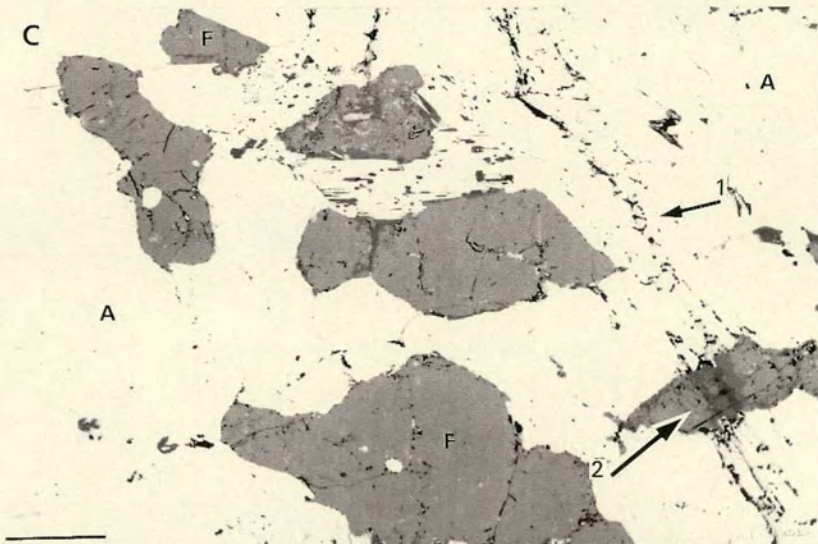
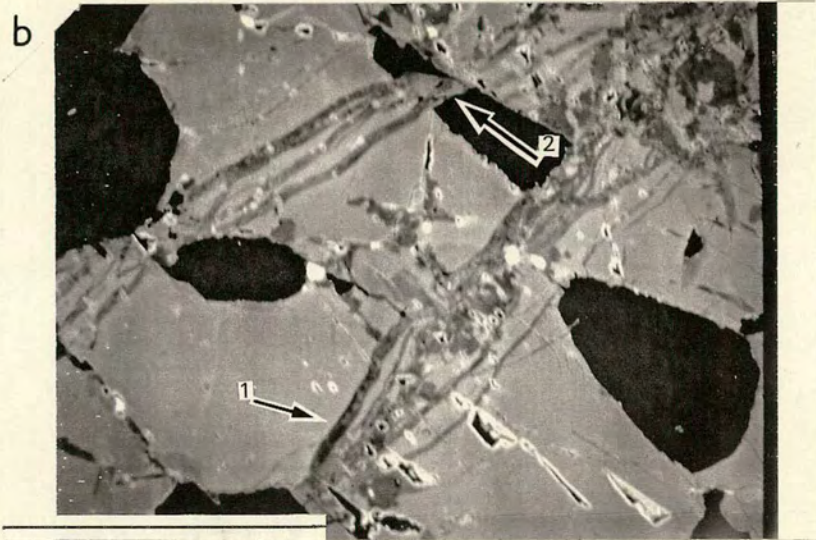
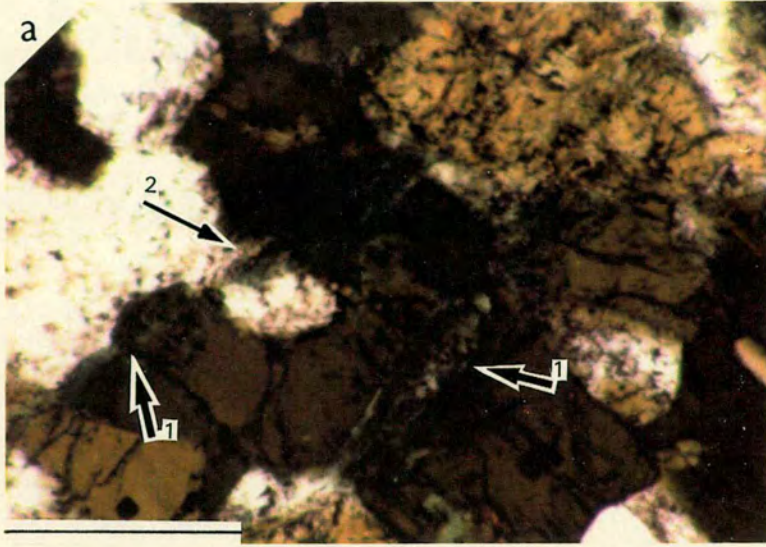


PLATE 47: MICROVEIN ALTERATION.

(a) B.S.E. image of an original amphibole crystal (pale-grey) traversed by darker-grey, sharply bounded, secondary amphibole microveins. Note the lack of alteration of the original amphibole immediately adjacent to the microveins (arrowed 1) and the irregular, bifurcating paths taken by the microveins. Arrow 2 points to a microvein amphibole which 'overgrows' a feldspar crystal (black) before entering an adjacent original amphibole.

Scale bar: 200 μ m. (E15)

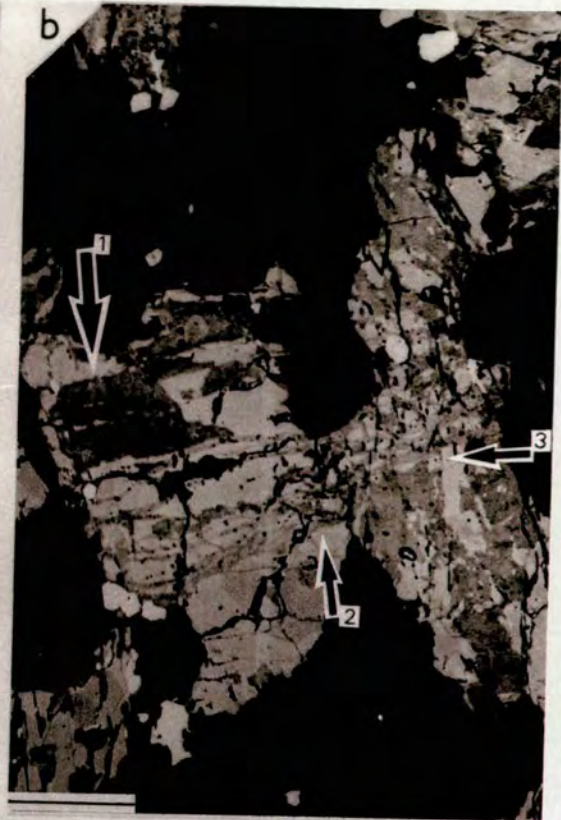
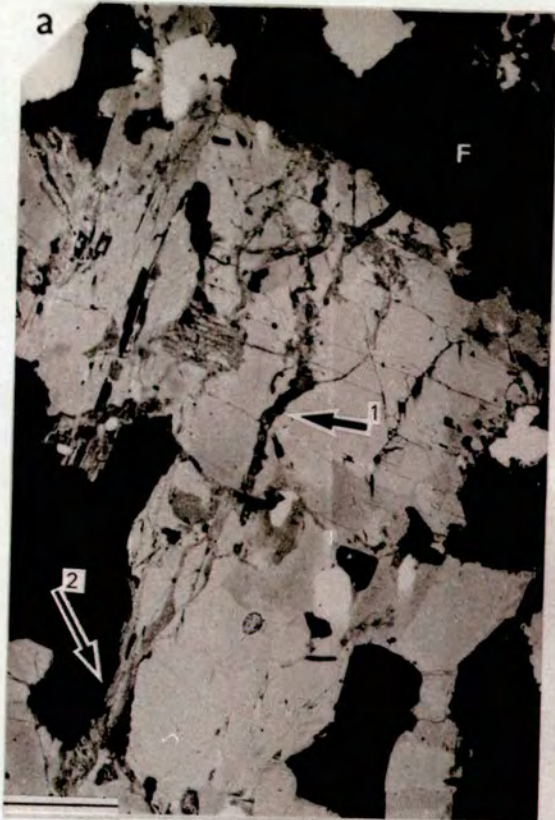
(b) B.S.E. image of an original amphibole crystal (pale-grey) within which a broad, dark-grey microvein (arrow 1) is clearly visible. Again note its sharply bounded interface with the host crystal. Narrower, paler-grey microveins (arrowed 2) can be linked to the extensive zonations in the adjacent amphibole crystal (arrow 3).

Scale bar: 200 μ m. (E15)

(c) and (d) B.S.E. images of highly irregularly shaped, dark-grey coloured secondary amphibole microveins within pale-grey coloured hosts. The interface between dark-grey and pale-grey amphiboles is very abrupt.

Scale bars (c): 50 μ m. (E16)

(d): 20 μ m. (E21)



3: Intracrystalline patchworks of irregularly shaped secondary amphibole. (Plate 48)

These patchworks commonly coincide with cracked and cleaved regions within the original hornblende crystals however, the detailed shapes of the individual patches themselves do not appear to be entirely crack/cleavage controlled. These are classified as microveins because of their obviously cross-cutting relationship with the host amphibole, contrasting with occasional spots adjacent to cleavages which usually show no continuity through the host and have thus been classified as boundary type alterations. Individual units within the patchworks are composed of a range of different secondary amphibole chemistries varying from edenitic-hornblendes to actinolite. Each chemically different amphibole forms a discrete, sharply bounded but often irregularly shaped unit within the altered patchwork. Occasionally a triangular shaped unit is present.

When viewed optically these microveins appear as anastomosing areas of homogeneous, blue-green coloured amphibole which retains optical continuity with the host crystal (Plate 48a). The composite nature of the microveins (as seen in B.S.E. images) cannot be distinguished in PPL; no individual grain-boundaries or sub-grains can be identified which coincide with the patches/units seen in the B.S.E. images.

A closely spaced (*c.*1.5 μm . interval) automatic electron microprobe traverse was performed across an actinolitic unit within one of the patchwork-like microveins described in 3 above (Plate 48). The right-hand region of the traverse (Figure 5.6) displays a quite rapid chemical gradient of *c.*5 μm . between the central actinolite "microvein" and the outer hornblende composition. It should be noted that the hornblende composition here is not that of an unaltered/original hornblende but actually represents a secondary amphibole unit adjacent to the actinolite microvein. The left-hand side of the traverse is more complicated due to the intersection of several chemically different units whose interfaces with one another are slightly smoothed. The first *c.*30 μm . represents a secondary magnesio-hornblende-rich plateau, an approximately 4-5 μm . gradient separates this from a very approximately 3 μm . wide secondary actinolitic-hornblende rich unit (whose plateau has not been intersected). The following *c.*6 μm . represents an additional secondary magnesio-hornblende unit (whose Si,Mg content is higher than seen previously); a *c.*6-8 μm . wide interface occurs between this unit and the actinolite microvein plateau.

PLATE 48: PATCHWORK MICROVEIN.

(a) PPL photograph of epitaxial, blue-green coloured secondary amphibole microvein within an original amphibole crystal.

Scale bar: 800 μm . (E21)

(b)-(e) Sequentially higher magnification views of the amphibole microvein depicted in (a). The blue-green amphibole is seen to comprise a "patchwork" of sharply bounded chemical units each with a characteristic shade of grey in these B.S.E. images.

Scale bars: (b) 400 μm .

(c) 100 μm .

(d) 40 μm .

(e) 20 μm .

PLATE 48

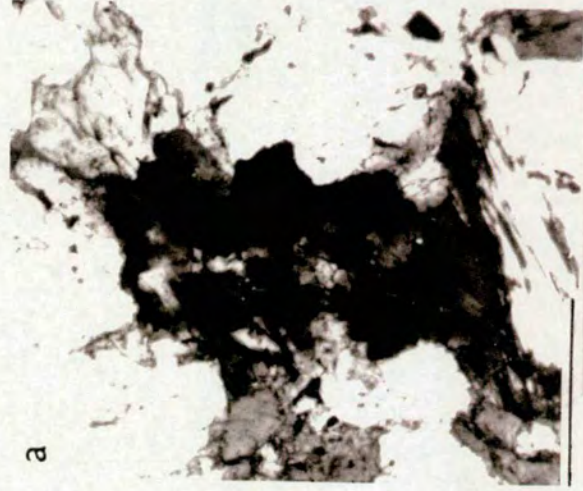


FIGURE 5.6.

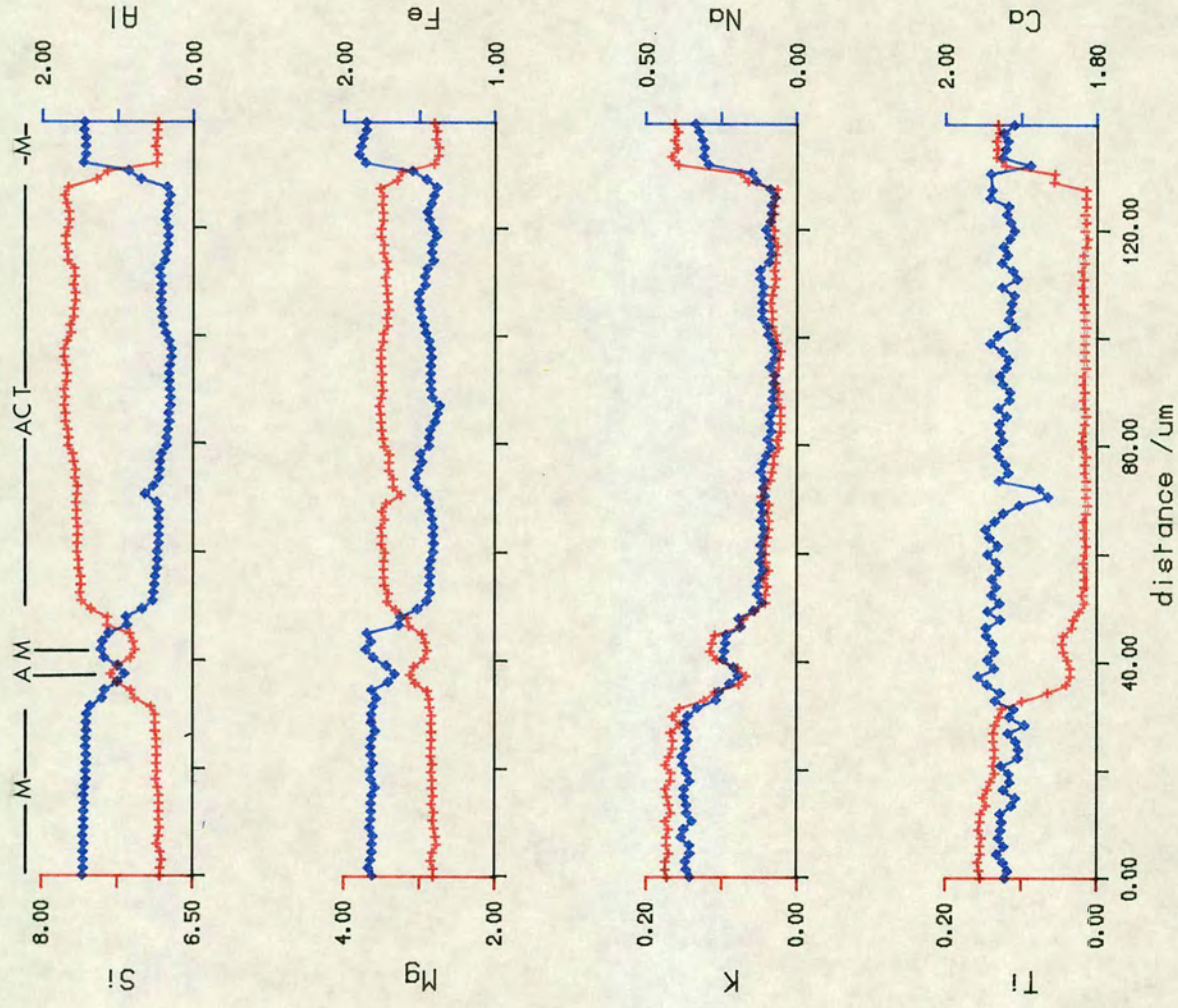
Plot of cation concentrations versus distance across an actinolite microvein. The line of the traverse is indicated in Plate 48d. The different secondary amphibole compositions intersected are shown:

M - Magnesio hornblende A - Actinolitic hornblende

ACT - Actinolite.

KEY: Red curve/crosses correspond to the element plotted on the red axis.

Blue curve/diamonds correspond to the element plotted on the blue axis.



The relative abundances of each of the microvein types discussed above is not known in detail because of the vast amounts of time required to image each thin-section. Combined B.S.E. and optical studies performed so far suggest type 1 microveins to be the most common.

SPATIAL DISTRIBUTION

Type 1 microveins have been optically identified in many of the rocks (see Table 4.1) irrespective of their distances from the intrusive Stock. Type 1 microveins are particularly abundant in the sample closest to the contact (E15).

(c) *Extensive single crystal alterations.*

The more extensive alterations described in the detailed thin-section description of E15, the closest sample to the contact (section 4.1.3.), were examined in some detail using both B.S.E. and microprobe techniques. The extensive epitaxial secondary amphibole growths in E15 were found in B.S.E. studies to be composed of patch-works of secondary actinolitic-hornblende and actinolite similar to the microvein type 3 described above. Each different amphibole chemistry forms a distinct, sharply bounded unit. The units again have very irregular shapes; Plate 49 displays both optical and B.S.E. photographs of several of the extensively altered amphibole crystals, Plate 50a,c,d exhibits some additional images of the almost pseudomorph-like secondary amphibole seen in E15. Several representative spot analyses of the secondary amphibole are presented in Table 5.3.

Low power B.S.E. image locality maps of E15, made as an aid to laser-beam positioning (see chapter 3), indicate that many of these actinolitic units can be linked to more obviously crystal penetrative microveins (1 above) within adjacent amphiboles (Plates 15b and 47b). This relationship was also observed optically. The extensive single-crystal alterations in this rock (E15) are therefore considered to be linked with a microvein formation event. This relationship has *only* been observed in E15.

SPATIAL DISTRIBUTION

Extensive single crystal alterations were only examined in E15; spatial distributions were identified optically (see Table 4.1).

PLATE 49: EXTENSIVE SINGLE CRYSTAL ALTERATIONS.

(a) PPL photograph of an original dark-brown coloured amphibole (arrow 1) within which large, deep-blue-green coloured zones can be seen (arrowed 2). The blue-green and host amphiboles are in optical continuity; both are single crystals.

Scale bar: 0.4mm. (E15)

(b) B.S.E. image of (a) within which the blue-green coloured amphibole of (a) is clearly visible as sharply-bounded, darker-grey areas (arrowed 1) within a pale grey host (arrowed 2). Note the host amphibole is also altered; arrow 2 indicates the area magnified in (c).

Scale bar: 0.4mm. (E15)

(c) Higher magnification B.S.E. image of the area pinpointed in (b). The 'original' amphibole can be seen to contain mid-grey coloured zones (arrow 1); these have sharply-bounded interfaces with the unaltered, paler-grey host (arrow 2). Note also altered pyroxene.

Scale bar: 100 μ m. (E15)

(d) PPL photograph of an original dark-brown coloured amphibole (arrowed 1) whose core is partially occupied by a blue-green coloured amphibole (arrow 2).

Scale bar: 0.3mm. (E15)

(e) B.S.E. image of (d); the blue-green amphibole in (d) produces large zoned patches of a darker-grey amphibole (arrowed 1 and 2) in the B.S.E. image. Note the slight mismatch between the detailed shapes of PPL and B.S.E. images.

Scale bar: 0.3mm. (E15)

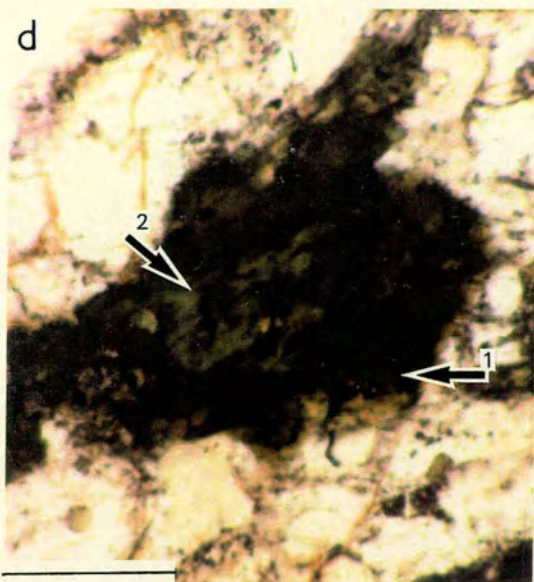
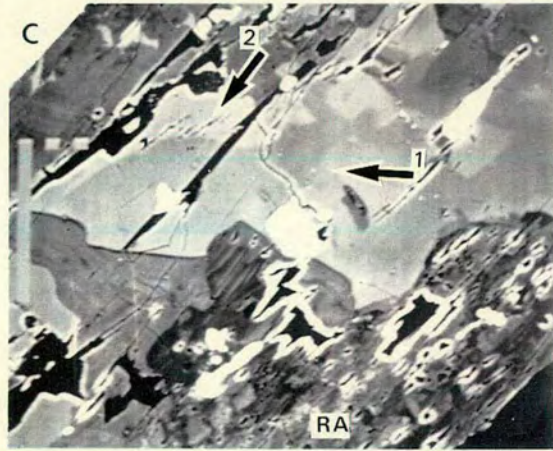
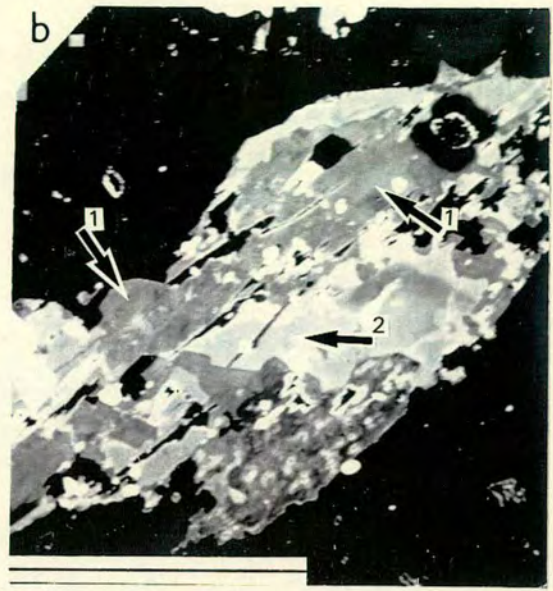
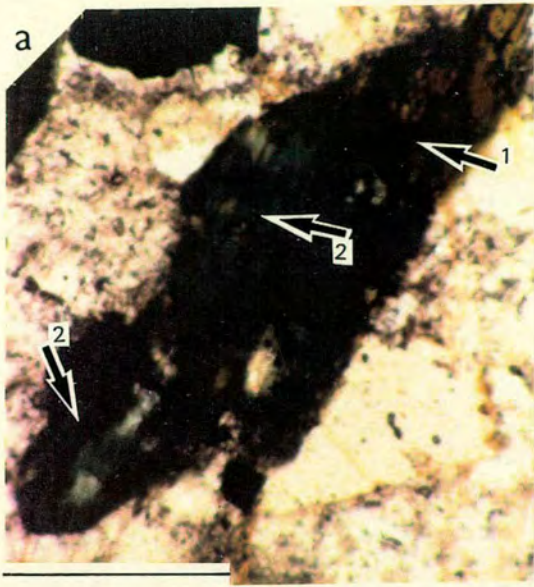


PLATE 50: EXTENSIVE SINGLE CRYSTAL ALTERATIONS.

(a),(c),(d) B.S.E. images of extensively altered amphibole grains. In each case the original pale-grey amphiboles contain large segments of sharply-bounded, dark-grey amphibole. Note mid-grey microveins in (c); arrow.

All scale bars: 200 μ m. (E15)

EXTENSIVE MULTI-CRYSTAL ALTERATION

(b) B.S.E. image of an amphibole which has partially recrystallised to an aggregate of dark-grey-black amphibole (arrow). In PPL the grain appears as a recrystallised aggregate of blue-green crystals; the retention of parts of the original crystal (OA) is only seen in B.S.E. images.

Scale bar: 100 μ m. (E15)



(d) *Extensive multi-crystal alterations.*

Completely or partially recrystallised amphibole grains were briefly investigated. B.S.E. images of partially recrystallised grains, see Plate 50b, indicate that some portions of the original hornblende remain intact. Microprobe analyses of the chemically modified areas of these grains indicates they are composed of secondary actinolite (see Table 5.3).

SPATIAL DISTRIBUTION

Extensive multi-crystal alterations were only investigated in E15; spatial distributions were determined optically (see Table 4.1).

COMPOSITIONS OF CRYSTALS NUCLEATING ALONG AMPHIBOLE GRAIN EDGES

Recrystallised crystal fringes composed of tiny $<1\mu\text{m}$. crystals adjacent to amphibole grain edges have been optically identified as being either biotite, amphibole, epidote or combinations of the three. Many of these crystals actually fall within the thickness of the thin-sections and as a result could not be either analysed or imaged. Those that are present at the section surface generally have a very poor polish which produces very poor and largely mineralogically unrecognisable analyses. Three rocks (E52, E16 and E50) within which the crystal fringes are particularly well developed were examined in some detail. A typical situation is presented in Plate 51, here the PPL photograph clearly displays a fringe of tiny crystals, but B.S.E. images reveal that few of these crystals are actually present at the sample surface. Both amphibole and biotite compositions have been identified amongst the more acceptable of the analyses obtained, the remaining analyses were not fully recognisable as either amphibole or biotite. No epidote was detected in these examples.

PLATE 51: RECRYSTALLISED GRAIN BOUNDARIES.

(a) PPL photograph of a relatively pristine amphibole grain. Alteration along the grain-margin (arrow) is optically identified as comprising recrystallised crystals of colourless amphibole in addition to tiny flakes of both biotite and epidote.
Scale bar: 0.2mm. (E52).

(b) B.S.E. image of the amphibole pictured in (a). Note that most of the tiny crystals which were seen optically within the recrystallised fringe are not present at the surface of the slide and therefore are not visible on the image. Note the amphibole is unaltered.
Scale bar: 100 μ m. (E52).

(c) Higher magnification B.S.E. image of the recrystallised fringe of (a) and (b) confirming the new growth crystals are within the thickness of the slide.
Scale bar: 100 μ m. (E52).

PLATE 51



5.1.2. SUMMARY OF THE OPTICAL AND CHEMICAL CHARACTERISTICS OF THE MAJOR AMPHIBOLE ALTERATION TYPES

In the great majority of situations amphibole alterations of Boundary, Microvein and Extensive single crystal types are characterised by:

- (i) an optical change from yellow-green-brown coloured original hornblende to bluish-green coloured secondary amphibole.
- (ii) optical continuity between original and secondary amphiboles.
- (iii) a change in B.S.E. images from pale-grey, original hornblende to darker-grey/black secondary hornblende/actinolite.
- (iv) increased concentrations of Si, Mg and decreased concentrations of Al, Fe, K, Na, Ti and Ca in the secondary amphibole relative to the original hornblende.

Boundary type secondary amphiboles are mostly edenites and magnesio-hornblendes, occasionally actinolitic hornblendes or actinolites. Extensive single and multi-crystal alterations and microveins are usually actinolitic hornblendes or actinolites. Some of the secondary amphibole patches/microveins are seen in B.S.E. images to be comprised of "patchworks" of sharply bounded units of variable compositions (each with a distinct grey shade in the B.S.E. image). Optically these patchworks correspond to blue-green coloured amphibole within which no sub-units can be clearly identified; no grain-boundaries can be observed in PPL which correlate to the secondary amphibole units seen in the B.S.E. images. Given the correlation in ages between geological events and alteration zones within the amphibolites established in section 4.4, the secondary hornblendes appear to be mostly PreCambrian and the secondary actinolites are largely Laramide in age.

5.1.3. SUMMARY OF CHEMICAL PROFILE TYPES

Two dominant types of chemical profile have been identified from the step-traverses performed using the electron microprobe:

- (i) those with abrupt changes in chemistry between original and secondary amphiboles
- (ii) those with gradual changes in chemistry between original and secondary amphiboles

Profiles such as those presented in Figure 5.2 can be readily interpreted as reflecting differences in the elemental concentrations between original and secondary amphiboles; a sharp ($<5\mu\text{m.}$) discontinuity occurs between the regions with the different chemistries. A smoothing of the true interface, due to overlapping of successive analysis points, has probably taken place in some of the closer spaced ($\leq 2\mu\text{m.}$) traverses such as those presented in Figures 5.5 and 5.6.

Many of the profiles obtained, such as those presented in Figures 5.1 and 5.4, are more difficult to interpret. Some elements (*e.g.* Si and Al in Figure 5.1) show a progressive change from original to secondary amphibole composition with an overall diffusion-type composition profile, whilst other elements (*e.g.* Mg, Fe in Figure 5.1) indicate that two distinct compositional plateaus were present and these have been extensively smoothed by some later diffusive event.

EXPERIMENTAL PROBLEMS

Experimental complexities add to the difficulty in interpreting some of the profiles. In the early stages of the research, concentration profiles were obtained without the use of B.S.E. imagery. Step traverses were performed with relatively widely spaced intervals ($\geq 10\mu\text{m.}$) to:

- (i) minimise beam overlap
- (ii) rapidly locate altered phases

In addition a conscious effort was made to avoid the edges of individual crystals thus minimising overlap with adjacent phases and avoiding intersections with the grain-boundaries themselves.

Amphibole crystals which, based on electron microprobe data were believed to have gradually changing chemical profiles, were later examined using B.S.E. imagery. A small proportion correlated with a gradual mean atomic number variation (Plates 42 and 43). However, the great majority actually reflected situations where the final analysis point of the electron microprobe traverse fell within a sharply bounded patch of secondary amphibole adjacent to the margin of the original hornblende. The true nature of the alteration types was fully characterised in later investigations performed using the combined analytical/B.S.E. facilities available on Edinburgh Universities Camebax Microprobe. Sufficient time was not available to perform closely spaced traverses across all of the grains that had already been examined, however, their B.S.E. images were recorded and representative situations were re-examined in

greater detail. Most of the diffusive-type composition profiles obtained were found to reflect situations in which experimental problems (as outlined above) had combined to generate misleading profiles.

5.1.4. DISCUSSION OF B.S.E. IMAGES

B.S.E. images of secondary amphiboles within original hornblende crystals are of two main types:

- (i) Secondary actinolites and hornblendes with abrupt interfaces against the host hornblende; Plates 40-41.

and

- (ii) Secondary hornblendes with apparently gradual interfaces against the host hornblende; Plates 42-43.

(i) ABRUPT INTERFACES BETWEEN HOST AND SECONDARY AMPHIBOLES.

Abruptly bounded secondary amphiboles are by far the most abundant of the two types (c.90%). They correspond to the discontinuous chemical profiles described in 5.1.3. Detailed B.S.E. imaging reveals that:

- 1: The abruptly bounded secondary amphiboles are very irregular in both size and shape, neither of which bears any relation to the shape of the original hornblende crystal.
- 2: The abruptly bounded secondary amphiboles occur widely throughout most of the amphibolitic rocks at Eldora.
- 3: An increased abundance of abruptly bounded secondary amphiboles is observed in the more mineralised rocks both adjacent to the contact and intermittently throughout the other amphibolitic rocks.

MULTIPLE EVENT EVIDENCE

Evidence for the presence of two generations of sharply bounded secondary amphiboles is evident within the rocks, though sparsely distributed. Sharply bounded patches of secondary amphibole have quite often been observed actually "within"/upon a presumably pre-existing secondary amphibole. An example of this sort of situation is presented in Plate 40d, here a secondary actinolite patch has "overgrown" a sharply bounded rim of secondary magnesio-hornblende. The secondary magnesio-hornblende has overgrown the original hornblende. The microvein "patchworks" of sharply bounded units (described

under Microvein alterations, microvein type 3) are also be considered to represent evidence to suggest multiple alteration events. In Plate 48 the actinolite 'microvein' and its surrounding sharply bounded units have overprinted a pre-existing secondary magnesio-hornblende. In the majority of situations the "younger" alterations are either actinolitic-hornblende or actinolites.

(ii) GRADUAL INTERFACES BETWEEN HOST AND SECONDARY HORNBLENDES

Gradual-type marginal amphibole alterations have been far less frequently encountered (Plates 42-43). Electron microprobe traverses from original hornblende cores to altered edges (Figures 5.1, 5.3 and 5.4) were interpreted in section 5.1.3 as suggesting that two originally homogeneous amphiboles were initially present and that the gradual-type gradients now existing between the original and secondary amphiboles is the result of variable degrees of diffusive exchange. Gradations in composition ranging over 10-100 μm .; averaging 20-40 μm . have been documented between such original and secondary amphibole compositions.

B.S.E. images reveal that:

- 1: Although the secondary hornblende is not always continuous within/around the original crystal their shapes do appear to reflect the shape of the original grain by forming partial to complete haloes adjacent to the original hornblendes grain-boundary (Plates 42, 43).
- 2: The widths of the gradual-type gradients is irregular both within individual crystals and generally within individual rocks (Plate 45b).
- 3: The widths of the gradual-type gradients do not obviously widen as the contact is approached; rocks within *c.*100m. of the contact have diffuse type rims with average widths of *c.*20-40 μm . (Plates 43b,c, 42b).

An excellent example of the irregularity in width of the gradual-type alteration is presented in Plate 45b. Here the gradual-type rim is *c.*20 μm . and 120 μm . in widths at opposing crystal margins. In Plates 42b and 43a however the alteration is seen as uniform, almost concentric haloes adjacent to the original hornblende grain boundaries.

Since only a minority (*c.*10%) of secondary hornblendes showing gradational composition contacts against the host hornblendes have been recognised within individual rocks, it is difficult to be certain whether the widths

and patterns observed are truly representative of those present (especially when one considers possible variations in the planes of cross-sections encountered).

Given that the widths and abundance of the gradual-type gradients do not noticeably increase as the contact is approached, their development shows no relation to a contact re-heating event. The widespread distribution of the gradual alteration patterns again suggests a regional event. If all the gradual-type alterations are assumed to be the same generation, two main interpretations can be drawn:

- (a) If two different amphiboles were present (as is suggested by the element profiles) it is reasonable to assume that an initial alteration event took place and that the secondary/original amphibole interfaces were once as sharply bounded as the abrupt interfaces (described under i). Diffusive activity responsible for smoothing the interface between original and secondary amphiboles must then have occurred during a subsequent PreCambrian or Laramide event. In this instance one of four PreCambrian events should be considered; migmatization, mineralisation or re-heating associated with the intrusions of either the Silver Plume or Pike's Peak Granites (see chapter 1). It is also feasible that the diffusive modification of the originally sharp boundaries may represent the combined effect of several diffusive exchanges brought about by re-heating associated with a combination of the PreCambrian and/or Laramide events.
- (b) If two different amphiboles were not present the diffusive rims may represent true zonations formed as a result of any one, or a combination of the four PreCambrian events or initial regional cooling. To date gradual-type alterations have only been recognised in less-pristine regions of the rocks, which optical studies have clearly shown to be related to the presence of rock-penetrative alteration zones (*i.e.* microfractures or permeation zones). The gradual alterations must therefore be in some way related to a regional, fluid controlled alteration event and are not "zonations" produced simply as a result of initial regional cooling or the PreCambrian re-heating events. In either of these two situations continuous-type haloes should have been encountered within the pristine areas of the rocks.

(iii) RELATIONSHIP BETWEEN ABRUPT AND GRADUAL TYPE ALTERATIONS.

Plate 45b clearly exhibits abruptly bounded secondary amphiboles (in this instance one of the peculiarly sawtooth shaped patterns) overprinting a gradual-type halo. A few similarly distinct situations have also been encountered during B.S.E. studies, Plates 42a, 41c, establishing that the abruptly bounded secondary amphiboles, in at least these specific cases, represent later alteration events. This relative age relationship is not always as obvious however; Plate 43c displays an amphibole with both gradual and abrupt alterations neither of which can be distinguished as a younger alteration (although younger alterations can be identified in an adjacent amphibole); Plates 43a, 42b and 42c display gradual-type haloes with no additional abruptly bounded secondary amphiboles, and Plate 43b shows a partially developed halo.

(iv) INTERPRETATION.

The relationships between secondary and original amphiboles outlined above provide strong evidence to support the theory that several alteration events have effected the Eldora Amphibolites.

Abruptly bounded amphibole alterations may be found superimposed upon both earlier abruptly bounded and gradually bounded secondary amphiboles. Thus at least two abruptly bounded amphibole alteration events are believed to have taken place:

- 1: A regional PreCambrian event (syn migmatization \pm /or mineralisation)
Epitaxial growths of secondary hornblendes and actinolite fillings to microveins developed upon/within original hornblende crystals.
- 2: A Laramide event (mineralisation + contact metasomatism)
Epitaxial growths of secondary actinolites, actinolitic hornblendes, secondary hornblendes and actinolite fillings to microveins developed upon/within both original hornblende crystals and some of the PreCambrian alterations. The development of one alteration upon another is presumably related to the routes taken by the respective "fluids" through the rocks.

The gradually bounded secondary hornblendes are believed to have developed as sharply bounded growths during one of the PreCambrian events. The interface between original and secondary hornblendes was then modified during a subsequent event. The diffusive modification of only a small fraction of the

PreCambrian alterations was controlled by the accessibility of the crystal grain boundaries to the younger fluids.

5.1.5. RELATION OF SECONDARY AMPHIBOLE COMPOSITIONS TO ALTERATION ZONES WITHIN THE AMPHIBOLITES

Border permeation zones were concluded in 4.4 to have formed in association with PreCambrian migmatization and thus the secondary hornblendes within these zones are also likely to be PreCambrian in age. Secondary hornblendes with both gradual and abrupt gradients against their host hornblendes have been encountered within border permeation zones.

The relative ages of the independent permeation zones within the amphibolites have not been satisfactorily resolved. Boundary type amphibole alterations which fall within these zones are mostly hornblendic, identical in composition to those which developed within the border permeation zones. The secondary hornblendes within the independent permeation zones have abrupt chemical interfaces against their hosts.

The Microvein portions of microfracture networks are almost exclusively actinolitic in composition, however the haloes of boundary alterations adjacent to the centrally located microfractures are usually hornblendic in composition. Microfractures were concluded from the optical evidence presented in chapter 4, to be the result of more than one event. The rock closest to the contact (E15) contains a particularly high percentage of Microveins which can be linked to Laramide Extensive single crystal alterations in adjacent amphibole grains. The actinolite Microveins in amphibolites immediately adjacent to the Stock are therefore considered to have developed as a result of Laramide metasomatism. Microfractures are common within the amphibolites at Eldora irrespective of their proximity to the Stock (see Table 4.1), thus a regional microfracture formation event must also have taken place. Since microfractures occur both adjacent to the Laramide ore shear (rock E7/E8) and elsewhere, their formation may be either related to the widespread movement of Laramide fluids or represent the result of an earlier PreCambrian alteration.

5.1.6. MISCIBILITY BETWEEN ORIGINAL AND SECONDARY AMPHIBOLES

The presence of more than one amphibole, particularly the original hornblendes and secondary actinolites within the Eldora Amphibolites, brings to the forefront the complex question of whether or not a miscibility gap or gaps

exist within the calcic amphibole series. The literature published on this topic is extensive (see section 2.2.3) however the presence of a solvus, at least between hornblende and actinolite, remains to be convincingly proven.

The possibility that some actinolite and/or secondary hornblende may have been present as part of the primary assemblage in *addition* to the original ferroan-pargasitic-hornblendes (and thus reflect a change in the P-T conditions of the initial regional metamorphism) is *not* considered because secondary amphibole is *not* present within pristine, unaltered parts of the rocks. Secondary amphibole has *only* been observed within and adjacent to definite bands and fracture networks within the rocks (as described in chapter 4).

The chemical sharpness of the interfaces between the original and secondary amphiboles (both actinolites *and* hornblendes), as depicted in their B.S.E. images and discontinuous chemical profiles, suggests several possibilities:

- (i) the secondary amphiboles are epitaxial overgrowths upon parts of the original ferroan-pargasitic-hornblendes.
- (ii) the secondary amphiboles represent single crystal replacements of parts of the original hornblendes.
- (iii) in case (ii) the secondary amphiboles are the result of diffusional exchange between a fluid and the original hornblende *combined* with the existence of a miscibility gap.
- (iv) the interface between the primary and secondary amphiboles is acting as a grain-boundary despite no such grain-boundary being detectable optically. A volume of the original hornblende is removed (dissolved) and secondary amphibole is re-precipitated. The secondary amphibole often grows as a single crystal in continuity with the host hornblende.

In the absence of either exsolution lamellae of hornblende in actinolite or clearly homogeneous grains of both hornblendes and actinolites within the Eldora Amphibolites, the best way to prove immiscibility/miscibility is to construct plots such as Na+K versus Al^{vi} (edenite v's tschermakite components) or Al^{vi} versus Si (tschermakite v's tremolite components). A scattering of analyses between ferroan-pargasitic-hornblendes and actinolites could be taken as suggesting complete miscibility, whilst distinct groups of analyses might perhaps suggest immiscibility. A review of the plots constructed using data obtained from other regional studies is given by Grapes and Graham (1978).

Plots of Al^{vi} versus Si, (Na+K) versus Al^{vi} and Mg versus Al^{vi} , presented in Figures 5.7, 5.8 and 5.9, represent the analytical data obtained from three different rocks. Figure 5.7 was constructed using data obtained from rock E15, the sample closest to the intrusive contact. Figure 5.8 was constructed using data obtained from rock E5, a fairly pristine rock originating approximately 15m. from the Stock contact. Figure 5.9 was constructed using data obtained from rock E52, a relatively pristine rock 663m. from the Stock contact which is pervaded by a network of microfractures (Plate 16). Each of these three rocks were described in detail in section 4.1.3.

The "composition gap" between hornblende and actinolite which has been postulated by some previous authors does not always fall exactly within the same area upon such plots and is apparently variable from region to region. A broad field, representing the approximate location of the majority of 'composition gaps' is illustrated by the boxes drawn in the Figures. It is clear from Figures 5.7 and 5.9 that compositions intermediate between original, ferroan-pargasitic-hornblende and secondary actinolite have been encountered. More data was available for the plots in Figure 5.9 and thus the transitional region between original hornblendes and actinolites is far better constrained. The field of secondary hornblendes in Figure 5.9 can be interpreted in two ways:

- (i) as a complete range of compositions intermediate between original hornblendes and actinolites which suggests complete miscibility.

or

- (ii) as four smaller bunches of secondary hornblende compositions (edenitic hornblendes, edenites, magnesio-hornblendes and actinolitic hornblendes).

FIGURE 5.7.

(a) Plot of Al^{vi} versus Si for rock E15 (0.15m. from the Eldora Stock contact).

(b) Plot of (Na+K) versus Al^{vi} for rock E15.

(c) Plot of Mg versus Al^{vi} for rock E15.

Boxes in a, b and c represent fields in which miscibility gaps have been reported in previous studies.

Tie-lines in a,b and c link co-existing compositions within individual amphibole grains.

End member compositions tremolite (TR), pargasite (PA) and edenite (ED) are shown where appropriate.

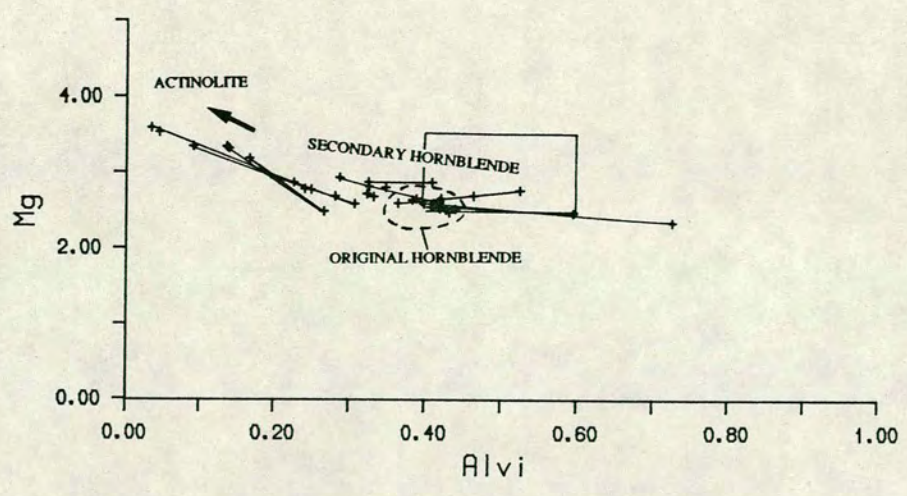
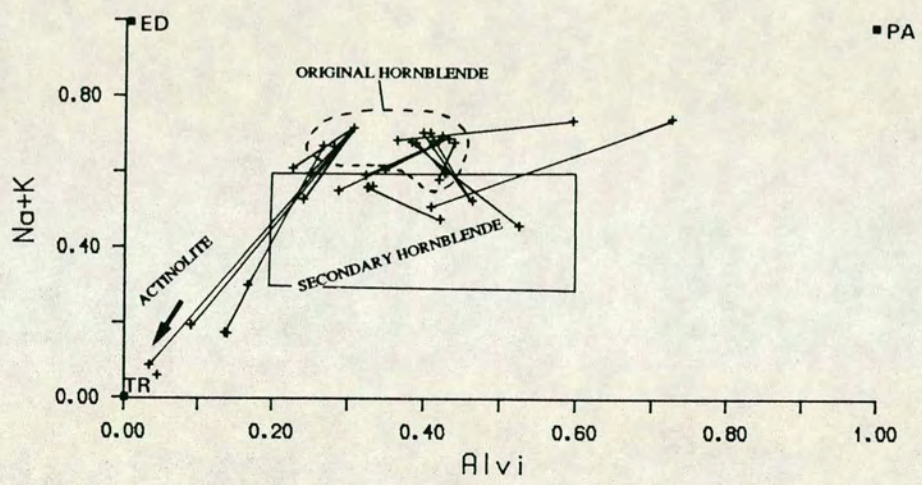
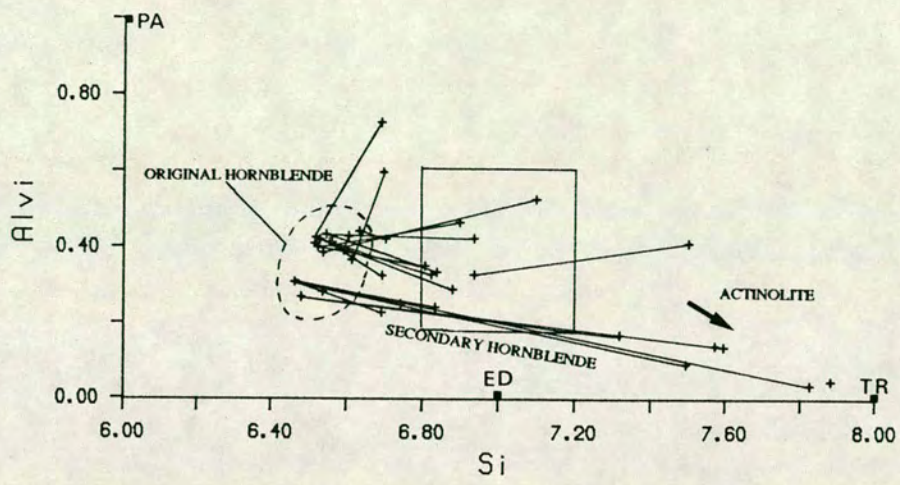


FIGURE 5.8.

(a) Plot of Al^{vi} versus Si for rock E5 (15m. from the Eldora Stock contact).

(b) Plot of (Na+K) versus Al^{vi} for rock E5.

(c) Plot of Mg versus Al^{vi} for rock E5.

Boxes in a, b and c represent fields in which miscibility gaps have been reported in previous studies.

Tie-lines in a,b and c link co-existing compositions within individual amphibole grains.

End member compositions tremolite (TR), pargasite (PA) and edenite (ED) are shown where appropriate.

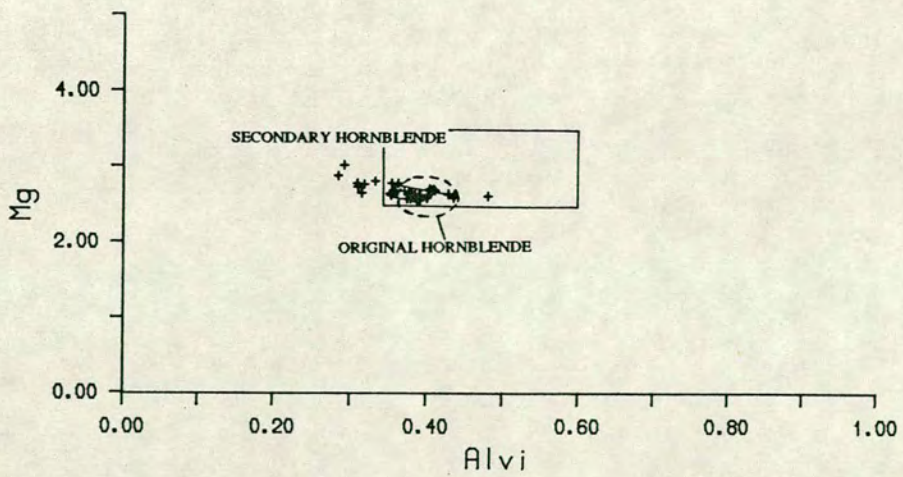
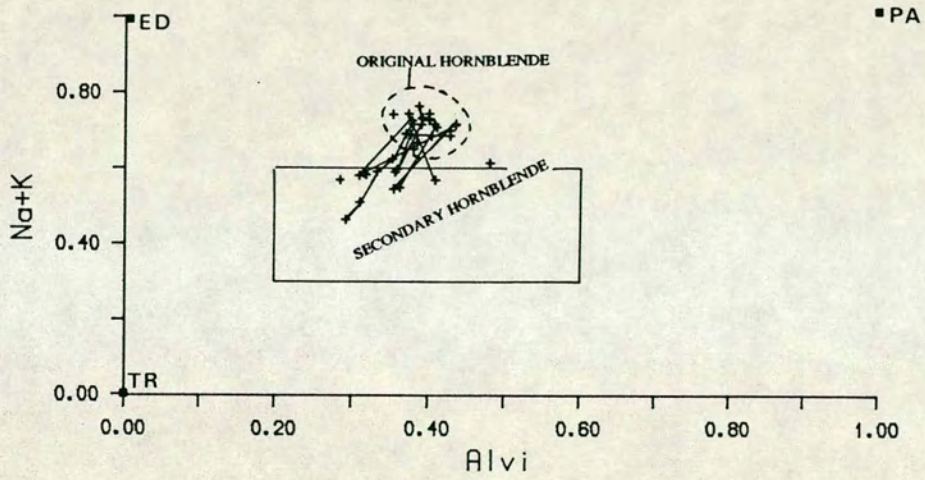
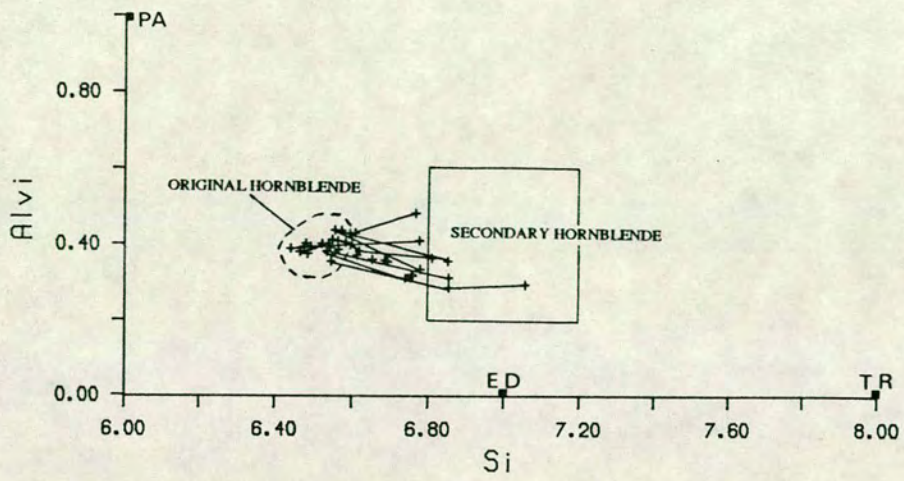


FIGURE 5.9.

(a) Plot of Al^{vi} versus Si for rock E52 (663m. from the Eldora Stock contact).

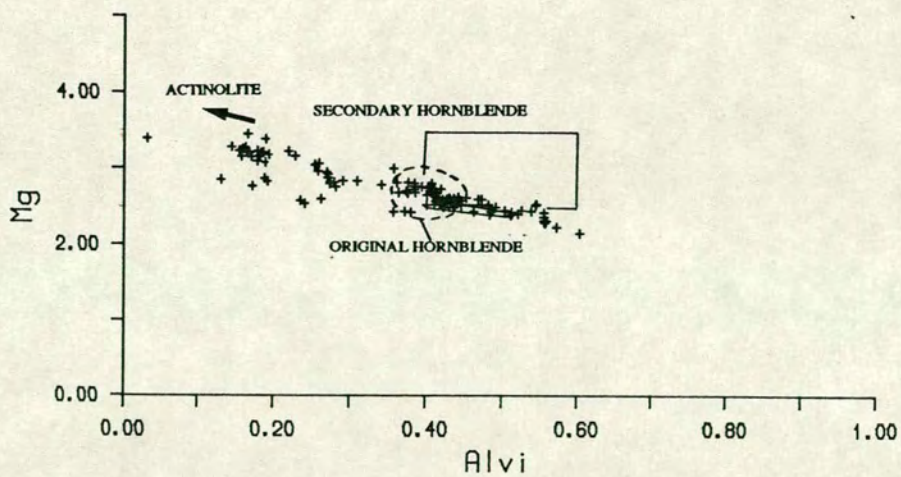
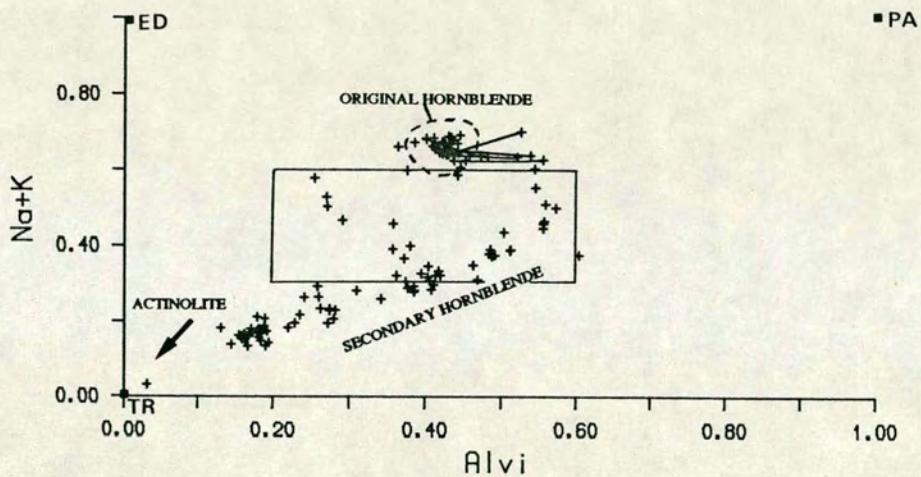
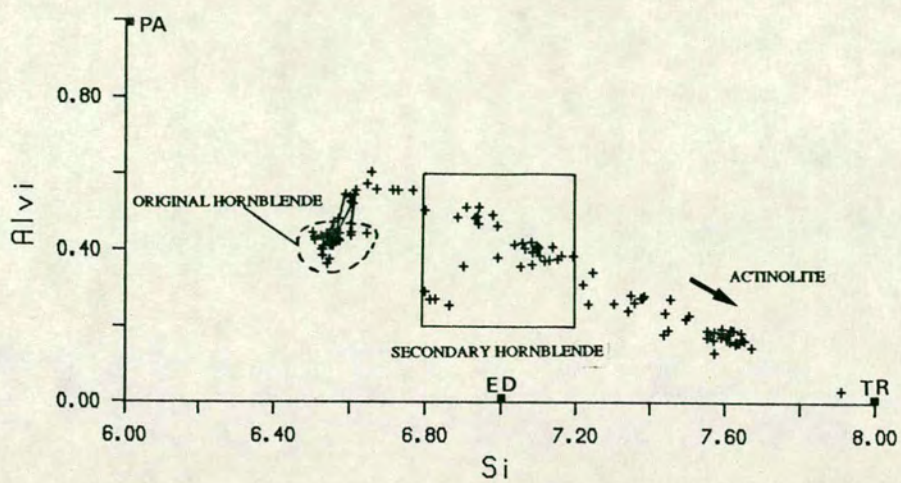
(b) Plot of (Na+K) versus Al^{vi} for rock E52.

(c) Plot of Mg versus Al^{vi} for rock E52.

Boxes in a, b and c represent fields in which miscibility gaps have been reported in previous studies.

Tie-lines in a,b and c link co-existing compositions within individual amphibole grains.

End member compositions tremolite (TR), pargasite (PA) and edenite (ED) are shown where appropriate.



The secondary amphibole analyses represented in the plots of Figure 5.9 originate from chemically sharply bounded secondary amphibole units within altered hornblende crystals. These occur as both patches adjacent to grain edges and as alteration patchworks similar to those presented in Plate 48. If the chemically sharp interfaces between the original hornblendes and secondary actinolites are to be interpreted as suggesting immiscibility then miscibility gaps must also be assumed to be responsible for the similarly sharp interfaces between the original and secondary hornblendes. To the authors knowledge no one has yet suggested immiscibility within the hornblende series.

Because fluids are believed to be ultimately responsible for the irregular distributions of the secondary phases within/adjacent to fracture networks and bands of alteration within the rocks (section 4.3) it is possible that the different secondary amphiboles reflect original amphibole alterations associated with:

- (i) several fluids whose compositions were slightly different.
- (ii) a fluid or several fluids whose compositions changed (*i.e.* evolved) over time.

In a simple case the secondary hornblendes might be considered to have resulted from one fluid-controlled alteration event and the secondary actinolites from a different fluid-controlled alteration event.

As the original hornblendes formed at high temperatures and the secondary hornblendes and actinolites developed during lower temperature, fluid-controlled alteration events, the amphibole compositions in question quite clearly *do not* represent an equilibrium assemblage. No evidence supporting the theory that a miscibility gap does exist within the calcic amphibole series has been distinguished within the figures presented in this section.

If there is no miscibility gap within the calcic amphibole series the sharp interfaces between many of the original and secondary amphiboles must be acting as a grain-boundary, despite the fact that often no such grain-boundary can be distinguished optically.

5.1.7. ION PROBE ANALYSIS

(i) MASS SURVEYS

Mass surveys of elements ranging in mass number from 1-238 were performed upon several amphibole crystals to establish the type and relative abundances of the different elemental and isotopic species present. One such survey is presented in Figure 5.10. The peaks represented in the histogram have not been corrected and therefore represent the combined emissions of both single- (*e.g.* ^{138}Ba , ^{28}Si) and multiple-ion species (*e.g.* BaO , $(2 \cdot ^{28}\text{Si})$, $(2 \cdot ^{24}\text{Mg}) + ^{48}\text{Ti}$ *etc.*). Several of the single isotope species measured in later analyses have been labelled; the ^{197}Au peak (caused by sputtering of the gold coating) indicates that the instrument was correctly aligned for both low and high mass resolution.

(ii) ELEMENT PROFILES FROM ALTERED GRAINS

The automatic step-scan facility available on the Ims 4F ion probe was utilised in attempts to obtain trace and rare-earth-element concentration profiles within individual amphibole crystals. The widest patches of secondary amphibole (*c.* 30-50 μm .) with the greatest difference in major/minor elemental concentrations to their host hornblendes which had (at least at that time) already been detected using electron-microprobe traverses were preferentially selected for further analysis. In order to minimise substantial beam-overlap whilst performing closely spaced traverses across the narrow compositional gradient between host and secondary amphiboles it was necessary to reduce the beam size at the expense of analytical sensitivity. Experimentation with both the field aperture and contrast diaphragm settings of the secondary column (performed by John Craven, Edinburgh University) enabled sampling of areas of between 1.5 μm and 15 μm of the primary beam spot to be obtained (*c.f.* the full primary beam-size of ~20-30 μm .). Closely spaced (*c.* 2-15 μm interval) traverses were then performed across zoned portions of several amphibole crystals.

One moderately strongly altered grain whose major/minor elemental profiles and subsequently obtained B.S.E. image are presented in Figures 5.11 and 5.12a was examined in some detail. The results obtained are typical of those seen within the other crystals examined. Three automated step-scans each with a different beam-size and step-interval were performed along the same line that the major/minor element profiles had been obtained (see Figure 5.12a).

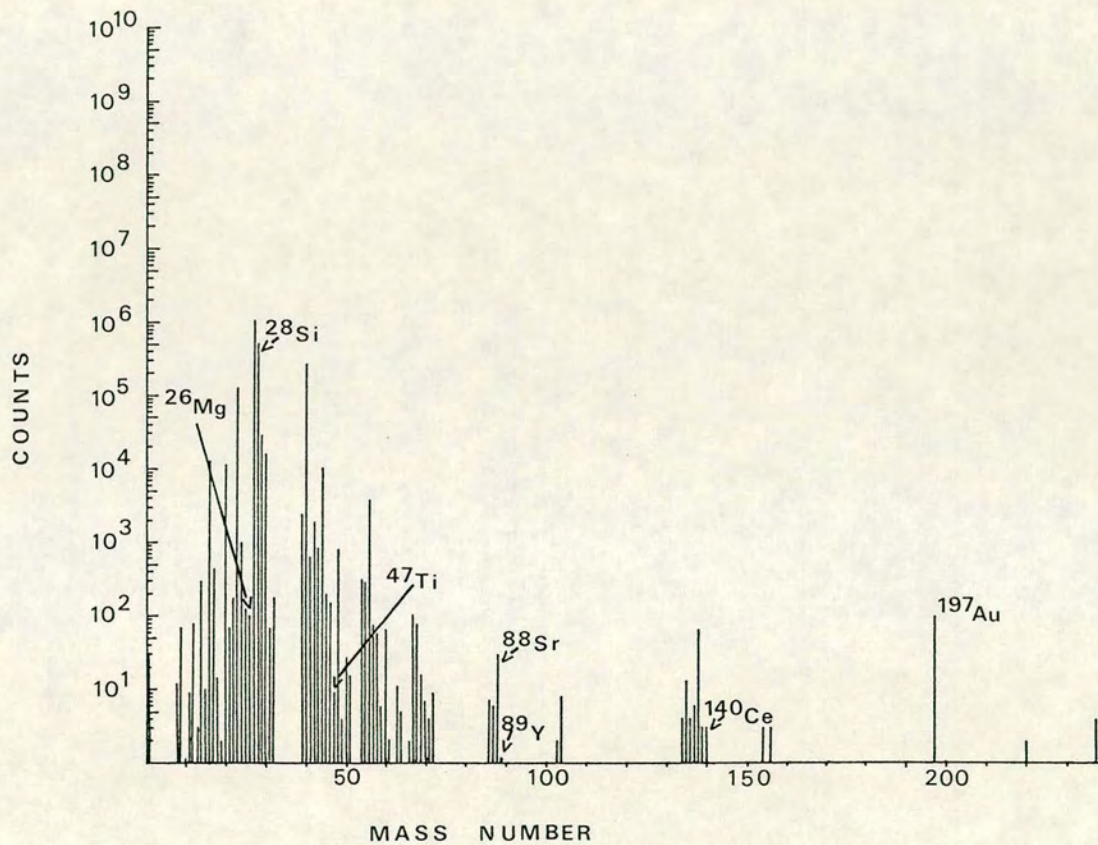


FIG. 5.10. Mass survey of an Eldora amphibole: both single and multiple ion species are depicted. Some of the isotopes examined in later analyses are labelled.

FIGURE 5.11.

Electron microprobe profiles depicting cation concentrations versus distance across the altered amphibole crystal used in later ion microprobe investigations (line of traverse indicated in Figure 5.12a).

KEY: Red curve/crosses correspond to the element plotted on the red axis.

Blue curve/diamonds correspond to the element plotted on the blue axis.

Step intervals $\sim 5\mu\text{m}$.

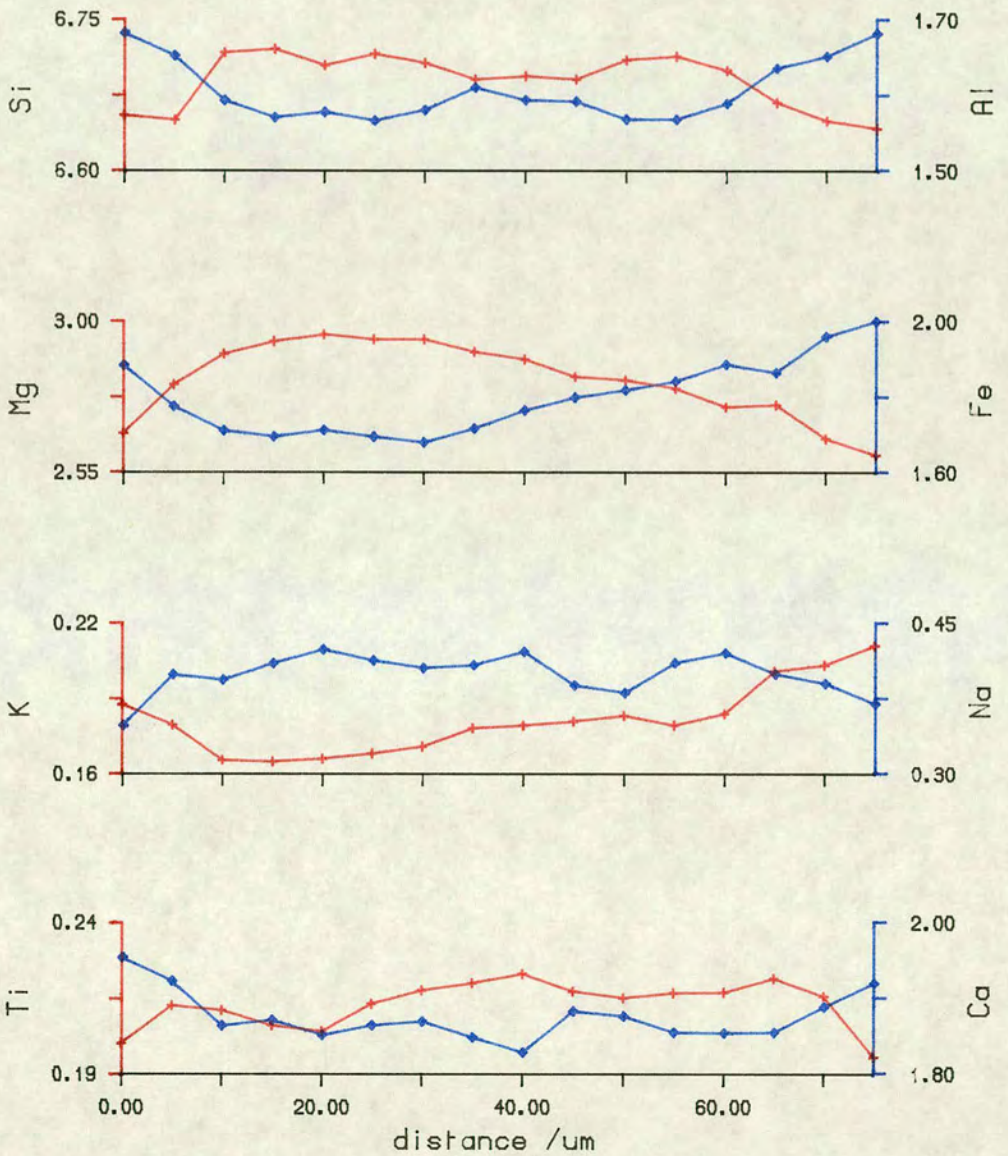


FIGURE 5.12.

(a) B.S.E. image of the altered amphibole crystal used to investigate trace/rare-earth element variations across secondary/original amphibole interfaces.

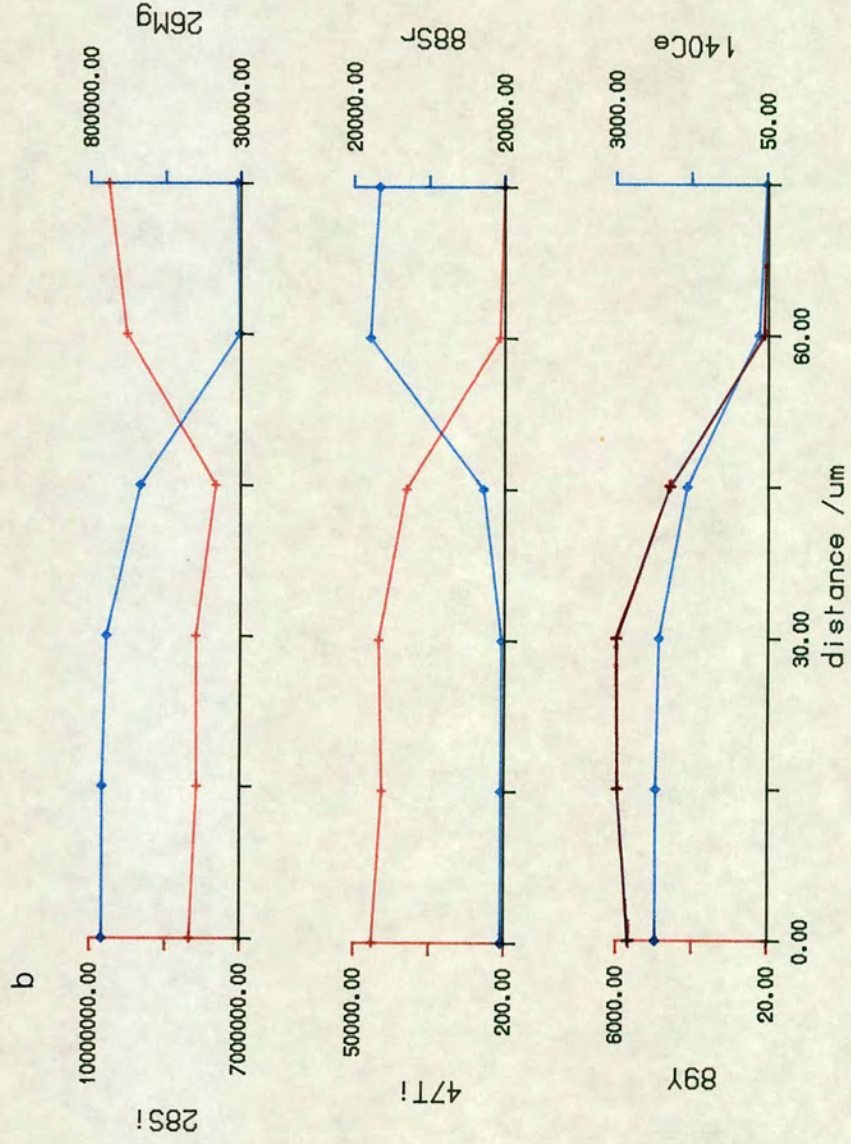
The "burn" line marks the position of both the electron and ion microprobe traverses within the amphibole; a dashed white line marks the continuation of the traverse into the feldspar.

(b) Elemental variations from original to secondary amphibole as measured on the ion microprobe (discussed in text).

KEY: Red curve/crosses correspond to the element plotted on the red axis.

Blue curve/diamonds correspond to the element plotted on the blue axis.

Step intervals $\sim 15\mu\text{m}$.



Counts of ^{26}Mg , ^{28}Si , ^{47}Ti , ^{88}Sr , ^{89}Y and ^{140}Ce were measured. Isotopes of Mg, Si and Ti were specifically detected to enable a direct comparison to be made with the pre-existing electron-microprobe profiles. This allowed the relative sensitivity (or lack of sensitivity!) of each technique to be assessed. One of the profiles obtained is presented in Figure 5.12b. The profiles are flat except where the interface between amphibole and plagioclase is intersected. At first inspection the interface might be interpreted as being a composition profile of the type expected. In reality the gradually curving profiles predominantly reflect the incrementally increasing incorporations of ions emitted from the adjacent phase. With each successive step toward and across the amphibole/plagioclase interface the beam produces ionic emissions representative of initially 100% amphibole then amphibole/plagioclase mixtures and ultimately 100% plagioclase. Any true marginal trace/rare-earth-element chemical variation present is therefore either obscured by these beam-overlap complexities or has not been detected (due to the reduced sensitivity of the apparatus). The electron-microprobe profiles suggest that some chemical variation should be present over a 30–40 μm . wide region toward the edge of the crystal examined. Since no such variation is detectable within the ion-probe profiles, in either major or trace element isotopes, it is assumed that the zonations concerned are too subtle and are not showing against the major effect of changing amphibole to plagioclase ratio at the beam sizes concerned.

(iii) SPOT ANALYSES OF DIFFERENT AMPHIBOLE CHEMISTRIES.

Since the combined analytical sensitivity and spatial resolutions obtained in the step-scans was too poor for the scale of the chemical zonations, single spot analyses of each amphibole chemistry were performed using normal beam-sizes of c.30 μm . Using a B.S.E. image to accurately locate the spot positions, analyses of original and secondary hornblende occurring within a single crystal were obtained, these are presented in Table 5.4. With the exception of Rb and Ce both secondary hornblende and actinolite are depleted in rare-earth-elements with respect to the original hornblende. The Rb^{and}Ce concentrations are more unusual; Rb increases from 2.49ppm within the original hornblende to 2.69ppm in the secondary hornblende, falling to 0.73ppm within the actinolite. A similar pattern is seen with Ce which increases from 3.60ppm within the original hornblende to 31.9ppm in the secondary hornblende, falling to 4.21ppm in the actinolite.

TABLE 5.4 RARE-EARTH-ELEMENT CONCENTRATIONS WITHIN THE DIFFERENT AMPHIBOLE CHEMISTRIES.

ELEM	MASS	ORIGINAL ⁱ	SECONDARY ⁱⁱ	ACTIN ⁱⁱⁱ
Rb	85	2.49	2.62	0.73
Sr	88	78.20	71.70	16.50
Y	89	9.22	6.38	4.90
Zr	90	38.40	35.60	10.80
Ba	138	193.00	156.00	8.37
Ce	140	3.60	31.90	4.21
Nd	142	14.40	12.30	3.40
Sm	152	3.00	1.30	1.30

Conversion of raw counts to ppm. made using
Edinburgh Ion Probe Software

ⁱ Weight/ppm relative to 43% SiO₂

ⁱⁱ Weight/ppm relative to 48% SiO₂

ⁱⁱⁱ Weight/ppm relative to 53% SiO₂

(iv) ION IMAGING

This was performed in order to investigate to what extent variations in trace elements could be imaged, thereby obtaining information on their relative spatial distributions. The small, triangular-shaped, secondary magnesio-hornblende patch discussed in 5.1.1(iiia) was selected as an ideal area upon which trace/rare-earth-element imaging could be performed. The major/minor elemental profiles, presented previously (Figure 5.5), indicate that a quite large difference in chemistry exists between hornblende host and secondary amphibole (*i.e.* 45-48wt% SiO₂; 12-14wt% MgO; 1.3-0.9wt% TiO₂ *etc.*). It was hoped that similarly large variations in trace/rare-earth-elements were also present in sufficiently large concentrations to be imaged using one of Edinburgh Universities Ion Probe imaging facilities (see chapter 3).

Dr R. Hinton (Edinburgh University) assisted in the running of both the Scanning Ion Beam Unit and R.A.E. imagers. The Scanning Ion Beam Unit proved to be insufficiently sensitive to the variations in relative abundances of a range of different major and trace-element concentrations within the host and secondary amphiboles. The differences in the relative Ti, K and Ba concentrations of the original and secondary amphiboles were just about visible on images obtained using the R.A.E. attachment. These images are presented in Plate 52. The R.A.E. could not distinguish the relative concentrations of elements present in lower concentrations (*e.g.* Sr, see Plate 52) between the original and secondary chemistries.

(v) SUMMARY OF ION PROBE ANALYSIS

Ion microprobe analyses reveal that both secondary hornblende and actinolite are depleted in ^{some} trace-elements (not Rb/Ce) with respect to the host hornblende. The fluid(s) from which the secondary hornblende and/or actinolite nucleated must, except for Rb/Ce, have had lower rare-earth concentrations than those of the original hornblende. Since secondary hornblendes and actinolites have different rare-earth-element concentrations they may either have been derived from different fluids or reflect differences in the partition coefficients of rare-earth-elements within different amphibole compositions.

PLATE 52: ION PROBE IMAGES.

(a) R.A.E. image of the relative Ti concentration differences between original/host hornblende and secondary magnesio-hornblende rich, triangular shaped secondary amphibole. Compare this image to the B.S.E. image presented in Figure 5.5a.

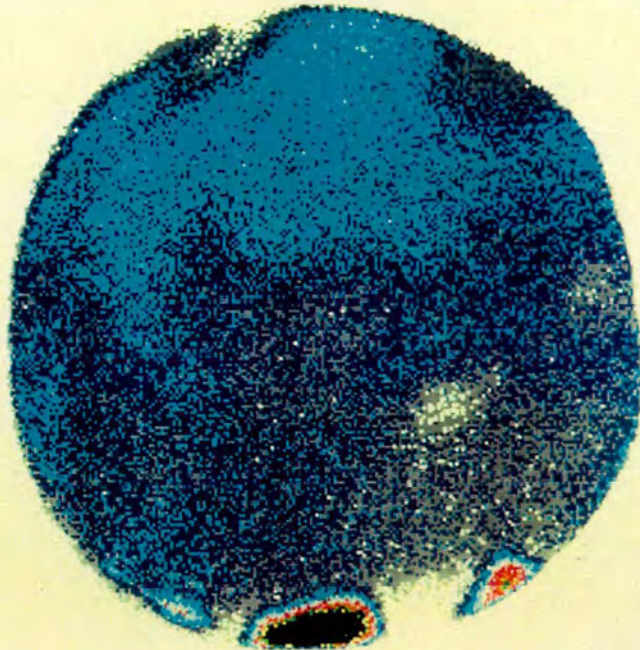
(b) R.A.E. images of the differences in elemental concentrations between host and secondary amphiboles.

Top left to bottom right: Ba, Sr, K, Ti. Note that the R.A.E. can only just distinguish differences in the K, Ti, and Ba concentrations. Sr variations (and other elements present in equally low levels) are not discernable.

a



\RAE\
KPTIH2
2 bytes

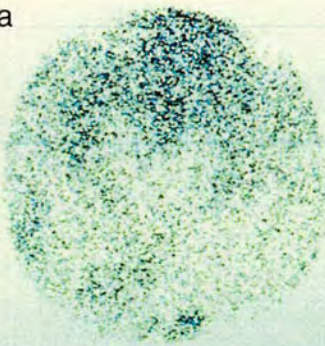


b



\RAE\
KPBH2
1 byte

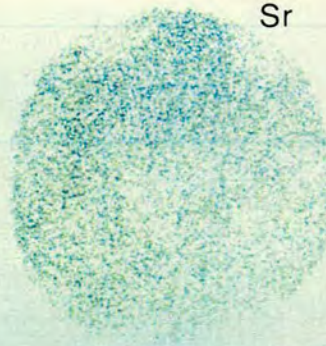
Ba



Sr

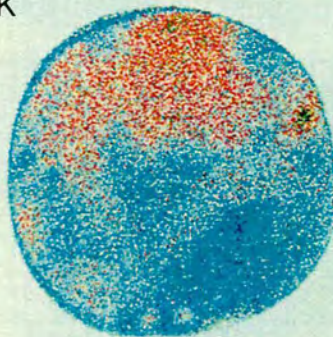


\RAE\
KPSRH2
1 byte



\RAE\
KPKH2
1 byte

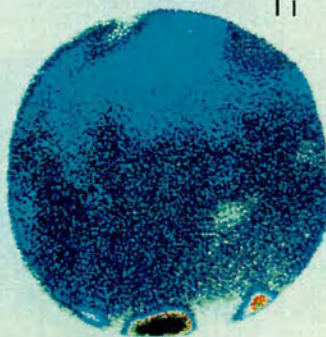
K



Ti



\RAE\
KPTIH2
2 bytes



5.2. FELDSPAR , PYROXENE AND BIOTITE CHEMISTRY

5.2.1. FELDSPAR CHEMISTRY

The plagioclase feldspars within the amphibolites were briefly investigated using both B.S.E. imagery and electron microprobe analysis. B.S.E. images of feldspar crystals occurring within rocks originating throughout the area sampled were studied but not in the intricate detail in which the amphibole alteration types were characterised. Individual crystals that were examined in detail are considered (from evidence of both optical and geochemical studies made) to be representative of those present within the rocks.

The plagioclase feldspar crystals examined within the rocks as a whole were found to have a range of compositions varying from labradorite to albite. Spot analyses of unaltered plagioclase crystals within both pristine and less pristine areas of the rocks are commonly andesine in composition (Table 5.5). Closely spaced electron microprobe traverses across, and point analyses within, several predominantly unaltered crystals within the more pristine parts of the rocks indicate that at least some of the feldspars are subtly zoned, with slightly more anorthite-rich rims. An example of the typical pattern observed is displayed in Figure 5.13. Only a small minority of crystals were examined in such detail; the extent of these zonations within the rocks as a whole is uncertain. B.S.E. images of pristine plagioclase grains are a constant, very pale shade of grey (Plate 53a,b): the subtle chemical zonations detected in the detailed electron microprobe studies have not been identified in B.S.E. images.

B.S.E. images of individual plagioclase crystals falling within the less pristine areas of the rock are clearly heterogeneous, being composed of both pale-grey shades similar to those described above and regions of a slightly darker grey. Chemically the darker grey regions correspond to albitic compositions (Table 5.5). These albitised areas were most commonly seen as patches along grain-edges or adjacent to intracrystalline cracks, an example of this type of image is displayed in Plate 53. In a few specific rocks (*e.g.* ELD19) a proportion of the plagioclase crystals exhibit an unusual "streaky" albitisation pattern (Plate 54a). These patterns are believed to correspond to intracrystalline "microveins" seen within the optical studies made.

Several particularly detailed studies of amphibole-feldspar interfaces were performed in addition to those described in section 5.1.1.(iia). Both the B.S.E.

and analytical facilities available on Edinburgh Universities Cameca Microprobe were used in an integrated approach to establish if any chemical pattern existed between altered/unaltered amphibole/plagioclase interfaces. Though altered patches were often distinguishable in both phases there was no apparent correlation between the two; an altered amphibole edge did not necessarily coincide with either an albitic plagioclase patch or a more calcic plagioclase composition. Plate 53c,d presents two images; 53c highlights the presence of patchy albitic alteration within the plagioclase, 53d reveals the unzoned nature of the adjacent amphibole.

The optically identified "epidotisation" of some plagioclase crystals within the rocks was confirmed in a geochemical study performed on a specific sample (E52). Spot analyses were obtained from several of the irregular, 'aggregate masses' described in section 4.1.3. Individual aggregates were found to have a range of slightly varying compositions; a selection of the different chemistries detected are displayed in Table 5.6. A B.S.E. image of an epidote aggregate is presented in Plate 54b.

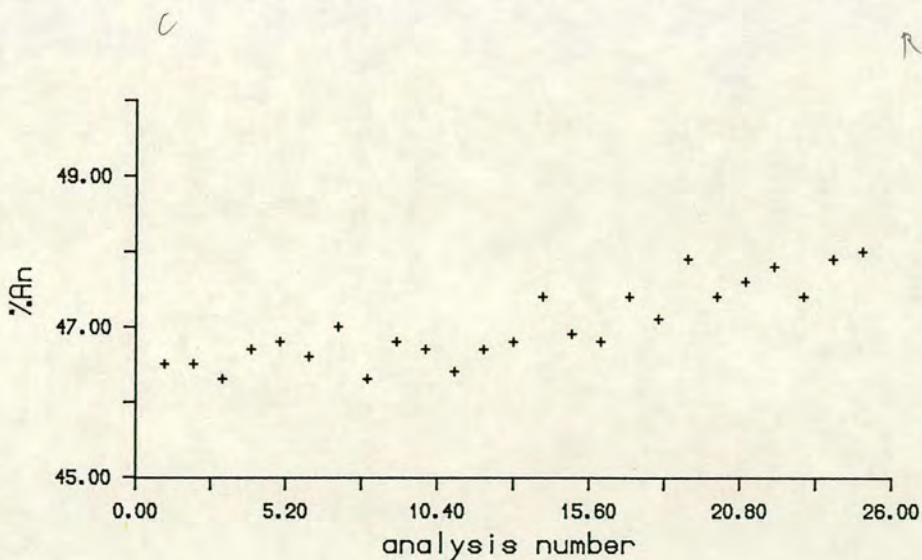


FIGURE 5.13. Plot of plagioclase anorthite content (%) versus distance from core to rim of a zoned plagioclase feldspar crystal. Spacing between analyses $\sim 2\mu\text{m}$.

TABLE 5.5 PLAGIOCLASE FELDSPAR COMPOSITIONS

OXIDE	9m.	15m. ⁱ	15m. ⁱⁱ	15m. ⁱⁱⁱ	2800m.
SiO ₂	55.993	55.208	54.825	57.316	57.226
Al ₂ O ₃	27.728	27.596	27.690	26.523	26.392
MgO	0.046	0.033	0.030	0.022	0.017
FeO	0.331	0.277	0.423	0.256	0.120
CaO	9.585	10.021	10.246	8.586	8.832
K ₂ O	0.123	0.214	0.090	0.160	0.143
Na ₂ O	5.957	5.984	5.935	6.761	6.543
TOTAL	99.807	99.366	99.353	99.684	99.327
Si	2.523	2.507	2.494	2.580	2.586
Al	1.473	1.477	1.484	1.407	1.406
Mg	0.003	0.002	0.002	0.001	0.001
Fe	0.012	0.011	0.016	0.010	0.002
Ca	0.463	0.487	0.499	0.414	0.426
K	0.007	0.012	0.010	0.160	0.008
Na	0.520	0.527	0.523	0.590	0.573
SUMCAT	5.001	5.023	5.028	5.000	5.002
AN	0.467	0.475	0.484	0.409	0.423
AB	0.526	0.513	0.507	0.582	0.569
OR	0.007	0.012	0.010	0.009	0.008

Recalculated on the basis of 8 oxygens using
Edinburgh Microprobe Unit Software

- ⁱ Core composition
ⁱⁱ Rim composition
ⁱⁱⁱ Secondary albitic alteration

PLATE 53: FELDSPAR B.S.E. IMAGES.

(a) and (b) B.S.E. images of pristine plagioclase crystals (F), amphibole (A) and "opaque" grain (O). The feldspar is a uniform shade of grey.

Scale bars: 100 μ m. (E52).

(c) B.S.E. image of an altered plagioclase crystal. Darker grey patches of more albitic feldspar (arrows) occur within the feldspar.

Scale bar: 15 μ m. (ELD19).

(d) B.S.E. image as (c) but with the contrast on the amphibole (A); feldspar (F) now black. Note that there are no zones at the margins of the amphibole crystal which coincide with the albitised feldspar seen in (c).

Scale bar: 15 μ m. (ELD19).

PLATE 53

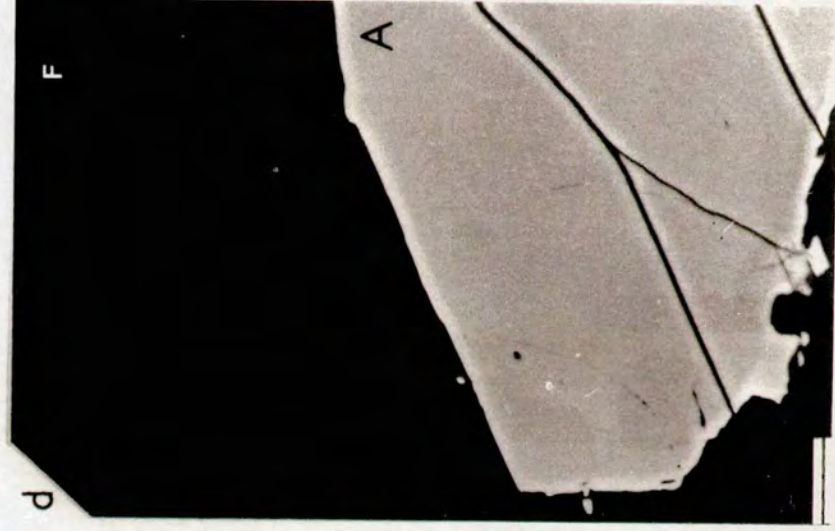
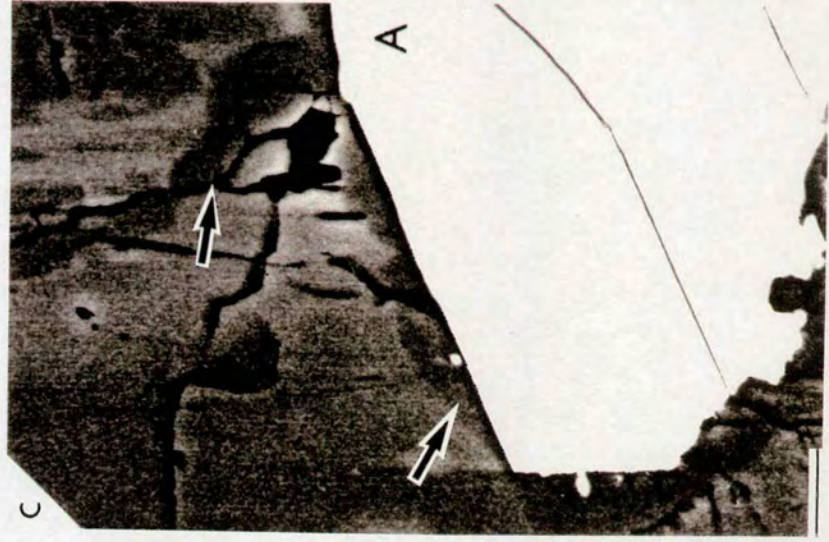


PLATE 54: B.S.E. IMAGES.

(a) B.S.E. image of 'streaky' albitisation pattern identified within some altered plagioclase crystals (arrows). Amphibole (A).

Scale bar: 40 μ m. (ELD19).

(b) B.S.E. image of amorphous epidote aggregates (E) nucleating at the interface between amphibole (A) and feldspar (F). Note the amphibole has been altered to a dark-grey-black colour (arrow).

Scale bar: 30 μ m. (E52).

(c) High-magnification B.S.E. image of an altered clinopyroxene (CPX) crystal. Small darker-grey patches (arrowed 1) correspond to sites at which amphibole neomineralisation has occurred.

Scale bar: 100 μ m. (E5).

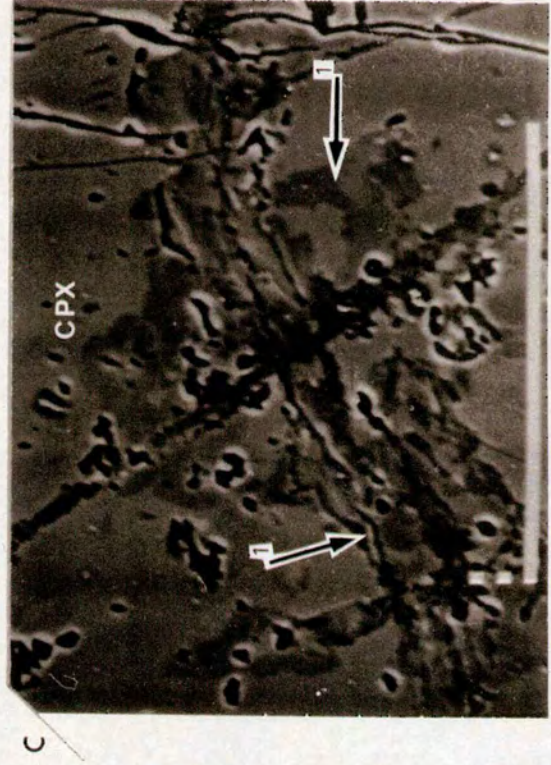
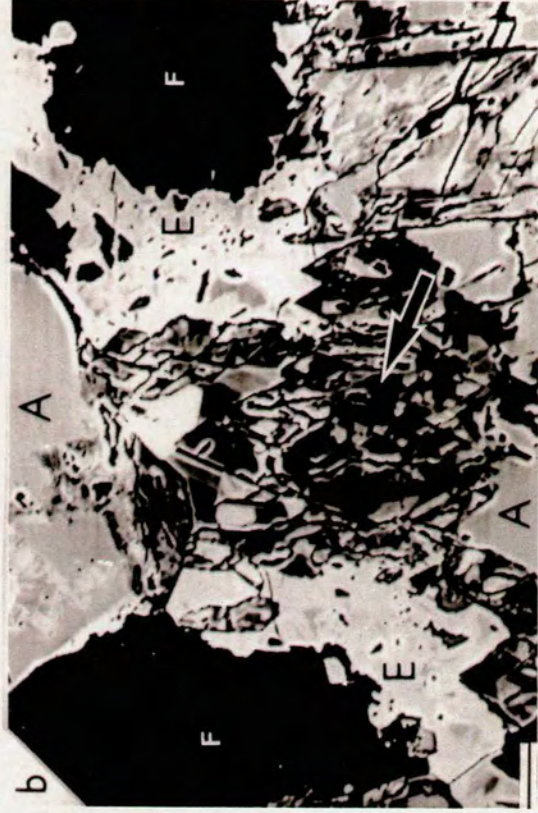


TABLE 5.6 "EPIDOTE" MINERAL COMPOSITIONS

OXIDE	E52				
SiO ₂	37.884	37.608	37.912	38.068	37.873
Al ₂ O ₃	23.520	22.955	23.564	25.104	24.244
MgO	0.048	0.088	0.085	0.053	0.041
FeO	11.396	11.685	11.261	9.499	10.623
TiO ₂	0.152	0.402	0.113	0.340	0.112
MnO	0.323	0.172	0.226	0.098	0.316
Cr ₂ O ₃	0.028	0.028	0.086	0.034	0.009
CaO	23.029	23.260	23.238	23.512	23.239
K ₂ O	0.014	0.013	0.002	0.018	0.012
Na ₂ O	0.032	0.020	0.022	0.000	0.019
F	0.000	0.030	0.000	0.000	0.000
OH	3.507	3.490	3.512	3.557	3.524
TOTAL	99.934	99.751	100.020	100.284	100.012
Si	3.236	3.228	3.234	3.205	3.219
Al	2.368	2.322	2.369	2.491	2.429
Mg	0.006	0.011	0.011	0.007	0.005
Fe	0.814	0.839	0.803	0.669	0.755
Ti	0.010	0.026	0.007	0.022	0.007
Mn	0.023	0.012	0.016	0.007	0.023
Cr	0.002	0.002	0.006	0.002	0.001
Ca	2.107	2.139	2.124	2.121	2.117
K	0.002	0.001	0.000	0.002	0.001
Na	0.005	0.003	0.004	0.000	0.003
F	0.000	0.008	0.000	0.000	0.000
OH	1.000	1.000	1.000	1.000	1.000
SUMCAT	9.573	9.593	9.573	9.526	9.560

Recalculated on the hydrous basis of 13 oxygens using
Edinburgh Microprobe Unit Software.

5.2.2. PYROXENE CHEMISTRY

Pyroxene crystals within pristine regions of the rock were chemically examined by spot analysis using the electron microprobe. Compositionally the pyroxenes fall within the 'Salite' field of the clinopyroxene series. Core and rim analyses obtained from individual crystals indicate the presence of a slight compositional zonation. Representative analyses of the compositions detected within the cores and rims of individual crystals are presented in Table 5.7. B.S.E. images obtained from several of the most pristine crystals confirms the presence of very fine scale exsolution lamellae; individual lamellae are $<1\mu\text{m}$. in width, too narrow to be analysed using the electron probe.

Pyroxene crystals falling within the less pristine areas of the rock retain salitic compositions but are variably neomineralised to actinolite (deep-blue-green coloured amphibole crystals of thin-section descriptions). A representative analysis of the actinolitic amphibole composition is displayed in Table 5.7. B.S.E images highlight the rather patchy nature of the actinolitic neomineralisation, one such image is presented in Plate 54c.

5.2.3. BIOTITE CHEMISTRY

Electron microprobe investigations of biotite micas within the Biotite Amphibolites were undertaken. Un-chloritised crystals within rocks both close to, and at greater distances from, the Stock contact were found to be chemically homogeneous and as a consequence few further analyses were made. A selection of the analyses that were obtained are presented in Table 5.8. Secondary chloritisation of the biotites was confirmed using E.D.S. spectrometry.

TABLE 5.7 PYROXENE COMPOSITIONS

OXIDE	2m.	15m. ⁱ	15m. ⁱⁱ	15m. ⁱⁱⁱ	663m.
SiO ₂	51.105	51.834	52.230	54.015	51.539
Al ₂ O ₃	1.776	1.833	1.513	1.495	2.288
MgO	14.258	12.830	13.111	15.639	12.011
FeO	7.356	9.182	8.986	12.529	9.596
TiO ₂	0.040	0.153	0.153	0.033	0.222
MnO	0.474	0.382	0.386	0.505	0.447
Cr ₂ O ₃	0.010	0.041	0.039	0.000	0.004
CaO	24.066	23.162	23.099	13.006	22.926
K ₂ O	0.022	0.000	0.000	0.082	0.010
Na ₂ O	0.286	0.480	0.372	0.166	0.492
TOTAL	99.393	99.989	99.891	97.507	99.535
Si	1.925	1.949	1.960	7.809	1.947
Al	0.079	0.081	0.067	0.255	0.102
Mg	0.800	0.719	0.733	3.370	0.676
Fe	0.232	0.289	0.282	1.515	0.303
Ti	0.001	0.004	0.004	0.004	0.006
Mn	0.015	0.012	0.012	0.062	0.014
Cr	0.000	0.001	0.001	0.000	0.000
Ca	0.971	0.933	0.929	2.014	0.928
K	0.001	0.000	0.000	0.015	0.000
Na	0.021	0.035	0.027	0.046	0.036
SUMCAT	4.045	4.023	4.015	15.090	4.012
WO	0.481	0.478	0.475		0.483
EN	0.397	0.368	0.375		0.352
FS	0.122	0.154	0.150		0.165

Recalculated on the basis of 6 oxygens using
Edinburgh Microprobe Software.

ⁱ Core composition

ⁱⁱ Rim composition

ⁱⁱⁱ Secondary actinolitic alteration (recalculated to 23 oxy.)

TABLE 5.8 BIOTITE COMPOSITIONS

OXIDE	9m.	27m.	35m.	2440m.	3863m.
SiO ₂	36.219	36.945	38.111	37.734	37.308
Al ₂ O ₃	14.447	13.489	14.367	14.700	15.067
MgO	11.758	12.597	14.689	16.677	13.673
FeO	18.535	16.861	15.218	12.473	15.784
TiO ₂	3.902	4.012	2.569	3.056	3.760
MnO	0.343	0.226	0.438	0.101	0.151
Cr ₂ O ₃	0.047	0.041	0.028	0.022	0.000
CaO	0.011	0.003	0.006	0.000	0.004
K ₂ O	9.298	9.531	9.237	8.965	9.002
Na ₂ O	0.090	0.113	0.067	0.224	0.171
F	0.257	0.709	0.567	1.466	0.969
TOTAL	94.907	94.525	95.296	95.417	95.889
Si	5.562	5.680	5.656	5.632	5.601
Al	2.615	2.444	2.513	2.586	2.666
Mg	2.691	2.887	3.248	3.710	3.060
Fe	2.380	2.168	1.888	1.557	1.982
Ti	0.451	0.464	0.287	0.343	0.424
Mn	0.045	0.029	0.055	0.013	0.019
Cr	0.006	0.005	0.003	0.003	0.000
Ca	0.002	0.000	0.009	0.000	0.001
K	1.822	1.869	1.749	1.707	1.724
Na	0.027	0.034	0.027	0.065	0.050
F	0.125	0.345	0.266	0.692	0.460
SUMCAT	15.725	15.926	15.685	16.307	15.987

Recalculated on the anhydrous basis of 22 oxygens using
Edinburgh Microprobe Software.

5.3. SUMMARY OF CHEMICAL DATA

The mineral alterations investigated reflect retrogressions from original amphibolite towards greenschist facies assemblages. Original ferroan-pargasitic-hornblendes are chemically altered to secondary edenitic-hornblendes, edenites, magnesio-hornblendes, actinolitic hornblendes and actinolites; plagioclase feldspars are patchily albitised and epidotised; pyroxene crystals are neomineralised to actinolite and chlorite, and biotite is chloritised.

Original, unaltered hornblende within both pristine and less pristine regions of the amphibolitic rocks have very similar chemistries (Table 5.1) suggesting that a regional equilibrium was once achieved. Secondary amphibole with compositions ranging from edenitic-hornblendes to actinolites (Tables 5.2-5.3) have been documented throughout the sample area.

The development of patches of secondary amphibole, located adjacent to original amphibole grain-boundaries have been shown to:

- (i) Bear no relation to the mineralogical nature of the adjacent phase.
- (ii) Bear no relation to strain or compositional features of the grain(s) undergoing replacement.
- (iii) Be unrelated to triple junctions.
- (iv) Be unrelated to the rocks distance from the intrusive contact.

Chapter 4 outlined the presence of distinct alteration zones (microfracture networks and permeation zones) within the rocks to which all the mineral alterations can be related. Since the presence of secondary amphibole does not appear to be dependent upon the nature of the adjacent phase its development must be controlled by the relative tightness of the grain-boundaries and the accessibility of fluids to certain grains. Boundary and some Microvein amphibole alterations both represent situations in which alteration has taken place adjacent to cracks, grain-boundaries and other pre-existing weakness within the original crystals. Other Microveins and the Extensive single and multi-crystal alterations represent the effects of the intrusion of a greater volume of fluids into the rocks.

Boundary amphibole alterations occurring within permeation zones (both border and independent types) *and* adjacent to microfracture networks, are predominantly composed of abruptly bounded secondary hornblendes (edenitic to magnesio-hornblendes). Where actinolitic hornblende and actinolite compositions are encountered these can usually be identified, using B.S.E.

imagery, as a younger alteration event (section 5.1.4). Gradual-type secondary hornblende alterations (section 5.1.3 and 5.1.4) are thought to represent original, abruptly bounded alterations which have suffered diffusive modification during a later event.

Microvein, Extensive single crystal *and* Extensive multi-crystal amphibole alterations are usually composed of abruptly bounded secondary actinolitic hornblendes and actinolites.

The abrupt interfaces between both original hornblendes and secondary hornblendes, and original hornblendes and secondary actinolites (section 5.17) are considered to be a consequence of the mechanism(s) by which alteration took place (*i.e.* overgrowths/replacements/dissolution *etc.*) and do not necessarily imply the presence of miscibility gaps within the hornblende series'. The original and secondary amphiboles do not represent an equilibrium assemblage; the secondary hornblendes and actinolites were probably derived from different fluids whose compositions evolved over time.

Combining the optical and geochemical conclusions of sections 4.4 and sections 5.1.2-5.1.5. it is likely that most of the secondary hornblendes formed during PreCambrian events and most of the actinolites developed during the Laramide orogeny.

5.4. THERMOBAROMETRY AND DIFFUSION CALCULATIONS

5.4.1. THERMOBAROMETRY

The geobarometers derived by Hammarstrom and Zen (1986), Hollister *et.al.* (1987) and Johnson and Rutherford (1989) (outlined in some detail in chapter 2) have each been used in attempts to constrain the pressures at which both original and secondary hornblende and actinolite were formed; the results are displayed in the following table.

		HAMMARSTROM & ZEN PRESSURE \pm 3kb	HOLLISTER ET.AL. PRESSURE \pm 1kb	JOHNSON & RUTHERFORD PRESSURE \pm 0.5kb
ORIG.HBDE ¹	1.88	5.5kb	5.8kb	4.5kb
SEC.HBDE ²	1.52	3.7kb	3.8kb	3.0kb
ACTIN. ³	0.33	-2.3kb	-2.9kb	-2.1kb

¹ ORIGINAL HORNBLLENDE

² SECONDARY HORNBLLENDE

³ ACTINOLITE

Considering the geobarometers are specifically stated as being strictly applicable to calc-alkaline rocks only, the estimates obtained should be regarded with caution. Since actinolite is not one of the stipulated phases (see chapter 2) the negative pressures obtained are a reflection that the geobarometer is unsuitable for use with such compositions.

Blundy and Holland's (1990) thermometer (again refer to chapter 2) is stated as being applicable to rocks from greenschist to granulite facies; being sensitive to hornblende-plagioclase equilibration temperatures $\pm 75^\circ\text{C}$. A prerequisite of this method is the knowledge of whether original/secondary hornblende or actinolite is in equilibrium with either unaltered or albitised plagioclase. Since this has not been fully established with certainty the temperatures at which each amphibole is in equilibrium with both unaltered and albitised plagioclase compositions have been determined; these are presented in the following table.

	X_{Ab}	Si	P	$T \pm 75^\circ\text{C}$
with more calcic plag.				
ORIG.HBDE ¹	0.51	6.52	3-6kb	852-803°C
SEC.HBDE ²	0.51	6.88	3-6kb	767-722°C
ACTIN. ³	0.51	7.74	0-6kb	550-483°C
with more sodic plag.				
ORIG.HBDE ¹	0.58	6.52	3-6kb	825-778°C
SEC.HBDE ²	0.58	6.88	3-6kb	744-701°C
ACTIN. ³	0.58	7.74	0-6kb	554-469°C

¹ ORIGINAL HORNBLLENDE

² SECONDARY HORNBLLENDE

³ ACTINOLITE

Assuming plagioclase ideality (since $X_{Ab} > 0.5$) and pressures between 0 and 6kb (agreeing with both reasonable estimates in the literature and the barometric results obtained above), equilibration temperatures were found to vary between 469° and 852°C. The lowest temperatures obtained correspond to actinolite in equilibrium with more albitic plagioclase - which seems reasonable. The model is applicable only to amphibole with <7.8 Si atoms p.f.u therefore these temperatures are at the limits to which the thermometer can be expected to generate valid results. It is probably sensible to assume that the unaltered plagioclase was at some point in equilibrium with original hornblende; the results obtained using Blundy and Holland's model (1990) suggest this regional equilibration to correspond to a temperature of *c.*803-852°C.

INTERPRETATION

The different temperatures obtained *may* be interpreted as suggesting three different temperature events:

- 1: Regional equilibration 803-852°C.
Original hornblende in equilibrium with unaltered plagioclase (Ab_{51}).
- 2: PreCambrian event 701-767°C.
Secondary hornblendes in equilibrium with altered/unaltered[?] plagioclase.
- 3: Laramide event 469-554°C.
Actinolite in equilibrium with altered plagioclase.

The temperatures obtained appear to confirm the theory that at least two alteration events have affected the amphibolites (evidence of which was presented in sections 4.4 and 5.1.4). It should be noted at this point that actinolic microveins, forming parts of microfracture networks, are often bordered by haloes within which original hornblendes are altered to secondary hornblendes of Boundary types (see section 4.3.1). In many cases the actinolite

microveins and the secondary hornblendes associated with the microfracture networks have not been conclusively tied to either Laramide or PreCambrian events (see sections 4.4 and 5.1.5.). Whatever the age of the alterations within and adjacent to individual microfracture networks, it is clear that both secondary hornblendes and actinolites, in at least in some cases, may have formed during the same event. It has been quite clearly shown that the border permeation zones are PreCambrian (see sections 4.4 and 5.1.5) so the temperature 701-767°C, may represent the temperature interval over which migmatization took place. Most of the actinolitic alteration adjacent to the contact has been linked with Laramide metasomatism (see sections 4.4, 5.1.4., 5.1.5.), the temperatures calculated above suggest this took place at 469-554°C.

5.4.2. DIFFUSION CALCULATIONS AND CURVE FITTING

Using the relationship $x^2=Dt$ (outlined in chapter 2) it is possible to derive approximate values of D for both abrupt and gradual-type amphibole alteration events.

If the interface between original and secondary amphiboles is taken as being ~2µm. and diffusive exchange continued to the present day *

- 1: for any alteration resulting from a c.60my (Laramide) event

$$D \approx 2.1 \times 10^{-23} \text{cm}^2 \text{s}^{-1}$$

- 2: for alteration caused by a PreCambrian event c.1100my associated with the intrusion of the Pike's Peak Granite

$$D \approx 1.2 \times 10^{-24} \text{cm}^2 \text{s}^{-1}$$

- 3: alteration associated with a PreCambrian event c.1410my

$$D \approx 9.0 \times 10^{-25} \text{cm}^2 \text{s}^{-1}$$

- 4: alterations resulting from a PreCambrian event c.1750my (associated with migmatization)

$$D \approx 7.2 \times 10^{-25} \text{cm}^2 \text{s}^{-1}$$

If diffusive exchange took place for approximately 10my following/during any one of the above events:

$$D \approx 1.3 \times 10^{-22} \text{cm}^2 \text{s}^{-1}$$

If diffusive exchange took place for c.0.5my following/during an event

$$D \approx 2.5 \times 10^{-21} \text{cm}^2 \text{s}^{-1}$$

* 3.1536×10^7 seconds per year.

If the width of the gradual-type alterations is taken as between 20 μm . and 100 μm . and the diffusive exchange took place until the present day:

- 1: Alteration associated with regional metamorphism *c.*1850my
 $D \approx 6.8 \times 10^{-23} \text{cm}^2\text{s}^{-1} - 1.7 \times 10^{-21} \text{cm}^2\text{s}^{-1}$ (20 μm . and 100 μm . respectively)
- 2: Alteration associated with PreCambrian re-heating *c.*1410my resulting from the intrusion of the Silver Plume Granite and causing the re-setting of K-Ar ages
 $D \approx 9.0 \times 10^{-23} - 2.2 \times 10^{-21} \text{cm}^2\text{s}^{-1}$
- 3: Alteration associated with a regional event at *c.*1100my
 $D \approx 1.2 \times 10^{-22} - 2.9 \times 10^{-21} \text{cm}^2\text{s}^{-1}$
- 4: Alteration associated with the 60my event
 $D \approx 2.1 \times 10^{-21} - 5.3 \times 10^{-20} \text{cm}^2\text{s}^{-1}$

If diffusive exchange took place for approximately 10my following/during any one of the above events:

$$D \approx 1.3 \times 10^{-20} \text{cm}^2\text{s}^{-1} - 3.2 \times 10^{-19} \text{cm}^2\text{s}^{-1}$$

If diffusive exchange took place for *c.*0.5my following/during an event

$$D \approx 2.5 \times 10^{-19} \text{cm}^2\text{s}^{-1} - 6.3 \times 10^{-18} \text{cm}^2\text{s}^{-1}$$

FITTING OF GRADUAL-TYPE PROFILES TO LASAGA AND ERROR FUNCTION CURVES

A range of the gradual-type profiles obtained were run through a computer programme written by Mike Matthews (Edinburgh University). This programme fits electron probe generated profiles to both standard error function curves, supplying an estimate of Dt , and Lasaga Curves (see reference and chapter 2). The spacings of most of the electron probe traverses made was typically $\sim 10\mu\text{m}$. (to minimise beam-overlap). Since the widths of the gradual-type profiles averages approximately 40 μm ., few points were obtained which actually fell within the gradient between original and secondary amphibole; as a consequence the fit achieved between the profiles and either Lasaga or isothermal curves was quite poor. In most instances however the fit between the isothermal curves and data provided was superior to that achieved with the Lasaga fit. A representative case is displayed in Figure 5.14. The electron-probe traverse performed was spaced at $\sim 5\mu\text{m}$. intervals and is therefore quite well constrained. The Fe gradients at both margins of the crystal have been modelled; these are displayed in Figure 5.14 (I and II). The values of Dt , and hence D , obtained compare fairly well with those estimated earlier in this section; see below.

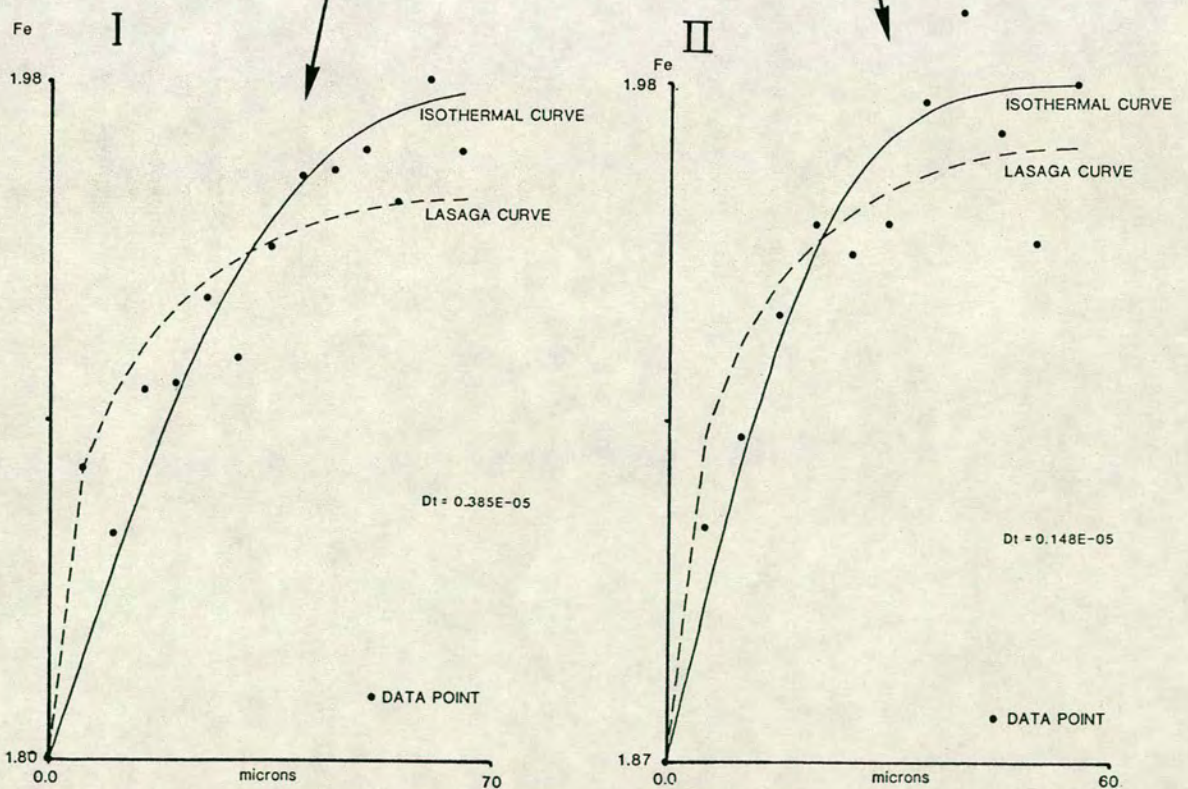
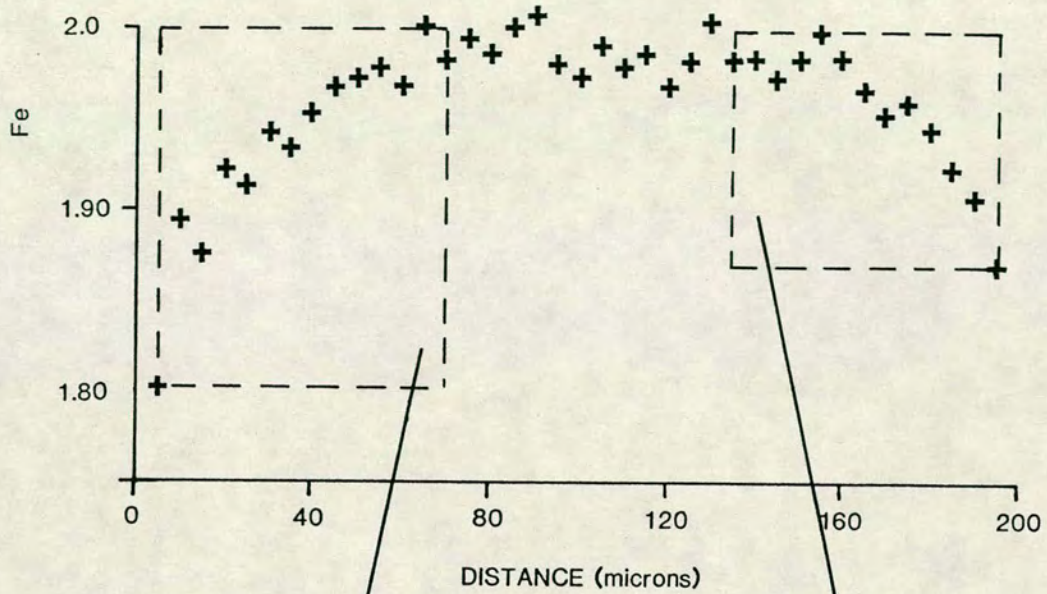


FIG. 5.14. (a) Plot of Fe concentration (in cations) versus distance across an altered amphibole grain. (b) Graphs illustrating the fit of data points indicated in (a) to both Lasaga and isothermal curves.

1: Given $Dt=0.385 \times 10^{-5}$ [$x=70\mu\text{m}$. (Figure 5.14 (I))

assuming diffusive exchange continued until the present day:

- | | |
|--------------------------|--|
| (a) If $t=1850\text{my}$ | $D \sim 6.6 \times 10^{-23} \text{cm}^2 \text{s}^{-1}$ |
| (b) If $t=1750\text{my}$ | $D \sim 7.0 \times 10^{-23} \text{cm}^2 \text{s}^{-1}$ |
| (c) If $t=1410\text{my}$ | $D \sim 8.7 \times 10^{-23} \text{cm}^2 \text{s}^{-1}$ |
| (d) If $t=1100\text{my}$ | $D \sim 1.1 \times 10^{-22} \text{cm}^2 \text{s}^{-1}$ |
| (e) If $t=60\text{my}$ | $D \sim 2.0 \times 10^{-21} \text{cm}^2 \text{s}^{-1}$ |

If diffusive exchange took place for 10my following/during an event:

$$D \sim 1.2 \times 10^{-20} \text{cm}^2 \text{s}^{-1}$$

If diffusive exchange took place for 0.5my following/during an event:

$$D \sim 2.4 \times 10^{-19} \text{cm}^2 \text{s}^{-1}$$

2: Given $Dt=0.148 \times 10^{-5}$ [$x=60\mu\text{m}$.] (Figure 5.14(II))

assuming diffusive exchange continued until the present day:

- | | |
|--------------------------|--|
| (a) If $t=1850\text{my}$ | $D \sim 2.5 \times 10^{-23} \text{cm}^2 \text{s}^{-1}$ |
| (b) If $t=1750\text{my}$ | $D \sim 2.7 \times 10^{-23} \text{cm}^2 \text{s}^{-1}$ |
| (c) If $t=1410\text{my}$ | $D \sim 3.3 \times 10^{-23} \text{cm}^2 \text{s}^{-1}$ |
| (d) If $t=1100\text{my}$ | $D \sim 4.3 \times 10^{-23} \text{cm}^2 \text{s}^{-1}$ |
| (e) If $t=60\text{my}$ | $D \sim 7.8 \times 10^{-22} \text{cm}^2 \text{s}^{-1}$ |

If diffusive exchange took place for 10my following/during an event:

$$D \sim 4.7 \times 10^{-21} \text{cm}^2 \text{s}^{-1}$$

If diffusive exchange took place for 0.5my following/during an event:

$$D \sim 9.4 \times 10^{-20} \text{cm}^2 \text{s}^{-1}$$

INTERPRETATION

The diffusivity values calculated range between approximately 10^{-18} - $10^{-25} \text{cm}^2 \text{s}^{-1}$ depending on the time available for diffusive exchange. These values of D have been calculated irrespective of the temperature(s) of the rocks and thus represent time-integrated values which might involve several changes in temperatures.

Each individual element within a mineral may diffuse at a different rate, and these rates may change with changing temperature, pressure and possible fluid presence of the rocks. The general diffusivity values presented thus only provide very approximate estimates of the possible time-integrated rates at which multi-element diffusion may have occurred. The D values obtained are much slower than those for elements within pyroxenes presented in chapter 2. The pyroxene experiments were however performed at much higher temperatures ($> 1100^\circ\text{C}$) than the sorts of temperatures the Eldora Amphibolites are likely to have experienced ($< 850^\circ\text{C}$; section 5.4.1.).

CHAPTER 6. SUMMARY AND DISCUSSION OF THE OPTICAL AND B.S.E./MICROPROBE INFORMATION OBTAINED ON THE ELDORA AMPHIBOLITES

This chapter presents an overall synopsis of the alteration history of the rocks using a "collation" diagram to bring together the conclusions drawn from the field studies, optical investigations and B.S.E./microprobe analyses of the Eldora amphibolites.

6.1. SUMMARY OF OPTICAL AND B.S.E./MICROPROBE OBSERVATIONS

A summary of the complex inter-relationships between the amphibole alteration types, compositions and chemical boundaries, and their distributions within the Eldora amphibolites is presented in a collation diagram (Figure 6.1). The construction of this diagram is based on the different amphibole alteration types and alteration zone types outlined in chapter four. No attempt has been made to link the amphibole alteration types directly with the alteration zone types in Figure 6.1 since their associations are complex and often inter-related (e.g. Boundary alterations form haloes around microfracture networks as described in section 5.1.5.).

The different types of secondary amphibole alterations, *i.e.* Boundary, Microvein, Extensive single and Extensive multi-crystal types, are described and illustrated in detail in chapter 4 section 4.2.2. These were found to have developed only within and adjacent to definite zones of alteration within the rocks, rather than being generally disseminated through rock matrices over extensive areas. Two principal types of alteration zones: (1) microfracture networks and (2) permeation zones, were identified and these are described in detail in chapter 4 section 4.3.1. Permeation zones were further sub-divided into:

- (i) Border permeation zones - those found adjacent to leucocratic seams.
- (ii) Independent permeation zones - zones which occur independently within the rocks and are not associated with leucocratic seams.

In the collation diagram the principal alteration types and alteration zone types are listed and their association with specific features/field distributions are shown. Amphibole alteration types are indirectly linked to the types of alteration zones via their relative distributions within the amphibolites. The most important correlations to note in Figure 6.1. are the presence of Extensive single and multi-

crystal alterations in rocks which only occur adjacent to the contact and adjacent to mineralised ore shears, and the widespread (*i.e.* regional) distribution of both Boundary and Microvein alterations.

The amphibole alteration types listed in Figure 6.1 are linked with their corresponding mineral compositions as determined from the electron-microprobe analyses described in detail in chapter 5 section 5.1.1.(ii) and summarised in 5.1.2. Boundary amphibole alterations are mostly comprised of secondary hornblendes whilst Microvein, Extensive single and Extensive multi-crystal alterations are almost always actinolites. Section 5.1.5. outlined how the compositions of the secondary amphiboles are related to the types of alteration zones in which they are located. Boundary amphibole alterations (secondary hornblendes) develop in all three types of alteration zones whilst secondary amphibole Microveins (actinolites) predominantly comprise components of microfracture networks. Extensive single and multi-crystal alterations (actinolites) develop in microfracture networks and independent permeation zones *only* in rocks which fall adjacent to the contact or adjacent to ore shears.

The secondary amphiboles investigated were found to have either abrupt or gradual chemical gradients against their host amphiboles; these were described in depth in chapter 5, section 5.1.1.(ii) and summarised in sections 5.1.3. and 5.1.4. The collation diagram shows that the secondary hornblendes have either abrupt or gradual chemical boundaries against their hosts whilst the secondary actinolites always have abrupt boundaries with the original hornblende crystals.

LINKS BETWEEN AMPHIBOLE ALTERATION TYPES, ALTERATION ZONE TYPES AND REGIONAL HISTORY

The distributions of the amphibole alteration types and the alteration zone types within the amphibolites (described in chapter 4 sections 4.3. and 4.4.) suggested that several alteration events have taken place. The widespread areal occurrence of Boundary and some Microvein alterations within microfracture networks and independent permeation zones (see Table 4.1 and Figure 6.1) indicates that a regional event or events may have occurred.

Microfracture networks and independent permeation zones have been widely documented within the rocks (see Table 4.1), however they are particularly well developed in the marginal contact zone and adjacent to mineralised shear zones (chapter 4 section 4.3.2.). Thus in some specific instances (*e.g.* adjacent to the Stock contact) the microfracture networks and

independent permeation zones seem to be Laramide, otherwise they may be either Laramide or PreCambrian in age. PreCambrian mineralisation of the amphibolites was reported by Lovering and Goddard (1950), but its exact age in relation to other PreCambrian events is not known. Microfracture networks within the Eldora Amphibolites are thus believed to have formed in association with both PreCambrian mineralisation and Laramide aged events (see Figure 6.1). The Laramide microfractures formed in association with both Stock emplacement/crystallisation and later, localised mineralisation episodes (see chapter 4 section 4.4.); a strong correlation between microfracture networks, abruptly bounded actinolites and Laramide aged events is shown in Figure 6.1.

Independent permeation zones have been particularly difficult to constrain in terms of their possible age. Their association with a high percentage of ore minerals and abruptly bounded secondary amphibole compositions suggests that they also developed during a mineralisation event. It is not known whether the mineralisation event which created the independent permeation zones was PreCambrian or Laramide in age. Given that the microfracture networks are believed to have formed during both Laramide and PreCambrian mineralisation events, it is most likely that the independent permeation zones also formed during both episodes.

Border permeation zones are observed at distances between 0-3.5km. from the Stock contact (see Table 4.1), thus they have been related to a regional metamorphic origin in Figure 6.1. Their development is believed to be related to the intrusion and/or crystallisation of material constituting the Leucocratic seams within the rocks (chapter 4 section 4.4). Border permeation zones are clearly migmatite related and are therefore PreCambrian (1750my). Some of the abruptly bounded secondary hornblendes formed during migmatisation and thus a strong correlation between the migmatisation event and abrupt secondary hornblendes is indicated in Figure 6.1. Gradually bounded secondary hornblendes probably formed during migmatisation and their contacts with the original amphibole crystals were modified during younger reheating and/or mineralisation events, as depicted in Figure 6.1.

Extensive single and Extensive multi-crystal alterations have been documented *only* within microfracture networks and independent permeation zones which occur either within 2m. of the contact, or adjacent to mineralised ore shears (see chapter 4 section 4.3., Table 4.1, section 4.4. and Figure 6.1).

Extensive single and multi-crystal alterations have not been observed within the border permeation zones.

Strong geochemical evidence was presented in chapter 5 (sections 5.1.3., 5.1.4.) showing that amphiboles with abrupt chemical boundaries formed during at least two events:

- (i) An initial abruptly bounded secondary hornblende formation event.
- (ii) A later abruptly bounded secondary actinolite forming event.

The gradually bounded secondary hornblende alterations are considered to represent initially abruptly bounded alterations which formed during event (i) above and were modified during later events.

Secondary amphibole compositions and types are indirectly linked with the regional history via their chemical gradients against their host crystals. Sharply bounded actinolites mostly formed in association with Laramide aged events (though a minority may have developed during PreCambrian mineralisation). Secondary hornblendes mostly developed during PreCambrian migmatization though younger secondary hornblende formation cannot be entirely discounted (see discussion in section 5.4.1.).

The temperatures at which the original and secondary hornblendes and actinolites formed are shown in the flow chart and discussed in more detail in chapter 5 section 5.4.1. Although the temperatures obtained are a simplification of the true alteration history (for reasons explained in section 5.4.1.) they do seem to agree with the multi-event picture already established from both the optical and chemical data described in the preceding chapters.

6.2. CONCLUSIONS

From the conclusions and interpretations made in sections 4.4., 5.1.2.-5.1.5. and discussions in the preceding section of this chapter it has been shown that the Eldora secondary amphiboles developed, with particular distributions and compositions, in association with at least three different events, as follows:

- (i) Secondary amphiboles which developed within Border permeation zones during PreCambrian migmatization are mostly hornblendic in composition and occur as Boundary type amphibole alterations.

- (ii) Secondary amphiboles which formed in association with PreCambrian mineralisation are both hornblendic and actinolitic in composition. The secondary hornblendes are mostly abruptly bounded Boundary type alterations, the actinolites are mostly seen as Microveins.
- (iii) Secondary amphiboles which formed during Laramide events are predominantly actinolitic in composition. These are seen as Microveins and Extensive single and multi-crystal alterations within/upon original hornblende grains.

Estimating the amounts of secondary amphibole which formed in association with these three events is difficult because where they overprint one another particular ages of formation of different crystals cannot be readily and widely assessed. It is particularly difficult to distinguish PreCambrian and Laramide mineralisation events, but emphasis is placed on Laramide events in Figure 6.1 because these may be seen in the igneous body and are most clearly documented in the literature. The bold lines in the collation diagram illustrated in Figure 6.1. therefore emphasise the PreCambrian migmatisation and Laramide mineralisation events as the major factors affecting amphibole alteration. In general the bold lines in Figure 6.1. represent the strongest correlations between the different sections; dashed lines represent weak or less abundant correlations or uncertainties.

As is quite clear from Figure 6.1., the alteration history of the Eldora amphibolites is far from being the "simple situation", involving initial PreCambrian events causing equilibration followed only by igneous-intrusion related re-heating, with diffusive exchange as the main process in this re-heating (Hart, 1964). Strong evidence has been presented which indicates that some of the mineral alterations within the amphibolites were formed during the PreCambrian and others in association with the Laramide orogeny. Only a fraction of the Laramide alteration is Stock-related and most of the Laramide alteration within the amphibolites is probably associated with the movement of Laramide aged mineralising fluids forming 'ore shears'. All the alterations identified within the Eldora amphibolites appear to be the result of volatile-fluid interactions associated with the crystallised minerals, as a result of the movement of fluids of various ages through the rocks.

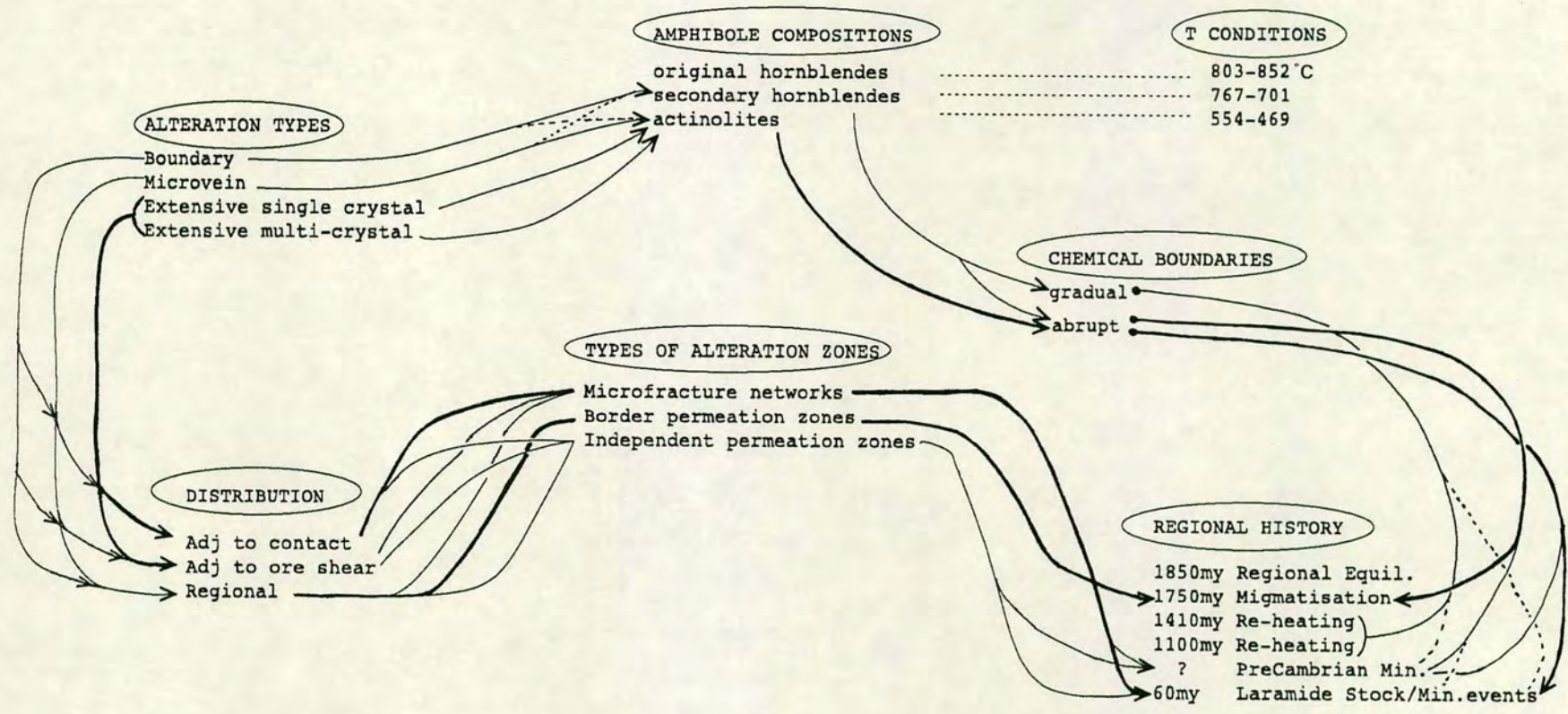


FIG. 6.1. Summary diagram illustrating the correlations between secondary amphibole types, compositions and chemical boundaries, and their distributions within the Eldora amphibolites. Both alteration types and zones are linked with the geological events which formed them. Bold lines represent strong correlations, dashed lines represent uncertainties.

CHAPTER 7. GEOCHRONOLOGY

This chapter reviews the previous geochronological studies performed within the Eldora amphibolites and presents new data obtained using both conventional K-Ar analysis of hornblende separates (as Hart, 1964) and $^{40}\text{Ar}^*$ - ^{39}Ar laser spot analysis of individual amphibole grains.

7.1. PREVIOUS WORK

The complex PreCambrian geological history of the now mostly high-grade metamorphic rocks of the Idaho Springs Formation was outlined in some detail in chapter 1; a re-capitulation of the most salient points is given below. This is followed, for comparison purposes, by a brief discussion of a geochronological study performed adjacent to a Laramide Stock close to Eldora and culminates with a review of the works carried out adjacent to the Eldora Stock itself.

The Idaho Springs Formation has been affected by four PreCambrian events (Peterman *et al.*, 1968), see Figure 1.2.

(i) 1850 to 1750my.

First regional metamorphism of greenschist facies.

Preserved only within the lower grade rocks of the north-east Front Range.

(ii) ~1750my.

Second regional metamorphism of amphibolite grade

Extensive migmatization of the Formation (Olsen, 1982, 1984) during the waning stages of which the Boulder Creek Granodiorite was emplaced (c.1700my.).

(iii) c.1410my.

Third event, second major plutonism, corresponds to the emplacement of the Silver Plume Granite and its correlatives.

Mainly thermal effects upon the surrounding rock, re-setting both the Rb-Sr and K-Ar mineral ages.

Cataclastic deformation occurred in localised zones between 1200 and 1400my.

(iv) c.1100my.

Fourth event, third major plutonic episode, involved the emplacement of the Pikes Peak Granite.

This had local thermal effects only.

In addition to these PreCambrian events two similar mineralisation episodes have taken place, one of PreCambrian age the other associated with the Laramide orogeny. The Laramide orogeny (c.60-100my ago) also resulted in the emplacement of a series of 'monzonitic' intrusives such as the Eldora stock.

CONTACT STUDIES:

The Boulder Creek Granite

A series of papers by Phair *et al.* (1971) report apparent Pb-alpha and U-Pb ages of zircons within the Boulder Creek Granodiorite ranging between 1850 and 910my. The lowest zircon ages (<1000my.) correlate with selective channelways within the granodiorite which strike toward a nearby Laramide intrusion (The Jamestown Stock see chapter 1 Figures 1.7 and 1.8). Phair *et al.(op.cit.)* examined the zircons microscopically and discovered the original purple-semi-opaque grains had partial or complete rims of colourless zircon which they interpreted as being overgrowths. Not all the zircons within any one sample were zoned. On the basis of the zircon textures observed and the reduction in ages adjacent to channelways within the rock Phair *et al.* (1971) conclude:

"warm solutions rather than heat as the agent of recrystallisation and lead loss".

The Eldora Stock

The Eldora Stock and adjacent country-rocks have been the setting of numerous geochronological studies (Doe and Hart, 1963; Davis *et al.*, 1962; Hart, 1964; Tilton *et al.*, 1964; Steiger and Hart, 1967; Wright, 1967; Berger, 1975). The early works of Doe and Hart (1963), Davis *et al.*(1962) and Tilton *et al.*(1964) established the presence of zircon (^{207}Pb - ^{206}Pb , ^{238}U - ^{206}Pb), hornblende (K-Ar) and biotite (Rb-Sr, K-Ar) age patterns within the rocks adjacent to the Stock. The results of these studies are incorporated into Figure 1.1 (chapter 1). Hart (1964) reports the experimental details of the K-Ar ages of both hornblende and biotite separates and the Rb-Sr ages of biotite separates from these studies, and additionally presents data on K-Ar/Rb-Sr ages of feldspar separates. Rb-Sr and K-Ar ages of biotite separates from the Eldora Stock itself suggest it is approximately 54my. old (Hart, 1964). The coarse biotite Rb-Sr/K-Ar ages (obtained from separates made from the pegmatites within the Idaho Springs Formation) reach a PreCambrian plateau age of c. 1200my. at distances approximately 10,000ft. (3148m.) from the contact; the hornblende K-Ar plateau age varies between 1172my. (134ft.; 42m.) and 1375my. (9400ft.; c.3000m.).

The apparent 'gradual' drop in ages toward the contact is considered by Hart (1964) to represent a re-setting of the ages due to thermally activated volume diffusion brought about by the intrusion of the Stock. Hart (*op.cit.*) suggests the discrepancies in the plateau ages are related to the variable response of the different mineral age systems during the PreCambrian metamorphic events. The K-Ar mineral ages reported by Hart (1964) have been recalculated using I.U.G.S. decay constants (Steiger and Jaeger, 1977) and are presented in Table 7.1.

The potassium feldspar K-Ar ages (obtained from pegmatite separates) are highly irregular. Hart (1964) reports the feldspar from 2ft. has a K-Ar age of 78my. and that those between 20ft. and 1000ft. have ages older than the intrusion despite their having been converted from microcline to orthoclase. Hart (*op.cit.*) suggests that either some part of the argon in the feldspars is bound very tightly and therefore is not easily re-distributed by diffusion or the erratic ages represent variations in the subunit diffusion size of the feldspar. The Rb-Sr ages of the feldspars plot near a 1400my. isochron suggesting the samples Rb-Sr ratios were unaffected by the contact metamorphism.

Both K-Ar and Rb-Sr ages of coarse biotites separated from pegmatites show a gradual progression from Laramide to PreCambrian ages, see Figure 1.1. No K-Ar ages were obtained closer than 248ft. (76m.) The fine biotites, separated from the amphibolitic rocks, have much more variable ages (see Table 7.1); these are consistently lower than the corresponding coarse biotite ages. Hart (1964) suggests the difference in ages within and between both coarse and fine-grained fractions represent variations in the physical grain-size, which controls diffusion.

Of the seven hornblende K-Ar ages obtained only two (samples collected 2 and 11 feet from the contact) show a major reduction in age. Hart (1964) suggests the presence of biotite impurities in these separates has almost certainly lowered their apparent ages. Similarly, sample 950 (the sample number reflects it's distance from the contact, in feet) has a 2% biotite impurity for which Hart (*op.cit.*) makes a correction for, changing the observed age from 1080my. to ~1200my. All the samples, except those closest to the contact (2 and 11), have fairly constant bulk-analysed potassium contents ranging from 1 to 1.2 wt% (Hart, 1964). Sample 11 has a K content of 0.77wt% and sample 2 ~0.5wt% (after a correction was performed to remove 10% biotite impurity). Hart (1964) speculates the reduction in K of the bulk separates close to the contact to be due to neomineralisation of the original hornblende crystals to biotite.

TABLE 7.1 HART'S K-Ar MINERAL AGES

DISTANCE feet (m)	K (wt%)	$^{40}\text{Ar}^*$ (Sccs/g) $\times 10^{-5}$	$\frac{^{40}\text{Ar}^*}{^{40}\text{Ar}_T}$ (%)	HART'S AGE(ma)	RECALC AGE(ma) #
K-FELDSPARS					
2 (0.6m)	11.250	3.600	89.0	78.5	80.4
20 (6m)	10.950	14.100	98.0	298	304.0
85 (26m)	8.880	10.300	98.0	270	275.7
248 (76m)	10.960	25.900	76.0	516	523.0
1070 (326m)	9.710	11.300	97.0	272	276.6
2400 (732m)	11.420	24.700	96.0	477	484.3
22500 (6858m)	10.690	50.000	99.0	916	920.7
COARSE BIOTITES					
COA (stock)	7.670	1.703	64.0	55.0	56.0
248 (76m)	7.400	2.430	69.0	80.6	82.4
1130 (344m)	7.220	12.690	97.0	397	402.9
2400 (732m)	6.180	15.410	95.0	540	548.1
3600 (1097m)	7.840	29.800	98.0	771	780.3
5200 (1585m)	7.530	40.800	99.0	1023	1031.5
7300 (2225m)	7.850	44.400	98.0	1058	1065.7
14100 (4298m)	7.540	48.900	99.0	1172	1180.0
22500 (6858m)	8.260	53.300	99.0	1168	1175.6
FINE BIOTITES					
58 (18m)	6.640	2.070	85.0	76	78.3
950 (290m)	7.130	1.707	73.0	59	60.5
1070 (326m)	5.130	4.370	69.0	203	206.5
2400 (732m)	5.520	9.900	92.0	407	410.3
HORNBLLENDE					
2 (0.6m)	1.210	0.598	40.0	120	123.0
11 (3m)	0.774	3.840	91.0	956	964.0
134 (41m)	1.026	6.650	94.0	1172	1179.0
248 (76m)	1.000	6.560	85.0	1180	1190.0
950 (290m)	1.450	7.950	74.0	1080	1041.0
1130 (344m)	1.150	7.870	98.0	1220	1227.0
9400 (2865m)	1.195	9.640	97.0	1375	1380.0

$\lambda_p = 4.962 \times 10^{-10} \text{a}^{-1}$ $\lambda_c = 0.581 \times 10^{-10} \text{a}^{-1}$ $^{40}\text{K} = 1.167 \times 10^{-4} \text{atoms}$ AGES $\pm 3\%$ $^{40}\text{Ar}^* = \text{radiogenic argon-40}$ $^{40}\text{Ar}_T = \text{Total argon-40}$

If one assumes Hart's samples are broadly similar to those studied in detail in this research (which is likely seeing as the samples were collected along the same traverse) it is possible that the reduction in the K content of the separates close to the contact reflects an increasing abundance of actinolitic overgrowths and microveins within the separates (as described in chapters 4 and 5). Since actinolite has a K content $< 0.5 \text{wt}\%$ sample 11 could be interpreted as being a mixture of original hornblende and partially actinolised hornblendes, sample 2 mostly actinolised hornblende and microveins. Hart's original separates

would need to be examined optically to confirm whether or not such a situation exists, however his separate description notes:

"hornblende olive-green with some bluish alteration".

Berger (1975) performed ^{40}Ar - ^{39}Ar step heating experiments (see section 3.3.2) on Hart's hornblende, coarse-grained biotite and K-feldspar separates hoping to distinguish between undisturbed, partially re-set and completely overprinted ages (following Turner, 1968). In principle geologically undisturbed samples should yield well defined apparent-age plateaus; partially disturbed samples should exhibit age gradients and completely re-set samples should generate age plateaus indicative of the age of overprinting (see Figure 7.1 from Turner, 1968). The total argon release ages obtained by Berger (1975) have been recalculated using I.U.G.S. decay constants (Steiger and Jager, 1977) and are presented in Table 7.2. In all but a minority of cases, (feldspars 2 and 85), Berger's dates are older than the K-Ar ages obtained by Hart (1964). Berger (*op.cit.*) reports a coarse-biotite age for the Stock of 64.5my. (*c.f.* Hart's 54my.). A reduction in total Ar release ages obtained from separates closest to the contact is retained. However, the incremental age patterns observed are not easily interpreted in terms of the gradual resetting of ages expected.

The coarse-biotite spectra of undisturbed biotite separates 22500 and 14100 and the completely re-set separate 20 have well defined plateaus at ~1220, 1242 and 64my. respectively for argon released above *c.*600°C (Berger, 1975) see Figure 7.2 a and b. Biotite separates between 14100 and 20 have more irregular spectra, argon released above 900°C is described by Berger (1975) as having "significantly anomalous dips or significantly anomalous rises". Berger (*op.cit.*) interprets these as being characteristic of the spectra generated by partially overprinted biotites.

The K-feldspar separates released their argon in two main intervals, one below 900°C the other below 1200°C (Berger, 1975). Berger suggests the argon released below 900°C represents the maximum age of thermal overprinting whilst that released above 900°C produces "geologically meaningless" ages and plateaus. The feldspar spectra have been reproduced in Figure 7.3.

TABLE 7.2 BERGER'S ^{40}Ar - ^{39}Ar MINERAL AGES

DISTANCE feet (m)	J $\times 10^{-3}$	$\frac{^{40}\text{Ar}^*}{^{39}\text{Ar}}$	BERGER'S AGE(ma)	RECALC AGE(ma) #
K-FELDSPARS				
COA (stock)	4.089	11.42±0.07	81.2±1.5	82.34
2 (0.6m)	3.918	11.27±0.07	76.8±1.4	77.94
85 (26m)	4.223	29.82±0.19	211.3±3.7	214.00
1070 (326m)	4.223	52.64±0.30	358.4±6.0	362.16
2400 (732m)	3.918	36.42±0.20	237.7±4.1	240.62
22500 (6858m)	4.086	166.80±1.20	946.0±1.4	937.52
COARSE BIOTITES				
COA (stock)	4.086	8.92±0.065	64.5±1.2	64.55
20 (6m)	6.266	5.70±0.081	63.3±1.4	63.32
248 (76m)	6.266	9.10±0.18	100.1±2.0	100.04
1130 (344m)	6.266	42.46±0.33	427.2±7.5	425.57
2400 (732m)	6.266	63.31±0.60	606.0±11	602.74
3600 (1097m)	6.266	105.60±3.4	924.0±27	916.14
5200 (1585m)	6.266	140.20±2.8	1150.0±23	1137.38
14100 (4298m)	6.266	155.70±1.5	1242.0±18	1228.32
22500 (6858m)	5.846	164.90±1.9	1223.0±19	1217.65
HORNBLENDSES				
2 (0.6m)	5.816	15.47±0.09	154.3±5.0	155.00
11 (3m)	5.816	141.20±0.9	1085.0±27	1082.00
134 (41m)	5.816	176.50±1.1	1281.0±30	1274.00
248 (76m)	5.846	171.80±2.4	1261.0±21	1254.00
950 (290m)	5.816	136.80±2.3	1060.0±33	1056.00
1130 (344m)	5.816	177.20±2.8	1285.0±39	1278.00
9400 (2865m)	5.816	200.00±4.1	1401.0±38	1392.00

$\lambda_{\beta}=4.962 \times 10^{-10} \text{a}^{-1}$ $\lambda_{\alpha}=0.581 \times 10^{-10} \text{a}^{-1}$ $^{40}\text{K}=1.167 \times 10^{-4} \text{atoms}$ $^{40}\text{Ar}^*=\text{radiogenic argon-40}$ $^{40}\text{Ar}_{\text{T}}=\text{Total argon-40}$

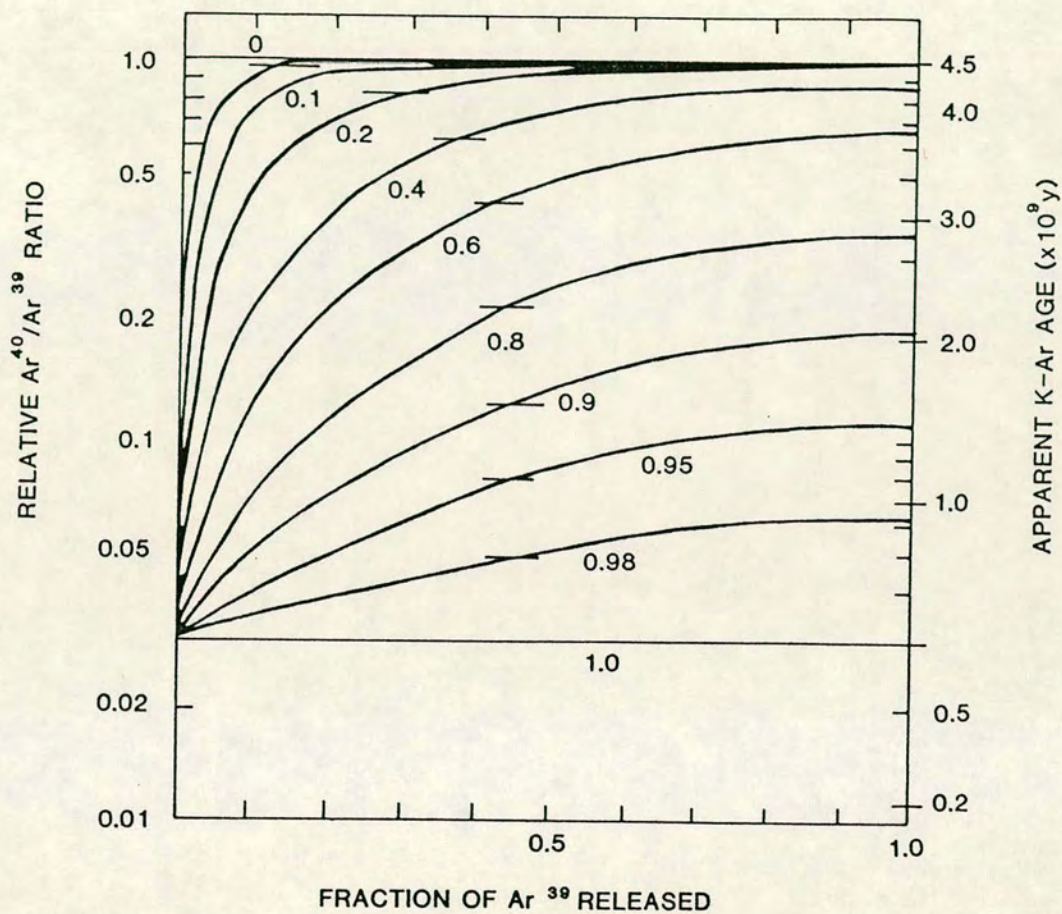


FIG. 7.1. Theoretical ⁴⁰Ar/³⁹Ar release patterns (reproduced from Turner, 1968).

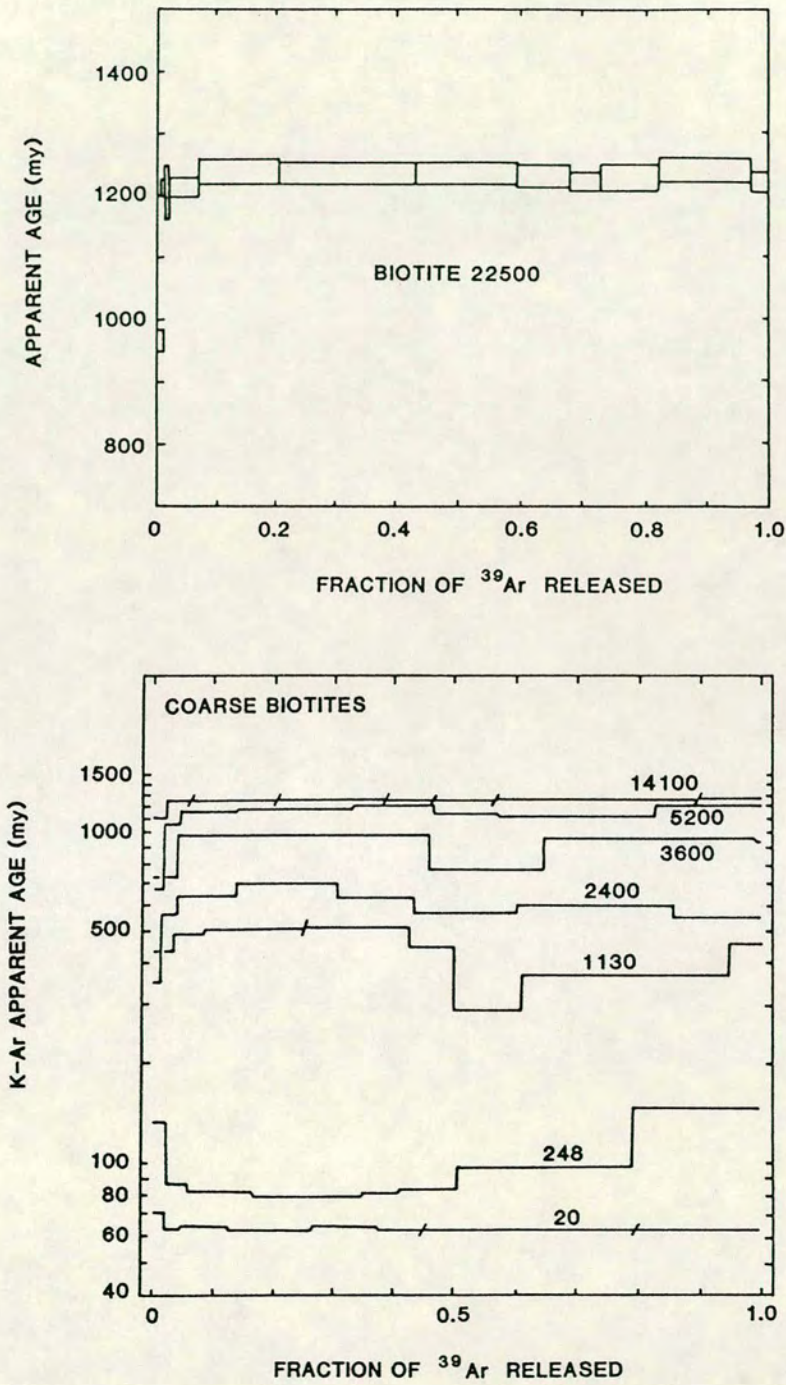


FIG. 7.2. $^{40}\text{Ar}/^{39}\text{Ar}$ age spectrum plots for coarse biotite fractions separated from Eldora amphibolites and biotite-pegmatites (reproduced from Berger, 1975).

- (a) Biotite separate 22500ft (6858m.) from the Stock contact. C.1200my age plateau retained.
- (b) Biotite separates 14100ft to 20ft (4298,6m.) from the Stock contact. Complex age patterns - discussed in text.

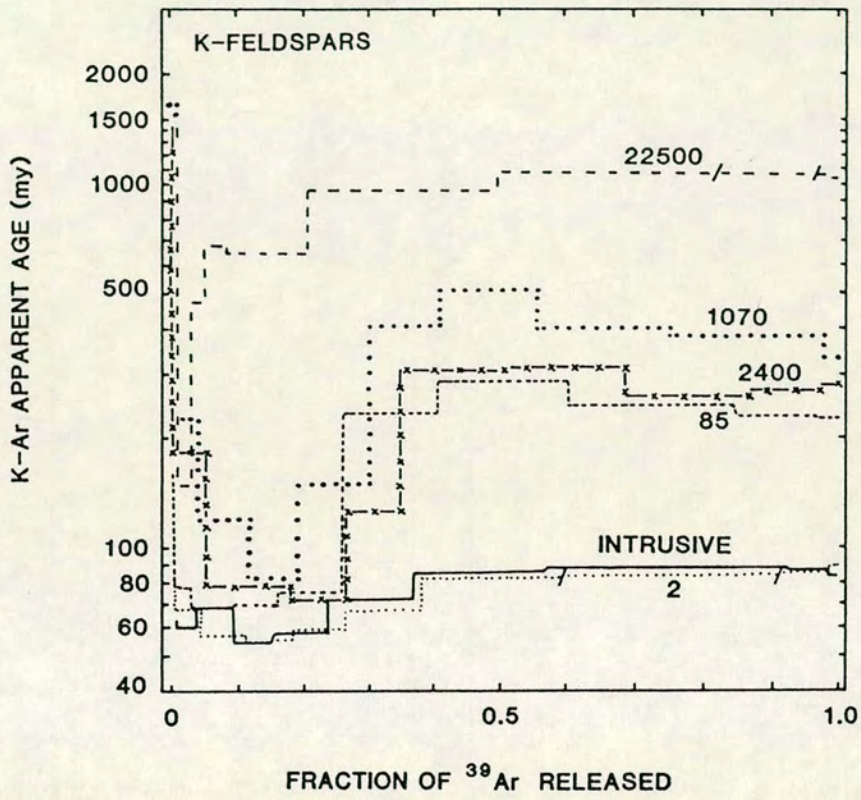


FIG. 7.3. ⁴⁰Ar/³⁹Ar age spectrum plots for K-feldspar fractions separated from the Eldora biotite-pegmatites (Berger, 1975).

Berger's hornblende $^{40}\text{Ar}/^{39}\text{Ar}$ spectra have been reproduced in Figure 7.4 (A,B,C). Most radiogenic argon was released between 950 and 1100°C. Hornblende 9400 (Figure 7.4A) has a well defined plateau representing ~98% of the argon released. The remaining ~2% argon was released below c.900°C (Berger, 1975). This is suggested by Berger to represent a phase change (amphibole-pyroxene) brought about by vacuum heating. Hornblendes 1130 and 950 (Figure 7.4B) display the sorts of apparent age gradients expected from partially disturbed samples (Turner, 1968). However, Hart (1964) reports a 1% fine-grained biotite impurity in sample 1130 and 2% in 950. Hart's K-Ar ages of fine-grained biotites at 1070ft. and 950ft. (see Table 7.1) are 203my. and 59my. respectively. Berger (1975) believes the spectra of 1130 and 950 obtained represent variable emissions of argon from the intergrown biotites and hornblendes and not true age gradients. Berger (1975) suggests the plateaus in spectra 1130 and 950 represent the original c.1400my. age of the hornblendes (c.f. 1285my and 1060my. K-Ar ages of Hart, 1964). Hornblendes 248, 134 and 11 display similar spectra to 1130 and 950 (Figure 7.4C). The c.1000my. plateau in sample 11 is considered by Berger (1975) to be "false" presumably because it is so close to the contact and "should" therefore be overprinted by the Laramide event. Samples 248 and 134 have well defined plateaus at ~1294my. and ~1320my. respectively. The age spectrum for hornblende 2 is far more irregular than the others; Berger (*op.cit.*) believes this reflects the presence of the 10-15% fine-grained biotite impurity reported by Hart (1964). Berger (1975) places an age of "at least" 390my. on the "hornblende component" of the spectra.

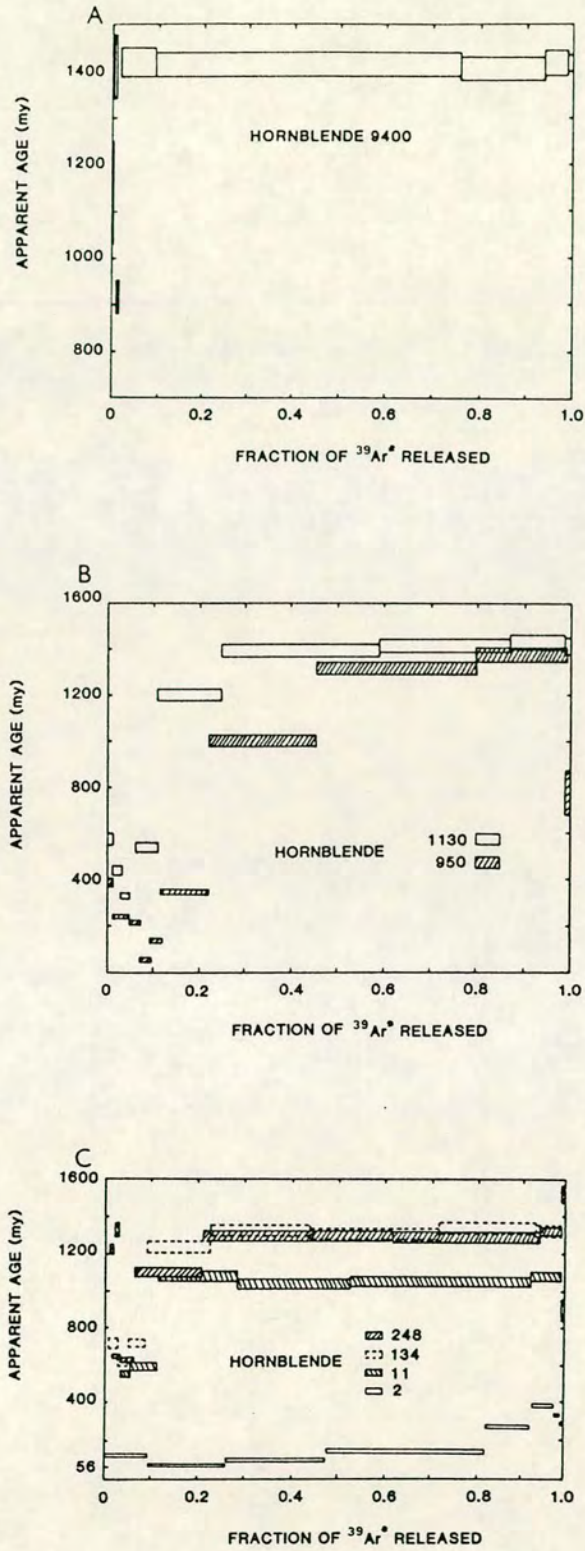


FIG. 7.4. $^{40}\text{Ar}/^{39}\text{Ar}$ age spectrum plots for hornblende fractions separated from the Eldora amphibolites (reproduced from Berger, 1975).

(A) Hornblende fraction 9400ft (2865m.) from the Stock contact. C. 1400my age plateau retained.

(B) Hornblendes 1130 and 950 (344m and 290m.) from the contact - apparent age gradients exist. See text for explanation.

(C) Hornblendes 248, 134, 11 (76m., 41m., 3m. from the contact) - partial age plateaus retained. Hornblende 2 (0.6m.) - completely re-set age plateau? See text for further explanations.

Lee *et al.* (1990) performed both laser microprobe analyses of single mineral grains and step-heating analyses of multigrain mineral separates in an investigation of biotite and hornblende ^{40}Ar - ^{39}Ar ages within the thermal aureole of a dyke. The hornblende spectra and single laser spot patterns obtained are believed to represent the partial re-setting of grains associated with dyke emplacement (Lee *et al.*, 1990). During the intrusion event amphibole rims were degassed but the cores remained unaffected; a subsequent elevation in the partial pressure of argon is believed to have caused diffusion of excess ^{40}Ar back into the hornblende grains where it is concentrated along both unaltered and altered grain margins. In an ideal situation the apparent ages should gradually decline from crystal cores toward their rims (reflecting diffusive loss due to re-heating); the outer most edges of the crystals should coincide with a rise in ages reflecting incorporation of the excess argon component. The patterns obtained by Lee *et al. (op.cit.)* are far more complicated than the "ideal" due to either experimental difficulties (involving the plane of cross-section intersecting the amphiboles studied) or effective radius of diffusion size variations related to the presence of exsolution lamellae within the amphiboles.

7.2. K-Ar AGE DETERMINATIONS FROM MINERAL SEPARATES

K-Ar age determinations were made using the experimental procedures outlined in chapter 3 section 3.3.1. Seven hornblende separates, six of which fall within 15m. of the Eldora Stock Contact were selected to provide additional data on the area within 100 feet of the contact, reported by Hart (1964) as having undergone argon loss due to volume diffusion processes. The seventh sample, originating 663m. from the contact was selected as a representative of the 'plateau region' retaining original PreCambrian ages (following Hart, 1964). The K-Ar results obtained are presented in the following table.

SAMPLE N ^o	DIST /m.	K (wt%)	K (C.V) ^a	⁴⁰ Ar* (Scgs/g) X10 ⁻⁵	⁴⁰ Ar* (%) ⁴⁰ Ar _T	AGE ^b (my)
E15	0.15	0.931	0.66	4.822	97.1	998
E16	1.45	0.859	0.42	3.532	97.2	832
E12	4.00	1.039	0.26	5.956	98.4	1078
E18	4.10	0.952	0.40	4.328	98.4	902
E21	8.70	0.864	0.29	3.382	97.2	800
E5	15.00	1.011	0.67	6.127	98.6	1124
E52	663.00	1.120	0.47	8.682	96.0	1343

^a=coefficient of variation on K determinations

^b $\lambda_p = 4.962 \times 10^{-10} \text{a}^{-1}$

$\lambda_c = 0.581 \times 10^{-10} \text{a}^{-1}$

⁴⁰K = 1.167×10^{-4} atoms

AGES $\pm 3\%$

⁴⁰Ar* = radiogenic argon-40

⁴⁰Ar_T = Total argon-40

No age younger than 800my. (rock E21) was obtained. Even the sample closest to the contact retains an age of 998my. There is thus no evidence of an extensive Laramide event causing extensive K-Ar re-equilibration.

A conscious effort was made during mineral separation to remove all traces of both blue-green, secondary hornblende and fine-grained biotite from the samples. Nonetheless the variabilities in the ages obtained are believed to represent intergrowths of biotite and secondary hornblende within the mineral separates which were not successfully removed during separation. It should be noted that both E16 and E21 are biotite-rich amphibolites. The rocks retaining the oldest ages (E52, E5 and E12) are optically composed of large areas of pristine amphibolite, from which altered hornblendes were reasonably easily removed during separation. The effects of alteration and biotite contamination also appear to be evident in aspects of Hart's original study. Thus he reports

"hornblende, ragged, green to brown. Biotite intergrown as alteration of the hornblende."

and

"hornblende, clear, brown-green to green, altered in places to blue-green."

These K-Ar ages clearly demonstrate that the reduction in the age of the rocks adjacent to the Stock contact reported by Hart (1964) is in fact due to the presence of a greater abundance of secondary actinolite/hornblendes than seen elsewhere within the amphibolites. Volume diffusion appears to have had little effect in the re-setting of the mineral ages; thus the best 'pristine' amphibole separates show little evidence of being reset by the Stock related re-heating event.

7.3. $^{40}\text{Ar}/^{39}\text{Ar}$ AGE DETERMINATIONS USING LASER SPOT ANALYSIS

$^{40}\text{Ar}/^{39}\text{Ar}$ analyses were performed upon individual amphibole, biotite and plagioclase crystals within irradiated slivers of six of the seven rocks from which mineral separates had been obtained (see section 7.2). An explanation of the laser technique employed for argon extraction and analysis is given in chapter 3 section 3.3.2.

Brief descriptions of the age data obtained from rocks E52, E5, E21, E18, E16 and E15 are given in section 7.3.1. Rock E12 was not examined using laser microanalysis. Section 7.3.2. presents an overall summary and interpretation of the age patterns documented within the individual amphibole grains. Section 7.4. contains the overall conclusions made from the geochronological studies made during this research and section 7.5 compares these results to those of the original study performed by Hart (1964).

The total release ages presented in this thesis were corrected using a computer programme written by Dr.R.Burgess, S.U.R.R.C. (see section 3.3.2). The atmospheric argon (^{36}Ar) content of the Eldora Amphibolites was found to be negligible ($c.0.001$). Any correction for ^{36}Ar content upon the ^{40}Ar ages obtained would therefore be insignificant and has not been performed.

The argon ratios and ages gathered from each of the six rocks investigated have been tabulated and are presented in Appendix A. All six rocks were irradiated in late January 1991. Three rocks (E16, E21 and E52) were analysed in May 1991, the remaining three rocks (E15, E18 and E5) were analysed late in

November 1991. During the time from January to November the ^{37}Ar within the rocks decayed to stable ^{37}Cl with a half life of 35.1 days. Corrections were performed upon the $^{40}\text{Ar}/^{39}\text{Ar}$ ages of the first three rocks dated however by November the ^{37}Ar had decayed by an amount equivalent to approximately 8 half lives (*pers.com.* Ray Burgess). Thus in rocks E15, E16 and E5 ^{37}Ar had decayed ~99.6%, i.e. almost all the ^{37}Ar produced during irradiation had converted to ^{37}Cl . The $^{37}\text{Ar}/^{39}\text{Ar}$ ratios measured in these rocks are effectively meaningless and thus have not been presented.

7.3.1. DESCRIPTIONS OF THE AGE PATTERNS OBSERVED WITHIN EACH ROCK

E52 (663m.)

Two relatively unaltered amphibole crystals and several patches of secondary amphibole were examined. The $^{37}\text{Ar}/^{39}\text{Ar}$, $^{38}\text{Ar}/^{39}\text{Ar}$ and $^{40}\text{Ar}/^{39}\text{Ar}$ ratios, total release ages and the error bars associated with each analysis are given in Appendix A, Tables 1 and 2.

Closely spaced analyses within 'pristine' amphibole crystals (E52 grains 1 and 2) indicated that there was a spread in $^{40}\text{Ar}/^{39}\text{Ar}$ ages within individual crystals. B.S.E. images of the two amphibole crystals examined, and line drawings depicting the approximate size and locations of the laser pits are shown in Figures 7.5a,b (E52G1) and 7.7a,b. (E52G2). Figures 7.6a,b,c and 7.8a,b,c illustrate how the $^{40}\text{Ar}/^{39}\text{Ar}$ ages, $^{37}\text{Ar}/^{39}\text{Ar}$ and $^{38}\text{Ar}/^{39}\text{Ar}$ ratios vary within the two crystals. Age chrontours and $^{38}\text{Ar}/^{39}\text{Ar}$ ratio chrontours have been added to Figures 7.6a,b and 7.8a,b. Grain E52G1 retains an age of *c.*1447my (analysis number Z053) within it's core, E52G2 is slightly younger at *c.*1430my (Z107). In both E52G1 and E52G2 the laser-spot ages were found to decrease from the cores of the grains toward their rims, a narrow region of variable width occurs around the perimeter of each crystal within which the $^{40}\text{Ar}/^{39}\text{Ar}$ ages are anomalously high and slightly erratic. In E52G1, Figure 7.6a, the ages fall from *c.*1447my in the core to approximately 1090my (Z081) before rising again to between 1100 (Z073) and 1300my (Z062) at the very edge of the crystal. An identical pattern is displayed in E52G2 were the ages drop from *c.*1430my in the 'core' to 1100my (Z099) before rising again to between ~1200 and 1380my (Z122) toward the crystal's margin.

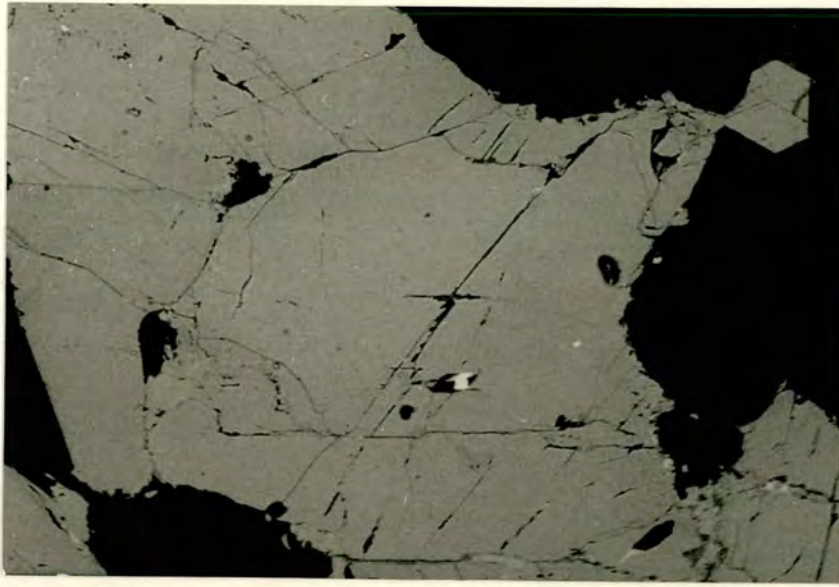


FIG. 7.5(a). B.S.E. image of hornblende grain 1 from rock E2 (E52G1). Scale bar: 400 μ m.

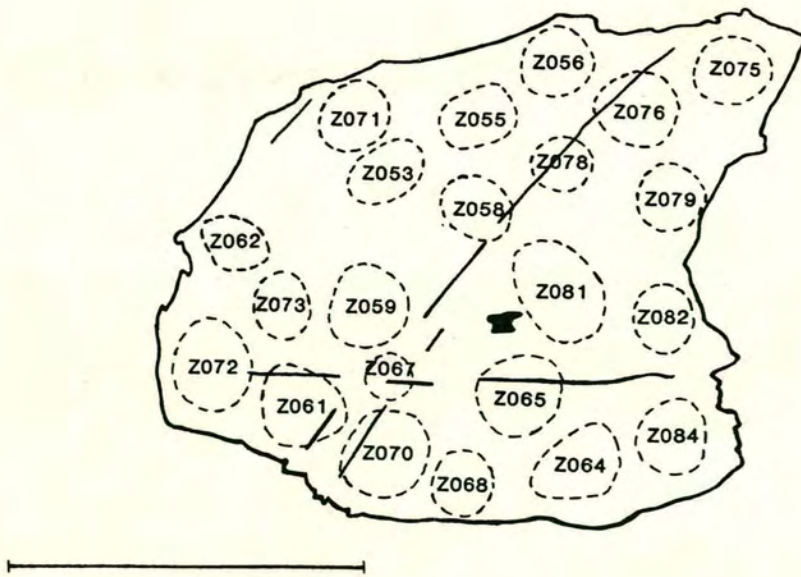


FIG. 7.5(b). Sketch of E52 hornblende grain 1 showing the approximate size and location of laser pits. Scale bar: 400 μ m.

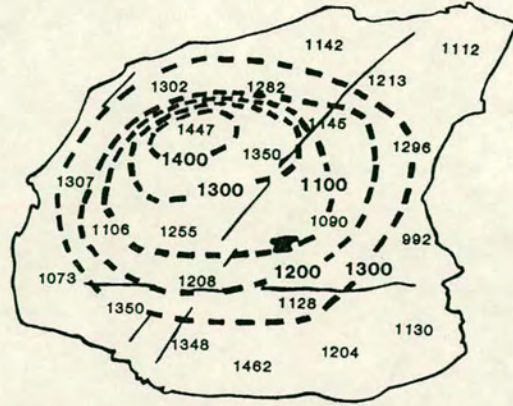


FIG. 7.6(a). Chrontour map of hornblende grain E52G1 as shown in Fig 7.5. Dates are in millions of years.

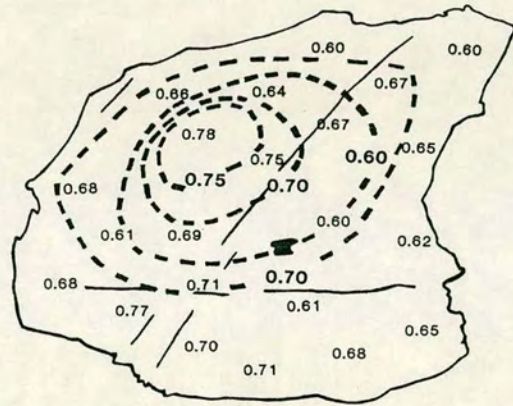


FIG. 7.6(b). $^{38}\text{Ar}_C/^{39}\text{Ar}_K$ contour map of hornblende E52G1.

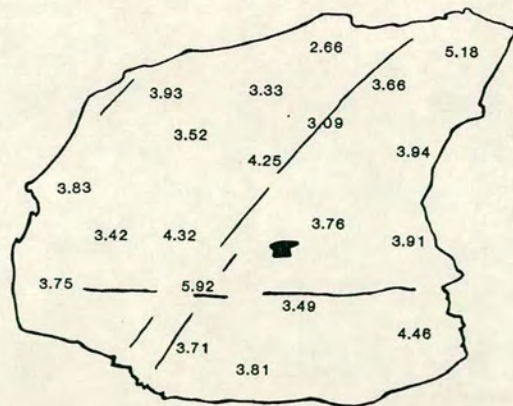


FIG. 7.6(c). Sketch showing $^{37}\text{Ar}_C/^{39}\text{Ar}_K$ ratios of E52G1.

All scale bars = 400 μm .

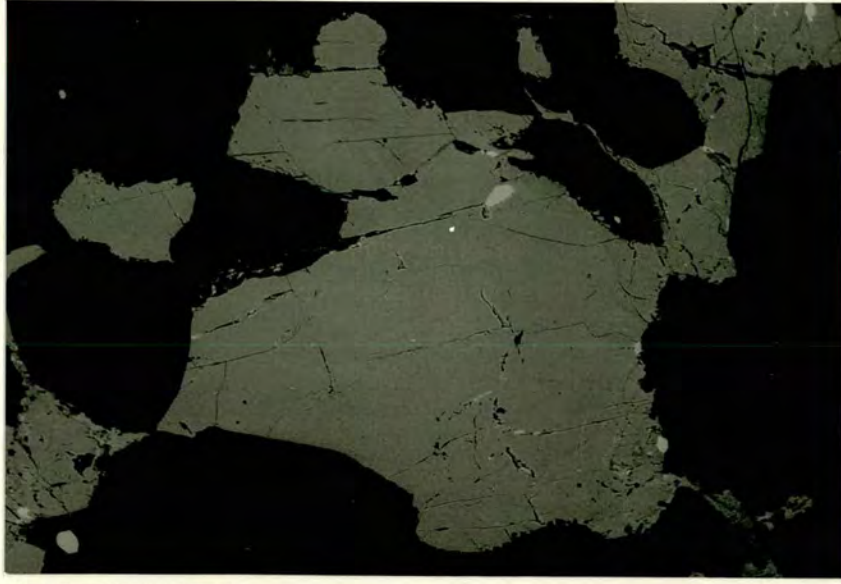


FIG. 7.7(a). B.S.E. image of hornblende grain 2 from rock E52. Scale bar: 400 μ m.



FIG. 7.7(b). Sketch of E52 hornblende grain 2 (E52G2) showing the approximate size and location of laser pits. Scale bar: 400 μ m.



FIG. 7.8(a). Chrontour map of hornblende grain E52G2 as shown in Fig 7.7. Dates are in millions of years.

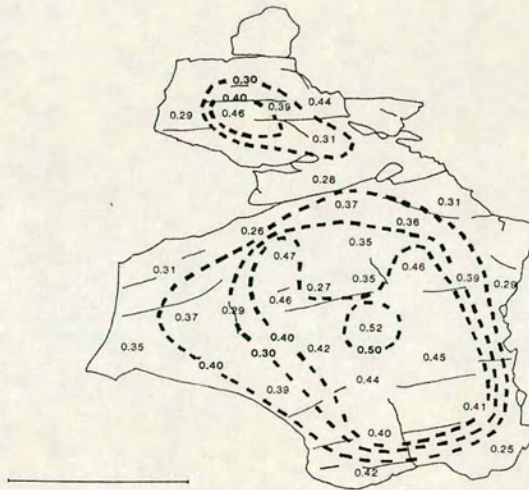


FIG. 7.8(b). $^{38}\text{Ar}_C/^{39}\text{Ar}_K$ contour map of hornblende E52G2.

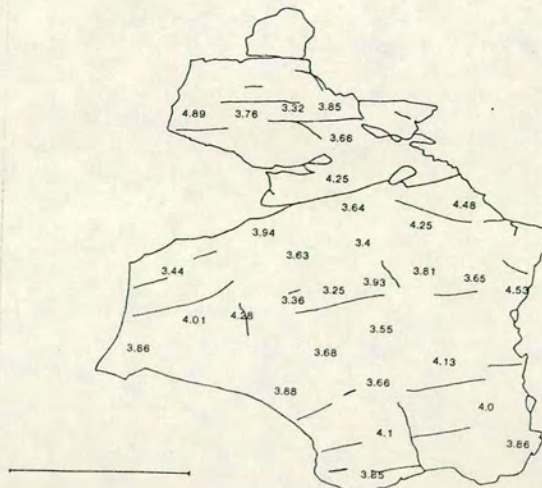


FIG. 7.8(c). Sketch showing $^{37}\text{Ar}_C/^{39}\text{Ar}_K$ ratios of E52G2.

All scale bars = 400 μm .

In both E52G1 and E52G2 it was possible to plot chrontours of the $^{38}\text{Ar}/^{39}\text{Ar}$ ratios. The $^{38}\text{Ar}/^{39}\text{Ar}$ chrontours show similar patterns to the total release ages (see Figures 7.6a,b and 7.8a,b). In both grains the $^{37}\text{Ar}/^{39}\text{Ar}$ ratios were too variable to be able to delimit chrontours.

Secondary amphiboles examined within E52 were mostly of Boundary amphibole alteration types which were hornblendic in composition. These were mostly narrow in width, usually less than $40\mu\text{m}$., and as a result it was difficult to obtain an 'uncontaminated' age from an individual analysis. Laser spots, though centred upon the secondary hornblendes, tended to overlap into the original hornblende causing partial volatilisation from both original and secondary hornblendes. The ages^{**} obtained in most instances are therefore believed to represent a mixture of the original and secondary hornblende ages. These 'mixed' ages are variable, ranging from 1020my to 1338my (see Appendix A Table 1 : Z085, 87 and 88), depending upon the proportion of Ar released from each amphibole within the area volatilised. The true ages of the secondary hornblendes are not known in these instances.

E5 (15m.)

A pristine amphibole from rock E5 was selected to ascertain whether the age pattern detected in E52 also exists in other rock samples. A B.S.E. image of the crystal investigated is presented in Figure 7.9a, Figure 7.9b shows the approximate size and location of the laser pits. Figure 7.10a,b illustrates the total release ages and the $^{38}\text{Ar}/^{39}\text{Ar}$ ratios within the amphibole grain. Table 3 Appendix A lists the argon ratios, ages and error bars associated with each analysis. The original amphibole is probably 1421-1433my old approximately (d137, d135), with younger, *c.*1100-1330my, ages (d138, d134 *etc.*). The anomalous 1823my age (d148) is interpreted as being the result of excess argon within the amphibole. The significant drop in ages from *c.*1300my to *c.*1100-640my (d140, e003) at localities at the edge of the original grain correspond to patches where secondary hornblende has developed (compare Figure 7.9a with Figure 7.10a - it is particularly clear for the youngest age). Secondary hornblende therefore seems to have formed at a different time to the original hornblende. The volatilised area from the widest patch of secondary hornblende (e003), located at the right hand side of the grain shown in Figure 7.9a, provides an age of 639my. As suggested in rock E52 this age is probably a combined age, representing argon released from both primary and secondary hornblendes. The

** Ages referred to in this context are better described as 'apparent ages' because it is not certain whether they represent (i) true ages for different amphibole growths, (ii) mixed ages resulting from partial argon emissions from different phases, or (iii) amphiboles of similar age but which have differing argon retentivities for some unknown reason.

secondary hornblende ages obtained are significantly lower than the ages of the original hornblende observed elsewhere within this grain.

E21 (8.9m.)

The thin, doubly polished sliver of rock prepared from sample E21 fractured during irradiation within the nuclear reactor (see section 3.3.2). The fragments of the sliver remaining did not include areas which had been characterised using the S.E.M. Laser analysis was therefore performed without the aid of S.E.M. images, however, it was possible to distinguish between altered and pristine amphibole using the optical apparatus available on the Laser microprobe. Table 4 Appendix A lists the argon ratios, total release ages and error bars associated with each analysis performed. An identical age pattern to those described in E52 and E5 was discovered. The unaltered cores of pristine grains retain ages ranging between 1201my (b120) and 1791my (b091) whilst edges to and altered patches within the original amphibole crystals have much lower ages ranging from 989my (b096) to 329my (b094). E21 is a biotite rich amphibolite and some of the younger ages obtained may represent argon emissions from amphibole-biotite mixtures.

Several larger biotite flakes visible within the rock were also analysed, these were found to have ages averaging *c.*60my (see Table 4 Appendix A). This suggests that the biotites either formed, or were re-set during, the Laramide orogeny.

Two plagioclase feldspar crystals within E21 gave ages of 1223my (b107) and 1500my (b108).

E18 (4m.)

E18 was loaded into the laser port with its upper surface in an inverse orientation to that examined using the S.E.M. Though the rock sliver is very thin (*c.*100µm.) its upper and lower surfaces are not identical. This meant that the S.E.M. photographs could only be used as a rough guide to the alteration state of individual amphibole grains and as a locator of secondary amphibole within original hornblende crystals. Since the age data for E18 is far less well constrained than that of the other five rocks it was not felt appropriate to discuss the data in great detail, however the analyses obtained are presented for reference in Appendix A, Table 5.

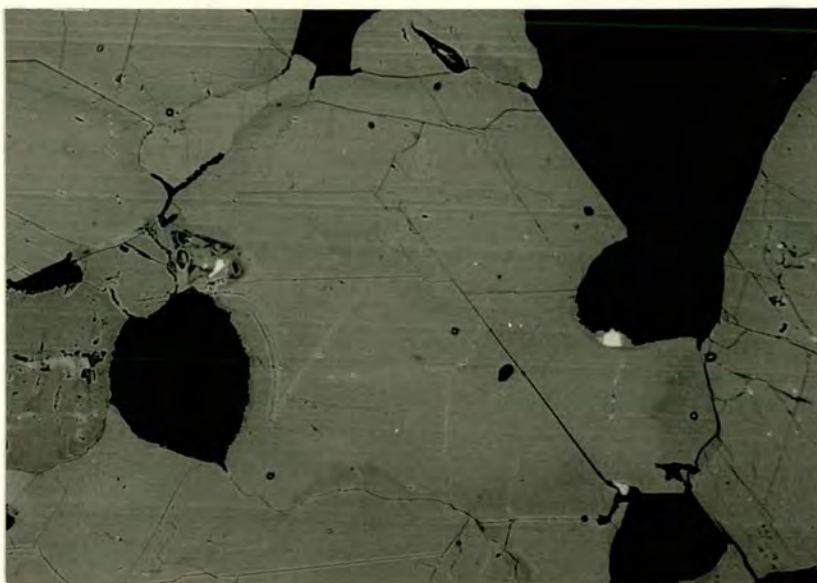


FIG. 7.9(a). B.S.E. of hornblende grain 1 from rock E5. Scale bar: 400 μ m.

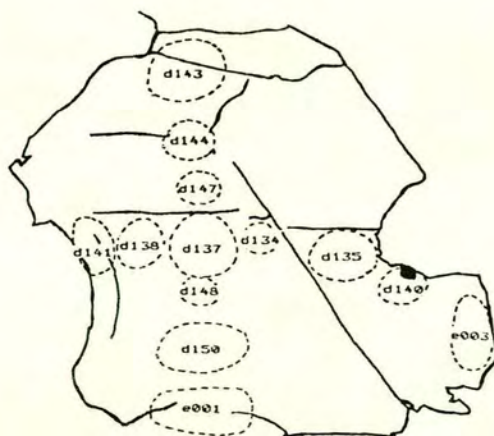


FIG. 7.9(b). Sketch of E5 hornblende grain 1 showing the approximate size and location of laser pits. Scale bar: 400 μ m.

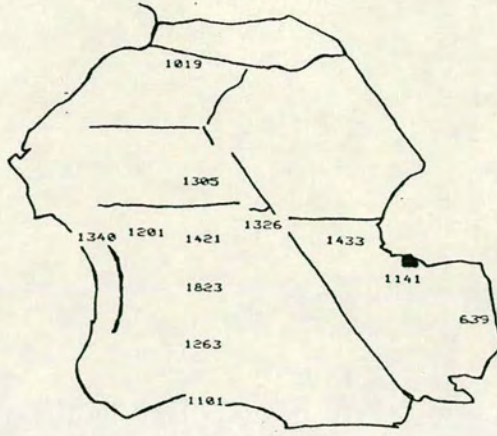


FIG. 7.10(a). Chrontour map of E5G1 as shown in Fig. 7.9. Dates are in millions of years.

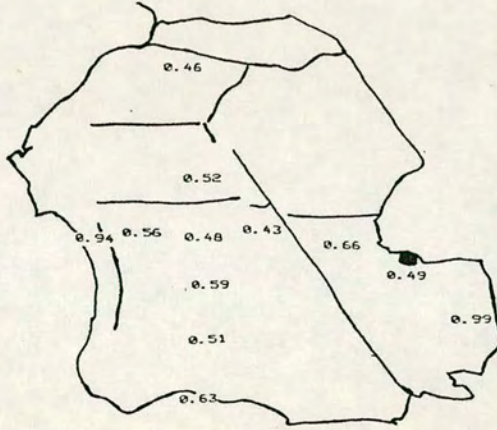


FIG. 7.10(b). $^{38}\text{Ar}_{\text{Cl}}/^{39}\text{Ar}_{\text{K}}$ contour map of hornblende E5G1.

All scale bars = 400 μm .

E16 (1.45m.)

E16 is a sample originating 1.45m. from the Eldora Stock. Optical examinations of a thin-section of the rock indicated that many of the original amphiboles are altered to blue-green coloured, secondary amphibole. Secondary amphibole occurs as Boundary, Microvein and Extensive single and multi-crystal amphibole alterations which are either hornblendic or actinolitic in composition.

A patchily altered amphibole crystal was investigated in some detail. In addition numerous single spot analyses of original and secondary hornblendes, secondary actinolite microveins and several biotite and plagioclase feldspar crystals were performed. The argon ratios, total release ages and the error bars associated with each analysis are presented in Appendix A, Tables 6 and 7.

A B.S.E. image of the patchily altered original amphibole crystal investigated in detail is presented in Plate 55. Figure 7.11 is a line drawing illustrating the approximate sizes and locations of each laser pit. Figures 7.12a,b and c depict the spatial locations of the total release ages, $^{38}\text{Ar}/^{39}\text{Ar}$ ratios and $^{37}\text{Ar}/^{39}\text{Ar}$ ratios within the crystal. The relatively unaltered upper portion of the crystal (see Plate 55) retains an age pattern similar to those described previously. The core of the amphibole is between 1300 and 1400my old; concentric rings of ages decreasing to *c.*500my (lower than seen before) occur almost symmetrically around the core region. Once again the extreme edge of the unaltered part of the grain exhibits much older, *c.*957my, ages. The remaining parts of the original amphibole grain have been partially altered to secondary amphibole with a few small biotite flakes. The ages obtained from the altered portions of the grain are erratic and usually lower than those documented within the unaltered core. Once again mixing between original and secondary amphiboles has probably masked the true age of the younger alteration phenomena. The youngest age obtained from the altered amphibole area is 255my. (a026).

The single spot analyses performed upon original and secondary amphiboles within E16 produced rather variable results. Some secondary hornblendes showed ages between 600 and 1500my, similar to those documented within the primary hornblendes (see analyses Z015, Z016, Z027, Z034, Z038 and Z049). Other secondary hornblende analyses such as Z028, Z030, Z031 and Z033 are much younger, ranging from *c.* 521my to 170my. Actinolite and actinolitic hornblende was more difficult to date with any degree of accuracy due to its very low potassium content (<1%).

Plate 55

B.S.E. image of altered amphibole grain 1 from rock E16 (E16G1). Compare the location of secondary amphibole with the analysis points shown in Fig. 7.11 and the ages presented in Figure 7.12.

Scale bar: 400 μ m.

PLATE 55

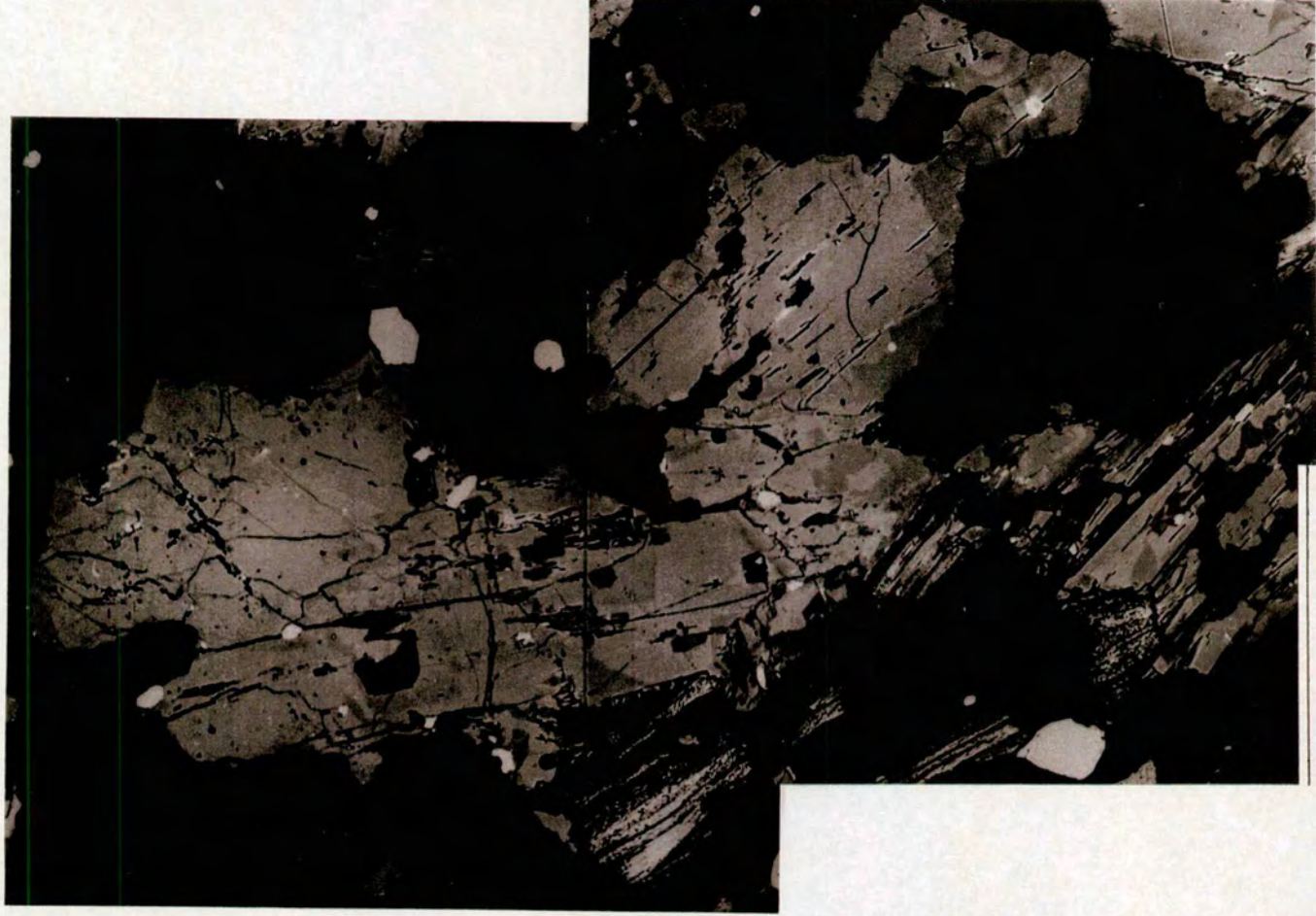




FIG. 7.11. Sketch of amphibole E16G1 showing the approximate size and locations of the laser pits. Scale bar 400 μ m.



FIG. 7.12(a). Chrontour map of altered hornblende grain E16G1 as shown in Plate 55 and Fig.7.11. Note that where secondary amphibole has developed the ages are generally much lower than those of the unaltered hornblende.



FIG. 7.12(b). $^{38}\text{Ar}_{\text{Cl}}/^{39}\text{Ar}_{\text{K}}$ ratios within altered hornblende E16G1.



FIG. 7.12(c). Sketch showing $^{37}\text{Ar}_{\text{Ca}}/^{39}\text{Ar}_{\text{K}}$ ratios of altered hornblende E16G1. All scale bars = 400 μm .

The ages generated from laser spots Z007, Z025 and Z040 (712, 1462 and 810my respectively) are thus difficult to interpret.

The biotite crystals analysed produced ages varying between 63 and 185my (see a028, a029, Z018, Z021 and Z041 in Table 7 Appendix A). Plagioclase feldspar ages were also found to be variable, ranging between 462 and 1731my (see Z019, Z022 and Z043 in Table 7 Appendix A).

E15 (0.15m.)

E15, the sample originating closest to the Eldora Stock, also fractured during irradiation with the nuclear reactor however several recognisable crystals have been examined in detail. The thin-section description of the rock presented in chapter 4 clearly established the more highly altered nature of this sample and subsequent S.E.M. investigations outlined the widespread occurrence of actinolite microveins and extensive single and multicrystal actinolitic amphibole alterations within original hornblende grains.

The B.S.E images of two of the highly altered amphibole crystals investigated are presented in Figures 7.13a and 7.15a. Figures 7.13b and 7.15b show the approximate size and locations of analysis points within the two altered crystals and Figures 7.14a,b,c and 7.16a,b are line drawings which illustrate the variations in ages and argon-38 ratios detected. The total release ages, argon ratios and error bars associated with the measurements made are presented in Tables 8 and 9, Appendix A.

Both altered crystals examined display a similar age pattern to those already described in rock E16. Much older ages, *c.*>1000my, were obtained from analyses falling within original hornblende patches in both E15G1 and E15G2 (Figure 7.13 analyses e113 and e114 ; Figure 7.15 analyses e068, e070, e071 and e072 and the relevant ages on Figures 7.14a and 7.16a respectively). Volatilisations falling almost entirely within the altered regions of the crystals, such as analyses e117, e120 from E15G1 and e063, e083, e075 in E15G2, give significantly younger ages (*c.*<500my). The remaining analyses in both crystals are rather erratic, reflecting combined emissions from original and secondary amphibole, plagioclase feldspar and opaques which fall within the original grain. No attempt has been made to contour the ages or $^{38}\text{Ar}/^{39}\text{Ar}$ ratios within either grain because the patterns are too variable.



FIG. 7.13(a). B.S.E. image of altered hornblende grain 1 from rock E15 (E15G1).
Scale bar: 400 μ m.



FIG. 7.13(b). Sketch of E15 hornblende grain 1 showing the approximate size and location of laser pits. Scale bar: 400 μ m.



FIG. 7.14(a). Sketch showing the age variations within hornblende grain E15G1 as shown in Fig 7.13. Dates are in millions of years.



FIG. 7.14(b). $^{38}\text{Ar}_{\text{Cl}}/^{39}\text{Ar}_{\text{K}}$ ratios within hornblende E15G1.

All scale bars = 400 μm .

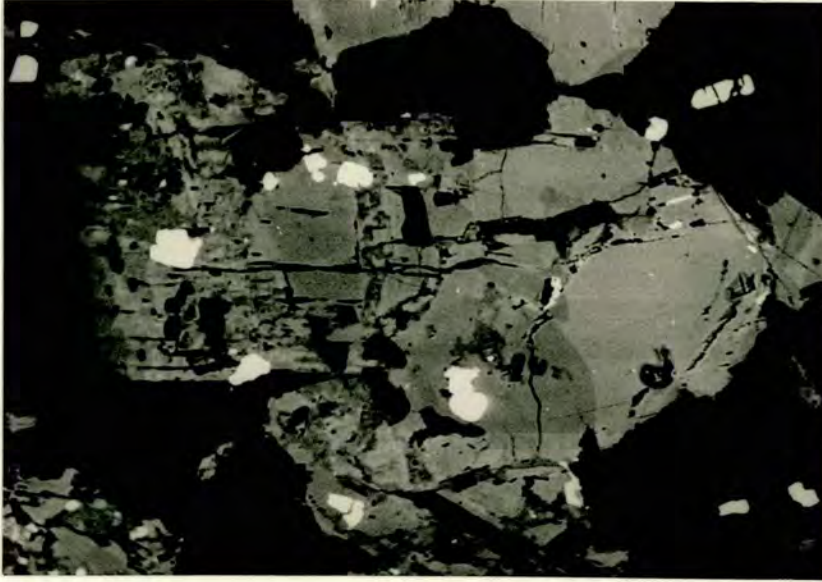


FIG. 7.15(a). B.S.E. image of altered hornblende grain 2 from rock E15 (E15G2). Scale bar: 400 μ m.



FIG. 7.15(b). Sketch of E15 hornblende grain 2 showing the approximate size and location of laser pits. Scale bar: 400 μ m.



FIG. 7.16(a). Sketch showing the age variations within hornblende grain E15G2 as shown in Fig 7.15. Dates are in millions of years.

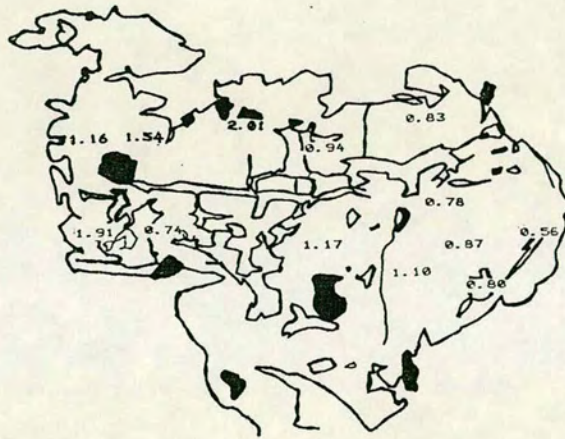


FIG. 7.16(b). $^{38}\text{Ar}_{\text{Cl}}/^{39}\text{Ar}_{\text{K}}$ ratios within hornblende E15G2.

All scale bars = 400 μm .

7.3.2. SUMMARY AND INTERPRETATION OF LASER SPOT AGES

Detailed examinations of the ages preserved within both pristine and altered amphibole grains within six samples of the Eldora amphibolite has revealed two different types of age pattern:

(i) PRISTINE AMPHIBOLES

Amphibole grains such as E52G1, E52G2 and E5G1, which have thus far been described as 'pristine' (*i.e.* they retain an original ferroan-pargasitic hornblende composition only), have been found to comprise 'cores' which vary in age from 1447-1421my. These central areas are rimmed by ages which gradually decrease to *c.*900my (except in E16 where the ages decrease to *c.*600my). The outermost edges of the grains in each case are associated with erratic, usually older ages. This distinct pattern is identical to the theoretical pattern of age re-setting associated with dyke emplacement described by Lee *et.al* (1990); argon is outgassed during the re-heating event resulting in a drop-off in ages towards the margins of the grains. The argon 'lost' forms an excess argon component within the rock which under favourable conditions may diffuse back into the original grain where it becomes concentrated along grain edges, cracks *etc.* and causes erroneous ages to be obtained (see section 7.1). The erratic ages found around the margins of the Eldora amphiboles, during laser analysis carried out as part of this research, are thus believed to reflect the re-incorporation of excess argon which was generated during diffusive loss caused by an earlier re-heating event. Since this diffusive-type pattern is distinguishable in rocks both near to the contact, such as E16 (1.45m.), and at distance from the Stock contact, such as E52 (663m.), it appears that the re-heating event in question is not related to the intrusion of the Laramide Stock.

(ii) ALTERED AMPHIBOLES

Altered amphibole grains such as E16G1, E15G1 and E15G2 have been found to comprise variable, but often much younger ages. Secondary hornblende and actinolite within both E16 and E15 is often less than 500my old. In most instances these younger ages appear to have superimposed upon the pre-existing 'pristine amphibole' age pattern within the grain. Some ages <200my have been documented, though many more ages of 400-600my have been obtained. Many of these ages are thought to represent volatilisations from mixtures of altered and more pristine amphiboles. Laramide ages (*c.* 60my) have been obtained from some biotites. Older ages, *c.*1000-1500my, have also been generated from secondary amphibole patches. It is not known whether these apparently PreCambrian alterations are truly PreCambrian in age or result from volatilisations comprising mixtures of original and secondary amphibole or regions of the original crystal occupied by excess argon.

7.4. CONCLUSIONS OF ISOTOPIC STUDIES

The K-Ar dating of amphibole mineral separates and Laser spot dating of individual amphibole crystals have both clearly shown that the age variations within the Eldora Amphibolites are not the result of re-heating associated with the intrusion of the Eldora Stock. The K-Ar ages, obtained from the analysis of fresh amphibole separates, showed that the apparent bulk age of the amphibolites does not gradually decrease to the age of the Stock as the Stock-amphibolite contact is approached. The results did demonstrate however that the bulk age of the rock was determined by the purity of the separate. Heavily altered rocks, such as E15 and E21 have apparently younger ages than the almost entirely unaltered rocks such as E5 and E52.

The Laser Spot ages enabled both a diffusive-type, PreCambrian age pattern and a much younger, rather erratic age pattern to be distinguished. Both types of age patterns were observed within the rocks irrespective of their proximity to the Stock contact. The re-heating age pattern appears to be unrelated to any re-heating caused by the intrusion of the Laramide Stock and is thus believed to represent one or a combination of the PreCambrian, regional metamorphic, re-heating events discussed in section 7.1. The younger alteration event has been difficult to date conclusively. Most analyses are between 400 and 600my suggesting a Late Cambrian-early PreCambrian event. Some analyses are <200my indicating that a Laramide alteration event may have occurred, some of

the apparently PreCambrian ages may in fact be mixtures of Laramide and original PreCambrian amphiboles.

The PreCambrian age pattern has been detected within both pristine and altered amphibole grains and does not appear to be restricted to alteration zones (i.e. microfracture networks or permeation zones) within the rock. The PreCambrian age pattern appears to have formed during a regional re-heating event. The regional history of the area suggests that the pattern may have developed as a result of regional re-heating associated with either the intrusion of the Silver Plume (c.1410my) or Pikes Peak Granites (c.1100my).

Secondary amphiboles occur **only** within alteration zones within the rocks. Chapter six illustrated the inter-relations between the different alteration zone types and the regional history of the rocks (Figure 6.1). Both PreCambrian and Laramide aged events resulted in the formation of alteration zones within the amphibolites. Migmatization (c.1750my) was responsible for the formation of the Border permeation zones whilst both PreCambrian and Laramide aged mineralisations produced independent permeation zones and microfracture networks. Laramide metasomatic fluids, originating from within the Stock (see section 4.), produced extensive alteration and the formation of microfracture networks and independent permeation zones within approximately 2m. of the Stock. Clearly the rather mixed nature of the ages obtained from secondary amphiboles within alteration zones within the Eldora amphibolites reflects the fact that they may have formed from either PreCambrian or Laramide events. Many of the younger ages (<200my) probably represent secondary amphiboles which grew during Laramide events.

7.5. DISCUSSION OF PREVIOUS WORK

Figure 7.17 presents a graph upon which Eldora amphibole age data (compiled from the isotopic studies of Hart (1964), Berger (1975), and those obtained from K-Ar analysis of amphibole separates during this research) have been plotted. The data from each study has been given a different symbol for ease of comparison. Both Hart's and Berger's data were discussed in detail in section 7.1 to which the reader is referred for further explanations. Of the 21 age measurements made, only two (those from a separate 2 feet (0.6m.) from the Stock) give ages less than 200my old. The remaining ages vary between 800 and 1400my and are believed by Hart, Berger and the author to reflect variabilities in the age of the PreCambrian plateau and perhaps also to be related to impurities

within the mineral separates. Both Hart and Berger concluded that the separate 0.6m. from the Stock had been at least partially re-set by diffusion related to a temperature increase brought about by the intrusion of a Laramide stock. Both reported a 10-15% biotite impurity within this separate. The mineral separates prepared by the author were made as pure as possible to remove any biotite and/or secondary amphibole constituents and the K-Ar ages obtained are much higher (>800my). Even a sample 0.15m. from the stock retained an age of 998my suggesting that stock-related age re-setting did not occur, or was insignificant.

The interpretation of the K-Ar and $^{40}\text{Ar}/^{39}\text{Ar}$ age data presented in this chapter (section 7.4) was based upon pre-requisite knowledge derived from the extensive optical, B.S.E. and microprobe examination of the amphibolites undertaken by the author (summarised in chapter 6). This interpretation clearly differs from that made by Hart (1964), who suggested the ages of the minerals were controlled by their position within a thermal aureole surrounding the Eldora Stock. Hart's investigation of the Eldora amphibolites was thorough and his results are of a consistently high standard, however the emphasis of Hart's study was geochronological. Despite performing accurate, routine thin section observations (in which both blue-green coloured, secondary amphibole and biotite were identified within the original amphiboles), Hart did not recognise the importance of the distributions of these alterations within the rocks. The thin section work performed by the author (presented in chapter 4) established the presence of distinct 'zones of alteration' (termed microfracture networks and permeation zones) within the amphibolites. Most of the amphibole alteration (as seen by both Hart and the author) was only ever visible within, or immediately adjacent to, one of these alteration zones. This suggests a fluid or fluids were responsible for the mineral alterations present within the amphibolites and not an increase in temperature (associated with stock emplacement) as suggested originally by Hart (1964) and built upon by many subsequent workers. Once the mineral alterations had been conclusively tied to fluid-related events it was possible to begin unravelling the complex history of the rocks. The variations in the ages of the Eldora amphibolites first recorded by Hart (1964) have now been successfully shown to be the consequence of a combination of PreCambrian and Laramide aged events. A zone of particularly high alteration bordering the Stock has been shown to have been produced from metasomatic fluids originating from the Stock itself (section 4.4), the remaining Laramide aged alterations detected within the amphibolites are the result of Laramide-aged mineralisation.

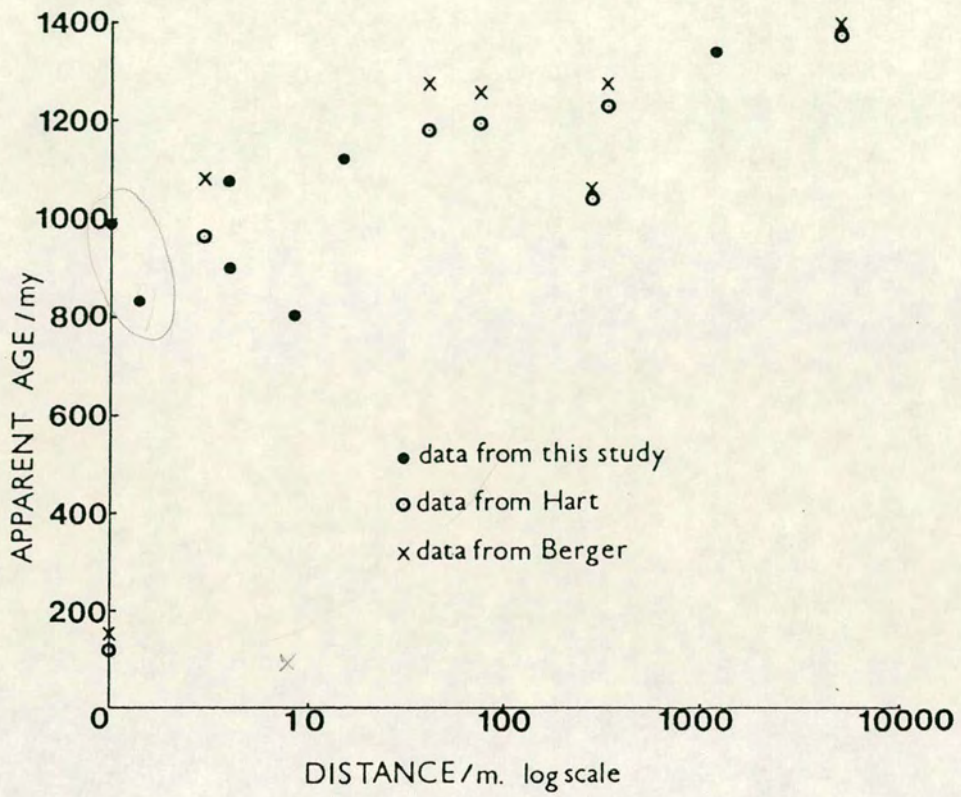


FIG 7.17. Plot of apparent amphibole age versus distance from the Eldora Stock. Data compiled from Hart (1964), Berger (1975) and this study. All ages have been calculated using I.U.G.S. decay constants (Steiger and Jaeger, 1977).

CHAPTER 8. CONCLUSIONS.

The conclusions arising from the studies presented in this thesis have already been comprehensively discussed towards the end of chapters four, five and seven. Chapter six presented a summary of the alteration history of the rocks which linked the optical, electron microscope, electron microprobe and thermobarometric results together in a collation diagram. To minimise repetition this chapter provides an outline of the most important findings of this research and suggests areas where further work could be carried out.

The most significant finding of this research was the fact that all the mineral alterations within the amphibolites are confined to definite alteration zones within the rocks (see section 4.3.). This and the irregular nature of the alterations themselves (i.e. they have no consistent relation to the nature of their adjacent phases; see section 5.1.1.(ii)) indicates that they formed from crystal-fluid interactions and are not the result of temperature-controlled diffusion as previously suggested by Hart (1964).

Most of the amphibole alteration types have optically and chemically sharp interfaces against their host crystals (see section 4.2 and chapter 5). This has been shown (sections 5.1.4. and 5.1.6.) to be due to either a replacement, or an overgrowth upon, the original crystal and is not due to a miscibility gap within the calcic amphibole series.

Combined optical and microprobe investigations (sections 4.4. and 5.1.5.) show that the secondary hornblendes formed during PreCambrian migmatitisation, PreCambrian mineralisation and Laramide-aged events. Secondary actinolite microveins formed during PreCambrian and Laramide mineralisation events and actinolitic Extensive single and Extensive multi-crystal alterations formed only during Laramide-aged events.

K-Ar analyses of fresh amphibole separates do not show a gradual re-setting from PreCambrian to Laramide ages as the Eldora Stock contact with the amphibolites is approached (section 7.2). This indicates that the age "re-setting" described by Hart (1964) is in fact due to the presence of secondary amphiboles and biotites within his separates and not the result of temperature-related diffusion (as outlined in theory in chapter 2).

The $^{40}\text{Ar}/^{39}\text{Ar}$ ages of the amphibole grains studied in-situ, though complicated due to the presence of a PreCambrian age pattern, show that the

secondary amphiboles are often significantly younger than the original hornblendes.

Each of the optical, chemical and geochronological studies performed during this research have provided a wealth of evidence which suggests that the age variabilities within the rocks at Eldora, originally documented by Hart (1964), are in fact the result of a complex combination of both PreCambrian and Laramide aged events.

Many unanswered questions have arisen during this research. Perhaps the most pressing of these questions revolves around the exact mechanism(s) by which the original amphibole crystals have been altered. Since immiscibility between hornblende and actinolite has still not been conclusively proven the author considers overgrowths and/or single crystal replacements to be the most likely mechanism of alteration, despite no grain boundaries being distinguishable optically (section 5.1.5.). Exactly how amphiboles alter is clearly a field which warrants future research.

Now the true alteration history of the Eldora Amphibolites has been established it may be feasible to undertake further similar studies which would enable a clearer delineation between Laramide and PreCambrian mineralisation to be made. Both the laser spot dating and ion microprobe techniques could, given future reductions in the size of the volatilisation areas, be re-applied to provide enhanced data on the differences between the original and secondary amphiboles. Finally it would be worth performing T.E.M. examinations of several altered amphibole grains in order to distinguish epitaxial overgrowths of secondary amphibole upon the original hornblendes from single crystal replacements of secondary amphibole within the original hornblendes.

Although it has been shown that the apparent age variabilities within the Eldora Amphibolites are *not* the result of diffusive exchange associated with the intrusion of the Eldora Stock this has not been proven for the Biotite Pegmatites which also occur within the country rocks adjacent to the Stock. Much of the original work of Hart (1964) was based upon ages obtained from biotites and feldspars separated from Biotite Pegmatites (see Table 7.1). Both the biotite and feldspar separates show apparent reductions in their "ages" as the contact is approached. These age reductions occur over a much wider distance than that suggested by Hart for the hornblendes (see Figure 1.1). Biotites and feldspars have much lower K-Ar closure temperatures (*c.*300°C and 150°C) than those of amphiboles (*c.*550°C). Hart (1964) suggests the country-rocks within approximately 2km. of the Stock were likely to have had their temperatures raised between 150-500°C. It is possible therefore that the large biotite and feldspar crystals within the Biotite Pegmatites were raised above their K-Ar closure temperatures and thus may have undergone partial argon loss in amounts related to their distances from the Stock. The same is not true for the amphiboles whose higher K-Ar closure temperatures may have prevented diffusive loss occurring at this particular time.

APPENDIX A: Laser Spot Dates

TABLE 1

SPOT No.	$\frac{37\text{Ar}}{39\text{Ar}}$	$\frac{38\text{Ar}}{39\text{Ar}}$	$\frac{40\text{Ar}^*}{39\text{Ar}}$	AGE(ma) $\pm 1\sigma$
E52 AMPHIBOLE GRAIN 1 (area c)				
Z053	3.52±0.42	0.78±0.04	349.1±14.8	1447±45
Z055	3.33±0.34	0.642±0.034	293.7±12.5	1282±42
Z056	2.66±0.62	0.604±0.041	250.8±14.7	1142±52
Z058	4.25±0.59	0.757±0.049	316.0±20.0	1350±62
Z059	4.32±0.56	0.687±0.041	285.2±17.2	1255±57
Z061	4.71±0.35	0.765±0.042	315.9±13.5	1350±44
Z062	3.83±0.47	0.682±0.034	302.0±14.8	1307±48
Z064	3.71±0.63	0.675±0.059	269.5±22.8	1204±76
Z065	3.50±0.46	0.607±0.030	246.7±12.5	1128±45
Z067	5.92±0.65	0.705±0.064	270.7±20.1	1208±67
Z068	3.81±0.49	0.708±0.039	354.5±17.2	1462±51
Z070	3.71±0.59	0.700±0.040	315.3±18.8	1348±59
Z071	3.93±0.53	0.664±0.044	300.2±17.4	1302±56
Z072	3.75±0.55	0.681±0.056	230.6±20.7	1073±74
Z073	3.42±0.38	0.614±0.040	240.0±12.6	1106±46
Z075	5.18±0.79	0.597±0.042	242.0±14.6	1112±52
Z076	3.66±0.23	0.669±0.024	272.2±9.7	1213±35
Z078	3.09±0.32	0.666±0.031	251.6±10.9	1145±39
Z079	3.94±0.28	0.650±0.031	298.3±13.1	1296±43
Z081	3.76±0.34	0.597±0.024	235.3±9.9	1090±37
Z082	3.91±0.53	0.619±0.036	208.0±10.7	992±41
Z084	4.46±0.35	0.654±0.040	247.2±15.3	1130±54
SECONDARY HORNBLLENDE ANALYSES				
Z085	4.67±0.63	0.543±0.045	215.8±18.6	1020±68
Z087	5.89±1.33	0.674±0.007	219.4±25.7	1033±93
Z088	4.15±0.48	0.803±0.045	311.8±19.8	1338±62
CORRECTED DATA IN MULTIPLIER VOLTS			J=0.00353±0.00006	

TABLE 2

SPOT No.	^{37}Ar ^{39}Ar	^{38}Ar ^{39}Ar	$^{40}\text{Ar}^*$ ^{39}Ar	AGE(ma) $\pm 1\sigma$
E52 AMPHIBOLE GRAIN 2				
Z090	3.93±0.43	0.3483±0.0208	274.4±16.5	1220±55
Z091	3.55±0.30	0.5214±0.0205	317.9±11.6	1356±37
Z093	3.66±0.29	0.4441±0.0203	272.5±13.2	1214±44
Z094	4.10±0.30	0.4029±0.0213	300.6±15.6	1303±50
Z096	3.85±0.28	0.4235±0.0100	248.7±9.4	1135±34
Z097	3.40±0.35	0.3540±0.0231	331.5±38.1	1396±112
Z099	3.64±0.35	0.3664±0.0259	298.6±19.4	1297±61
Z100	4.25±0.33	0.2835±0.0228	292.0±20	1276±64
Z102	3.66±0.30	0.3090±0.0107	274.5±11.8	1221±40
Z104	3.85±0.44	0.4442±0.0229	257.1±17.1	1163±58
Z105	3.25±0.27	0.2673±0.0147	336.7±4.44	1412±28
Z107	3.36±0.23	0.4616±0.0148	343.2±14.2	1430±43
Z108	4.28±0.46	0.2870±0.0196	315.6±21.9	1349±67
Z110	4.01±0.34	0.3669±0.0170	282.4±14.4	1246±47
Z111	3.86±0.31	0.3502±0.0183	303.2±15.3	1311±49
Z113	3.81±0.20	0.4559±0.0175	296.6±9.6	1291±32
Z114	3.65±0.22	0.3864±0.0183	259.6±12.4	1172±43
Z116	4.53±0.54	0.2940±0.0199	289.1±12.5	1267±41
Z117	3.86±0.34	0.2479±0.0228	298.0±44.3	1295±138
Z119	4.02±0.30	0.4101±0.0211	257.3±16	1164±55
Z120	4.13±0.20	0.4503±0.0152	275.4±10.6	1223±36
Z122	4.48±0.43	0.3149±0.0200	325.2±21.2	1377±64
Z123	4.25±0.26	0.3586±0.0138	338.7±18.1	1417±54
Z125	3.88±0.48	0.3867±0.0219	266.5±16.5	1194±55
Z126	3.68±0.30	0.4246±0.0150	312.9±15.7	1341±49
Z128	3.44±0.38	0.3086±0.0170	247.7±12.6	1132±44
Z129	3.94±0.31	0.2576±0.0152	303.6±18.6	1312±58
Z131	3.63±0.33	0.4656±0.0109	279.5±9	1237±31
Z132	4.89±0.30	0.2923±0.0253	349.6±28.9	1448±83
Z134	3.76±0.19	0.4589±0.0130	313.2±11.5	1341±37
Z135	3.32±0.30	0.3948±0.0157	296.3±10.6	1289±35
CORRECTED DATA IN MULTIPLIER VOLTS J=0.00353±6E-05				

TABLE 3

SPOT No.	$\frac{^{38}\text{Ar}}{^{39}\text{Ar}}$	$\frac{^{40}\text{Ar}^*}{^{39}\text{Ar}}$	AGE(ma) $\pm 1\sigma$
E5 AMPHIBOLE DATA			
d134	0.427±0.71	317.9±41.3	1326±123
d135	0.660±0.041	355.3±19.6	1433±56
d137	0.479±0.065	351.2±35.3	1421±100
d138	0.562±0.049	277.1±17.5	1201±57
d140	0.491±0.045	258.5±11.4	1141±39
d141	0.941±0.046	322.7±12	1340±38
d143	0.457±0.046	222.3±14.3	1019±51
d147	0.515±0.029	310.9±15.3	1305±48
d148	0.591±0.163	511.7±93.9	1823±211
d150	0.514±0.020	297.2±9.4	1263±32
e001	0.633±0.026	246.4±9.5	1101±34
e003	0.987±0.041	124.5±5.2	639±24
e004	1.297±0.068	373.5±19.5	1488±55
CORRECTED DATA IN MULTIPLIER VOLTS		J=0.00341±5E-05	

TABLE 4

SPOT No.	^{37}Ar ^{39}Ar	^{38}Ar ^{39}Ar	$^{40}\text{Ar}^*$ ^{39}Ar	AGE(ma) $\pm 1\sigma$
E21 PRISTINE AMPHIBOLE GRAIN 1				
b091	9.869±1.181	1.0395±0.0571	439.7±20.3	1791.9±53.8
bo92	5.205±1.421	0.6632±0.0269	138.2±6.8	772.4±31.5
bo94	1.153±0.375	0.4022±0.0143	51.8±3.6	329.2±21
bo95	5.107±0.422	0.6077±0.0158	174.9±4.1	931.9±18.5
b096	4.477±0.851	0.8376±0.0291	188.8±8.1	988.9±33.7
bo98	4.864±1.273	0.4228±0.0190	169.7±5.9	910±25.8
bo99	2.554±0.569	0.3947±0.0093	92.2±2.3	549.9±12.6
b100	6.499±0.469	0.8234±0.0199	135.1±3.7	758.3±18.2
PRISTINE AMPHIBOLE GRAIN 2				
b109 (core)	1.518±6.094	0.5482±0.1086	338.7±36.8	1509.9±111.5
b110 (edge)	4.795±0.772	0.7799±0.0186	116.7±4.7	671.6±23.5
b112 (edge)	6.880±0.807	1.0796±0.0355	96.7±4.6	572.8±24.1
SINGLE SPOT AMPHIBOLE ANALYSES				
b088 (core)	1.082±0.658	0.3445±0.0151	103.2±5.9	605.6±30.1
b113 (edge)	5.012±0.951	0.7102±0.0266	214.4±8.1	1089.1±32.1
b114 (edge)	5.325±0.428	0.6080±0.0183	183.6±4.5	967.7±19.8
b116 (whole grain)	3.201±0.166	0.4553±0.0085	110.5±1.1	641.5±7.6
b117 (whole grain)	4.693±0.228	0.6003±0.0089	142.9±1.4	793.6±9.3
b118 (whole grain)	4.256±0.325	0.6778±0.0106	120.6±1.9	690.6±10.8
b120 (fresh core)	4.132±1.843	0.6898±0.0382	244.9±11.2	1201.9±41.1
b121 (altered core)	1.341±0.267	0.4274±0.0084	113.8±1.7	657.7±10
b123 (fresh core)	3.869±1.766	0.6764±0.0602	344.7±20.3	1528±61.8
b124 (altered core)	2.754±1.211	0.7563±0.0412	64.8±8.7	403.5±48.5
BIOTITES				
b085	0.061±0.066	0.231±0.0034	8.90±0.6	60.9±3.8
bo86	0.027±0.050	0.217±0.0022	8.70±0.30	59.9±2.1
b103	0.119±0.042	0.2253±0.0025	8.80±0.20	60.1±1.8
b104	0.072±0.048	0.2308±0.0021	8.80±0.30	60.1±2.4
b105	0.177±0.023	0.2315±0.0018	8.90±0.20	61.2±1.4
FELDSPARS				
b107	6.427±0.766	0.4916±0.0284	250.9±8.2	1223.1±30.3
b108	4.422±0.374	1.091±0.0234	335.6±6.9	1500.6±23.4
CORRECTED DATA IN MULTIPLIER VOLTS J=0.003866±4E-05				

TABLE 5

SPOT No.	$\frac{^{38}\text{Ar}}{^{39}\text{Ar}}$	$\frac{^{40}\text{Ar}^*}{^{39}\text{Ar}}$	AGE(ma) $\pm 1\sigma$
E18 AMPHIBOLE DATA			
e144	1.462±0.132	284.4±24.7	1199±77
e145	1.206±0.045	185.3±7.1	865±28
e147	1.970±0.111	612±32	2001±66
e148	1.052±0.042	295.9±8.5	1235±29
e149	1.092±0.084	334±24.1	1346±70
f001	1.068±0.035	229.3±7	1021±27
f002	1.126±0.054	380±16.8	1472±47
f003	0.904±0.028	154.8±4.7	748±21
f005	1.251±0.033	193±2.2	893±22
f006	5.069±1.099	502.6±118.8	1771±267
f007	1.543±0.058	389.2±13.8	1497±39
f008	1.936±0.112	539.2±27.9	1851±62
f009	1.031±0.029	286.6±6.8	1206±25
f011	1.241±0.024	243.2±3.6	1068±17
f012	1.54±0.069	418.4±16.8	1571±45
f013	1.298±0.029	233.2±6.2	1034±24
CORRECTED DATA IN MULTIPLIER VOLTS		J=0.00332±5E-05	

TABLE 6

SPOT No.	$\frac{37}{39}\text{Ar}$	$\frac{38}{39}\text{Ar}$	$\frac{40}{39}\text{Ar}^*$	AGE(ma) $\pm 1\sigma$
E16 AMPHIBOLE GRAIN 1				
Z006	3.34±0.94	0.3325±0.0439	283.09±30.77	1248±98.7
Z010	3.79±0.45	0.4219±0.0308	303.06±11.13	1310.5±36.7
Z012	4.22±0.97	0.6352±0.1036	266.41±35.90	1194.1±118.3
Z013	2.17±1.10	1.4224±0.2106	132.71±38.38	692±166.4
Z141	3.24±0.37	0.4121±0.0370	137.87±9.050	714.2±39.6
Z143	2.68±0.46	0.5823±0.0482	198.54±16.38	956.6±62.2
Z144	3.98±0.49	0.3159±0.0287	105.14±15.80	568.5±73.6
Z146	3.32±0.37	0.3373±0.0164	137.19±5.180	711.3±23.7
Z147	4.08±0.22	0.3257±0.0219	247.32±8.260	1130.4±30.5
Z149	4.28±0.57	0.4664±0.0427	392.32±29.53	1565.8±80.2
a002	3.17±0.38	0.3966±0.0146	70.12±5.52	398.2±28.6
a003	4.61±0.28	0.2492±0.0321	46.72±1.94	274.9±11.2
a005	4.59±0.10	0.4689±0.0084	185.46±2.02	907.1±12.8
a006	5.55±0.80	0.5496±0.0446	188.28±13.58	917.9±52.9
a008	4.62±0.16	0.4894±0.0144	75.31±2.26	424.5±12.5
a009	4.68±0.56	0.2533±0.0222	44.47±7.46	262.5±41.2
a011	5.96±0.49	0.5813±0.0242	99.08±6.80	540.1±32.7
a013	4.12±0.35	0.4752±0.0162	106.08±4.33	572.8±21.2
a014	4.77±0.26	0.5085±0.0147	102.41±3.33	555.7±17
a016	4.43±0.32	0.4616±0.0205	128.29±4.57	672.7±21.5
a017	2.05±0.56	0.5361±0.0484	55.88±15.06	324.2±80.1
a019	4.29±0.21	0.4644±0.0175	110.61±4.2	593.6±20.5
a020	4.8±0.23	0.4574±0.0137	136.52±3.9	708.4±18.7
a022	4.6±0.32	0.4644±0.016	119.69±3.99	634.7±19.4
a023	3.08±0.45	0.2933±0.027	168.92±7.78	842.3±32.4
a025	4.1±0.36	0.4432±0.0195	70.66±4.4	401±23
a026	5.13±0.34	0.5814±0.0201	43.09±3.88	254.9±21.7
a031	4.52±0.58	0.6679±0.0295	156.32±7.91	791.4±33.7
a032	1.75±0.58	0.5861±0.0482	137.98±16.05	714.7±69.2
a034	4.55±0.41	0.5000±0.0171	128.62±4.53	674.2±21.4
a035	5.29±0.27	0.4389±0.018	95.39±5.17	522.7±25.4
E16 SINGLE SPOT AMPHIBOLE ANALYSES				
Z007 (ACT)	13.51±6.81	1.501±0.6250	138.7±102.3	717.6±436.9
Z015 (SH)	4.06±0.30	0.7104±0.0335	264.7±10.7	1188.6±37.3
Z016 (SH)	6.056±0.98	0.9027±0.1212	200.1±32.2	962.3±120.6
Z024 (OH)	7.02±1.61	0.4387±0.0672	320.6±31	1363.6±93.4
Z025 (M-V)	7.91±1.21	1.0003±0.1231	354.4±41.3	1461.6±117.6
Z027 (SH)	5.04±1.39	0.4211±0.0912	118.5±27.9	629.4±125.1
Z028 (SH)	8.30±1.55	0.8716±0.1354	27.9±38.8	169.3±224.5
Z030 (SH)	13.64±1.82	1.32±0.1572	51.4±34.9	300.1±187.7
Z031 (SH)	5.81±0.61	0.7368±0.060	73.9±11.8	417.6±59.6
Z033 (SH)	3.85±0.28	0.5622±0.027	95.2±6.5	521.9±31.5
Z034 (SH)	4.77±0.39	0.5406±0.0363	131.5±10.8	686.8±47.5
Z037 (OH)	3.706±0.54	0.4369±0.0251	245.9±13.4	1125.4±47.1
CORRECTED DATA IN MULTIPLIER VOLTS		J=0.003526±6E-05		
OH=ORIGINAL HORNBLENDE		SH=SECONDARY HORNBLENDE		
ACT=SECONDARY ACTINOLITE		M-V=ACTINOLITE MICROVEIN		

TABLE 7

SPOT No.	^{37}Ar ^{39}Ar	^{38}Ar ^{39}Ar	$^{40}\text{Ar}^*$ ^{39}Ar	AGE(ma) $\pm 1\sigma$
E16 SINGLE SPOT AMPHIBOLE ANALYSES (continued)				
Z038 (SH)	4.87±0.39	0.6046±0.0267	179.2±10	882.8±40.4
Z040 (ACT)	7.305±0.61	0.8983±0.0417	161.0±9.3	810.5±38.7
Z044 (OH)	4.678±0.59	0.4095±0.0414	355.2±32	1464±91.5
Z046 (OH)	5.82±1.65	0.5144±0.1096	205.±45.6	980.6±168.7
Z047 (OH)	4.68±0.36	0.5067±0.0254	224.8±9.90	1052±35.8
Z049 (SH)	6.65±0.54	0.8446±0.0584	360.7±22.4	1479.5±64.4
Z050 (OH)	3.71±1.07	0.5477±0.0612	326.2±26.4	1380.1±79.2
BIOTITES				
a028	0.00±9.0	0.2361±0.0046	30.61±1.4	184.7±8.40
a029	-0.25±0.10	0.1508±0.0038	15.02±1.27	93.0±7.8
Z018	0.003±0.087	0.2105±0.0094	10.2±2.2	63.7±
Z021	0.06±0.084	0.1917±0.0086	10.2±1.9	63.5±11.7
Z041	0.149±0.238	0.1559±0.0105	16.3±2.2	100.6±13.5
PLAGIOCLASE				
Z019	4.69±0.37	0.357±0.0191	126.5±6.9	665±31.6
Z022	3.63±0.08?	0.3794±0.0098	82.9±4.4	462.1±22.3
Z043	5.92±0.38	1.0077±0.0363	457.1±15	1731±39.9
CORRECTED DATA IN MULTIPLIER VOLTS		J=0.003526±6E-05		
OH=ORIGINAL HORNBLLENDE		SH=SECONDARY HORNBLLENDE		
ACT=SECONDARY ACTINOLITE		M-V=ACTINOLITE MICROVEIN		

TABLE 8

SPOT No.	$\frac{^{38}\text{Ar}}{^{39}\text{Ar}}$	$\frac{^{40}\text{Ar}^*}{^{39}\text{Ar}}$	AGE(ma) $\pm 1\sigma$
E15 AMPHIBOLE DATA			
e062	2.008±0.169	308.34±29.84	1501.2±99.1
e063	1.536±0.007	84.9±4.29	551.3±24.4
e064	1.162±0.036	141.82±5.25	844.6±25.8
e066	1.907±0.171	106.61±19.59	668.9±102.8
e067	0.827±0.029	385.53±9.65	1739.8±29.9
e068	0.784±0.038	248.55±8.58	1291.9±33
e070	0.871±0.042	365.70±12.85	1681.4±39.8
e071	0.800±0.034	255.46±9.57	1317.3±36.1
e072	0.562±0.047	176.71±8.10	1003.3±36
e074	1.095±0.041	121.37±5.06	744.6±26.1
e075	1.166±0.043	34.85±5.01	247±33.3
e083	0.736±0.015	18.13±0.89	132.7±6.4
e084	0.944±0.038	96.95±3.88	617.5±21.5
e085	0.863±0.037	151.07±6.17	888.1±29.4
e087	0.918±0.13	472.07±60.37	1974.4±153.9
e088	0.45±0.026	243.69±10.93	1273.8±41.9
e089	0.718±0.056	286.06±19.27	1426±67
e091	0.644±0.033	370.18±13.65	1694.8±41.9
e092	0.75±0.038	301.33±11.96	1477.8±41.2
e095	0.645±0.031	241.5±5.81	1265.5±23.5
e096	0.682±0.049	235.34±13.17	1242.2±51
e097	0.598±0.018	184.98±4.74	1039±21.6
e099	0.690±0.021	222.3±4.26	1191.7±18.7
e100	1.097±0.042	196.35±6.76	1086.9±29.2
e101	1.271±0.033	93.71±4.06	599.9±22.7
e103	0.603±0.049	152.32±8.52	893.9±40
e104	0.944±0.075	95.24±8.09	608.3±44.1
e105	1.131±0.066	160.02±10.42	929.2±47.8
e107	0.65±0.032	67.44±4.57	450.9±27.3
e108	0.674±0.036	64.26±2.51	432±15.5
e109	0.574±0.011	33±0.95	234.7±6.7
e112	1.323±0.142	115.02±17.53	712.4±89.9
e113	1.069±0.036	260.52±7.74	1335.8±29.4
e114	0.711±0.045	204.47±10.81	1120.4±44.8
e116	2.818±0.155	222.88±17.08	1194±67.5
e117	1.51±0.152	108.84±14.22	680.5±74.3
e118	0.701±0.022	156.91±4.11	915±20
e120	0.558±0.017	33.7±2.11	239.3±14.2
e121	0.632±0.027	268.07±7.22	1362.9±27.3
CORRECTED DATA IN MULTIPLIER VOLTS		J=0.00421±4E-05	

TABLE 9

SPOT No.	$\frac{^{38}\text{Ar}}{^{39}\text{Ar}}$	$\frac{^{40}\text{Ar}^*}{^{39}\text{Ar}}$	AGE(ma) $\pm 1\sigma$
E15 AMPHIBOLE DATA (cont.)			
e122	0.79±0.022	142.79±3.44	849.2±17.6
e124	0.827±0.036	213.04±6.37	1155±26.8
e125	0.723±0.052	244.95±12.23	1278.5±46.6
e127	0.695±0.036	227.87±8.21	1213.4±32.9
e128	0.45±0.011	152.66±2.49	895.4±13.3
e129	0.545±0.02	139.4±5.99	833.1±29.4
e131	0.547±0.012	70.84±1.58	470.9±10
e132	1.145±0.033	103.03±4.18	650±22.8
e133	1.152±0.041	149.59±5.73	881.2±27.5
e135	1.01±0.036	128.27±5.93	779±29.9
e136	1.086±0.036	148.07±4.4	874.1±21.6
e137	0.658±0.013	93.18±1.96	597±11.7
e139	0.863±0.012	75.28±2.12	496.7±12.9
PLAGIOCLASE			
e140	0.056±0.002	23.34±0.33	169.1±2.7
e141	0.189±0.011	82.52±2.81	538±16.5
CORRECTED DATA IN MULTIPLIER VOLTS		J=0.00421±4E-05	

BIBLIOGRAPHY

- ADAMS, C.J., BISHOP, D.G. and GABITES, J.E. 1985. K-Ar ages of a low grade progressively metamorphosed greywacke sequence, Dansey Pass, South Island, New Zealand. *J.Geol.Soc.*, **142** (2), 339-349.
- ALDRICH, L.T., DAVIS, G.L., TILTON, G.R. and WETHERILL, G.W. 1956. Radioactive ages of minerals from the Brown Derby Mine and the Quartz Creek Granite near Gunnison, Colorado. *J.Geophys.Res.*, **61**, 215-232.
- ALLEN, J.M. and GOLDIE, R. 1978. Coexisting amphiboles from the Noranda area, Quebec: extension of the actinolite-hornblende miscibility gap to iron-rich bulk compositions. *Am.Mineral.*, **63**, 205-209.
- AMIRKHANOFF, K.H.L., BARTNITSKIY, E.N., BRANDT, S.B. and VOITKEVITCH, G.V. 1959. *Dokl.Akad.Nauk.SSSR. Earth Sci.Sect.*, **126**, 394-395.
- ANDERSON, D.E. and BUCKLEY, G.R. 1973. Zoning in garnets - diffusion models. *Contrib.Mineral.Petrol.*, **40**, 87-104.
- ANDERSON, D.H. 1964. Uranium-thorium-lead ages of zircons and model lead ages of feldspars from the Saganaga, Snowbank and Giants Range Granites of northeastern Minnesota. Unpublished Ph.D. Thesis, University of Minnesota.
- ANDERSON, G.E. 1956. Copper-nickel mineralisation at the base of the Duluth Gabbro. Unpublished M.S. Thesis. University of Minnesota.
- ANDREWS, M.S. and RIPLEY, E.M. 1989. Mass Transfer and Sulphur Fixation in the contact aureole of the Duluth Complex, Dunka Road Cu-Ni Deposit Minnesota. *Can. Mineral.*, **27**, 293-310.
- APTED, M.J. and LIU, J.G. 1983. Phase relations among greenschist, epidote-amphibolite and amphibolite in a basaltic system. *Am.J.Sci.*, **283-A**, 328-354.
- BAKER, D.J., DALLMEYER, R.D. and SUTTER, J.F. 1973. Significance of differences between $^{40}\text{Ar}/^{39}\text{Ar}$ and K-Ar uplift ages of the northwesternmost Reading Prong: New York-Jersey. *Geol.Soc.Amer.Abstr. with Programs*, **5**, 540.
- BALDWIN, S.L. and HARRISON, T.M. 1989. Geochronology of blueschists from west-central Baja California and the timing of uplift in subduction complexes. *J.Geol.*, **97**, 149-163.
- BALDWIN, S.L., HARRISON, T.M. and FITZGERALD, J.D. 1990. Diffusion of ^{40}Ar in metamorphic hornblende. *Contrib.Mineral.Petrol.*, **105**, 691-703.
- BALK, R.R. and GROUT, F.F. 1934. Structural study of Snowbank Stock. *Bull.Geol.Soc.Amer.*, **45**, 621-636.
- BARKER, A.J. 1990. *Introduction to Metamorphic Textures and Microstructures*. Blackie, Glasgow, London.
- BARNES, C.G. 1987. Mineralogy of the Wooley Creek batholith, Slinkard Pluton, and related dikes. Klamath mountains Northern California. *Am.Mineral.*, **72**, 879-901.
- BARNES, V.E. 1930. Changes in hornblende at about 800°C. *Am.Mineral.*, **15**, 393.
- BARRER, R.M. 1931. *Diffusion in and through solids*. McMillan Co., New York.

- BARRER, R.M. 1978. *Zeolites and clay minerals as sorbents and molecular sieves*. Academic Press, London New York, 256-338.
- BEAR, J. 1972. *Dynamics of fluids in porous media*. American Elsevier, 764pp.
- BELL, T.H. and CUFF, C. 1989. Dissolution, solution transfer, diffusion versus fluid flow and volume loss during deformation/metamorphism. *J.Met.Geol.*, 7, 425-447.
- BENCE, A.E. and RAJAMANI, V. 1972. $^{40}\text{Ar}/^{39}\text{Ar}$ incremental heating "ages" of muscovites and biotites from a progressive metamorphic terrane. *Geol.Soc.Amer Abstr. with Programs*, 4, 449.
- BERGER, G.W. 1975. $^{40}\text{Ar}/^{39}\text{Ar}$ step heating of thermally overprinted biotite, hornblende and K-feldspar from Eldora, Colorado. *E.P.Sci.Letts.*, 26, 387-408.
- BERGER, G.W. and YORK, D. 1981. Geothermometry from $^{40}\text{Ar}/^{39}\text{Ar}$ experiments. *Geochim.Cosmochim.Acta*, 45, 795-811.
- BERGER, G.W., YORK, D. and DUNLOP, D.J. 1979. Calibration of Grenvillian palaeopoles by $^{40}\text{Ar}/^{39}\text{Ar}$ dating. *Nature*, 277, 46-48.
- BEST, M.G. 1982. *Igneous and Metamorphic Petrology*. Freeman, New York.
- BICKLE, M.J. and MCKENZIE, D. 1987. The transport of heat and matter by fluids during metamorphism. *Contrib.Mineral.Petrol.*, 95 (3), 384-392.
- BIERMANN, C. 1981. (100) deformation twins in naturally deformed amphiboles. *Nature*, 292, 821-823.
- BIERMANN, C. and VAR ROERMUND, H.L.M. 1983. Defect structures in naturally deformed clin amphiboles - A TEM study. *Tectonophysics*, 95, 267-278.
- BINNS, R.A. 1969. Hydrothermal investigations of the amphibolite-granulite facies boundary. *Spec.Publ.Geol.Soc.Australia*, 2, 341-344.
- BIRCH, F. 1950. Flow of heat in the Front Range, Colorado. *Bull.Geol.Soc.Amer.*, 61, 567-630.
- BLUNDY, J.D. 1989. The geology of the Southern Adamello Massif. Unpublished Ph.D. Thesis, University of Cambridge.
- BLUNDY, J.D. and HOLLAND, T.J.B. 1990. Calcic amphibole equilibria and a new amphibole-plagioclase geothermometer. *Contrib.Mineral.Petrol.*, 104, 208-224.
- BOTTINGA, Y. and JAVOY, M. 1973. Oxygen partitioning among the minerals in igneous and metamorphic rocks. *Rev.Geophys.Space.Phys.*, 13, 410-418.
- BRADY, J.B. 1974. Coexisting actinolite and hornblende from west-central New Hampshire. *Am.Mineral.*, 59, 529-535.
- BRADY, J.B. 1975. Reference frames and diffusion coefficients. *Am.J.Sci.*, 275, 954-983.
- BRADY, J.B. and McCALLISTER, R.H. 1983. Diffusion data for clinopyroxenes from homogenization and self diffusion experiments. *Am.Mineral.*, 68, 95-105.
- BRASAEMLE, B.L. and WEIBLEN, P.W. 1988. Estimated pressures of equilibration for granitic rocks from the Giants Range Batholith, N.E. Minnesota. *Abstract from GSA Meeting 1988*.

- BRODIE, K.H. and RUTTER, E.H. 1985. Deformation and Metamorphism of Basic Rocks. *In*: Thompson, A.B. and Rubie, D.C. (eds.) *Metamorphic Reactions, Kinetics, Textures and Deformation*. Advances in Physical Geochemistry, Vol 4. Springer-Verlag, New York.
- BROPHY, J.H., ROSE, R.M. and WULFF, J. 1964. *The structure and properties of materials (Vol II). Thermodynamics of structure*. J.Wiley & Sons Inc., New York.
- BUENING, D.K. and BUSECK, P.R. 1973. Fe-Mg Lattice Diffusion in Olivine. *J.Geophys.Res.*, **78**, 6852-6862.
- BURGESS, R., KELLY, S.P., PARSONS, I., WALKER, F.D.L., and WORDEN, R.H. (in press). $^{40}\text{Ar}/^{39}\text{Ar}$ analysis of perthite microtextures and fluid inclusions in alkali feldspars from the Klokken Syenite, South Greenland. *E.P.Sci.Letts*.
- BUSECK, P.R., NORAL, G.L.Jr. and VEBLEN, D.R. 1980. Subsolidus phenomena in pyroxenes. *In*: C.J.Prewitt (ed.) *Pyroxenes, Reviews in Mineralogy Vol.7.*, *Min.Soc.Amer.*, 117-211.
- CARSLAW, H.S. and JAEGER, J.C. 1959. *Conduction of heat in solids*. Oxford, Clarendon Press.
- CARTER, N.L. and RALEIGH, C.B. 1969. Principal stress directions from plastic flow in crystals. *Geol.Soc.Amer.Bull.*, **80**, 1231-1264.
- CATHLES, L.M. 1977. An analysis of the cooling of intrusives by ground-water convection which includes boiling. *Econ.Geol.*, **72**, 804-826.
- CHAKRABORTY, S. and GANGULY, J. 1990. Compositional zoning and cation diffusion in garnets. *In*: J.Ganguly (ed.) *Diffusion, atomic ordering and mass transport : Selected Problems in Geochemistry*. Springer-Verlag.
- CHALOKWU, C.I. and GRANT, N.K. 1987. Reequilibration of olivine with trapped liquid in the Duluth Complex, Minnesota. *Geology*, **15**, 71-74.
- CHALOKWU, C.I. and GRANT, N.K. 1990. Petrology of the Partridge River Intrusion, Duluth Complex, Minnesota : 1. Relationship between Mineral Compositions, Density and Trapped Liquid Abundance. *J.Petrol.*, **31**, 265.
- CHAN *et.al.* 1970. Natural convection in enclosed porous media with rectangular boundaries. *J.Heat.Tran.*, **92**, 21-27.
- CHAO, E.C.T. 1967. Shock effects in certain rock forming minerals. *Science*, **156**, 192-202.
- CHIVAS, A.R. 1978. Porphyry Copper Mineralization at the Koloua Igneous Complex, Guadalcanal, Soloman Islands. *Econ.Geol.*, **73**, 645-677.
- CHIVAS, A.R. 1981. Geochemical evidence for magmatic fluids in porphyry copper mineralization Part I. Mafic silicates from the Kolanula Igneous Complex. *Contrib.Mineral.Petrol.*, **78**, 389-403.
- CLIFF, R.A. 1985. Isotopic dating in metamorphic belts. *J.Geol.Soc.*, **142**, 97-110.
- CLOWE, C.A., POPP, R.K. and FRITZ, S.J. 1988. Experimental investigation of the effect of oxygen fugacity on ferric-ferrous ratios and unit-cell parameters of four natural clin amphiboles. *Am.Mineral.*, **73**, 487-499.
- COMPTON, R.R. 1958. Significance of amphibole paragenesis in the Bidwell Bar region, California. *Am.Mineral.*, **43**, 890-907.

- COOPER, A.F. 1972. Progressive metamorphism of metabasic rocks from the Haast Schist Group of Southern New Zealand. *J.Petrol.*, **13**, 457-492.
- COOPER, A.F. and LOVERING, J.F. 1970. Greenschist amphiboles from Haast River, New Zealand. *Contrib.Mineral.Petrol.*, **27**, 11-24.
- COOPER, A.J.Jr. 1968. The use and limitations of the concept of an effective binary diffusion coefficient for multi-component diffusion. In: J.B. Wachtman Jr and A.D. Franklin (eds.) *Mass transport in oxides* p79-84. National Bureau of Standards Spec.Publ., 296. U.S. Government Printing Office, Washington D.C.
- COOPER, J.A. 1963. The flame photometric determination of potassium in geological materials used for potassium-argon dating. *Geochim.Cosmochim.Acta*, **27**, 525-46.
- COX, K.G., PRICE, N.B. and HARTE, B. 1974. *A practical study of Crystals, Minerals and Rocks*. McGraw-Hill, London.
- CRANK, J. 1975. *The mathematics of diffusion*. Oxford Press.
- CREE, A. 1948. Tertiary intrusives in the Hessie-Tolland area, Boulder and Gilpin Counties, Colorado. Unpublished Ph.D. Thesis, University of Colorado, Chronic Catalogue number 2046, Denver, Colorado.
- CUMBEST, R.J., DURY, M.R., VAN ROERMUND, H.L.M. and SIMPSON, C. 1989. Dynamic recrystallisation and chemical evolution of clinoamphibole from Senja, Norway. *Contrib.Mineral.Petrol.*, **101**, 339-349.
- CYGAN, R.T. and LASAGA, A.C. 1982. Crystal growth and the formation of chemical zoning in garnets. *Contrib.Mineral.Petrol.*, **79**, 187-200.
- CZAMANSKE, G.K. and WONES, D.R. 1973. Oxidation during magmatic differentiation Finnmarka Complex, Oslo area Norway: Part 2, The mafic silicates. *J.Petrol.*, **14**, 349-380.
- DALLMEYER, R.C. 1975. $^{39}\text{Ar}/^{40}\text{Ar}$ ages of biotites and hornblendes from a prograde re-metamorphosed basement terrain : their bearing on the interpretation of release spectra. *Geochim.Cosmochim.Acta*, **39**, 1655-69.
- DALLMEYER, R.D. 1974. $^{40}\text{Ar}/^{39}\text{Ar}$ incremental release ages of biotite and hornblende from Pre-Kenoran gneisses between the Matagami-Chibougamau and Frotet-Troilus greenstone belts, Quebec. *Can.J.Earth.Sci.*, **11**, 1586-1593.
- DALLMEYER, R.D. 1974. Metamorphic history of the n-e Reading Prong, New York and northern New Jersey. *J.Petrol.*, **15**, 325-359.
- DALLMEYER, R.D. 1975. Incremental $^{40}\text{Ar}/^{39}\text{Ar}$ ages of biotite and hornblende from retrograded basement gneisses of the southern Blue Ridge: their bearing on the age of Palaeozoic metamorphism. *Am.J.Sci.*, **275**, 444-460.
- DALLMEYER, R.D. 1975. Incremental $^{40}\text{Ar}/^{39}\text{Ar}$ ages of biotite from the Cherokee Ore body, Ducktown, Tennessee : their bearing on the age of sulphide mineralization. *Econ.Geol.*, **70**, 341-345.
- DALLMEYER, R.D., BAKER, D.J. and SUTTER, J.F. 1974. $^{40}\text{Ar}/^{39}\text{Ar}$ incremental ages of biotite and hornblende from retrograded Grenville gneisses of the ne Reading Prong, New York. *Geol.Soc.Amer.Abstr. with Programs*, **6**, 703-704.
- DALRYMPLE, G.B. and LANPHERE, M.A. 1969. *Potassium-argon dating*. W.H. Freeman, San Francisco, 258pp.

- DALRYMPLE, G.B. and LANPHERE, M.A. 1971. $^{40}\text{Ar}/^{39}\text{Ar}$ technique of K/Ar dating: A comparison with the conventional technique. *E.P.Sci.Letts.*, **12**, 300-308.
- DAVIS, G.L., TILTON, G.R., ALDRICH, L.T., HART, S.R., STEIGER, R.H. and KOUVO, O. 1962. The ages of rocks and minerals. *Carnegie Inst. Washington Yearb.*, **62**, 218-229.
- DAVIS, G.L., TILTON, G.R., DOE, B.R., ALDRICH, L.T., and HART, S.R. 1960. Ages of rocks and minerals. *Carnegie Inst. Washington Yearb.*, **60**, 190-199.
- DEL MORO, A. et.al. 1982. Rb-Sr and K-Ar ages on minerals at temperatures of 300-400°C from deep wells in the Lardarello geothermal field. *Contrib.Mineral.Petrol.*, **81**, 340-349.
- DEMPSTER, T.J. 1985. Garnet zoning and metamorphism of the Barrovian type area, Scotland. *Contrib.Mineral.Petrol.*, **89**, 30-38.
- DENNIS, P.F. 1984. Oxygen self diffusion in quartz under hydrothermal conditions. *J.Geophys. Res.*, **89**, 4047-4057.
- DEWEY, J.F. and PANKHURST, R.P. 1970. The evolution of the Scottish Caledonides in relation to their radiometric age patterns. *Trans.R.Soc.Edinburgh*, **68**, 361-89.
- DODSON, M.H. 1973. Closure temperatures in cooling geochronological and petrological systems. *Contrib.Min.Petrol.*, **40**, 259.
- DODSON, M.H. 1976. Kinetic processes and thermal history of slowly cooling solids. *Nature*, **259**, 551.
- DODSON, M.H. 1979. Theory of Cooling Ages. In : Jager, E. and Hunziker, J.C. (eds.) *Lectures in Isotope Geology*. Springer-Verlag, Berlin Heidelberg.
- DODSON, M.H. 1986. Closure profiles in cooling systems. *Materials Science Forum*, **7**, 145-154.
- DODSON, M.H. and McCLELLAND-BROWN, E. 1985. Isotopic and palaeomagnetic evidence for rates of cooling, uplift and erosion. In: Snelling, N.J. (ed.) *Chronology and the Geological Record*. Spec.Publ.Geol.Soc.Lond.
- DOE, B.R. and HART, S.R. 1963. The effect of contact metamorphism on lead in potassium feldspars near the Eldora Stock, Colorado. *J.Geophys.Res.*, **68**, 3521.
- DOLLINGER, G. and BLACIC, J.D. 1975. Deformation mechanisms in experimentally and naturally deformed amphiboles. *E.P.Sci.Letts.*, **26**, 409-416.
- ELIAS, E.M., MACINTYRE, R.M. and LEAKE, B.E. 1988. The cooling history of Connemara, western Ireland, from K-Ar and Rb-Sr age studies. *J.Geol.Soc.*, **145**, 649-660.
- ELPHICK, S.C. and GRAHAM, C.M. 1988. The effects of hydrogen on oxygen diffusion in quartz : evidence for fast proton transients ? *Nature*, **335**, 243.
- ELPHICK, S.C., DENNIS, P.F. and GRAHAM, C.M. 1986. An experimental study of the diffusion of oxygen in quartz and albite using an overgrowth technique. *Contrib.Mineral.Petrol.*, **92**, 322-330.
- ELPHICK, S.C., GANGULY, J., and LOOMIS, T.P. 1981. Experimental study of Fe-Mg interdiffusion in aluminosilicate garnet. *Trans.Am.Geophys.Union (Eos)*, **62**, 411.
- ELPHICK, S.C., GANGULY, J., and LOOMIS, T.P. 1985. Experimental determination of cation diffusivities in aluminosilicate garnets. I. Experimental methods and interdiffusion data. *Contrib.Mineral.Petrol.*, **90**, 36-44.

- ELPHICK, S.C., GRAHAM, C.M. and DENNIS, P.F. 1988. An ion microprobe study of anhydrous oxygen diffusion in anorthite: a comparison with hydrothermal data and some geological implications. *Contrib.Mineral.Petrol.*, **100**, 490-495.
- ELPHICK, S.C., GRAHAM, C.M., WALKER, F.D.L., and HOLNESS, M.B. 1991. The application of SIMS ion imaging techniques in the experimental study of fluid-mineral interactions. *Min.Mag.*, **55**, 347-356.
- ENGLAND, P.C. and RICHARDSON, S.W. 1977. The influence of erosion upon the mineral facies of rocks from different metamorphic environments. *J.Geol.Soc.*, **134**, 201-213.
- ERNST, W.G. 1960. Diabase-Granophyre Relations in the Endion Sill, Duluth, Minnesota. *J.Petrol.*, **1** (3), 286-303.
- ERNST, W.G. and WAI, C.M. 1970. Mossbauer, infrared, x-ray and optical study of cation ordering and de-hydrogenation in natural and heat-treated sodic amphiboles. *Am.Mineral.*, **55**, 1226-1258.
- EVERNDEN, J.F., CURTIS, G.H., KISTLER, P.W. and OBRADOVICH, J. 1960. Argon diffusion in glauconite, microcline, sanidine, leucite and phlogophite. *Am.J.Sci.*, **258**, 583-604.
- FARVER, J.R. and GILETTI, B.J. 1985. O Diffusion in Amphiboles. *Geochim.Cosmochim.Acta*, **49**, 1403-1411.
- FAURE, G. 1986. *Principles of Isotope Geology*. Wiley and Sons, New York.
- FAURE, G., CHAUDHURI, S. and FENTON, M.D. 1969. Ages of the Duluth Gabbro Complex and of the Endion Sill, Duluth, Minnesota. *J.Geophys.Res.*, **74** (2), 720-725.
- FECHTIG, H., GENTNER, W. and ZHRINGER, J. 1960. Argon Bestimmungen an Kaliummineralien-vii: Diffusion-verluste von Argon in Mineralien und ihre Auswirkung auf die Kalium-Argon-Alterbestimmung. *Geochim.Cosmochim.Acta*, **19**, 70-79.
- FEDKIN, V.V. 1986. Chemical inhomogeneity in minerals and evolution of metamorphism. In: Borrev, I. and Korozirski, M. (eds) *Morphology and phase equilibria of minerals*, 323-332.
- FERNANDEZ-MORON, H. et.al. 1971. Correlated electron-microscopy and diffraction of lunar clinopyroxene from Apollo 12 samples. *Proc.2nd.Lunar Sci.Confr.*, **1**, 109-116.
- FERRY, J.M. 1980. A case study of the amount and distribution of heat and fluid during metamorphism. *Contrib.Mineral.Petrol.*, **71**, 373-385.
- FERRY, J.M. and DIPPLE, G.M. 1991. Fluid Flow, Mineral Reactions and Metasomatism. *Geology*, **19**, 211-214.
- FINLAY, L.A. and KERR, A. 1979. Garnet growth in a metapelite from the Moinian rocks of northern Sutherland, Scotland. *Contrib.Mineral.Petrol.*, **71**, 185-191.
- FORTIER, S.M. and GILETTI, B.J. 1991. Volume self diffusion of oxygen in biotite, muscovite and phlogophite micas. *Geochim.Cosmochim.Acta*, **55**, 1319-1330.
- FREER, R. 1979 An experimental measurement of cation diffusion in almandine garnet. *Nature*, **280**, 220-222.
- FREER, R. 1980. Self-diffusion and impurity diffusion in oxides. *J.Mater.Sci.*, **15**, 803-824.
- FREER, R. 1981. Diffusion in silicate minerals and glasses : A Data Digest and Guide to the Literature. *Contrib.Mineral.Petrol.*, **76**, 440-454.

- FREER, R. and DENNIS, P.F. 1982. Oxygen diffusion studies I. A preliminary ion microprobe investigation of oxygen in some rock-forming minerals. *Min.Mag.*, **45**, 179-192.
- FREER, R., CARPENTER, M.A., LONG, J.V.P. and REED, S.J.B. 1982. 'Null result' diffusion experiments with diopsides : implications for pyroxene equilibria. *E.P.Sci.Letts.*, **58**, 285-292.
- FRITZ, S.J. and POPP, R.K. 1985. A single dissolution technique for determining FeO and Fe₂O₃ in rock and mineral samples. *Am.Mineral.*, **70**, 961-968.
- GABER, L.J., FOLAND, K.A. and CORBATO, C.E. 1988. On the significance of argon release from biotite and amphibole during ⁴⁰Ar/³⁹Ar vacuum heating. *Geochim.Cosmochim.Acta*, **52**, 2457-2465.
- GABLE, D.J. 1969. Geologic map of the Nederland Quadrangle, Boulder and Gilpin Counties, Colorado. *U.S. Geological Survey*, Washington D.C.
- GANGULY, J. 1979. Garnet and clinopyroxene solid solutions and geothermometry based on Fe-Mg distribution coefficients. *J.Petrol.*, **43**, 1021-9.
- GANGULY, J., BHATTACHARYA, R.N. and CHAKRABORTY, S. 1988. Convolution effect in the determination of compositional profiles and diffusion coefficients by microprobe step scans. *Am.Mineral.*, **73**, 901-909.
- GAST, P.W. and LONG, L.E. 1957. Absolute age determinations from the basement rocks of the Beartooth Mountains and Bighorn Mountains. *Geol.Soc.Am.Bull.Abst.*, **68**, 1732-1733.
- GAST, P.W., KULP, J.L. and LONG, L.E. 1958. Age of early PreCambrian rocks in the Bighorn Basin of Wyoming and Montana and Southeastern Manitoba. *Trans.Am.Geophys.Union.* **39**, 323-334.
- GAVASCI, A.T. 1973. Investigations on deformation in amphibole and amphibole-bearing xenoliths from the Kimberlite-bearing diatremes on the Colorado Plateau. *Air Force Cambridge Research Lab. Final Contract Rep. AFCRL-TR-73-0765*, 1-12.
- GERLING, E.K., KOL'TSOVA, T.V., PETROV, B.V. and ZUL'FIKAROVA, Z.K. 1965. On the suitability of amphiboles for age determination by the K-Ar method. *Geochem.Int.*, 148-154.
- GILBERT, M.C., HELZ, R.T., POPP, P.K. and SPEAR, F.S. 1982. Experimental studies of amphibole stability. In: Veblen, D.R. and Ribbe, P.H. (eds.) *Amphiboles: Petrology and Experimental Phase Relations. Reviews in Mineralogy Vol.9B*, Min.Soc.Am., 229-353.
- GILETTI, B.J. 1974(a). Diffusion related to geochronology In : Hofmann, A.W. et.al. (eds) 1974. *Geochemical Transport and Kinetics*. Carnegie Institution of Washington Publication 634.
- GILETTI, B.J. 1974(b). Studies in diffusion I: Argon in phlogophite mica. In: Hofman, A.W., Giletti, B.J., Yoder, H.S. Jr and Yund, R.A. (eds.) *Geochemical transport and kinetics*. Carnegie Institution of Washington Publication 634, 107-115.
- GILETTI, B.J. 1986. Diffusion effects on oxygen isotope temperatures of slowly cooled igneous and metamorphic rocks. *E.P.Sci.Letts.*, **77**, 218-228.
- GILETTI, B.J. 1991. Rb and Sr diffusion in alkali feldspars with implications for cooling histories of rocks. *Geochim.Cosmochim.Acta*, **55**, 1331-1343.
- GILETTI, B.J. SEMET, M.P., and YUND, R.A. 1978. Studies in diffusion III : Oxygen in feldspars : an ion microprobe determination. *Geochim.Cosmochim.Acta*, **42**, 45-57.
- GILETT, B.J. and YUND, R.A. 1984. Oxygen diffusion in quartz. *J.Geophys.Res.*, **89**, 4039-4046.

- GITTO, M.F., LORIMER, G.W. and CHAMPNESS, P.E. 1974. An electron-microscopic study of precipitation (exsolution) in an amphibole (the hornblende-grunerite system). *J.Mater.Sci.*, **9**, 184-192.
- GITTO, M.F., LORIMER, G.W. and CHAMPNESS, P.E. 1976. The phase distributions in some exsolved amphiboles. *In*: Wenk, H.R. (ed.) *Electron Microscopy in Mineralogy*, 238-247. Springer-Verlag, Berlin.
- GOLDICH, S.S. 1968. Geochronology in the Lake Superior region. *Can.J Earth Sci*, **5**, 715.
- GOLDICH, S.S., NIER, A.O., BAADSGAARD, H., HOFFMAN, J.H. and KRUEGER, H.W. 1961. The PreCambrian geology and geochronology of Minnesota. *Minn.Geol.Surv.Bull.*, **41**.
- GOLDSTEIN, J.I. and SHORT, J.U. 1967. Cooling rates of 27 iron and stony-iron meteorites. *Geochim.Cosmochim.Acta*, **31**, 1001-1023.
- GRAHAM, C.M. 1974. Metabasite amphiboles of the Scottish Dalradian. *Contrib.Mineral.Petrol.*, **47**, 165-185.
- GRAHAM, C.M. 1981. Experimental Hydrogen Isotope Studies III : diffusion of hydrogen in hydrous minerals, and stable isotope exchange in metamorphic rocks. *Contrib.Mineral.Petrol.*, **76**, 216-228.
- GRAHAM, C.M. and ELPHICK, S.C. 1990. Some experimental constraints on the role of oxygen and hydrogen diffusion and Al-Si interdiffusion in silicates. *In*: Ganguly, J. (ed.) *Diffusion , Atomic Ordering and Mass Transport, Advances in Physical Geochemistry, Vol 8*. Springer-Verlag, New York.
- GRAHAM, C.M. and NAVROTSKY, A. 1986. Thermochemistry of the tremolite-edenite amphiboles using Fluorine analogues, and applications to amphibole-plagioclase-quartz equilibria. *Contrib.Mineral.Petrol.*, **93**, 18-32.
- GRAHAM, C.M. and POWELL, R. 1984. A garnet-hornblende geothermometer: calibration, testing and application to the Pelona Schist, S.California. *E.P.Sci.Letts.*, **31**, 142-152.
- GRAHAM, C.M. *et.al.* 1984. Experimental H-isotope studies : hydrogen isotope exchange between amphibole and water. *Am.Mineral.*, **69**, 128-138.
- GRAHAM, C.M., MARESCH, W.V., WELCH, M.D. and PAWLEY, A.R. 1989. Experimental studies on amphiboles : a review with thermodynamic perspectives. *European Journal of Mineralogy*, **1**, 535-555.
- GRAPES, R.H. 1975. Actinolite-hornblende pairs in metamorphosed gabbros, Hidaka Mountains, Hokkaido. *Contrib.Mineral.Petrol.*, **49**, 125-140.
- GRAPES, R.H. 1977. Chemical inhomogeneity of amphiboles in relation to section orientation in routine EPMA analysis. *Geochem.J.*, **11**, 253-255.
- GRAPES, R.H. and GRAHAM, C.M. 1978. The actinolite-hornblende series in metabasites and the so-called miscibility gap: a review. *Lithos*, **11**, 85-97.
- GRAPES, R.H., HASHIMOTO, S. and MIYASHIA, S. 1977. Amphiboles of a Metagabbro-Amphibolite Sequence, Hidaka Metamorphic Belt, Hokkaido. *J.Petrol.*, **18**, 285-318.
- GREEN, J.C. 1970. Lower Precambrian Rocks of the Gabbro Lake Quadrangle, N.E. Minnesota. *Minnesota Geological Survey, Special Publication*, **13**, 69pp.

- GREEN, J.C., PHINNEY, W.C. and WEIBLEN, P.W. 1966. Gabbro Lake Quadrangle, Lake County, Minnesota. Miscellaneous Map Series, Map M2, Minnesota Geological Survey.
- GREEN, T.H. and PEARSON, N.J. 1985. Experimental determination of R.E.E. partition coefficients between amphibole and basaltic to andesitic liquids at high pressure. *Geochim.Cosmochim.Acta*, **49**, 1465-1468.
- GREENWOOD, H.J. 1979. Thermodynamic properties of edenite. *In*: Current Research, Part B, *Geol.Surv.Canada Paper 79-1B*, 365-370.
- GROUT, F.F. 1918. The lopolith; an igneous form exemplified by the Duluth Gabbro. *Am.J.Sci.*, **46**, 516-522.
- GRUNER, J.W. 1941. Structural geology of the Knife area of northeastern Minnesota. *Bull.Geol.Soc.Amer.*, **52**, 1577-1642.
- HACKER, B.R. and CHRISTIE, J.M. 1991. Observational evidence for a possible new diffusion path. *Science*, **251**, 67-70.
- HALLIMOND, A.F. 1943. On the graphical representation of calciferous amphiboles. *Am.Mineral.*, **28**, 65-89.
- HAMMARSTROM, J.M. and ZEN, E-AN. 1986. Aluminium in hornblende : An empirical igneous geobarometer. *Am.Mineral.*, **71**, 1297-1313.
- HANSON, G. 1968. K-Ar ages for hornblende from granites and gneisses and for basaltic intrusives in Minnesota. *Minnesota.Geol.Surv.Rep.Of Investigations*, **8**, 20pp.
- HANSON, G.N. and GAST, P.W. 1967. Kinetic Studies in Contact Metamorphic Zones. *Geochim.Cosmochim.Acta*, **31**, 1119-1153.
- HANSON, G.N., CATANZARO, E.J and ANDERSON, D.H. 1971. U-Pb Ages for Sphene in a Contact Metamorphic Zone. *E.P.Sci.Letts.*, **12**, 231-237.
- HANSON, G.S., SIMMONS, K.R. and BENCE, A.E. 1975. $^{40}\text{Ar}/^{39}\text{Ar}$ spectrum ages for biotite, hornblende and muscovite in a contact metamorphic zone. *Geochim.Cosmochim.Acta*, **39**, 1269-1277.
- HARPER, C. 1967. The geological interpretation of potassium-argon ages of metamorphic rocks from the Scottish Caledonides. *Scott.J.Geol.*, **3**, 46-66.
- HARRIS, R.L.Jr. 1959. Geological evolution of the Beartooth Mountains, Montana and Wyoming. *Bull.Geol.Soc.Amer.*, **70**, 1185-1216.
- HARRISON, T.M. 1981. Diffusion of ^{40}Ar in Hornblende. *Contrib.Mineral.Petrol.*, **78**, 324-331.
- HARRISON, T.M. and CLARKE, G.K.C. 1979. A model of igneous intrusion and uplift as applied to Quottoon Pluton, British Columbia. *Can.J.Earth.Sci.*, **16**, 411-420.
- HARRISON, T.M. and FITZGERALD, J.D. 1986. Exsolution in hornblende and its consequences for $^{40}\text{Ar}/^{39}\text{Ar}$ age spectra and closure temperatures. *Geochim.Cosmochim.Acta*, **50**, 247-253.
- HARRISON, T.M. and McDUGALL, I. 1980a. Investigations of an intrusive contact, Northwest Nelson, New Zealand - I Thermal, Chronological and Isotopic Constraints. *Geochim.Cosmochim.Acta*, **44**, 1985-2003.

- HARRISON, T.M. and McDOUGALL, I. 1980b. Investigations of an intrusive contact, Northwest Nelson, New Zealand - II Diffusion of radiogenic and excess ^{40}Ar in hornblende revealed by $^{40}\text{Ar}/^{39}\text{Ar}$ spectrum analysis. *Geochim.Cosmochim.Acta*, **44**, 2005-2020.
- HARRISON, T.M. and McDOUGALL, I. 1981. Excess ^{40}Ar in metamorphic rocks from Broken Hill, New South Wales : Implications for $^{40}\text{Ar}/^{39}\text{Ar}$ age spectra and the thermal history of the region. *E.P.Sci.Letts.*, **55**, 123-149.
- HARRISON, T.M. and McDOUGALL, I. 1982. The thermal significance of K-feldspar K-Ar ages inferred from $^{40}\text{Ar}/^{39}\text{Ar}$ age spectrum results. *Geochim.Cosmochim.Acta*, **46**, 1811-1820.
- HARRISON, T.M., ARMSTRONG, R.L., NAESER, C.W. and HAKAL, J.E. 1979. Geochronology and thermal history of the coast plutonic complex near Prince Rupert, British Columbia. *Can.J.Earth.Sci.*, **16**, 400-410.
- HARRISON, T.M., DUNCAN, I.J. and McDOUGALL, I. 1985. Diffusion of ^{40}Ar in Biotite: Temperature, pressure and compositional effects. *Geochim.Cosmochim.Acta*, **49**, 2461-2468.
- HART, E.W. 1957. On the rate of dislocations in bulk diffusion. *Acta Metallurgica*, **5**, 597.
- HART, S.R. 1961. A study of mineral ages in a contact metamorphic zone (abstract). *J.Geophys.Res*, **66**, 2533.
- HART, S.R. 1964. The petrology and isotopic-mineral age relations of a contact zone in the Front Range, Colorado. *J.Geol.*, **72**, 493-525.
- HART, S.R. 1981. Diffusion compensation in natural silicates. *Geochim.Cosmochim.Acta*, **45**, 279-291.
- HART, S.R., DAVIS, G.L., STEIGER, R.H. and TILTON, G.R. 1969. Isotopic mineral age variations and petrologic changes. In: Hamilton, E.I. and Farquhar, R.H. (eds.) *Radiometric dating for geologists*. Interscience Publishers, London, New York, Sydney.
- HARTE, B. 1977. Rock Nomenclature with particular relation to deformation and recrystallisation textures in olivine-bearing xenoliths. *J.Geol.*, **85**, 279-288.
- HARTE, B. and GRAHAM, C.M. 1975. The graphical analysis of Greenschist to Amphibolite facies mineralogical assemblages in metabasites. *J.Petrol.*, **16**, 347.
- HARTE, B. and HENLEY, K.J. 1966. Occurrence of compositionally zoned almanditic garnets in regionally metamorphosed rocks. *Nature*, **210**, 689-692.
- HAWTHORNE, F.C. 1981. Crystal chemistry of the Amphiboles. In: Veblen, D. (ed.) *Amphiboles and other hydrous pyriboles - Mineralogy. Reviews in Mineralogy Vol.9A*, Min.Soc.Am.
- HAWTHORNE, F.C. 1983. Quantitative characterisation of site occupancies in minerals. *Am.Mineral.*, **68**, 287-306.
- HAWTHORNE, F.C. 1983. The crystal chemistry of the Amphiboles. *Can.Mineral.*, **21**, 173-480.
- HAWTHORNE, F.C. and GRUNDY 1973. The crystal chemistry of the amphiboles: I:Refinement of the crystal structure of ferrotschermakite. *Min.Mag.*, **39**, 36-48.
- HAYNES, A. 1982. A comparison of Amphiboles from Medium- and Low-Pressure Metabasites. *Contrib.Mineral.Petrol.*, **81**, 119-125.
- HELTZ, R.T. 1982. Phase relations and compositions of amphiboles produced in studies of the melting behaviour of rocks. *Min.Soc.Amer.Reviews In Mineralogy Vol.9B*, 279-346.

- HENDRY, D.A.F., CHIVAS, A.R., LONG, J.V.P. and REED, S.J.B. 1985. Chemical difference between minerals from mineralizing and barren intrusions from some North American porphyry copper deposits. *Contrib.Mineral.Petrol.*, **89**, 317-329.
- HIETANEN, A. 1974. Amphibole Pairs, Epidote Minerals, Chlorite and Plagioclase in Metamorphic Rocks, Northern Sierra Nevada, California. *Am.Mineral.*, **59**, 22-40.
- HOFMAN, A.W. 1980. Diffusion in silicate melts : A critical review. *In*: Hargraves, R.B. (ed.) *Physics of magmatic processes*. Princeton Univ.Press, Princeton, New Jersey, 385-417.
- HOFMANN, A.W. and HART, S.R. 1978. An assessment of local and regional isopopic equilibrium in the mantle. *E.P.Sci.Letts.*, **38**, 44-62.
- HOFMANN, A.W., GILETTI, B.J., YODER, H.S.Jr. and YUND, R.A. 1974. *Geochemical Transport and Kinetics*. Carnegie Institution of Washington Publication 634.
- HOLLAND, T.J.B. and POWELL, R. 1990. An enlarged and updated internally consistent thermodynamic data set with uncertainties and correlations: the system $K_2O-Na_2O-CaO-MgO-MnO-FeO-Fe_2O_3-Al_2O_3-TiO_2-SiO_2-C-H_2O-O_2$. *J.Met.Geol.*, **8**, 89-124.
- HOLLAND, T.J.B., and RICHARDSON, S.W. 1979. Amphibole zonation in metabasites as a guide to the evolution of metamorphic conditions. *Contrib.Mineral.Petrol.*, **70**, 143-148.
- HOLLISTER, L.S. 1966. Garnet zoning: An interpretation based on the Rayleigh fractionation model. *Science*, **154**, 1647-1651.
- HOLLISTER, L.S., GRISSOM, G.C., STOWELL, H.H., and SISSON, V.B. 1987. Confirmation of the empirical correlation of Al in hornblende with pressure of solidification of calc-alkaline plutons. *Am.Mineral.*, **72**, 231-239.
- HOLLOWAY, J.R. 1973. The system pargasite-H₂O-CO₂ : a model for melting of a hydrous mineral with a mixed-volatile fluid. I : Experimental results to 8Kbar. *Geochim.Cosmochim.Acta*, **37**, 651-666.
- HUEBNER, J.S. and NORD, G.L. Jnr. 1981. Assessment of diffusion in pyroxenes : What we do and do not know. *Lunar.Planet.Sci.*, **12**, 479-481.
- HUEBNER, J.S., ROSS, M. and HICKLING, N. 1975. Significance of exsolved pyroxenes from lunar breccia 77215. *Proc.Lunar.Sci.Conf.6th.*, 529-546.
- HUTCHISON, . 1970. Metamorphic framework and plutonic styles in the Prince Rupert region of the Central Coast Mountains, British Columbia. *Can.J.Earth.Sci.*, **7**, 376-405.
- JAEGER, J.C. 1959. Temperatures outside a cooling intrusive sheet. *Am.J.Sci.*, **257**, 44-54.
- JAGER, E. NIGGLI, E. and WENK, E. 1967. Rb-Sr Altersbestimmungen an Glimmern der Zentralalpen. Beitrage zur Geol. Karte der Schweiz. Neue Folge, 134. Lieferungen.
- JAIN, S.C. 1958. Simple solution of the partial differential equation for diffusion (or heat conduction). *Proc.R.Soc.Lond.*, **243**, 359-374.
- JAVOY, M. 1977. Stable isotopes and geothermometry. *J.Geol.Soc.*, **133**, 609-636.
- JENKINS, D.M. 1988. Experimental study of the join tremolite-tschermakite: A reinvestigation. *Contrib.Mineral.Petrol.*, **99**, 392-400.

- JOESTEN, R. 1990. Diffusion Kinetics in Polycrystalline Silicate and Oxide Minerals. *In*: Ganguly, J. (ed.) *Diffusion, Atomic Ordering and Mass Transport*, Advances in Physical Geochemistry, Vol 8. Springer-Verlag, New York
- JOHNSON, M.C. and RUTHERFORD, M.J. 1988. Experimental calibration of an Aluminium-in-Hornblende geobarometer applicable to calc-alkaline rocks. *Eos*, **69**, 1511.
- JOHNSON, M.C. and RUTHERFORD, M.J. 1989. Experimental calibration of the aluminium-in-hornblende geobarometer with application to Long Valley Caldera (California) volcanic rocks. *Geology*, **17**, 837-841.
- JOST, W. 1952. *Diffusion in solids, liquids and gases*. Academic Press, New York.
- KELLY, S. (in press). Laser probe ^{40}Ar - ^{39}Ar age profiles across single hornblende grains from the Giants Range Granite, N.E Minnesota, U.S.A.
- KELLY, S., TURNER, G., BUTTERFIELD, A.W., and SHEPHERD, T.J. 1986. The source and significance of argon isotopes in fluid inclusions from areas of mineralization. *E.P.Sci.Letts.*, **79**, 303-318.
- KIMBALL, K.L. 1988. High-temperature hydrothermal alteration of ultramafic cumulates from the base of the sheeted dikes in the Josephine ophiolite, NW California. *J.Geophys.Res.*, **93**, 4675-4687.
- KINGERY, W.D. 1960. *Introduction to ceramics*. J.Wiley & Sons Inc., New York.
- KLEIN, C. Jr. 1969. Two-amphibole assemblages in the system actinolite-hornblende-glaucophane. *Am.Mineral.*, **54**, 212-237.
- LABOTKA, T.C., WHITE, C.E. and PAPIKE, J.J. 1984. The evolution of water in the contact-metamorphic aureole of the Duluth Complex, N.E. Minnesota. *Bull.Geol.Soc.Amer.*, **95**, 788-804.
- LAIRD, J. and ALBEE, A.L. 1981. High Pressure metamorphism in mafic schist from Northern Vermont. *Am.J.Sci.*, **281**, 97-126.
- LAIRD, J. and ALBEE, A.L. 1981. Pressure, Temperature and time indicators in mafic schist: Their application to reconstructing the polymetamorphic history of Vermont. *Am.J.Sci.*, **281**, 127-175.
- LAIRD, J., THOMPSON, A.B. and THOMPSON, J.B. 1978. Amphibole reactions in mafic schist [abs]. *Trans.Am.Geophys.Union (Eos)*, **59**, 408.
- LAIRD, J., THOMPSON, A.B. and THOMPSON, J.B. 1979. P,T calibration of amphibole reactions in mafic schist [abs]. *Trans.Am.Geophys Union (Eos)*, **60**, 424.
- LASAGA, A.C. 1979. Multicomponent exchange and diffusion in silicates. *Geochim.Cosmochim.Acta*, **43**, 455-69.
- LASAGA, A.C. 1983. Geospeedometry: An Extension of Geothermometry. *In*: Saxena, S.K. (ed.) *Kinetics and Equilibrium in Mineral Reactions*. Advances in Physical Geochemistry Vol 3, Springer-Verlag, New York.
- LASAGA, A.C. 1989. Fluid flow and chemical reaction kinetics in metamorphic systems : a new simple model. *E.P.Sci.Letts.*, **94**, 417.

- LASAGA, A.C., RICHARDSON, S.M. and HOLLAND, H.D. 1977. The mathematics of cation diffusion and exchange between silicate minerals during retrograde metamorphism. *In*: Saxena, S.K. and Bhattacharji, S (eds.) *Energetics of Geological Processes*, 353-388. Springer-Verlag, New York.
- LEAKE, B.E. 1978. Nomenclature of amphiboles. *Am.Mineral.*, **63**, 1023-1052.
- LEAKE, B.E. 1989. The metagabbros, orthogneisses and paragneisses of the Connemara Complex, western Ireland. *J.Geol.Soc.*, **146**, 575-596.
- LEAKE, B.E., ELIAS, E.M. and FARROW, C.M. 1988. The relationship of argon retentivity and chemical composition of hornblende. *Geochim.Cosmochim.Acta*, **52**, 2165.
- LEE, J.K.W., LO, C-H. and ONSTOTT, T.C. 1990. On the argon release mechanisms of hydrous minerals in vacuo. *Seventh International Conference on Geochronology, Cosmochronology and Isotope Geology, Canberra*, **58**.
- LEE, J.K.W., ONSTOTT, T.C. and HANES, J.A. 1987. A laser microprobe investigation of argon distribution in biotite and hornblende: A comparison with conventional ^{40}Ar - ^{39}Ar step heating spectra. *Eos*, **68**, 1514.
- LEE, J.K.W., ONSTOTT, T.C. and HANES, J.A. 1990. An $^{40}\text{Ar}/^{39}\text{Ar}$ investigation of the contact effects of a dyke intrusion, Kapuskasing Structural Zone, Ontario. A comparison of laser microprobe and furnace extraction techniques. *Contrib.Mineral.Petrol.*, **105**, 87-105.
- LESTER, A.P. 1987. Hydrothermal Fluid Circulation in a Contact Aureole: Ordering and Exsolution Characteristics in K-feldspar, Paleomagnetic and Oxygen Isotope Data. *Eos*, **68**, 1663.
- LIGWIG, N. *et.al.* 1981. Geochemical and K-Ar isotopic behaviour of Alpine sheet silicates during polyphase deformation. *Tectonophysics*, **78**, 273-90.
- LIN, T.H. and YUND, R.A. 1972. Potassium and sodium self diffusion in alkali feldspar. *Contrib.Mineral.Petrol.*, **34**, 177-184.
- LINDNER, R. 1955. Studies of solid state reactions with radiotracers. *J.Chem.Phys.*, **23**, 410-411.
- LLOYD, G.E. 1987. Atomic number and crystallographic contrast images with the S.E.M. : A review of backscattered electron techniques. *Min.Mag.*, **51**, 3-19.
- LLOYD, G.E. and HALL, M.G. 1981. Application of scanning electron microscopy to the study of deformed rocks. *Tectonophysics*, **78**, 687-98.
- LOOMIS, T.P. 1975. Reaction of zoning of garnet. *Contrib.Mineral.Petrol.*, **52**, 285-305.
- LOOMIS, T.P. 1977. Kinetics of a garnet granulite reaction. *Contrib.Mineral.Petrol.*, **62**, 1-22.
- LOOMIS, T.P. 1978 (a). Multicomponent diffusion in garnet: I. Formulation of isothermal models. *Amer.J.Sci.*, **278**, 1099-1118.
- LOOMIS, T.P. 1978 (b). Multicomponent diffusion in garnet: II. Comparison of models with isothermal data. *Am.J.Sci.*, **278**, 1119-1137.
- LOOMIS, T.P. 1983. Compositional Zoning of Crystals: A Record of Growth and Reaction History. *In*: Saxena, S.K. (ed.) *Kinetics and Equilibrium in Mineral Reactions*. Advances in Physical Geochemistry Vol 3, Springer-Verlag, New York.

- LOOMIS, T.P., GANGULY, J. and ELPHICK, S.C. 1985. Experimental determination of cation diffusivities in aluminosilicate garnets II. Multicomponent simulation and tracer diffusion coefficients. *Contrib.Mineral.Petrol.*, **90**, 45-51.
- LOVERING, T.S. and GODDARD, E.N. 1950. Geology and ore deposits of the Front-Range, Colorado. *U.S.Geol.Surv.Prof.Paper*, **223**.
- MABOKO, M.A.H., McDOUGALL, I., ZEITLER, P.K. and FITZGERALD, J.D. 1991. Discordant ^{40}Ar - ^{39}Ar ages from the Musgrove Ranges, central Australia: Implications for the significance of hornblende ^{40}Ar - ^{39}Ar spectra. *Chemical Geology (isotope Geoscience Section)*, **86**, 139-160.
- MAKINO, K. and KATSUTOSHI, T. 1989. Cation distribution in the octahedral sites of hornblendes. *Am.Mineral.*, **74**, 1097-1105.
- MANNING, J.R. 1968. *Diffusion kinetics of atoms in crystals*. Dannos Van Nostrand.
- MANNING, J.R. 1974. Diffusion kinetics and mechanisms in simple crystals. In: Giletti, B.J. (ed.) *Geochemical Transport and Kinetics*. Carnegie Institute of Washington Yearbook **634**, 107-115.
- MARESCH, W.V. and CZANK, M. 1983. Problems of compositional and structural uncertainty in synthetic hydroxyl-amphiboles; with an annotated atlas of the realbau. *Periodico di Mineralogia - Roma.*, **52**, 463-542.
- MARESCH, W.V. and CZANK, M. 1988. Crystal chemistry, growth kinetics and phase relationships of structurally disordered (Mn^{2+} , Mg)-amphiboles. *Fortschr.Mineral.*, **66**, 69-121.
- MASON, D.R. 1978. Compositional variation in ferromagnesian minerals from porphyry copper-generating and barren intrusions in the Western Highlands, Papua New Guinea. *Econ.Geol.*, **73**, 878-890.
- MASON, R. 1978. *Petrology of the metamorphic rocks*. George, Allen & Unwin Ltd., London.
- McCALLISTER, R.H. 1980. Determination of major cation diffusion constants in pyroxenes. *Geol.Soc.Amer.Abstr.Progr.*, **12**, 479.
- McCALLISTER, R.H. BRADY, J.B. and MYSEN, B.O. 1979. Self diffusion of Ca in diopside. *Carnegie Inst.Washington Yearb.*, **78**, 574-577.
- McCONVILLE, P. KELLY, S. and TURNER, G. 1988. Laser probe ^{40}Ar - ^{39}Ar Peace River Shocked LG chondrite. *Geochim. Cosmochim. Acta.*, **52**, 2487-2499.
- MILLER, J.D. and WEIBLEN, P.W. 1990. Anorthositic Rocks of the Duluth Complex : Examples of Rocks formed from Plagioclase Crystal Mushes. *J.Petrol.*, **31**.
- MISCH, P. and RICE, J.M. 1975. Miscibility of Tremolite and Hornblende in Progressive Skagit Metamorphic Suite, North Cascades, Washington. *J.Petrol.*, **16**, 1-21.
- MISENER, D.J. 1974. Cationic diffusion in olivine to 1400°C and 35kBar. In: Hofman, A.W., Giletti, B.J., Yoder, H.S.Jr and Yund, R.A. (eds.) *Geochemical Transport and Kinetics*. Carnegie Inst.Washington Yearb.Publ. **634**.
- MIYAMOTO, M. and TAKEDA, H. 1977. Evaluation of a crust model of eucrites from the width of exsolved pyroxene. *Geochem.Intl.*, **11**, 161-169.
- MIYASHIRO, A. 1957. The chemistry optics and genesis of the alkali amphiboles. *Fac.Sci.Univ.Tokyo.J.*, SecII, **11**, 57-83.

- MIYASHIRO, A. 1958. Regional metamorphism of the Gasaisyo-Takanuki district in the central Abukuma Plateau. *Jnl.Fac.Sci.University of Tokyo, Section II*, **11**, 219-272.
- MIYASHIRO, A. 1973. *Metamorphism and metamorphic belts*. George Allen & Unwin, London.
- MOODY, J.B., MEYER, D. and JENKINS, J.E. 1983. Experimental characterisation of the greenschist/amphibolite boundary in mafic systems. *Am.J.Sci.*, **283**, 48-92.
- MONTGOMERY, C.W. and BRACE, W.F. 1975. Micropores in plagioclase. *Contrib.Mineral.Petrol.*, **52**, 17-28.
- MORRISON-SMITH, D.J. 1974. A mechanism of exsolution in amphiboles. *Geol.Soc.Amer.Abstr.Programs* **6**, 878.
- MORRISON-SMITH, D.J. 1976. Transmission electron microscopy of experimentally deformed hornblende. *Am.Mineral.*, **61**, 272-280.
- MOTT, N.F. 1948. Slip at grain boundaries in metals. *Proc.Phys.Soc.Lond.*, **60**, 391.
- NABELEK, C.R. and LINDSLEY, D.H. 1985. Tetrahedral Al in amphibole: a potential thermometer for some mafic rocks. *Geol.Soc.Amer.Abst with Prog.*, **17**, 673.
- NICHOLLS, I.A. and HARRIS, K.L. 1980. Experimental r.e.e. partition coefficients for garnet, clinopyroxene and amphiboles coexisting with andesitic and basaltic liquids. *Geochim.Cosmochim.Acta*, **44**, 287-308.
- NORRIS, R.J. and HENLEY, R.W. 1976. Dewatering of a metamorphic pile. *Geology*, **4**, 333-6.
- NORTON, D. and KNAPP, R. 1977. Transport phenomena in hydrothermal systems : the nature of porosity. *Am.J.Sci.*, **277**, 913-936.
- NORTON, D. and KNIGHT, J. 1977. Transport phenomena in hydrothermal systems : cooling plutons. *Am.J.Sci.*, **277**, 937-981.
- NYMAN, M.W., TRACY, R.J. and LAW, R.L. 1989. Chemical and microstructural variation within an amphibolite shear zone as a function of shear strain. *Eos*, **70**, 1391.
- O'NIONS, R.K., SMITH, D.G.W., BAADSGAARD, H. and MORTON, R.D. 1969. Influence of chemical composition on argon retention in calcic amphiboles from S.Norway. *E.P.Sci.Letts.*, **5**, 339-355.
- OBA, T. 1980. Phase relation - the tremolite-pargasite join. *Contrib.Mineral.Petrol.*, **71**, 247-256.
- OBA, T. and YAGI, K. 1987. Phase relations on the actinolite-pargasite join. *J.Petrol.*, **28**, 23-36.
- OBA, T., YAMAMOTO, M. and OBA, N. 1977. Chemical compositions of coexisting biotites and hornblendes from Okveyama granodiorite, Kyushu, Japan. *J.J.Assoc.Mineral.Petrol.Econ.Geol.*, **72**, 433-442.
- OLSEN, S.N. 1982. Open- and closed-system migmatites in the Front Range, Colorado. *Am.J.Sci.*, **282**, 1596-1622.
- OLSEN, S.N. 1984. Mass-balance and mass-transfer in migmatites from the Colorado Front Range. *Contrib.Mineral.Petrol.*, **85**, 30-44.
- OLSEN, S.N. and GRANT, J.A. 1991. Isocon analysis of the Front Range Migmatites. *J.Met.Geol.*, **9**, 151-164.

- ONSTOTT, T.C. and PEACOCK, M.W. 1987. Argon retentivity of hornblendes: A field experiment in a slowly cooled metamorphic terrane. *Geochim.Cosmochim.Acta*, **51**, 2891-2903.
- ONSTOTT, T.C. and PRINGLE-GOODSELL, L. 1988. The influence of microstructures on the relationship between argon retentivity and chemical composition of hornblende. *Geochim.Cosmochim.Acta*, **52**, 2167-2168.
- PE-PIPER, G. 1988. Calcic amphiboles of mafic rocks of the Jeffers Brook plutonic complex Nova Scotia, Canada. *Am.Mineral.*, **73**, 993-1006.
- PERRY, E.C. Jnr. and BONNICHSEN, B. 1966. Quartz and Magnetite : Oxygen-18-Oxygen-16 Fractionation in Metamorphosed Bibabik Iron Formation.
- PETERMAN, Z.E. and HEDGE, C.E. 1967. Chronology of Precambrian events in the Front Range, Colorado. *Can.J.Earth Sci.*, **5**, 749-756.
- PETERMAN, Z.E., HEDGE, C.E. and BRADDOCK, W.A. 1968. Age of Precambrian Events in the Northeastern Front Range, Colorado. *J.Geophys.Res.*, **73**, 2277-2296.
- PHAIR, G., STERN, T.W. and GOTTFRIED, D. 1971. Boulder Creek Batholith, Colorado. Part III : Fringerprinting Discordant Zircon Ages in a Complex Intrusion. *Geol.Soc.Amer.Bull.*, **82**, 1635-1656.
- PHILLIPS, M.W., DRAHEIM, J.E., POPP, R.K., CLOWE, C.A. and PINKERTON, 1989. Effects of oxidation-dehydrogenation in tschermakitic hornblende. *Am.Mineral.*, **74**, 764-773.
- PHILLIPS, M.W., POPP, R.K. and CLOWE, C.A. 1988. Structural adjustments accompanying oxidation-dehydrogenation in amphiboles. *Am.Mineral.*, **73**, 500-506.
- PHILLIPS, R. 1963. The recalculation of amphibole analyses. *Min.Mag.*, **33**, 701-711.
- PHINNEY, W.C. 1969. *The Duluth Complex in the Gabbro Lake Quadrangle, Minnesota*. Report of Investigations of University of Minnesota, Minneapolis.
- PIERCE, W.G. 1965. Geologic map of the Deep Lake Quadrangle, Park County, Wyoming. U.S. Geological Survey, Washington D.C.
- POTTS, P.J. 1987. *A handbook of silicate rock analysis*. Blackie, London, 630pp.
- POWELL, R. 1975. Thermodynamics of co-existing cummingtonite-hornblende pairs. *Contrib.Mineral.Petrol.*, **51**, 29-37.
- POWELL, R. 1987. Darken's quadratic formalism and the thermodynamics of minerals. *Am.Mineral.*, **72**, 1-11.
- PRICE, G.D. 1981. Diffusion in the titanomagnetite solid solution series. *Min.Mag.*, **44**, 195-200.
- PRINTZ, M. 1964. Geologic evolution of the Beartooth Mountains, Montana and Wyoming, Part 5. Mafic dike swarms of the southern Beartooth Mountains. *Bull.Geol.Soc.Amer.*, **75**, 1217-1248.
- PURDY, J.W. and JAGER, E. 1976. K-Ar ages on rock forming minerals from the Central Alps. *Mem.Ist.Geol.Univ.Padova*, Vol. XXX.
- PUTNIS, A. and McCONNELL, J.D.C. 1980. *Principles of Mineral Behaviour*. Blackwell Scientific Publications, Oxford.
- RAMBALDI, E.R. 1973. Variation in the composition of plagioclase and epidote in some metamorphic rocks near Bancroft, Ontario. *Can.J.Earth.Sci.*, **10**, 852-868.

- RANKAMA, K. 1963. *Progress In Isotope Geology*. Interscience Publishers; J.Wiley & Sons, New York-London.
- RASSE, P. 1974. Al and Ti contents of hornblendes as indicators of pressure and temperature of regional metamorphism. *Contrib.Mineral.Petrol.*, **45**, 231-236.
- RAUDSEPP, M. TURNOCK, A.C., HAWTHORNE, F.C., SHERRIFF, B.L. and HARTMAN, J.S. 1987. Characterisation of synthetic pargasitic amphiboles ($\text{NaCa}_2\text{Mg}_4\text{M}^{3+}\text{Si}_6\text{Al}_2\text{O}_{22}(\text{OH},\text{F})_2$; $\text{M}^{3+}=\text{Al,Cr,Ga,Sc,In}$) by infrared spectroscopy, Rietveld structure refinement and ^{27}Al , ^{29}Si , ^{19}F MAS NMR spectroscopy. *Am.Mineral.*, **72**, 580-593.
- RAYCHAUDHURI, B. 1964. Relation of atomic constitution to lattice parameters in some hornblendes from the Black Hills, S.Dakota. *Am.Mineral.*, **49**, 198-208.
- REED, S.J.B. 1975. *Electron Microprobe Analysis*. Cambridge University Press, Cambridge.
- REED, S.J.B. 1989. Ion microprobe analysis - a review of geological applications. *Min.Mag.*, **53**, 3-24.
- RICHARD, L.R. and CLARKE, D.B. 1990. AMPHIBOL: A program for calculating structural formulae and for classifying and plotting chemical analyses of amphiboles. *Am.Mineral.*, **75**, 421-423.
- RICHARDSON, S.W. and HOLLAND, T.J.B. 1979. Metamorphic consequences of crustal eclogite production in overthrust orogenic zones. *E.P.Sci.Letts.*, **42**, 183-190.
- RIPLEY, E.M. and TAIB, N.I. 1989. Carbon isotopic studies of meta-sedimentary and igneous rocks at the Babbit Cu-Ni deposit, Duluth Complex, Minnesota, U.S.A. *Chem.Geol.*(isotope geoscience section), **73**, 319-342.
- ROBINSON, K. GIBBS, G.V., RIBBE, P. and HALL, M.R. 1973. Cation distribution in 3 hornblendes. *Am.J.Sci.*, **273-A**, 522-535.
- ROBINSON, P., JAFFE, H., KLEIN, C. and ROSS, M. 1969. Equilibrium coexistence of three amphiboles. *Contrib.Mineral.Petrol.*, **22**, 248-258.
- ROBINSON, P., SPEAR, F.S., SCHUMACHER, J.C., LAIRD, J., KLEIN, C., EVANS, B.W. and DOOLAN, B.L. 1982. Phase relations of metamorphic amphiboles: natural occurrence and theory. In: Veblen, D.R. and Ribbe, P.H. (eds.) *Amphiboles: Petrology and Experimental Phase Relations. Reviews in Mineralogy Vol.9B*. Min.Soc.Am.
- RODDICK, J.C. 1983. High Precision Intercalibration of ^{40}Ar - ^{39}Ar Standards. *Geochim.Cosmochim.Acta*, **47**, 887-898.
- ROONEY, T.P., GAVASCI, A.T. and RIECKER, R.E. 1974. Mechanical twinning in experimentally and naturally deformed hornblende. *Air Force Cambridge Research Lab., Environmental Research Pap.*, **484**, AFCRL-TR-74-0361.
- ROONEY, T.P., RIECKER, R.E. and GAVASCI, A.T. 1975. Hornblende deformation features. *Geology*, **3**, 364-368.
- ROONEY, T.P., RIECKER, R.E. and ROSS, M. 1970. Deformation twins in hornblende. *Science*, **169**, 173-175.
- ROSS, M., PAPIKE, J.J. and SHAW, K.W. 1969. Exsolution textures in amphiboles as indicators of subsolidus thermal histories. *Min.Soc.Amer.Spec.Paper* **2**, 275-299.
- ROWBOTHAM, G. and FARMER, V.C. 1973. The effect of 'A' site occupancy upon the hydroxyl stretching frequency in clinoamphiboles. *Contrib.Mineral.Petrol.*, **38**, 147-149.

- RUTTER, M.J. and WYLLIE, P.J. 1989. Experimental study of interaction between hydrous granite melt and amphibolite. *Geol.Mag.*, **126**, 633-646.
- RUTTER, M.J., VAN DER LAAN, S.R. and WYLLIE, P.J. 1989. Experimental data for a proposed empirical igneous geobarometer: Aluminium in hornblende at 10kbar pressure. *Geology*, **17**, 897-900.
- SAMPSON, G.A. and FAWCETT, J.J. 1977. Coexisting amphiboles from the Hastings Region of South-Eastern Ontario. *Can.Mineral.*, **15**, 283-296.
- SANDERS, C.W.Jr. 1929. A composite sotch at Snowbank Lake northeastern Minnesota. *J.Geol.*, **37**, 135-149.
- SANFORD, R.F. and HUEBNER, J.S. 1979. Re-examination of diffusion processes in 77115 and 77215. *Lunar Planet.Sci.*, **10**, 1052-1054.
- SANFORD, R.F. and HUEBNER, J.S. 1979. Re-examination of diffusion processes in 77115 and 77215 (abst). *In: Lunar and Planetary Science, Vol X*, 1052-1054. Lunar and Planetary Science Institute, Houston, Texas.
- SAUTTER, V. and HARTE, B. 1988. Diffusion gradients in an eclogite xenolith from the Roberts Victor Kimberlite Pipe :1. Mechanism and Evolution of Garnet Exsolution in Al₂O₃-rich clinopyroxene. *J.Petrol.*, **29**, 1325-1352.
- SAUTTER, V., JAOU, O. and ABEL, F. 1988. Aluminium diffusion in diopside using the ²⁷Al(P,γ) ²⁸Si nuclear reaction : preliminary results. *E.P.Sci.Letts.*, **89**, 109-114.
- SAXENA, S.K. 1972. Retrieval of thermodynamic data from a study of inter-crystalline and intracrystalline ion-exchange equilibrium. *Am.Mineral.*, **57**, 1782-1800.
- SAXENA, S.K. (ed.) 1983. *Kinetics and equilibrium in mineral reactions*. Springer-Verlag, New York.
- SEIFERT, F. and VIRGO, D. 1975. Kinetics of the Fe²⁺-Mg order-disorder reaction in Anthophyllites : Quantitative Cooling Rates. *Science*, **188**, 1107-1109.
- SEITZ, M.G. 1973. Uranium and thorium diffusion in diopside and fluorapatite. *Carnegie Inst.Washington Yearb.*, **72**, 586-588,
- SHAFFER, E.W. *et.al.* 1974. Diffusion of tritiated water in β-Quartz. *In: Hofmann, A.W. et.al. (eds.) Geochemical Transport and Kinetics*. Carnegie Inst.Wash.Publ., 634.
- SHIEH, Y.N. and TAYLOR, H.P. 1969. Oxygen and hydrogen isotope studies of contact metamorphism in the Santa Rosa Range, Nevada and other areas. *Contrib.Mineral.Petrol.*, **20**, 306-356.
- SHIMIZU, N. Cameca Ion Microprobe Ims 3F : Physical Properties (translation).
- SIMS, P.K. and MOREY, G.B. (eds.) 1972. *Geology of Minnesota: A Centennial Volume*, Minnesota Geological Survey.
- SIPPEL, R.F. 1963. Sodium diffusion in natural minerals. *Geochim.Cosmochim.Acta*, **27**, 107-120
- SMELIK, E.A., NYMAN, M.W. and VEBLEN, D.R. (submitted). Pervasive exsolution within the calcic amphibole series: TEM evidence for a miscibility gap between actinolite and hornblende in natural samples. *Am.Mineral*.
- SMITH, J.V. 1974. *Felspar Minerals, Vol 2*. Springer, Berlin Heidelberg New York, 152-195.

- SNEERINGER, M., HART, S.R. and SHIMIZU, N. 1984. Strontium and samarium diffusion in diopside. *Geochim.Cosmochim.Acta*, **48**, 1589-1608.
- SNEERINGER, M., HART, S. 1978. Sr diffusion in diopside (abstr.) *Eos*, American Geophysical Union Transactions, **59**, 402.
- SPEAR, F.S. 1980. NaSi \rightleftharpoons CaAl exchange equilibrium between plagioclase and amphibole. An empirical model. *Contrib.Mineral.Petrol.*, **72**, 33-41.
- SPEAR, F.S. 1981. Amphibole-Plagioclase Equilibria: An empirical Model for the Relation Albite + Tremolite = Edenite + 4Quartz. *Contrib.Mineral.Petrol.*, **77**, 355-364.
- SPEAR, F.S. 1981. An experimental study of hornblende stability and compositional variability in amphibolites. *Am.J.Sci.*, **281**, 697-734.
- SPEAR, F.S. 1982. Phase equilibria of amphibolites from the Post Pond volcanics, Mt.Cube quadrangle, Vermont. *J.Petrol.*, **23**, 383-426.
- SPEAR, F.S. 1991. On the interpretation of peak metamorphic temperatures in the light of garnet diffusion during cooling. *J.Met.Geol.*, **9**, 379-388.
- SPEAR, F.S. and KIMBALL, K.L. 1984. Recamp - A Fortran IV program for estimating Fe³⁺ contents in amphiboles. *Computers & Geosciences*, **10**, 317-325.
- SPRAY, J.G. and RODDICK, J.C. 1980. Petrology and ⁴⁰Ar/³⁹Ar Geochronology of some Hellenic Sub-Ophiolite Metamorphic Rocks. *Contrib.Mineral.Petrol.*, **72**, 43-55.
- SPRY, S. 1983. *Metamorphic Textures*. Pergamon Press, Oxford. New York.
- STEIGER, R.H. and HART, S.R. 1967. The microcline-orthoclase transition within a contact aureole. *Am.Mineral.*, **52**, 87-116.
- STEIGER, R.H. and JAGER, E. 1977. Submission on Geochronology: Convention on the use of decay constants in geo- and cosmochronology. *E.P.Sci.Letts.*, **36**, 359-362.
- STERN, T.W., PHAIR, G. and NEWELL, M.F. 1971. Boulder Creek Batholith, Colorado. Part II : Isotopic Age of Emplacement and Morphology of Zircon. *Bull.Geol.Soc.Amer.*, **82**, 1615-1634.
- STOUT, J.H. 1972. Phase petrology and mineral chemistry of co-existing amphiboles from Telemark, Norway. *J.Petrol.*, **13**, 99-145.
- SWEATMAN, T.R. and LONG, J.V.P. 1969. Quantitative electron-probe microanalysis of rock forming minerals. *J.Petrol.*, **10**, 332-379.
- TAYLOR, H.P. 1978. Oxygen and hydrogen isotope studies of plutonic granitic rocks. *E.P.Sci.Letts.*, **38**, 177-210.
- THIEL, E. 1956. Correlation of gravity anomalies with the Keweenawan geology of Wisconsin and Minnesota. *Bull.Geol.Soc.Amer.*, **67**, 1079-1100.
- THOMPSON, J.B., Jr. 1982. Composition space: An algebraic and geometric approach. *Mineralogical Society of America Reviews in Mineralogy*, **10**, 1-31.
- THOMPSON, J.B., LAIRD, J. and THOMPSON, A.B. 1982. Reaction in Amphibolite, Greenschist and Blueschist. *J.Petrol.*, **23**, 1-27.
- TILTON, G.R., DAVIS, G.L., HART, S.R. and ALDRICH, L.T. *Carnegie Inst.Wash.Yearb.*, **61**, 173-9.

- TILTON, G.R., DAVIS, G.L., HART, S.R., ALDRICH, L.T., STEIGER, R.H. and GAST, P.W. 1964. Geochronology and Isotope Geochemistry. *Carnegie Inst.Wash.Yearb.*, **63**, 240-256.
- TROLL, G. and GILBERT, M.C. 1972. Fluorine-hydroxyl substitutions in tremolite. *Am.Mineral.*, **57**, 1386-1403.
- TURNER, F.J. 1968. *Metamorphic Petrology, Mineralogy, Field and Tectonic Aspects*. Hemisphere Publishing Co., New York.
- TURNER, G. 1968. The Distribution of Potassium and Argon in Chondrites. In: Ahrens, L.H. (ed.) *Origins and Distributions of The Elements*. Pergamon Press. Oxford, New York.
- TURNER, G. 1969. Thermal histories of meteorites by the $^{39}\text{Ar}/^{40}\text{Ar}$ method. In: P.M. Millman (ed.) *Meteoritic Research*. D.Reidel.Publ.Co.
- TURNER, G. 1971. ^{40}Ar - ^{39}Ar dating: The Optimization of Irradiation Parameters. *E.P.Sci.Letts.*, **10**, 227-234.
- TURNER, D.L. and FORBES, R.B. 1976. K-Ar studies in deep basement drill holes : a new geologic estimate of argon blocking in biotite (abstr). *Eos*, **57**, 353.
- TWETO, O. and SIMS, P.K. 1963. Precambrian Ancestry of the Colorado Mineral Belt. *Bull.Geol.Soc.Amer.*, **74**, 991-1014.
- UNGARETTI, L., SMITH, D.C. and ROSSI, G. 1981. Crystal-chemistry by X-ray structure refinement and electron microprobe analysis of a series of sodic-calcic to alkali amphiboles from the Nybo eclogite pod, Norway. *Soc.Franc.Mineral.Crist.Bull.*, **104**, 400-412.
- VAN BREEMAN, O., AFTALION, M., PANKHURST, R.J. and RICHARDSON, S.W. 1979. Age of the Glen Dessary Syenite Invernesshire: diachronous Palaeozoic Metamorphism across the Great Glen. *Scott.J.Geol.*, **15**, 49-62.
- VAN BREEMER, O. and DALLMEYER, R.D. 1984. The scale of Sr isotopic diffusion during post-metamorphic cooling of gneisses in the Inner Piedmont of Georgia, Southern Appalachians. *E.P.Sci.Letts.*, **68**, 141-150.
- VEBLEN, D.R. (ed.) 1981. *Amphiboles and other hydrous pyriboles - mineralogy. Reviews in Mineralogy Vol.9B*. Min.Soc.Am., Bookcrafts Inc., Michigan.
- VEBLEN, D.R. and RIBBE, P.H. (eds.) 1982. *Amphiboles : petrology and experimental phase relations. Reviews in Mineralog Vol.9A*. Min.Soc.Amer., Bookcrafts Inc., Michigan.
- VERNON, R.H. 1976. *Metamorphic Processes*. George, Allen & Unwin Ltd., London.
- VIDALE, R.J. 1969. Metasomatism in a chemical gradient and the formation of calc-silicate bands. *Am.J.Sci.*, **267**, 857-874.
- VILLA, H., BAUER, G., MORTEANI, R.H. and STEIGER, R.H. 1989. Time calibration of a PT-path from the western Tavern Window, Eastern Alps ; the problem of closure temperature. *Contrib.Mineral.Petrol.*, **101**, 1-11.
- VYHNAL, C.R., McSWEEN, H.Y.Jr. and SPEER, J.A. 1991. Hornblende chemistry in southern Appalachian granitoids: Implications for aluminium hornblende thermobarometry and magmatic epidote stability. *Am.Mineral.*, **76**, 176-188.
- WAGNER, G.A. and REIMER, G.M. 1972. Fission track tectonics: The tectonic interpretation of fission track apatite ages. *E.P.Sci.Letts.*, **14**, 263-268.

- WALKER, F.D.L., 1990. Ion microprobe study of intragrain micropermeability in alkali feldspars. *Contrib.Mineral.Petrol.*, **106**, 124-128.
- WALKER, K.L. and HOMSY, G.M. 1978. Convection in a porous cavity. *J.Fluid.Mech.*, **87**, 449-474.
- WALTHER, J.V. and WOOD, B.J. 1984. Rate and mechanism in prograde metamorphism. *Contrib.Mineral.Petrol.*, **88**, 246-259.
- WALTON, M. 1982. Geologic Map of Minnesota: Two Harbors Sheet. Minnesota Geological Survey.
- WARTHON, J. DODSON, M.H., REX, D.C. and GUISE, P.G. 1991. Mechanisms of argon release from Himalayan metamorphic hornblendes. *Am.Mineral.*(letter) July/August edition.
- WEIBLEN, P.W. and MOREY, G.B. 1980. A summary of the stratigraphy, petrology and structure of the Duluth Complex. *Am.J.Sci.*, **280-A**, 88-133.
- WELCH, M.D. 1987. Experimental Studies of Selected Amphiboles In The System Na₂O-CaO-MgO-Al₂O₃-SiO₂-H₂O-F₂ and it's Subsystems. Unpubl.Ph.D.Thesis. University of Edinburgh.
- WENK, H.R. (ed.). 1976. *Electron Microscopy in Mineralogy*. Springer, Berlin.
- WENK, H.R. 1985. *Preferred Orientation in Deformed Metals and Rocks: An Introduction to Modern Texture Analysis*. Academic Press Inc., London.
- WESCOTT, M.R. 1966. Loss of Argon from Biotite in a Thermal Metamorphic Event. *Nature*, **210**, 83-84.
- WESTRICH, H.R. 1981. F-OH exchange equilibria between mica-amphibole pairs. *Contrib.Mineral.Petrol.*, **78**, 318-323.
- WESTRICH, H.R. and HOLLOWAY, J.R. 1981. Experimental dehydration of pargasite and calculation of it's entropy and Gibb's energy. *Am.J.Sci.*, **281**, 922-934.
- WIJBRONS, J.R., SCHLIESTEDT, M. and YORK, D. 1990. Single grain argon laser probe dating of phengites from the blueschist to greenschist transition on Sifnos (Cyclades, Greece). *Contrib.Mineral.Petrol.*, **104**, 582-593.
- WONES, D.R. and EUGSTER, H.P. 1965. Stability of biotite : experiment, theory and application. *Am.Mineral.*, **50**, 1228-1272.
- WOOD, B.J. 1976. The partitioning of Fe and Mg between co-existing garnet and clinopyroxene. *Carnegie Inst.Wash.Yearb.*, **75**, 571-574.
- WOOD, B.J. and HEMMING, R.F. 1978. Major and trace element disequilibrium during partial melting. In: *Short Papers, 4th International Conference on Geochronology, Cosmochronology and Isotope Geology*, Snormass, U.S.A., U.S.Geol.Surv.Open File Rep., 78-701, 459-462.
- WORDEN, R.H., WALKER, F.D.L., PARSONS, I., and BROWN, W.L., 1990. Development of microporosity, diffusion channels and deuteric coarsening in perthitic alkali feldspars. *Contrib.Mineral.Petrol.*, **104**, 507-515.
- WRIGHT, T.L. 1967. The microcline-orthoclase transformation in the contact aureole of the Eldora Stock, Colorado. *Am.Mineral.*, **52**, 117.
- WRIGHT, N., LAYER, P.W. and YORK, D. 1991. New insights into thermal history from single grain ⁴⁰Ar/³⁹Ar analysis of biotite. *E.P.Sci.Letts.*, **104**, 59-69.

- YAMAGUCHI, Y. 1985. Hornblende-cummingtonite and hornblende-actinolite intergrowths from Koyama calc-alkaline intrusion, Susa, southwest Japan. *Am.Mineral.*, **709**, 980-986.
- YORK, D. 1984. Cooling Histories from $^{40}\text{Ar}/^{39}\text{Ar}$ Age Spectra. Implications for Precambrian Palaeotectonics. *Ann.Rev.E.P.Sci.Letts.*, **12**, 383-409.
- YUND, R.A., QUIGLEY, J. and TULLIS, T. 1989. The effect of dislocations on bulk diffusion in feldspars during metamorphism. *J.Met.Geol.*, **7**, 337.
- ZIELINSKI, R.A. and FREY, F.A. 1974. An experimental study of the partitioning of a R.E.E. (Gd) in the system diopside-aqueous vapour. *Geochim.Cosmochim.Acta*, **38**, 545-565.

ADDITIONAL REFERENCES CITED

- GREEN, J.C. 1982. Geologic map of Minnesota, Two Harbors Sheet. Publ. Minnesota Geological Survey.
- MITCHELL, J.G. 1968. The argon $^{40}\text{Ar}/^{39}\text{Ar}$ method for potassium-argon age determinations. *Geochim.Cosmochim.Acta.*, **32**, 781-790.
- TWETO, O. 1966. Regional features of Precambrian rocks in northcentral Colorado. In: The Geological Society of America Abstracts for 1965. *Geol.Soc.Am.Spec.Paper* **87**.

